UNIVERSITY OF OKLAHOMA

GRADUATE COLLEGE

INTERPRETATION OF PRESSURE TRANSIENT TESTS OF HORIZONTAL WELLS WITH MULTIPLE HYDRAULIC FRACTURES AND ZONAL ISOLATIONS

A DISSERTATION

SUBMITTED TO THE GRADUATE FACULTY

in partial fulfillment of the requirements for the

Degree of

DOCTOR OF PHILOSOPHY

By

SALAM J. HUSSAIN AL RBEAWI
Norman, Oklahoma
2012

INTERPRETATION OF PRESSURE TRANSIENT TESTS OF HORIZONTAL WELLS WITH MULTIPLE HYDRAULIC FRACTURES AND ZONAL ISOLATIONS

A DISSERTATION APPROVED FOR THE
MEWBOURNE SCHOOL OF PETROLEUM AND GEOLOGICAL ENGINEERING

BY

_____

Dr. Djebbar Tiab, Chair

_____

Dr. Maysam Pournik

_____

Dr. B.J. Ben Shiau

_____

Dr. Deepak Devegowda

_____

Dr. Miguel Bagajewicz

DEDICATION

To my lovely wife, **SABAH**, my dear son, **NAWAR**, and my dear daughter, **WUD**.

To our family in Norman, **JIM** and **BETTY BROWN**

ACKNOWLEDGMENTS

I wish to express my gratitude to Dr. Djebbar Tiab for his continuous guidance and encouragement during graduate and research studies at the University of Oklahoma. I really believe without his support, advice and comment, this project would not have been possible. I would like also to thank Dr. Ben Shiau, Dr. Maysam Porunik, Dr. Deepak Devegowda, and Dr. Miguel Bagajewicz for their willingness to serve as members of my doctoral committee.

It was a pleasure and valuable professional experiences to associate with all the faculty members of Mewbourne School of Petroleum and Geological Engineering. I thank all of them for their cooperation, friendship, and kindness that made my study at the University of Oklahoma meaningful and enjoyable. I also appreciate all the help and cooperation provided by the MPGE staff that made my attendance at the school during my study very easy and comfortable.

Deep appreciations are extended to my family for their patience and help all the way during my Ph.D. journey. Without their sacrifices and challenges, I would not have been able to get the opportunity to pursue our goals in study and life.

Finally, great gratitude, deep appreciation and all thanks to **JIM** and **BETTY BROWN** for their caring, guidance and inspiration. Their friendship extremely changed my life and my family's life positively and developed our sights about everything. Their association with us has been the motivation to do all the best in our daily lives. Thank you again and again **JIM** and **BETTY**.

TABLE OF CONTENTS

	Page
TABLE OF CONTENT	v
LIST OF TABLES	viii
LIST OF FIGURES	ix
ABSTRACT	xiii
CHAPTER ONE: INTRODUCTION AND LITERATURE REVIEW	
1-1- Zonal isolations	1
1-2- Hydraulic fractures	5
CHAPTER TWO: MATHEMATICAL MODELS FOR A HORIZONTAL WELL WITH ZONAL ISOLATIONS	
2-1- Short horizontal well headed by a zonal isolation	15
2-2- Long horizontal well headed by a zonal isolation	23
2-3- Short horizontal well headed by a perforated zone	26
2-4- Long horizontal well headed by a perforated zone	27
CHAPTER THREE: PRESSURE TRANSIENT ANALYSIS FOR HORIZONTAL WELLS WITH ZONAL ISOLATIONS	
3-1- Pressure behavior for horizontal wells without zonal isolations	30
3-2- Pressure behavior for horizontal wells with zonal isolations	36
3-3- Flow regimes for horizontal well with zonal isolations	40
3-4- Intersection points	47
3-5- Relationships between flow regimes	49

3-6- Skin factor 51

3-7- The effect of the number and length of zonal isolation on pseudo-skin factor 53

3-8- Application of type-curve matching 55

3-9- Application of TDS technique 57

3-10- Malfunction of zonal isolations 71

CHAPTER FOUR: MATHEMATICAL MODELS FOR MULTIPLE-INCLINED HYDRAULIC FRACTURES

4-1- State of in-situ stress 78

4-2- Inclined hydraulic fractures 79

4-3- Models derivation 80

4-4- Model for anisotropic formation 102

4-5- Models validation 104

CHAPTER FIVE: PRESSURE TRANSIENT ANALYSIS FOR HORIZONTAL WELL WITH MULTIPLE-INCLINED HYDRAULIC FRACTURES

5-1- Pressure behavior 106

5-2- Flow regimes 111

5-3- Intersection points 115

5-4- Pseudo-skin factor 117

5-5- Application of type-curve matching 119

5-6- Application of TDS technique 121

5-7- Hydraulic fractures malfunction 133

CHAPTER SIX: MATHEMATICAL MODELS FOR PARTIALLY PENETRATING MULTIPLE-INCLINED HYDRAULIC FRACTURES

6-1- Models derivation 139

6-2- Partially penetrating multiple inclined transverse hydraulic fractures 145

CHAPTER SEVEN: PRESSURE TRANSIENT ANALYSIS FOR PARTIALLY PENETRATING MULTIPLE-INCLINED HYDRAULIC FRACTURES

7-1- Pressure behavior 147

7-2- Effect of inclination angle 156

7-3- Flow regimes 157

7-4- Intersection points 163

7-5- Relationships between flow regimes 164

7-6- Pseudo-skin factor 166

7-7- Application of type-curve matching 166

7-8- Application of TDS technique 168

SUMMURY AND CONCLUSIONS 180

RECOMMENDATIONS 183

NOMENCLATURES 184

REFERNCES 186

APPENDIXES 192

LIST OF TABLES

Page

Table 3-1-Summury of results of Example 3-1. 65

Table 3-2-Summury of results of Example 3-2. 71

Table 3-3-Summury of results of Example 3-3. 76

Table 5-1-Summury of results of Example 5-1. 128

Table 5-2-Summury of results of Example 5-2. 133

Table 7-1-Summury of results of Example 7-1. 175

Table 7-2-Summury of results of Example 7-2. 179

LIST OF FIGURES

Page

2-1- Horizontal well headed by zonal isolation. 15
2-2- The monitoring point and the sources of production for a horizontal well. 16
2-3- Horizontal well headed by perforated zone. 27
3-1- Pressure behavior for horizontal wells in infinite reservoirs. 31
3-2- Pressure behavior for horizontal wells in finite reservoirs. 31
3-3- Early radial flow for horizontal wells. 31
3-4- Early linear flow for horizontal wells. 33
3-5- Pseudo-radial flow for horizontal wells. 34
3-6 Channel flow for horizontal wells acting in finite reservoirs. 35
3-7- Pressure behavior for short horizontal well with single zone isolation (L_D=1). 37
3-8- Pressure behavior for short horizontal well with multiple zonal isolations (L_D=1, L_{sD}=0.1). 37
3-9- Pressure behavior for short horizontal well with multiple zonal isolations (L_D=1, L_{sD}=0.4). 37
3-10- Pressure behavior for short horizontal well with multiple zonal isolations (L_D=1, L_{sD}=0.8). 37
3-11- Pressure behavior for moderate length horizontal well without zonal isolation (L_D=10). 39
3-12- Pressure behavior for moderate length horizontal well with multiple zonal isolations (L_D=10, L_{sD}=0.1). 39
3-13- Pressure behavior for moderate length horizontal well with multiple zonal isolations (L_D=10, L_{sD}=0.4). 39
3-14- Pressure behavior for moderate length horizontal well with multiple zonal isolations (L_D=10, L_{sD}=0.8). 39
3-15- Pressure behavior for long horizontal well without zonal isolations (L_D=50). 40
3-16- Pressure behavior for long horizontal well with multiple zonal isolations (L_D=50, L_{sD}=0.1). 40
3-17- Pressure behavior for long horizontal well with multiple zonal isolations (L_D=50, L_{sD}=0.4). 41
3-18- Pressure behavior for long horizontal well with multiple zonal isolations (L_D=50, L_{sD}=0.8). 41
3-19- Early radial flow for horizontal well with zonal isolations. 41
3-20- System radial flow for horizontal well with zonal isolations. 42
3-21- Intermediate radial flow for horizontal well with zonal isolations. 43
3-22- Pseudo-spherical flow for horizontal well with zonal isolations. 44
3-23- Early linear flow for horizontal well with zonal isolations. 45
3-24- Second linear flow for horizontal well with zonal isolations. 45
3-25- Elliptical flow regime for horizontal well with zonal isolations. 46
3-26- Multi-regression analysis for elliptical flow for horizontal well with zonal isolations. 46
3-27- Pseudo-radial flow for horizontal well with zonal isolations. 47
3-28- Effect of skin factor on pressure behavior of horizontal well without zonal isolations (L_D=16, L_{sD}=0.0). 53
3-29- Effect of skin factor on pressure behavior of horizontal well with zonal isolations (L_D=16, L_{sD}=0.5). 53
3-30- Effect of skin factor on pressure behavior of horizontal well with zonal isolations (L_D=16, L_{sD}=0.8). 54
3-31- Effect of number and length of zonal isolations on pseudo-skin factor. 54
3-32- Pressure and pressure derivative plot for Example 3-1. 61
3-33- Type-curve matching technique for Example 3-1. 61
3-34- TDS technique for Example 3-1. 62
3-35- Pressure and pressure derivative plot for Example 3-2. 67
3-36- Type-curve matching technique for Example 3-2. 67
3-37- TDS technique for Example 3-2. 69
3-38- Pressure and pressure derivative plot for single failed zonal isolation Single perforation zone and single zone isolator). 72
3-39- Pressure and pressure derivative plot for single failed zonal isolation (Double perforation zones and double zone isolators). 72
3-40- Pressure and pressure derivative plot for single failed zonal isolation (Triple perforation zones and triple zone isolators). 72

3-41- Pressure and pressure derivative plot for double failed zonal isolation (Double perforation zones and double zone isolators). 72
3-42- Pressure and pressure derivative plot for single failed zonal isolation (Four perforation zones and four zone isolators). 72
3-43- Pressure and pressure derivative plot for double failed zonal isolation (Four perforation zones and four zone isolators). 72
3-44- Pressure and pressure derivative plot for triple failed zonal isolation (Four perforation zones and four zone isolators). 72
3-45- Pressure and pressure derivative plot for Example 3-3. 74
3-46- Type-curve matching technique for Example 3-3. 74
4-1- Horizontal fracture for $\sigma_v < \sigma_h < \sigma_H$. 77
4-2- Vertical fractures for $\sigma_h < \sigma_H < \sigma_v$. 77
4-3- Effect of depletion production on hydraulic fracture orientation. 80
4-4- Horizontal well intersected by multiple-inclined transverse hydraulic fractures. 83
4-5- The monitoring point and the source points for multiple-inclined transverse hydraulic fractures. 84
4-6- Schematic diagram for horizontal well intersected by multiple-inclined transverse hydraulic fractures 85
4-7- The distance between the monitoring point and production points. 85
4-8- Superposition principles for multiple-inclined fractures. 86
4-9- Horizontal well intersected by multiple-inclined longitudinal hydraulic fractures. 94
4-10- The monitoring point and the source points for multiple-inclined longitudinal hydraulic fractures.94
4-11- Horizontal well intersected by deviated hydraulic fractures. 98
4-12- The distance between the monitoring point and production point for deviated hydraulic fractures 99
4-13- The result of three vertical fractures using the new model and Ozkan's model. 105
4-14- The result of single inclined fractures using the new model and Cinco-Ley's model. 105
5-1- Pressure behavior of two inclined transverse hydraulic fractures (h_D=1, D_D=2). 107
5-2- Pressure behavior of ten inclined transverse hydraulic fractures (h_D=1, D_D=2). 107
5-3- Pressure behavior of two inclined transverse hydraulic fractures (h_D=1, D_D=10). 108
5-4- Pressure behavior of ten inclined transverse hydraulic fractures (h_D=1, D_D=10). 108
5-5- Pressure behavior of five inclined longitudinal hydraulic fractures (h_D=1, D_D=1). 109
5-6- Pressure behavior of five inclined longitudinal hydraulic fractures (h_D=1, D_D=5). 109
5-7- Pressure behavior of five semi-transverse inclined hydraulic fractures (h_D=1, D_D=1, Thetav=0.0).110
5-8- Pressure behavior of five semi-transverse inclined hydraulic fractures (h_D=1, D_D=1, Thetav=60). 110
5-9- Pressure behavior of five semi-transverse inclined hydraulic fractures (h_D=1, D_D=5, Thetav=0.0).110
5-10- Pressure behavior of five semi-transverse inclined hydraulic fractures (h_D=1, D_D=5, Thetav=60)110
5-11- Linear flow regime of multiple-inclined hydraulic fractures. 112
5-12- Pseudo-radial flow regime for multiple-inclined hydraulic fractures. 113
5-13- Early radial flow regime for multiple-inclined hydraulic fractures. 113
5-14- Elliptical flow regime for multiple-inclined hydraulic fractures. 115
5-15- Multivariate regression analysis for elliptical flow regime (transverse and longitudinal fractures)115
5-16- Multivariate regression analysis for elliptical flow regime (semi-transverse fractures). 115
5-17- Pseudo-skin factor for transverse and longitudinal hydraulic fractures. 119
5-18- Pseudo-skin factor for semi-transverse hydraulic fractures. 119
5-19- Pressure and pressure derivative plot for Example 5-1. 125
5-20- Type-curve matching plot for Example 5-1. 125
5-21- TDS technique for Example 5-1. 126
5-22- Pressure and pressure derivative plot for Example 5-2. 129
5-23- Type-curve matching plot for Example 5-2. 129
5-24- TDS technique for Example 5-2. 131
5-25- Pressure behavior of three vertical fractures with one malfunction fracture. 134
5-26- Pressure behavior of four vertical fractures with one malfunction fracture. 134
5-27- Pressure behavior of five vertical fractures with one malfunction fracture. 135
5-28- Pressure behavior of six vertical fractures with one malfunction fracture. 135
5-29- Pressure behavior of seven vertical fractures with one malfunction fracture. 135

5-30- Pressure behavior of eight vertical fractures with one malfunction fracture. 135
5-31- Pressure behavior of nine vertical fractures with one malfunction fracture. 135
5-32- Pressure behavior of ten vertical fractures with one malfunction fracture. 135
5-33- Pressure behavior of eight vertical fractures with several malfunction fractures for short spacing 137
5-34- Pressure behavior of eight vertical fractures with several malfunction fractures for long spacing 137
5-35- Pressure and pressure derivative of Example 5-3. 138
5-36- Type-curve matching of Example 5-3. 138
6-1- Horizontal well intersected by partially penetrating multiple hydraulic fractures. 140
6-2- The monitoring point and the source points of partially penetrating multiple transverse hydraulic fractures. 141
6-3- Schematic diagram of partially penetrating hydraulic fractures. 142
6-4- Horizontal well intersected by partially penetrating multiple-inclined hydraulic fractures. 146
7-1- Pressure behavior of two partially penetrating vertical hydraulic fractures (h_{xfD}=2, D_D=1). 148
7-2- Pressure behavior of two partially penetrating vertical hydraulic fractures (h_{xfD}=8, D_D=1). 148
7-3- Pressure behavior of two partially penetrating vertical hydraulic fractures (h_{xfD}=2, D_D=8). 149
7-4- Pressure behavior of two partially penetrating vertical hydraulic fractures (h_{xfD}=8, D_D=8). 149
7-5- Pressure behavior of sixteen partially penetrating vertical hydraulic fractures (h_{xfD}=2, D_D=1). 149
7-6- Pressure behavior of sixteen partially penetrating vertical hydraulic fractures (h_{xfD}=8, D_D=1). 149
7-7- Pressure behavior of sixteen partially penetrating vertical hydraulic fractures (h_{xfD}=2, D_D=8). 149
7-8- Pressure behavior of sixteen partially penetrating vertical hydraulic fractures (h_{xfD}=8, D_D=8). 149
7-9- Pressure behavior of two partially penetrating vertical hydraulic fractures (h_{xfD}=16, D_D=1). 150
7-10- Pressure behavior of two partially penetrating vertical hydraulic fractures (h_{xfD}=32, D_D=1). 150
7-11- Pressure behavior of two partially penetrating vertical hydraulic fractures (h_{xfD}=16, D_D=8). 150
7-12- Pressure behavior of two partially penetrating vertical hydraulic fractures (h_{xfD}=32, D_D=8). 150
7-13- Pressure behavior of sixteen partially penetrating vertical hydraulic fractures (h_{xfD}=16, D_D=1). 151
7-14- Pressure behavior of sixteen partially penetrating vertical hydraulic fractures (h_{xfD}=32, D_D=1). 151
7-15- Pressure behavior of sixteen partially penetrating vertical hydraulic fractures (h_{xfD}=16, D_D=8). 151
7-16- Pressure behavior of sixteen partially penetrating vertical hydraulic fractures (h_{xfD}=32, D_D=8). 151
7-17- Pressure behavior of two partially penetrating vertical hydraulic fractures (h_{xfD}=2, D_D=1). 153
7-18- Pressure behavior of two partially penetrating vertical hydraulic fractures (h_{xfD}=8, D_D=1). 153
7-19- Pressure behavior of two partially penetrating vertical hydraulic fractures (h_{xfD}=2, D_D=8). 153
7-20- Pressure behavior of two partially penetrating vertical hydraulic fractures (h_{xfD}=8, D_D=8). 153
7-21- Pressure behavior of sixteen partially penetrating vertical hydraulic fractures (h_{xfD}=2, D_D=1). 153
7-22- Pressure behavior of sixteen partially penetrating vertical hydraulic fractures (h_{xfD}=8, D_D=1). 153
7-23- Pressure behavior of sixteen partially penetrating vertical hydraulic fractures (h_{xfD}=2, D_D=8). 154
7-24- Pressure behavior of sixteen partially penetrating vertical hydraulic fractures (h_{xfD}=8, D_D=8). 154
7-25- Pressure behavior of two partially penetrating vertical hydraulic fractures (h_{xfD}=16, D_D=1). 155
7-26- Pressure behavior of two partially penetrating vertical hydraulic fractures (h_{xfD}=32, D_D=1). 155
7-27- Pressure behavior of two partially penetrating vertical hydraulic fractures (h_{xfD}=16, D_D=8). 155
7-28- Pressure behavior of two partially penetrating vertical hydraulic fractures (h_{xfD}=32, D_D=8). 155
7-29- Pressure behavior of sixteen partially penetrating vertical hydraulic fractures (h_{xfD}=16, D_D=1). 155
7-30- Pressure behavior of sixteen partially penetrating vertical hydraulic fractures (h_{xfD}=32, D_D=1). 155
7-31- Pressure behavior of sixteen partially penetrating vertical hydraulic fractures (h_{xfD}=16, D_D=8). 156
7-32- Pressure behavior of sixteen partially penetrating vertical hydraulic fractures (h_{xfD}=32, D_D=8). 156
7-33- Pressure behavior of two partially penetrating inclined hydraulic fractures (h_{hfD}=0.5, h_{xfD}=10, D_D=1). 157
7-34- Pressure behavior of two partially penetrating inclined hydraulic fractures (h_{hfD}=0.5, h_{xfD}=10, D_D=8). 157
7-35- Pressure behavior of ten partially penetrating inclined hydraulic fractures (h_{hfD}=0.5, h_{xfD}=10, D_D=1). 157
7-36- Pressure behavior of ten partially penetrating inclined hydraulic fractures (h_{hfD}=0.5, h_{xfD}=10, D_D=8). 157
7-37- First linear flow regime for partially penetrating multiple hydraulic fractures. 158
7-38- Early radial flow regime for partially penetrating multiple hydraulic fractures. 159
7-39- Second linear flow regime for partially penetrating multiple hydraulic fractures. 160
7-40- Third linear flow regime for partially penetrating multiple hydraulic fractures. 161

7-41- Intermediate radial flow regime for partially penetrating multiple hydraulic fractures. 162
7-42- Pseudo-radial flow regime for partially penetrating multiple hydraulic fractures. 162
7-43- Elliptical flow regime for partially penetrating multiple hydraulic fractures. 163
7-44- Relationships between flow regimes for partially penetrating multiple hydraulic fractures. 166
7-45- Pressure and pressure derivative plot for Example 7-1. 171
7-46- Type-curve matching plot for Example 7-1. 171
7-47- TDS technique for Example 7-1. 173
7-48- Pressure and pressure derivative plot for Example 7-2. 177
7-49- Type-curve matching plot for Example 7-2. 177
7-50- TDS technique for Example 7-2. 178

ABSTRACT

The oil and gas industry has long recognized the importance of understanding the behaviors and trends of pressure and fluid flow dynamics for damaged and stimulated horizontal wells. It has also been recognized that the existing theories to predict these behaviors and trends have not been effective due to the geologic factors, as well as drilling, completion, and production processes. Previous researches and studies over the last two decades have shown different types of factors such as the presence of multi-damaged zones, multi-segmented fractures, branching, asymmetry, and deviation from either the vertical direction or the horizontal direction of the wellbores as a result of in-situ stress distribution.

The main purpose of this study is to find new applications for the well test analysis rather than the classic applications that are focusing basically on the characterization of formation and determination of the permeability and skin factor. The new applications for the well test analysis are evaluating performance of the zonal isolations and hydraulic fractures and determining the locations of the isolations and fractures that do not perform as designed. Another objective is to investigate pressure behavior and flow regimes of a horizontal well containing either zonal isolations or hydraulic fractures.

The objectives in this study are achieved by using different analytical models. These models have been derived to simulate the pressure responses and flow regimes in the vicinity of the wellbore and the outer boundaries of the formations. Based on the new derived models, different analytical solutions and type-curve matching sets have been developed to characterize formations.

The first part of this study focuses on the impact of the zonal isolations on pressure behaviors and flow regimes of horizontal wells. Horizontal wells with multiple zonal isolations have become a common completion technique in the oil and gas industry. Sand and asphalt production problems, damaged zones and water cresting or gas coning are the main reasons for using isolators to sustain or improve oil and gas recovery. However, the use of such isolators introduces negative effects on the pressure behavior of horizontal wells.

This research introduces new analytical models for studying the effect of this completion technique on pressure behavior of wells with multiple isolated zones. These models have been derived based on the assumption that reservoirs can be divided into multi-subsequent segments of producing and non-producing intervals. Based on the pressure and pressure derivative, the models can be used to estimate the impact of isolators on the pressure behavior. The effects of the number and length of isolators have been investigated for wells having different lengths.

A set of type-curves of dimensionless pressure and pressure derivative versus dimensionless time have been generated for two cases. The first case is for wells in an infinite reservoir having short dimensionless wellbore length and multiple-isolated zones, while the second case concentration on very long wells in an infinite reservoir. These plots can be used to verify the number and length of zonal isolations originally installed, as well as to determine the number and locations of malfunctioning isolators. These plots can also be used to locate segments where sand is produced and intervals of water cresting or gas coning are present.

The main finding is that the pressure of these wells behaves similarly for all cases. The dominant effect of the isolators can be noticed only during the early time flow regimes, i.e. during the early radial or early linear. The behavior of the late time flow regimes, i.e. pseudo radial is not affected by the presence of isolators.

The second part of this study focuses on the pressure behavior and flow regimes that are developed for horizontal wells intersected by multiple-inclined hydraulic fractures. The fractures either fully or partially penetrate the formations. Horizontal wells with multiple hydraulic fractures have become a common occurrence in the oil and gas industry, especially in tight formations. Recent studies have shown that fractures are asymmetric, inclined with respect to the vertical direction and the axis of the wellbore, and partially penetrate the formation in many cases.

This study introduces new analytical models for interpreting the pressure behavior of horizontal wells with multiple hydraulic fractures. The hydraulic fractures in this model could be longitudinal or transverse, vertical or inclined, symmetrical or asymmetrical. The fractures propagate in isotropic or anisotropic formations. In addition, they have different dimensions and different spacing. These models can be solved to calculate various reservoir parameters, including directional permeability, fracture length, skin factors, angle of inclination and penetration ratio.

Type-curve matching technique has been applied using the plots of the pressure and pressure derivative curves. A set of type curves have been generated for the inclined transverse and longitudinal hydraulic fractures associated with horizontal wells having different inclination angles from the vertical and different penetration ratios.

Tiab's Direct Synthesis (TDS) technique has been applied also using the plots of the pressure and pressure derivative curves. Several unique features of the pressure and pressure derivative plots of both longitudinal and transverse fractures models were identified including the points of intersection of straight lines for different flow regimes. These points can be used to verify the results or to calculate unknown parameters. Equations associated with these features were derived and their usefulness was demonstrated in this study.

1- INTRODUCTION AND LITERATURE REVIEW

1-1- ZONAL ISOLATIONS

The use of horizontal wells for producing oil and gas from low-permeability and unconventional reservoirs is now well established within the petroleum industry. The great increase of the surface area of the wellbore that allows fluids to flow freely from the reservoir to the wellbore is the main advantage of the horizontal well. Reducing the effects of the damaged zones and increasing the well deliverability are the direct results of this type of wells. Therefore, over the last two decades the number of horizontal wells that have been drilled worldwide has increased significantly due to the significant improvement in well productivity and ultimate oil and gas recovery. Low-permeability and unconventional reservoirs are not the only common applications for horizontal well technology. It has been used successfully in: (1) Fractured reservoirs to intersect natural fractures and effectively drain the reservoir, (2) Water and gas driven reservoirs to minimize water cresting and gas coning, (3) Both low and high permeability gas reservoirs to reduce the number of producing wells, and (4) Tertiary recovery applications to enhance the contact between the well and the reservoir. In addition, this technique has been applied in offshore reservoirs as well as in environmentally sensitive areas to reduce the cost of drilling and production facilities.

The completion of horizontal wells is of great importance due to its impact on current well deliverability and future reservoir management regarding the effective control of fluid movements from the reservoir drainage area toward the wellbore. An open-hole horizontal well completion may cost less than other types of completion. As a result, it

has been used, especially in the shale gas reservoirs where it has also led to higher production rates (Alison et al, 2009). However, this type of completion leaves the operators with little or no opportunity to perform future diagnostic or remedial work (Rentano and Muhammed, 1999). Many horizontal wells which were completed as open holes have had considerable decline in production in spite of producing for the first few years without significant problems.

Three common types of completion techniques have been used in recent years for horizontal wells instead of open hole: slotted linear, linear with external casing packers, and cemented and perforated casing. Different considerations should be taken into account when deciding what completion type should to be used. The competence of the rock is the first consideration while borehole instability and formation sensitivity is the second. Expected problems such as sand production should also be taken into consideration in addition to the damaged zones that might be produced either from the drilling and completion of the horizontal well itself or from the hydraulic fracturing processes. Water cresting and gas breakthrough are possible problems that may occur later in the life of the well that can lead to decreased productivity.

As a consequence of these potential problems, zonal isolation is perceived as an ideal solution. This approach not only helps the operators in controlling well deliverability and eliminates the negative effects of the damaged zones, sand production intervals, and water and gas coning sectors, but also compartmentalizes the horizontal section and optimizes the fracture treatment. There are several ways to establish the zonal isolations including traditional cement, open-hole hydraulic set packers, and inflatable packers. However, each technique adds complexity whether by adding extra operations process

to complete the installation or by introducing additional mechanical components, which increases the risks associated with the use of the isolators. Even though zonal isolations provide reasonable solutions to many production problems, they also have undesirable effects such as increasing the skin factor by reducing the horizontal section. At the same time they have a significant effect on the pressure response of horizontal wells and the type of flow regimes in the drainage area close to the wellbore.

Unfortunately, there are very few studies concerning the effects either positive or negative that result from the use of the zonal isolations. Robison et al 1993 explained that the use of zonal isolations in highly deviated or horizontal wells is likely to be the preferred solution for the problem of water and gas coning. Frick et al 1995 were the first to study the well testing in horizontal wells with isolated segments. They explained that segmented testing can provide information about the local skin factor. A high local skin factor provides an indication of damaged sections and is a necessary variable for the optimization of the stimulation process. Rentano and Muhammed 1999 suggested that in many cases the open length of the well can be reduced without a substantial decrease in the productivity index over a fully open well by using zonal isolations. East et al 2000 investigated the use of sealants before the primary cementing operation to improve zonal isolations performance for production and injection wells.

Henriksen et al 2005 stated that the integration of open-hole zonal isolation technology contributes to improving reserve recovery. They experimentally investigated the horizontal completions with formation segmentation by installing packers at strategically chosen locations along the wellbore. Kelbie and Garfield 2006 explained that the intermediate zonal isolation for the upper zone can be performed in several

ways. One way is setting a bridge plug below the target interval or deploying an inflatable straddle acidizing packer; thus shutting off gas zones. For the lower zone, different zonal isolation configuration should be used in which the packer is positioned below the perforations that require the isolations. Maddox et al 2008 provided field examples for the use of the zonal isolations in horizontal wells' completion for the hydraulic fracturing process. In these examples five inflatable packer isolation systems were used to create five separate hydraulically fractured zones along the wellbore. Brooks and Steven 2009 also have introduced field examples for well testing procedures for multi-zones open hole completion wells where the hydraulic isolation between zones is achieved by using casing annulus packers rather than cement. They found that the pressure transient test generally showed low mechanical skin and minimal formation damage in all intervals.

Del Rio et al 2011, explained how the using of the temporary zonal isolations minimizes reservoir damage during workover operations in Ecuador. They stated that cross linked polymer system can be spotted across the low pressure and/or highly permeable reservoirs to temporarily isolate and protect them from fluids invasion during the workover operations. This technique has led to increased production in more than fifteen wells. Gomez et al 2011, expressed that the long term zonal isolation is required to correctly exploit the Brazilian ultra deep water well of Santos basin to effectively perform stimulation operations and control water and/or unwanted gas production. They described the methods used to design a salt and CO_2 cement slurry and the laboratory testing performed to meet the cement requirement and the field implementation of the designed zonal isolation for a well in ultra deep waters.

1-2- HYDRAULIC FRACTURES

During the last two decades, horizontal wells have become a common applied completion technology in the petroleum industry. With a large reservoir contact area, horizontal wells can greatly improve well productivity and effectively handle problems with water cresting and gas coning. It is most advantageous to drill horizontal wells in thin and tight reservoirs with vertical fractures. However, there are certain situations, where fracturing a horizontal well is an economically attractive completion option. This is especially true in the case of tight formations. Wells in low to moderate permeability reservoirs that are not naturally fractured may be candidates for hydraulic fracturing.

Fracturing a horizontal well may take place under several scenarios, some of which are listed below:

(1) In low-permeability formations to enhance the drainage volume.

(2) Restricted flow in the vertical direction caused by low vertical permeability or the presence of shale slabs in order to create vertical fractures resulting in enhanced vertical permeability and thus enhanced well productivity.

(3) In a layered reservoir to create vertical fractures along the well length so that different producing layers can be connected at different elevations.

(4) Drilling and completion considerations in cemented horizontal wells may require cementing the wells. Therefore, by creating several fractures along the length of the wellbores, it is possible to achieve at least the same productivity as an open hole horizontal well.

(5) The existence of natural fractures in a direction different from the direction of induced fractures. Therefore, induced fractures will intercept the natural fractures.

Based on the above, hydraulic fracturing is an important stimulation technique that has been widely used in conventional and unconventional oil and gas reservoirs all over the world. The technique involves creation of fracture or fracture system in porous medium to overcome wellbore damage, to improve oil and gas productivity in low permeability reservoirs or to increase production in secondary recovery operations. Depending on the stresses' orientation relative to the wellbore, the fractures may be transverse or longitudinal, vertical or inclined.

For hydraulically fractured horizontal wells, transient well testing is commonly used to determine reservoir parameters and to estimate well productivity. One of the big challenges is the three dimensions' nature of flow geometry in the formations. The radial flow symmetry no longer exists. Instead, several flow regimes may occur in and around the fractures. These flow regimes generally can't be defined very well based on the test data. Moreover, many factors, such as vertical permeability or the vertical anisotropy, inclination angle from the vertical direction, the spacing between fractures, and the penetration ratio (the ratio of the fracture's height to the formation's height) can affect the transient pressure behavior.

Most of the pressure transient analysis techniques of fractured wells are derived based on many assumptions such as;

(1) Homogeneous reservoirs with constant thickness.

(2) Darcy's law is applicable.

(3) Gravitational and fractional effects are negligible.

(4) Isothermal flow.

(5) Single phase flow.

(6) Constant porosity, viscosity and compressibility.

Howard and fast 1970, defined hydraulic fracturing as a process of establishing a fracture or fracture system in a formation by injecting a fracturing fluid (usually water and sand) under high pressure in order to overcome local stresses and to cause breaking the porous medium. In general, for an isotropic medium, the over-all plane of a hydraulic fracture is parallel, inclined, or perpendicular to the axis of the borehole from which it is extending. Accordingly, these fractures will be called axial, inclined or normal respectively (often termed vertical, inclined or horizontal in the petroleum industry) (Daneshy, 1973).

Since 1972, several attempts have been done to model the pressure transient behavior for either horizontal or vertical wells, with or without hydraulic fractures. All these attempts were developed based on the using of the source solution and Green's function to solve unsteady-state flow problems in the reservoir which was presented by Gringarten and Ramey (1973). They used the source function and Newman product method for solving transient flow problems. Although this approach is extremely powerful in solving two and three dimensions' problem, it has some limitations such as incorporating the influence of storage and skin effects. The transient flow solutions have been extended to predict the behavior of the infinite conductivity vertical fracture in homogenous formations or in dual-porosity media. Cinco-Ley et al (1974, 1975) solved the problem for uniform flux and infinite conductivity inclined fracture in infinite slab reservoirs. They developed analytical models for the pressure behavior at the wellbore for a slanted hole and an inclined fracture associated with vertical wells. Cinco-Ley and Samaniego-V (1981) presented a method for the determination of the

orientation of a fully penetrating vertical fracture by means of analysis of transient pressure data recorded at one active well and two observation wells due to production or injection at the active fractured well.

Barker et al (1978) used a finite element model to study pressure behavior of a well intersecting a vertical fracture at the center of closed square reservoirs. Rodriguez and Cinco-Ley (1984) developed semi-analytical solution for the transient flow behavior of a reservoir with a well intersecting a partially-penetrating vertical fracture of finite conductivity. The results of this study explained that the flow behavior of partially penetrating fractures during the early time period is equivalent to that of totally penetrating fractures. Wong and Harrington (1985) analyzed the data using type curve matching and pressure and pressure derivative for cases of vertical fractured wells with no skin and no wellbore storage and cases with both skin and wellbore storage during the bi-linear flow period. Cinco-Ley and Meng (1988) studied the results obtained from the transient behavior of a well intersected by a vertical fracture in a double porosity reservoir. They introduced two models; the first one was a general semi-analytical and the second one was a simplified fully analytical model. Ozkan (1988) presented a complete set of different solutions for diffusivity equation in terms of the Laplace transform variable. He considered a wide variety of wellbore configurations, different bounded systems, and homogeneous or double-porosity reservoirs.

Early techniques for interpreting pressure transient tests included conventional semi-log and log-log type curve methods. In these techniques, flow regimes of reservoir's fluid must be observed in the pressure and pressure derivative curves over a sufficient period of time. If they not present, type curve matching will not be

sufficiently used. In multiple hydraulically fractured horizontal wells, different flow regimes are possible, but almost never observed from the pressure data. Therefore, it is important to use an alternative method known as "TDS-Tiab's Direct Synthesis Technique" introduced by Tiab in (1988) for hydraulically fractured wells with multiple fractures.

Olarewaju and Lee (1989) presented an analytical solution for pressure transient tests from layered reservoirs with or without cross flow. They noticed that the pressure behavior of a well in a two-layer reservoir with unsteady state interlayers' cross flow is identical to that of a commingled system. Rodriguez et al (1992) introduced a graphical technique to evaluate the asymmetry of hydraulically fractured wells. The technique was derived from an analytical solution for the pressure response of the wells during the pseudolinear flow period and the known bilinear flow solution.

Tiab (1993) applied the direct synthesis technique (TDS) to uniform flux, infinite conductivity and finite conductivity vertically fractured wells. This study extends the method to hydraulically fractured horizontal wells. The cases of uniform flux, infinite conductivity and finite conductivity models are considered.

Poe and Elbel (1994) suggested an analytical solution for the pressure transient behavior of a well intersected by a vertical fracture in infinite acting reservoirs or in cylindrical or rectangular bounded finite reservoirs. This solution included the practical effects of reservoir permeability, anisotropy and dual porosity behavior. Leif and Hegre (1994) provided a comprehensive investigation of the pressure transient behavior of horizontal wells with single or multiple vertical fractures, either longitudinal or transverse. Four flow regimes have been observed in their study; fracture radial, radial-

linear, formation linear, and pseudo-radial flow. Kuchuk and Habusky (1994) examined the pressure response of horizontal wells with single and multiple fractures in homogenous systems. They showed that the effect of the wellbore can't be neglected in the modeling unless the fracture conductivity is high.

Wright and Conant (1995) provided field examples where the hydraulic fractures reoriented due to production. Inclined fractures reorientation led to new inclination angles after refracturing. They introduced examples from Chevron Lost Hills field where the inclination angle has changed from 82 degrees to 45 degrees. This was the result of the production depletion between two fracturing treatments. This is clear evidence that production activities can affect the in-situ stress state and thus change the direction of principle stresses. Valko and Economides (1996) developed rigorous semi-analytical procedures for the purpose of modeling a horizontal well with a longitudinal vertical fracture. Raghavan (1997) developed a mathematical model to discern the characteristic response of multiply-fractured horizontal wells. Three significant flow periods have been observed based on their model; the early time period in which the system behaved like the one with n-layers, the intermediate time period in which the system reflected the interference between fractures and the late time period in which the system behaved as a single fractured horizontal well with length equal the distance between the outermost fractures.

Wright et al (1998) provided a number of case studies where surface tiltmeter arrays were used for fracture mapping. The results obtained from data of over (2000) fracture treatments using tiltmeters revealed that fractures are almost never perfectly vertical. Quite often they dip 5 to 15 degrees from the vertical and very few fractures

dip less than two degrees off vertical. In their study, they showed that "horizontal" fractures dipping less than 35 degrees with respect to the horizontal plane are not as rare as commonly known. Another conclusion from the study is fracture azimuth and dip may be very different locally across a field as the local stress field may be changed by location on the structure or with respect to local faults. Hydrocarbon production, steam and water injection and infill drilling in mature primary and secondary recovery reservoirs may alter the local stress field and thus affect the fracture orientation.

Wan and Aziz (1999) developed a general solution for horizontal wells with multiple fractures. They showed that four flow regimes can be observed; the early linear, transient, late linear, and late time radial flow. Zerzar and Bettam (2003) combined the boundary element method and Laplace transformation to present a comprehensive solution for horizontal wells with multiple vertical fractures. Seven flow regimes have been noticed; bilinear, first linear, elliptical, radial, pseudo-radial, second linear, and pseudo-steady state. Al-Kobaisi and Ozkan (2004) presented a hybrid numerical-analytical model for the pressure transient response of horizontal wells intercepted by a vertical fracture.

Dinh and Tiab (2009a,b) solved the analytical model presented by Cinco-Ley (1974) for the pressure transient behavior caused by an inclined fracture associated with vertical wellbore. The model used the uniform flux and infinite conductivity fracture solution for different inclination angles from the vertical direction. Both type curve and TDS technique have been used to estimate the formation parameters such as permeability, skin factor, and fracture length. Brown et al (2009) suggested an analytical trilinear flow solution to simulate the pressure transient and production

behavior of fractured horizontal wells in unconventional reservoirs. This model can be used to estimate petrophysical characteristics such as intrinsic properties of the matrix and the fracture.

All the definitions of symbols are given in the nomenclatures at the end of the dissertation text body.

2- MATHEMATICAL MODELS FOR HORIZONTAL WELLS WITH ZONAL ISOLATIONS

The primary goal of this chapter is to introduce various analytical models for the pressure behaviors and flow regimes of horizontal wells containing multiple zonal isolations. Four analytical models will be introduced in this chapter, two for short horizontal wells having dimensionless wellbore length -the ratio of the wellbore length and formation height- (L_D<20) and two for long horizontal wells having dimensionless wellbore length (L_D>20). Two different configurations for the two above cases of horizontal wells will be investigated. The first one is for horizontal wells headed by a zonal isolation while the second is for wells headed by a perforated zone. The following assumptions are important for the derivation of the models:

1- The reservoir is homogenous, having constant and uniform thickness with two impermeable layers at the top and bottom of the formation.
2- There is constant porosity and permeability in each direction, but the formation is anisotropic.
3- Gravitational and frictional effects are negligible.
4- The well is extending in the midpoint of the formation height (symmetrical).
5- Single phase fluid of small and constant compressibility, constant viscosity, and formation volume factor, flows from the reservoir to the wellbore.

For general purpose, the following facts are important to be mentioned:

1- Reservoir pressure is initially constant.

$$P\big|_{t=0} = P_i \tag{2-1}$$

2- The pressure at the outer boundaries of the reservoir is assumed to be constant and equal to the initial reservoir pressure.

$$P_e = P_i \tag{2-2}$$

3- The pressure at the upper and lower impermeable boundaries is assumed to be constant so that:

$$\left.\frac{\partial P}{\partial Z}\right|_{Z=0} = 0 \tag{2-3}$$

$$\left.\frac{\partial P}{\partial Z}\right|_{Z=h} = 0 \tag{2-4}$$

Fortunately, the effects of the zonal isolations on the pressure behavior of the horizontal wells can be investigated using the solution of the diffusivity equation. In this case the well can be considered as multiple-horizontal segments of production intervals separated by zonal isolations. In addition, the pressure drop at a certain point in the reservoir is considered resulting from the production from each production point. Therefore, the pressure drop at this point is equal to the sum of the pressure drop resulting from the production from each production interval.

Based on the above, the solution for the diffusivity equation can be used for this purpose using one of the techniques that are applicable for the transient flow of fluid in porous media. Gringarten and Ramey (1973) initially introduced the use of the source and Green's function in solving unsteady state flow problems in a reservoir. They stated that the infinite line source can be visualized as the intersection of two perpendicular infinite plane sources normal to two of the three principal axes of permeability while the point source can be visualized as the intersection of three perpendicular infinite plane

sources normal to the principal axes of permeability. Ozkan (1988) introduced new source solutions to the diffusivity equation using the Laplace space to overcome the difficulties that might result when the Gringarten and Ramey's source solution is applied in complex geometrical configurations such as dual porosity and dual permeability porous media.

2-1- Short horizontal well headed by a zonal isolation:

"Short horizontal well" in this study refers to a horizontal well having a ratio of wellbore length to the height of formation (L_D<20). Consider a horizontal well, such as in Fig. (2-1), producing slightly compressible petroleum fluids from an infinite-acting reservoir at a constant rate. The horizontal well consists of two altered sections; one is the producing interval and the other is the zone isolator.

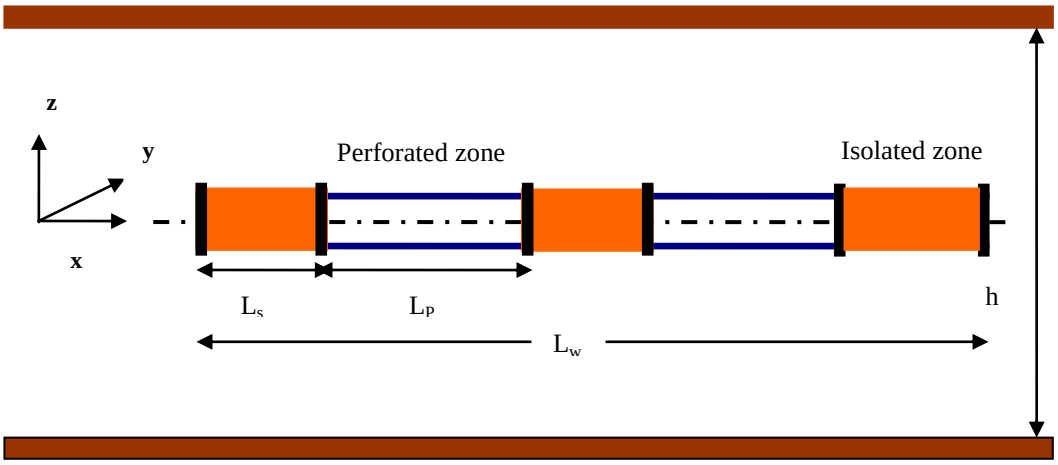

Figure 2-1: Horizontal well headed by zonal isolation.

The mathematical model that can be used to simulate the effects of the zonal isolations on the pressure behavior is created based on an assumption of constant production rate. The horizontal well is assumed having a known length (L_w), multiple-perforation intervals of equal length (L_P) separated by multiple-zonal isolations of

equal length (L_s), and extending in the midpoint of an infinite formation having a known height (h). The model can be derived as follow:

Assume equal and constant flow rate from the perforation intervals:

$$q_i = \frac{q_t}{nL_P} \tag{2-5}$$

where n is the number of the producing intervals.

The pressure drop at any point in the reservoir is:

$$\Delta P_t = \sum \Delta P_i \tag{2-6}$$

Using the instantaneous source functions for the pressure distribution in porous media which results from production process, the pressure behavior can be found as:

$$\Delta P_t = \frac{q}{\phi c_t}\int S(x,t)\times S(y,t)\times S(z,t)dt = \frac{q}{\phi c_t}\int \left(\frac{1}{2\sqrt{\pi\eta_x t}}e^{-\frac{d_x^{\,2}}{4\eta_x t}}\right)\times \left(\frac{1}{2\sqrt{\pi\eta_y t}}e^{-\frac{d_y^{\,2}}{4\eta_y t}}\right)\times\left(\frac{1}{2\sqrt{\pi\eta_y t}}e^{-\frac{d_z^{\,2}}{4\eta_z t}}\right)dt \tag{2-7}$$

where:

d_x , d_y , d_z = Distances between the source point and the monitoring point in the X, Y and Z direction.

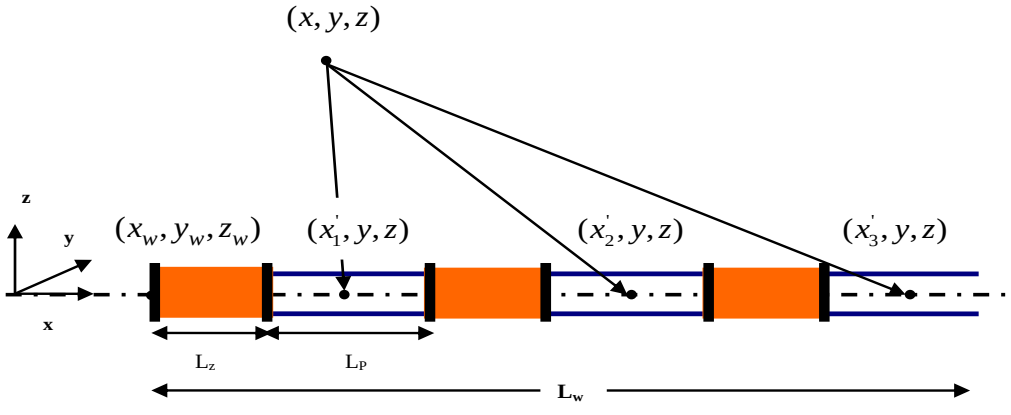

Figure 2-2: The monitoring point and the sources of production for a horizontal well.

It is clear that the pressure drop, represented in Eq. (2-7), consists of three instantaneous source functions which are S(x, t), S(y, t), and S(z, t). S(x, t) represents the infinite slab source in an infinite reservoir and S(y, t) represents the infinite plane source in an infinite reservoir while S(z, t) represents the infinite plane source in an infinite slab reservoir.

Applying Eq. (2-7) to the case of the horizontal well shown in Fig. (2-2):

$$\Delta P_t(x,y,z,t)=\frac{q_i}{8\phi c_t(\pi t)^{3/2}\sqrt{\eta_x\eta_y\eta_z}}\left[\begin{array}{l} e^{-\left[\frac{(x-x_1')^2}{4\eta_x t}+\frac{(y-y_1')^2}{4\eta_y t}+\frac{(z-z_1')^2}{4\eta_z t}\right]}+ \\ e^{-\left[\frac{(x-x_2')^2}{4\eta_x t}+\frac{(y-y_2')^2}{4\eta_y t}+\frac{(z-z_2')^2}{4\eta_z t}\right]}+ \\ e^{-\left[\frac{(x-x_3')^2}{4\eta_x t}+\frac{(y-y_3')^2}{4\eta_y t}+\frac{(z-z_3')^2}{4\eta_z t}\right]} \end{array}\right] \quad (2\text{-}8)$$

Since the horizontal well is extending along the (x) direction and both (y) and (z) are the same for all points along the wellbore of the well, Eq. (2-8) can be written as:

$$\Delta P_t(x,y,z,t)=\frac{q_i}{8\phi c_t(\pi)^{3/2}\sqrt{\eta_x\eta_y\eta_z}}\int_0^t\frac{1}{t^{3/2}}\left[e^{-\left[\frac{(y-y')^2}{4\eta_y t}+\frac{(z-z')^2}{4\eta_z t}\right]}\right]\times\left\{\int_{(x_w+L_s)}^{(x_w+L_s+L_p)}e^{-\frac{(x-x_1')^2}{4\eta_y t}}dx_1'\right.$$

$$\left.+\int_{(x_w+2L_s+L_p)}^{(x_w+2L_s+2L_p)}e^{-\frac{(x-x_2')^2}{4\eta_y t}}dx_2'+\int_{(x_w+3L_s+2L_p)}^{(x_w+3L_s+3L_p)}e^{-\frac{(x-x_3')^2}{4\eta_z t}}dx_3'\right\}dt \quad (2\text{-}9)$$

Assume:

$$u=\frac{x-x_1'}{2\sqrt{\eta_x t}}\Rightarrow dx_1'=-2\sqrt{\eta_x t} \quad (2\text{-}10)$$

$$v=\frac{x-x_2'}{2\sqrt{\eta_x t}}\Rightarrow dx_2'=-2\sqrt{\eta_x t} \quad (2\text{-}11)$$

$$w=\frac{x-x_3^{'}}{2\sqrt{\eta_x t}}\Rightarrow dx_3^{'}=-2\sqrt{\eta_x t} \tag{2-12}$$

Eq. (2-9) can be written as:

$$\Delta P_t(x,y,z,t)=\frac{q_i}{8\phi c_t(\pi)^{3/2}\sqrt{\eta_x\eta_y\eta_z}}\int_0^t\frac{1}{t^{3/2}}\left[e^{-\left[\frac{(y-y')^2}{4\eta_y t}+\frac{(z-z')^2}{4\eta_z t}\right]}\right]\times\left\{\int_{\frac{x-(x_w+L_s)}{2\sqrt{\eta_x t}}}^{\frac{x-(x_w+L_s+L_p)}{2\sqrt{\eta_x t}}}e^{-u^2}du+\int_{\frac{x-(x_w+2L_s+L_p)}{2\sqrt{\eta_x t}}}^{\frac{x-(x_w+2L_s+2L_p)}{2\sqrt{\eta_x t}}}e^{-v^2}dv+\int_{\frac{x-(x_w+3L_s+2L_p)}{2\sqrt{\eta_x t}}}^{\frac{x-(x_w+3L_s+3L_p)}{2\sqrt{\eta_x t}}}e^{-w^2}dw\right\}dt \tag{2-13}$$

Integrating for u, v, and w using the error function features, Eq. (2-13) becomes:

$$\Delta P_t(x,y,z,t)=\frac{q_i}{8\phi c_t\pi\sqrt{\eta_y\eta_z}}\int_0^t\frac{1}{t}\left[e^{-\left[\frac{(y-y')^2}{4\eta_y t}+\frac{(z-z')^2}{4\eta_z t}\right]}\right]\times\sum_{n=1}^{n=\infty}\left[erf\left(\frac{(x-x_w)-nL_s-(n-1)L_p}{2\sqrt{\eta_x t}}\right)-erf\left(\frac{x-x_w-n(L_s+L_p)}{2\sqrt{\eta_x t}}\right)\right]dt \tag{2-14}$$

To reflect the effect of the top and bottom impermeable layers on the pressure behavior of the horizontal well, superposition theory should be applied:

$$e^{-\frac{(z-z_1^{'})^2}{4\eta_z t}}=e^{-\frac{(z-z_w)^2}{4\eta_z t}}+e^{-\frac{(z+z_w)^2}{4\eta_z t}}+\sum_{N=1}^{N=\infty}\left[e^{-\frac{(z-z_w+2Nh)^2}{4\eta_z t}}+e^{-\frac{(z-z_w-2Nh)^2}{4\eta_z t}}\right]+\sum_{N=1}^{N=\infty}\left[e^{-\frac{(z+z_w+2Nh)^2}{4\eta_z t}}+e^{-\frac{(z+z_w-2Nh)^2}{4\eta_z t}}\right] \tag{2-15}$$

Eq. (2-15) can be rearranged in the following form:

$$e^{-\frac{(z-z_1^{'})^2}{4\eta_z t}}=\sum_{N=-\infty}^{N=\infty}\left[e^{-\frac{(z-z_w+2Nh)^2}{4\eta_z t}}+e^{-\frac{(z-z_w-2Nh)^2}{4\eta_z t}}\right] \tag{2-16}$$

Substitute Eq. (2-16) on Eq. (2-14):

$$\Delta P_t(x,y,z,t)=\frac{q_i}{8\phi c_t\pi\sqrt{\eta_y\eta_z}}\int_0^t\frac{e^{-\left[\frac{(y-y_w)^2}{4\eta_y t}\right]}}{t}\left\{\sum_{n=1}^{n=\infty}erf\left(\frac{(x-x_w)-nL_s-(n-1)L_p}{2\sqrt{\eta_x t}}\right)-\right.$$

$$\left.erf\left(\frac{x-x_w-n(L_s+L_p)}{2\sqrt{\eta_x t}}\right)\right\}\times\sum_{N=-\infty}^{N=\infty}\left[e^{-\frac{(z-z_w+2Nh)^2}{4\eta_z t}}+e^{-\frac{(z-z_w-2Nh)^2}{4\eta_z t}}\right]dt \qquad (2\text{-}17)$$

Applying Poisson's summation formula, Eq. (2-17) can be written as:

$$\Delta P_t(x,y,z,t)=\frac{q_i}{4\phi c_t\pi^{1/2}h\sqrt{\eta_z}}\int_0^t\frac{e^{-\left[\frac{(y-y_w)^2}{4\eta_y\tau}\right]}}{\sqrt{\tau}}\left\{\sum_{n=1}^{n=\infty}erf\left(\frac{(x-x_w)-nL_s-(n-1)L_p}{2\sqrt{\eta_x\tau}}\right)-\right.$$

$$\left.erf\left(\frac{x-x_w-n(L_s+L_p)}{2\sqrt{\eta_x\tau}}\right)\right\}\times\left[1+2\sum_{N=1}^{N=\infty}e^{-\frac{N^2\pi^2\eta_z\tau}{h^2}}\cos\left(N\pi\frac{z}{h}\right)\cos\left(N\pi\frac{z_w}{h}\right)\right]d\tau \qquad (2\text{-}18)$$

In dimensionless form, Eq. (2-18) becomes:

$$P_D(x_D,y_D,z_D,t_D)=\frac{\sqrt{\pi}}{2nL_{pD}}\int_0^{t_D}\frac{e^{-\frac{y_D^2}{4t_D}}}{\sqrt{\tau_D}}\left[\sum_{n=1}^{n=\infty}\left[erf\left(\frac{x_D-nL_{sD}-(n-1)L_{pD}}{2\sqrt{\tau_D}}\right)+erf\left(\frac{x_D-n(L_{sD}+L_{pD})}{2\sqrt{\tau_D}}\right)\right]\right]\times$$

$$\left[1+2\sum_{N=1}^{N=\infty}e^{\left(-N^2\pi^2L_D^2\tau_D\right)}\cos(N\pi z_{wD})\cos\left(N\pi(z_D+z_{wD})\right)\right]d\tau_D \qquad (2\text{-}19)$$

Where the dimensionless parameters in the above model are defined as follow:

$$x_D=\frac{x-x_w}{L_w} \qquad (2\text{-}20)$$

$$y_D=\frac{y-y_w}{L_w}\sqrt{\frac{k_x}{k_y}}=\frac{r_w}{L_w}\sqrt{\frac{k_x}{k_y}} \qquad (2\text{-}21)$$

$$z_D=\frac{z-z_w}{L_w}\sqrt{\frac{k_x}{k_z}} \qquad (2\text{-}22)$$

$$z_{wD} = \frac{z_w}{h} \tag{2-23}$$

$$\bar{z_D} = \frac{z - z_w}{h} = z_D L_D \tag{2-24}$$

$$L_D = \frac{L_w}{h}\sqrt{\frac{k_z}{k_x}} \tag{2-25}$$

$$L_{sD} = \frac{L_s}{L_w} \tag{2-26}$$

$$L_{pD} = \frac{L_p}{L_w} \tag{2-27}$$

$$t_D = \frac{k_x t}{\phi \mu c_t L_w^2} = \frac{\eta_x t}{L_w^2} \quad \text{where:} \quad \eta_x = \frac{k_x}{\phi \mu c_t} \tag{2-28}$$

$$P_D(x_D, y_D, z_D, t_D) = \frac{2\pi\sqrt{k_x k_y}\, h \Delta P_t(x, y, z, t)}{q_t \mu} \tag{2-29}$$

To solve the model given by Eq. (2-19), two approximations should be done for the three functions based on the fluid flow dynamic and flow regimes in the early and late time.

2-1-1- Early time approximation

This approximation is very important since the major effects of the zonal isolations are expected to happen at the flow regimes which are developed in the areas nearby the wellbore. These flow regimes usually are the early radial and to some extent the early linear flow when the top and bottom impermeable layers are reached. Therefore the short-time approximation can be obtained by considering the first term in Eq. (2-7) using dimensionless form as:

$$S(x_D, t_D) = \frac{1}{2\sqrt{\pi \eta_x t}} e^{-\frac{(x-x')^2}{4\eta_x t}} = \frac{1}{2} \tag{2-30}$$

The proper time limit for the above equation to be applied as determined by Gringarten and Ramey (1973) is:

$$t_D \leq \left[\frac{\left[x_D - nL_{sD} - (n-1)L_{pD}\right]^2}{20} \quad \frac{\left[x_D - n(L_{sD} + L_{pD})\right]^2}{20} \right] \tag{2-31}$$

The second term of Eq. (2-7), the instantaneous function S(y, t), remains as it is. Therefore its formula for the short time approximation using the dimensionless units is:

$$S(y_D, t_D) = \frac{1}{2\sqrt{\pi \eta_y t}} e^{-\frac{(y-y_w)}{4\eta_y t}} = \frac{1}{2\sqrt{\pi t_D} L_w} \sqrt{\frac{\eta_x}{\eta_y}} e^{-\frac{y_D^2}{4t_D}} \tag{2-32}$$

And the proper time for this approximation to be applicable is:

$$t_D = \frac{y_D^{\ 2}}{20} \tag{2-33}$$

The third term in Eq. (2-7) which represents the effect of the upper and lower boundaries also remains unchanged and the early time approximation of this term using dimensionless units is:

$$S(z_D, t_D) = \frac{1}{2\sqrt{\pi \eta_z t}} e^{-\frac{(z-z_w)^2}{4\eta_x t}} = \frac{1}{2\sqrt{\pi t_D} L_w} \sqrt{\frac{k_x}{k_z}} e^{-\frac{z_D^2}{4t_D}} \tag{2-34}$$

The proper time for this approximation to be applicable is:

$$t_D \leq \min \left[\frac{\left[\left(z_D^- + 2z_{wD}\right) / L_D\right]^2}{20} \quad \frac{\left[\left(z_D^- + 2z_{wD} - 2\right) / L_D\right]^2}{20} \right] \tag{2-35}$$

Based on the above approximations, Eq. (2-19) can be written as:

$$P_D(x_D, y_D, z_D, t_D) = \frac{1}{4nL_{pD}L_D}\int_0^{t_D}\frac{1}{\tau_D}e^{-\frac{\left[y_D^2+z_D^2\right]}{4\tau_D}}d\tau_D = -\frac{1}{4nLpDL_D}Ei\left(-\frac{y_D^2+z_D^2}{4t_D}\right)$$
$$= \frac{1}{4nL_{pD}L_D}\left(\ln\left(\frac{t_D}{y_D^2+z_D^2}\right)+0.80907\right) when Ei\left(-\frac{y_D^2+z_D^2}{4t_D}\right) \le 0.01 \quad (2\text{-}36)$$

2-1-2- Late time approximation

At late time, the pressure behaviors and flow regimes begin to be affected by the conditions at the outer boundary. Therefore, the long time approximation of Eq. (2-7) takes this fact into consideration. The first instantaneous function that represents the infinite slab source in an infinite reservoir is approximated as follows:

$$S(x_D, t_D) = \frac{1}{2\sqrt{\pi\eta_x t}}e^{-\frac{(x-x')^2}{4\eta_x t}} = \frac{L_{pD}}{2\sqrt{\pi t_D}} \quad (2\text{-}37)$$

and the starting time is:

$$t_D = \begin{bmatrix} \frac{25}{3}\left[xD - nLsD - (n-1)LpD\right]^2 \\ \frac{25}{3}\left[xD - n(LsD + LpD)\right]^2 \end{bmatrix} \quad (2\text{-}38)$$

The approximation for the second term and the time limit are:

$$S(y_D, t_D) = \frac{1}{2\sqrt{\pi\eta_y t}}e^{-\frac{(y-y')^2}{4\eta_y t}} = \frac{1}{2\sqrt{\pi t_D}L_w}\sqrt{\frac{k_x}{k_y}} \quad (2\text{-}39)$$

$$t_D = 25y_D^{\ 2} \quad (2\text{-}40)$$

The approximation and the time limit for the third term are:

$$S(Z_D, t_D) = \frac{1}{2\sqrt{\pi\eta_z t}}e^{-\frac{(z-z')^2}{4\eta_z t}} = \frac{1}{h} \quad (2\text{-}41)$$

$$t_D = \frac{5}{\pi^2 L_D^2} \quad (2\text{-}42)$$

Therefore the late time approximation of Eq. (2-19) can be written as follow:

$$P_D(x_D,y_D,z_D,t_D)=\frac{q_t}{nL_p\phi\mu}\left[\begin{array}{l}\int_0^{t_{D1}}\frac{1}{2\sqrt{\pi\eta_x t}}e^{-\frac{(x-x')^2}{4\eta_x t}}\times\frac{1}{2\sqrt{\pi\eta_y t}}e^{-\frac{(y-y')^2}{4\eta_y t}}\times\frac{1}{2\sqrt{\pi\eta_z t}}e^{-\frac{(z-z')^2}{4\eta_z t}}d\tau_D\\ +\frac{1}{2}\int_{t_{D1}}^{t_D}\frac{1}{\tau_D}d\tau_D\end{array}\right] \quad (2\text{-}43)$$

$$=P_D(x_D,y_D,z_D,t_{D1})+\frac{1}{2}\ln(\frac{t_D}{t_{D1}})$$

Where:

$$t_{D1}\geq Max\left[\begin{array}{l}\frac{25}{3}\left[x_D-nL_{sD}-(n-1)L_{pD}\right]^2\\ \frac{25}{3}\left[x_D-n(L_{sD}+L_{pD})\right]^2\\ 25y_D^2\\ \frac{5}{\pi^2L_D^2}\end{array}\right] \quad (2\text{-}44)$$

2-2- Long horizontal wells headed by a zonal isolation

"Long horizontal well" in this study refers to horizontal wells having a ratio of wellbore length to the height of formation (L_D>20) [L_D >50 (Spivak 1988), L_D >10 (Joshi 1991)]. The only difference between short and long horizontal wells is the early time flow regime that is expected to develop. Spivak (1988) explained that the long horizontal well behaves similarly to the vertical hydraulic fractures where the first flow regime that is expected to develop is the early linear flow while the first flow regime for short horizontal well is the early radial flow. Therefore the early time approximation for long horizontal wells will not be the same as for short horizontal wells.

For long horizontal wells, pressure behaviors and flow regimes of horizontal wells become exactly the same behavior as vertical hydraulic fracture. This fact is related to

the function of the infinite plane source in an infinite slab reservoir which is converging to:

$$S(z_D,t_D)=\frac{e^{-\frac{(z-z')^2}{4n_z t}}}{2\sqrt{\pi n_z t}}=\frac{1}{h} \tag{2-45}$$

Therefore the model for long horizontal wells can be modified from Eq. (2-7) as follows:

$$\Delta P_t=\frac{1}{8\phi c_t(\pi t)^{3/2}\sqrt{\eta}}e^{-d^2/4\eta t}=\frac{q_i}{\phi c_t}\int\left[\frac{e^{-\frac{(x-x')^2}{4\eta_x t}}}{2\sqrt{\eta_x \pi t}}\right]\times\left[\frac{e^{-\frac{(y-y')^2}{4\eta_y t}}}{2\sqrt{\eta_y \pi t}}\right]\times\left[\frac{1}{h}\right]dt \tag{2-46}$$

Following the same steps for the instantaneous function of an infinite slab source in an infinite reservoir S(x, t) and the instantaneous function of an infinite plane source in an infinite slab reservoir S(z, t) for short horizontal wells. The dimensionless model for pressure distribution of long horizontal wells extending in porous media can be written as:

$$P_D(x_D,y_D,z_D,z_{wD},L_D,t_D)=\frac{\sqrt{\pi}}{2nL_{pD}}\int_0^{t_D}\frac{e^{-\frac{y_D^2}{4t_D}}}{\sqrt{\tau_D}}\left[erf\left(\frac{1-nL_{sD}-(n-1)L_{pD}}{2\sqrt{\tau_D}}\right)+erf\left(\frac{1-n(L_{sD}+L_{pD})}{2\sqrt{\tau_D}}\right)\right]d\tau_D \tag{2-47}$$

2-2-1- Early time approximation

The short-time approximation for the instantaneous function S(x, t) can be obtained by considering:

$$S(x_D,t_D)=\frac{1}{2\sqrt{\pi\eta_x t}}e^{-\frac{(x-x')^2}{4\eta_x t}}=\frac{1}{2} \tag{2-48}$$

The proper time limit for the above equation to be applied as determined by Gringarten and Ramey (1973) is:

$$t_D \le \left[\begin{array}{c} \frac{\left[x_D - nL_{sD} - (n-1)L_{pD}\right]^2}{20} \\ \frac{\left[x_{_D} - n(L_{sD} + L_{pD})\right]^2}{20} \end{array} \right] \tag{2-49}$$

The second term, the instantaneous function S(y, t), remains as it is. Therefore, its formula for the short time approximation as follows:

$$S(y_D, t_D) = \frac{1}{2\sqrt{\pi \eta_y t}} e^{-\frac{(y-y_w)}{4\eta_y t}} = \frac{1}{2\sqrt{\pi t_D} L_w} \sqrt{\frac{\eta_x}{\eta_y}} e^{-\frac{y_D^2}{4t_D}} \tag{2-50}$$

The proper time for this approximation to be applicable is:

$$t_D = \frac{y_D^{\ 2}}{20} \tag{2-51}$$

The approximation and the time limit for the third instantaneous function S(z, t) are:

$$S(Z_D, t_D) = \frac{1}{2\sqrt{\pi \eta_z t}} e^{-\frac{(z-z')^2}{4\eta_z t}} = \frac{1}{h} \tag{2-52}$$

$$t_D = \frac{5}{\pi^2 L_D^2} \tag{2- 53}$$

Therefore, the short time approximation for Eq. (2-47) can be written as:

$$P_D(x_D, y_D, z_D, z_{wD}, L_D, t_D) = \sqrt{\pi t_D} e^{-\frac{y_D^2}{4t_D}} - \frac{\pi y_D}{2} erfc\left(\frac{y_D}{2\sqrt{t_D}}\right) \tag{2-54}$$

Assuming that $y_{_D} = 0$ and solving for the pressure at the wellbore:

$$P_{wD} = \frac{\sqrt{\pi t_D}}{2nL_{pD}} \tag{2-55}$$

It can be seen from Eq. (2-55) that early time approximation for long horizontal wells yields linear flow regimes similar to the early time approximation of vertical hydraulic fracture. For this time period the pressure behavior is linearly proportional

with time on log-log plots of dimensionless wellbore pressure and dimensionless time. The slope of the line is (0.5).

2-2-2- Late time approximation

Late time approximation does not change with the change of the wellbore length. The late time approximation for long horizontal wells is the same for short ones. Therefore, Eqs. (2-37) through (2-44) are applicable for long horizontal wells.

2-3- Short horizontal well headed by a perforated zone

The same concepts that have been used to derive the mathematical model for the pressure distribution of horizontal wells headed by zonal isolation can be used to derive the pressure distribution model for wells headed by perforated zone such as in Fig. (2-3). The only difference is the instantaneous function of infinite slab source in an infinite reservoir S(x, t). The limits of integration for this function should be changed based on the locations of the perforated zones. Therefore, the mathematical model for short horizontal wells headed by perforated zone is:

$$P_D(x_D,y_D,z_D,t_D)=\frac{\sqrt{\pi}}{2nL_{pD}}\int_0^{t_D}\frac{e^{-\frac{y_D^2}{4t_D}}}{\sqrt{\tau_D}}\left[\sum_{n=1}^{n=\infty}\left[erf(\frac{x_D-(n-1)(L_{pD}+L_{sD})}{2\sqrt{\tau_D}})+erf(\frac{x_D-nL_{pD}-(n-1)L_{sD}}{2\sqrt{\tau_D}})\right]\right]\times$$
$$\left[1+2\sum_{N=1}^{N=\infty}e^{\left(-N^2\pi^2L_D^2\tau_D\right)}\cos(N\pi z_{wD})\cos\left(N\pi(z_D^{-}+z_{wD})\right)\right]d\tau_D \qquad (2\text{-}56)$$

Early and late time approximations will be the same as the horizontal wells headed by zonal isolation except that Eqs (2-31), (2-38), and (2-44) should be written as follow:

$$t_D\le\left[\frac{\left[x_D-nL_{pD}-(n-1)L_{sD}\right]^2}{20}\right] \qquad (2\text{-}57)$$
$$\left[\frac{\left[x_D-(n-1)(L_{sD}+L_{pD})\right]^2}{20}\right]$$

$$t_D = \begin{bmatrix} \frac{25}{3}\left[xD - nLpD - (n-1)LsD\right]^2 \\ \frac{25}{3}\left[xD - (n-1)(LsD + LpD)\right]^2 \end{bmatrix} \tag{2-58}$$

$$t_{D1} \geq Max \begin{bmatrix} \frac{25}{3}\left[x_D - nL_{pD} - (n-1)L_{sD}\right]^2 \\ \frac{25}{3}\left[x_D - (n-1)(L_{sD} + L_{pD})\right]^2 \\ 25y_D^2 \\ \frac{5}{\pi^2 L_D^2} \end{bmatrix} \tag{2-59}$$

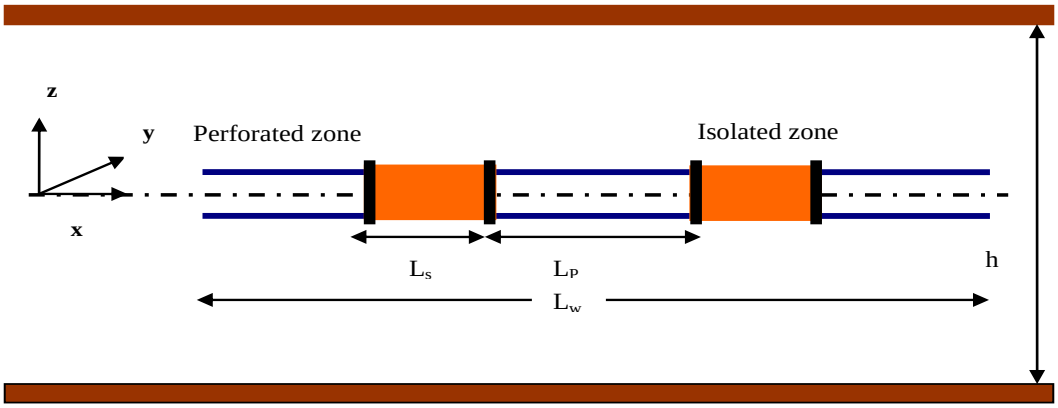

Figure 2-3: Horizontal well headed by perforated zone.

2-4- Long horizontal well headed by a perforated zone

Pressure distribution for long horizontal wells headed by perforated zone can be modified from Eq. (2-47):

$$P_D(x_D, y_D, z_D, z_{wD}, L_D, t_D) = \frac{\sqrt{\pi}}{2nL_{pD}} \int_0^{t_D} \frac{e^{-\frac{y_D^2}{4t_D}}}{\sqrt{\tau_D}} \left[erf\left(\frac{1-(n-1)(L_{pD}+L_{sD})}{2\sqrt{\tau_D}}\right) + erf\left(\frac{1-nL_{pD}-(n-1)L_{sD}}{2\sqrt{\tau_D}}\right) \right] d\tau_D \tag{2-60}$$

Early and late approximations will be the same as long horizontal wells headed by zonal isolation except that Eq. (2-49) should be modified to:

$$t_D \leq \begin{bmatrix} \frac{\left[x_D - nL_{pD} - (n-1)L_{sD}\right]^2}{20} \\ \frac{\left[x_D - (n-1)(L_{sD} + L_{pD})\right]^2}{20} \end{bmatrix} \tag{2-61}$$

3- PRESSURE TRANSIENT ANALYSIS FOR HORIZONTAL WELLS WITH ZONAL ISOLATIONS

Since the mid 1980's, horizontal well technology has provided the solution for oil and gas production process where the conventional vertical technique either had failed or produced less than the desired rate. The increase in the application of this technology during this period rapidly led to a need for the development of analytical models that are capable of evaluating the performance of these horizontal wells. Giger, F. (1985) and Joshi, S. D. (1986) presented the applicability of horizontal wells in heterogeneous reservoirs and the impact of the well productivity using slanted or horizontal wells respectively. Spivak, D. (1988) explained that the advantages of horizontal wells, such as productivity increase and better sweep efficiency, while reduction of water and gas coning have been reported by many researchers. At the same time, many attempts have been made by researchers to develop practical models to study the performance and productivity of horizontal wells.

Over time, pressure transient analysis techniques have been favorably applied for the evaluation of horizontal well performance and reservoir characterization. A few solutions for infinite limited isotropic reservoirs as well as for isotropic reservoirs with constant pressure at the outer boundaries, using the Newman product method have been introduced since 1970's. At the same time, the earliest analytical models for horizontal well test analysis, based on the line source approximation of the partially penetrating vertical fracture solution, have been developed. Ozkan et al (1989) have shown the effect of the production length of horizontal wells on the pressure derivative and

introduced a mathematical model for pressure evaluation in infinite conductivity horizontal wells. Odeh, A.S. and Babu, D.K. (1990) studied the transient flow behavior for horizontal wells, either for the pressure drawdown test or pressure build-up test.

Due to the increased complexity in the geometrical configuration of the wellbore, as a result of different horizontal well completion techniques, many concerns and questions regarding the pressure behavior in the vicinity of the wellbore and outer no-flow boundaries have remained unanswered. These concerns are based on the fact that the ideal behavior is seldom seen in real production tests. This is due to differing pressure derivative trends depending on the geometrical configuration of the whole system, the petrophysical properties of the formation, and zonal damage. Therefore, the validity of horizontal well models and the well test concepts adopted from vertical fracture analogue have been extensively investigated and new trends of horizontal well solutions were developed beginning in the 1990's. These solutions have been established under more realistic conditions to provide answers for previous concerns and questions.

Automatic type curve matching for horizontal wells was introduced and used for pressure transient interpretation several decades ago. Many researchers investigated the transient dual-porosity pressure response of two horizontal wells and introduced numerical models to reproduce the reservoir internal geometry and simulate the pressure trend monitored at the wells. Khelifa and Taib (2002) proposed a technique for analyzing the variable rate tests in horizontal wells, either a continuously changing flow rate test or a series of constant rate tests. It is important to note that Escobar et al (2004) used the TDS technique to analyze the pressure behavior of a horizontal well inside

channel systems. The last ten years has seen a focus on using the convolution and deconvolution technique in well test analysis. Gringarten et al (2003) proposed the use of downhole pressure gauges to diagnose production problems in North Sea horizontal wells. Whittle et al (2009) introduced a technique for well production forecasting by extrapolation of the deconvolution of pressure transient data and explained the practical use of the well test convolution and the various usages of deconvolution in tests of short and long durations.

Even though great attention has been focused on horizontal well technology, either in the drilling and completion aspect or in the production and reservoir characterization aspect, more study is required to overcome the concerns and limitations of the models that are used to evaluate the performance of wells or to predict the pressure behavior around and in the wellbore. This fact is supported by the idea of the great complexity of the horizontal well systems and the difficulties that are involved in recognition of the flow dynamics and types of flow regimes, especially in the area near the well where the geometrical configuration of flow becomes of great importance. In this chapter, the impact of the existence of the zonal isolations on pressure behavior of horizontal wells will be studied.

3-1- Pressure behavior of horizontal wells without zonal isolations:

The pressure response of horizontal wells without zonal isolations acting in infinite reservoirs can be shown in Fig. (3-1) while Fig. (3-2) shows the pressure behavior of horizontal wells acting in finite reservoirs.

Normally three flow regimes are easily identified for horizontal wells acting in infinite reservoirs: the early radial, early linear and pseudo-radial flow. Five flow

regimes can be developed for horizontal wells acting in finite reservoirs: early radial, linear, channel, pseudo-radial and pseudo-steady state flow.

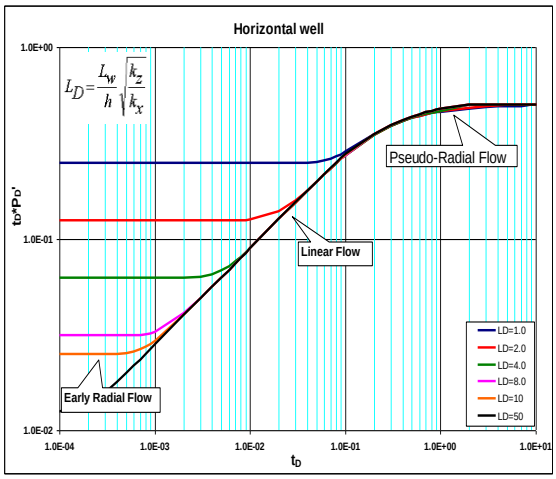

Figure 3-1: Pressure behavior for horizontal wells in infinite reservoirs.

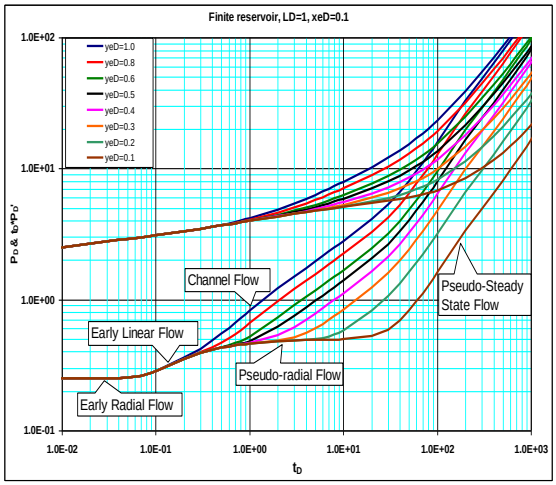

Figure 3-2: Pressure behavior for horizontal wells in finite reservoirs.

3-1-1- Early radial flow:

For horizontal wells with dimensionless length $L_D \le 20$, early vertical radial flow is expected to develop at early time as the fluid flows from all directions into the wellbore in the normal plane to the horizontal wellbore as shown in Fig. (3-3). However, for horizontal wells with $L_D \ge 20$, early radial flow regime can not be observed. This flow regime is characterized by a slope equal to $(1/4L_D)$ on the pressure curve or having the following value on the pressure derivative curve:

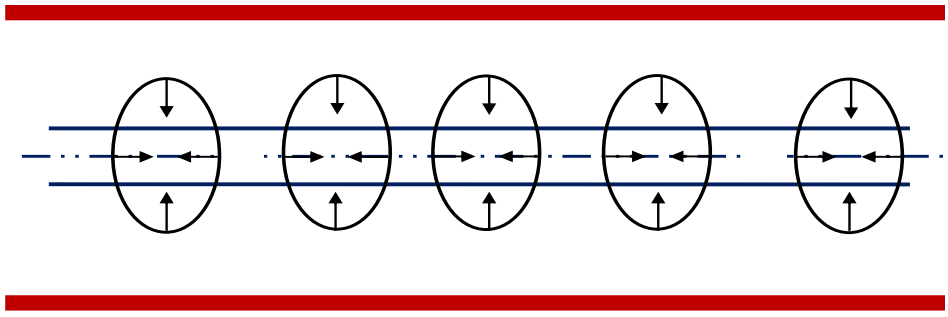

Figure 3-3: Early radial flow for horizontal wells.

$$(t_D \times P_D^{'})_{ER} = \frac{0.5}{2L_D} \tag{3-1}$$

therefore:

$$(t \times \Delta P')_{ER} = \frac{70.6q\mu B}{\sqrt{k_z k_y}\, L_w} \tag{3-2}$$

or:

$$(\Delta P)_{ER} = \frac{162.6q\mu B}{\sqrt{k_z k_y}\, L_w} \log(t) + C \tag{3-3}$$

where:

$$C = \ln\left(\frac{k_y}{\phi\mu c r_w^2}\right) - 7.43 + 2S_d \tag{3-4}$$

and:

$$S_d = S\left(\frac{L_w}{h}\sqrt{\frac{k_z}{k_y}}\right) \tag{3-5}$$

A semi-log plot of (ΔP) vs. (t) yields a straight line during the early data. The slope of this line can be used to calculate:

$$\sqrt{k_z k_y} = \frac{162.56q\mu B}{m_{ER} L_w} \tag{3-6}$$

3-1-2- Early linear flow:

After both upper and lower boundaries are reached, the early linear flow is developed as shown in Fig. (3-4). This flow is characterized by a slope of (0.5) on the pressure derivative curve. The governing equation for early linear flow (Goode 1987) is:

$$(\Delta P)_{EL} = \frac{8.128qB}{L_w h}\sqrt{\frac{\mu t}{k_y \phi c_t}} + C \tag{3-7}$$

where:

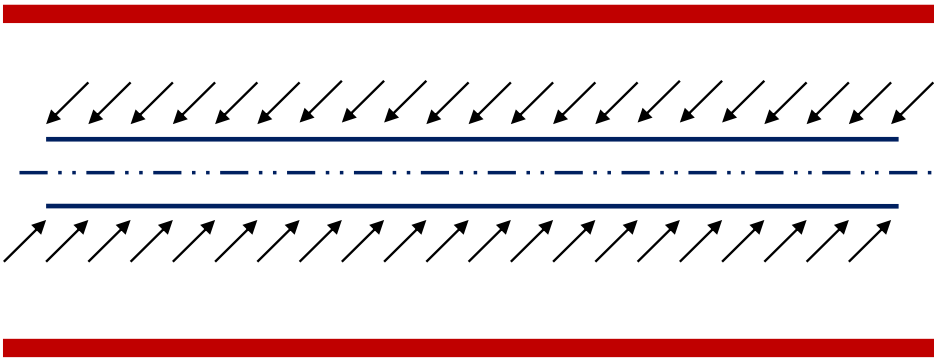

Figure 3-4: Early linear flow for horizontal wells.

$$C = \frac{141.2 q \mu B}{L_w \sqrt{k_z k_y}} S_d \tag{3-8}$$

and:

$$S_d = \left. \frac{L_w \sqrt{k_z k_y}}{141.2 q \mu b} \right|_{\Delta P = 0} - \ln\left(\frac{h}{r_w}\right) - 0.25 \ln\left(\frac{k_y}{k_z}\right) + 1.838 \tag{3-9}$$

Eq. (3-7) indicates that the plot of ΔP vs. $t^{1/2}$ yields a straight line. The slope of this line m_{EL} can be used to estimate k_y.

$$\sqrt{k_y} = \frac{8.128 qB}{L_w h m_{EL}} \sqrt{\frac{\mu}{\phi c}} \tag{3-10}$$

3-1-3- Pseudo radial flow:

This type of flow is developed at late time when the pressure pulse reaches a remote distance from the wellbore in an infinite reservoir as shown in Fig. (3-5). This flow regime is characterized by a horizontal line on pressure derivative curve:

$$(t_D \times P_D^{'})_{PR} = 0.5 \tag{3-11}$$

$$(t \times \Delta P')_{PR} = \frac{70.6 q \mu B}{\sqrt{k_x k_y}\, h} \tag{3-12}$$

$$(\Delta P)_{PR} = \frac{162.6 q \mu B}{\sqrt{k_x k_y}\, h} \log(t) + C \tag{3-13}$$

$$C = \frac{162.6 q \mu B}{\sqrt{k_x k_y}\, h} [\log(\frac{k_x}{\phi \mu c L_w^{\,2}}) - 2.023] + \frac{141.2 q \mu B}{L_w \sqrt{k_y k_z}} S_d \tag{3-14}$$

$$S_d = 1.151 \sqrt{\frac{k_z}{k_x}} \frac{L_w}{h} \left[\frac{\Delta P_{1hr}}{m_{PR}} - \log(\frac{k_x}{\phi \mu c L_w^{\,2}}) + 1.76 \right] \tag{3-15}$$

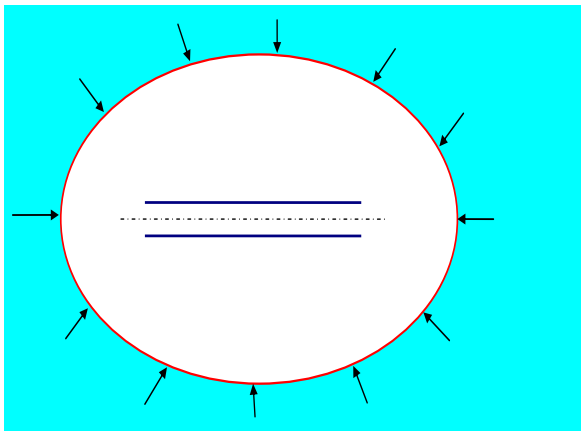

Figure 3-5: Pseudo-radial flow regime for horizontal wells.

A semi-log plot of (ΔP) vs. (t) yields straight line during the pseudo-radial flow period. The slope of this line can be used to calculate:

$$\sqrt{k_x k_y} = \frac{162.6 q \mu B}{m_{PR} h} \tag{3-16}$$

3-1-4 - Channel Flow:

This flow starts when the pressure behavior is affected by the closest outer boundaries of the bounded reservoirs as shown in Fig. (3-6). It is characterized by a

slope of (0.5) on the pressure derivative curve. The governing equation for this flow is (Goode 1987):

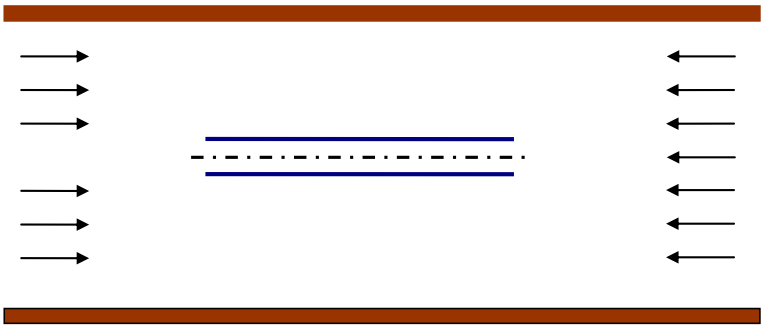

Figure 3-6: Channel flow for horizontal wells acting in finite reservoirs.

$$(\Delta P)_{CF} = \frac{8.128qB}{2hx_e}\sqrt{\frac{\mu t}{k_y \phi c_t}} + C \tag{3-17}$$

$$C = \frac{141.2q\mu B}{L_w\sqrt{k_z k_y}} S_t \tag{3-18}$$

$$S_t = \frac{L_w}{2x_e}\left[\left.\frac{2x_e\sqrt{k_z k_y}}{141.2q\mu b}\right|_{\Delta P=0} - S_p - \ln(\frac{h}{r_w}) - 0.25\ln(\frac{k_y}{k_z}) + 1.838\right] \tag{3-19}$$

where S_P represents the partial penetration skin factor.

The plot of ΔP vs. $t^{1/2}$ yields a straight line. The slope of this line m_{CF} can be used to estimate the distance to the closest boundary (x_e) as follows:

$$x_e = \frac{8.128qB}{2hm_{CF}}\sqrt{\frac{\mu}{k_y \phi c_t}} \tag{3-20}$$

3-1-5- Pseudo-Steady State Flow:

For long producing times in closed reservoir, pseudo-steady state flow regime appears as a result of the pressure being influenced by all four closed boundaries at the

same time. It is characterized by the unit-slope line on the pressure derivative curve. The equation of this straight line is:

$$\left(t_D \times P_D'\right)_{pss} = 2\pi t_{DA} \tag{3-21}$$

This flow can be used to estimate drainage area of the reservoir as follows:

$$A = \frac{0.2338qB}{\phi c_t h}\sqrt{\frac{k_x}{k_y}}\left(\frac{t_{PSS}}{\left(t \times \Delta P'\right)_{PSS}}\right) \tag{3-22}$$

3-2- Pressure behavior of horizontal wells with zonal isolations:

Because of the existence of zonal isolations, pressure responses and flow regimes of horizontal wells are expected to be changed. The primary impact will be on the early time flow regimes taking place in the vicinity of the wellbore. This impact depends on the effective length of the wellbore and the length and number of the zonal isolations. The following pressure behaviors and flow regimes can be classified based on the length of the horizontal well and the length and number of zonal isolations.

3-2-1- Short horizontal wellbore (L_D=1 for example):

Because of the extreme short length of the wellbore, the impact of the zonal isolations on pressure behavior will be easy to identify. This impact increases significantly as the total length of the isolated sections increases. The following cases can be identified:

1- Normal case with early radial, linear and pseudo radial flow regime if there is no zonal isolation as shown in Fig. (3-1).

2- If the wellbore contains a single zonal isolation having different lengths, early radial, transition or linear, pseudo-spherical, and pseudo radial flow will be observed for short isolators. For long isolators, early radial, pseudo-spherical, and

pseudo-radial flow will result as shown in Fig. (3-7). Pseudo-spherical flow is observed for the cases where the horizontal well is extremely short and the length of the zonal isolation represents (90%) of the total length of the wellbore. Physically this is understandable as the perforated section of horizontal well tends to be like single point in the formation.

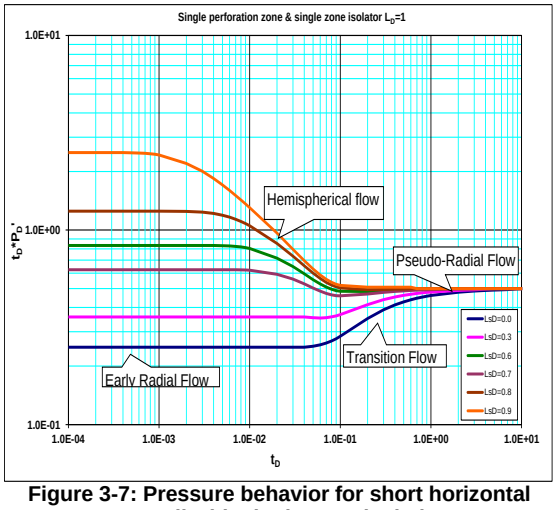

Figure 3-7: Pressure behavior for short horizontal well with single zone isolation.

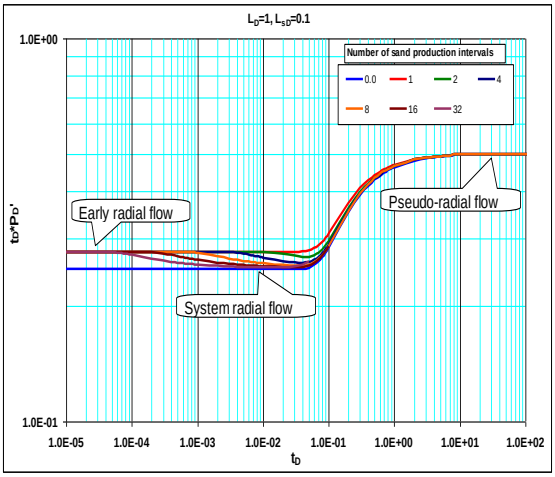

Figure 3-8: Pressure behavior for short horizontal well with multiple zonal isolations.

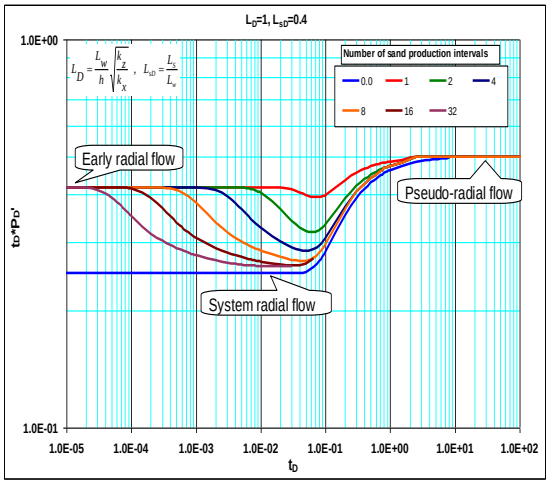

Figure 3-9: Pressure behavior for short horizontal well with multi zonal isolations.

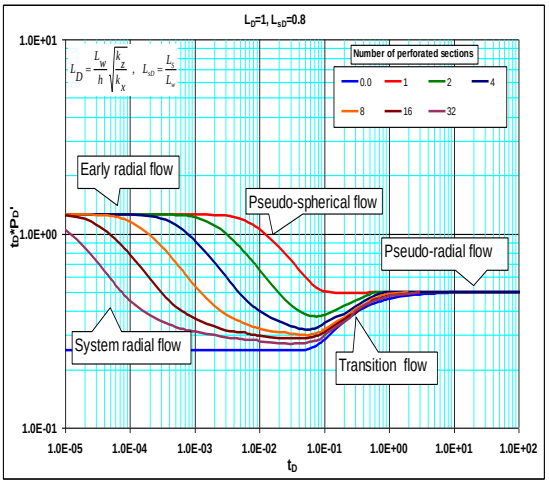

Figure 3-10: Pressure behavior for short horizontal well with multi zonal isolations

3- Early radial flow disappears gradually when the wellbore contains large numbers of zonal isolations. Pseudo-spherical flow is expected to develop for small numbers of zonal isolations. New flow regime is observed after early radial flow

in the case of a great numbers of zonal isolations. This flow regime is radial flow also (System radial flow) and develops in the normal plane to the horizontal wellbore (isolated zones and perforated zones) as shown in Figs. (3-8), (3-9), and (3-10).

3-2-2-Horizontal wellbore with moderate length (L_D=10):

The following cases may develop for moderate length horizontal wells in which early radial, linear, and pseudo-radial are the dominant flow regimes. However, there is a possibility to develop another new radial flow regime that is an intermediate radial flow between the early radial and the pseudo-radial flow regimes. Intermediate radial flow represents the flow of reservoir fluid toward the wellbore in the horizontal plane parallel to the wellbore.

1- Normal case with early radial flow, linear flow, and pseudo-radial flow regimes if the wellbore does not contain isolated zones as shown in Fig. (3-1).
2- For wellbores containing single zonal isolation, having different lengths, early radial, linear flow, and pseudo radial flow are expected to occur for both short and long isolated zones as shown in Fig. (3-11).
3- Linear flow will be affected more than early radial flow if the wellbore contains multi zonal isolations. The time interval for early radial flow will be reduced gradually as shown in Fig. (3-12).
4- In the existence of multi long zonal isolations, intermediate radial flow will develop as shown in Fig. (3-13) and the possibility for the system radial flow to occur will increase as shown in Fig. (3-14).

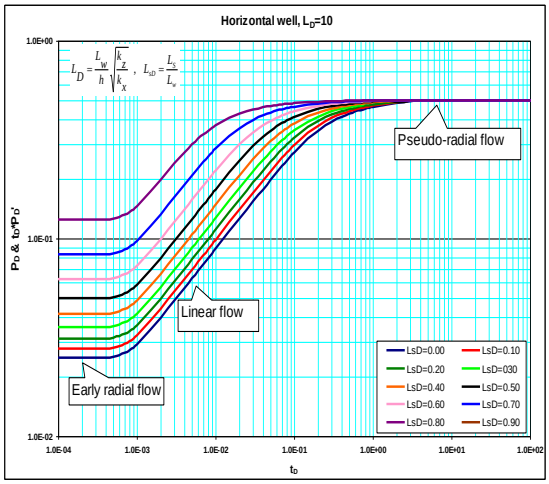

Figure 3-11: Pressure behavior for moderate length horizontal well without zonal isolation.

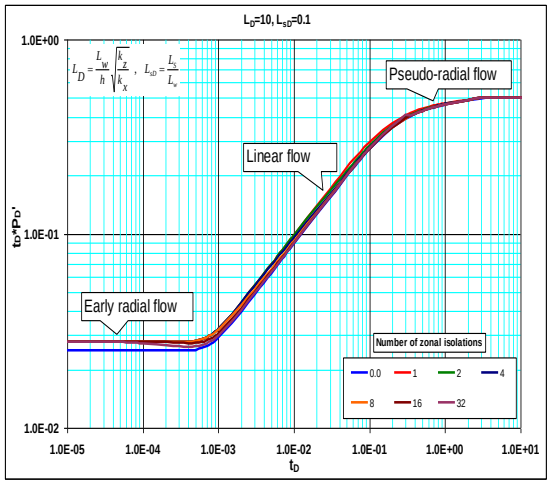

Figure 3-12: Pressure behavior for moderate length horizontal well with multiple zonal isolations.

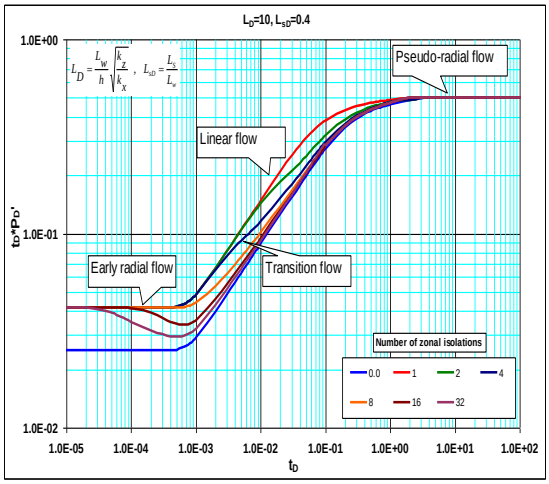

Fig. 3-13: Pressure behavior of moderate length horizontal well with multiple zonal isolations.

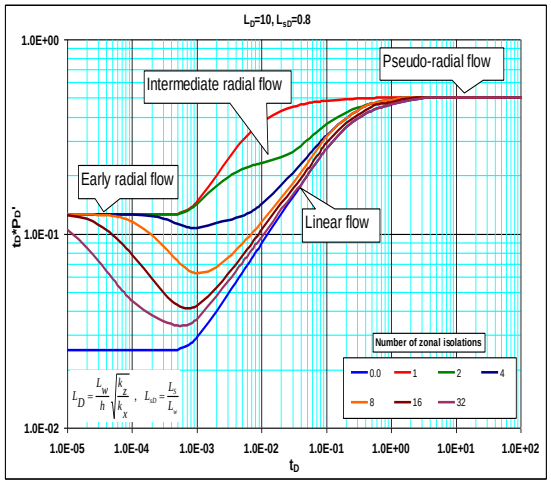

Fig. 3-14: Pressure behavior of moderate length horizontal well with multiple zonal isolations.

3-2-3- Long horizontal wellbore with moderate length (L_D=50):

In general, early radial flow will not be observed for long horizontal wells where pressure behavior tends to be similar to the pressure behavior of vertical hydraulic fractures. Linear flow and pseudo-radial flow are the dominant types of flow regimes.

1- Normal case with early radial, linear and pseudo-radial flow regimes if the wellbore does not contain isolated zones as shown in Fig. (3-1).

2- Pressure behavior of a horizontal wellbore having a single zonal isolation having different lengths up to (L_{sD}=90%), will be similar to the normal horizontal well

with only two flow regimes; linear and pseudo-radial as shown in Fig. (3-15).

3- Pressure behavior of a horizontal wellbore will not be affected if multiple short isolated zones exist as shown in Fig. (3-16).

4- Pressure behavior of a long horizontal wellbore containing multiple long zonal isolations (L_{sD}=40% for example) is expected to have early linear, transition, second linear and pseudo-radial flow as shown in Fig. (3-17). The second linear flow represents the flow to the whole system (isolated zones and perforated zones).

5- If the wellbore contains large numbers of long zonal isolations (L_{sD}=80% for example), early linear and intermediate radial flow will appear followed by second linear and pseudo-radial flow regimes as shown in Fig. (3-18).

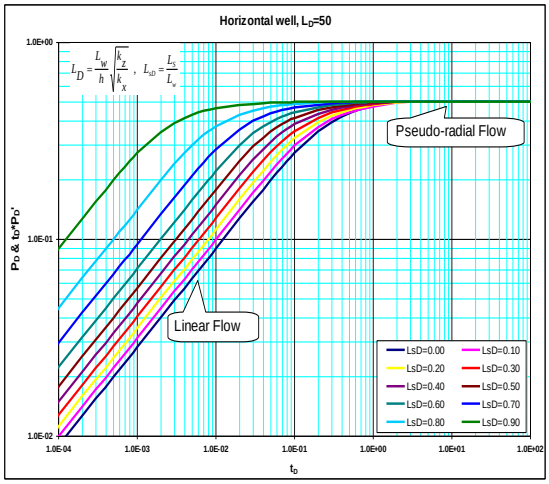

Figure 3-15: Pressure behavior for long horizontal well without zonal isolation.

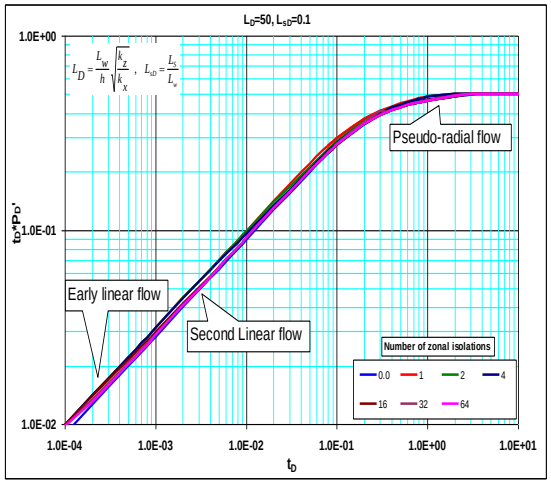

Figure 3-16: Pressure behavior for long horizontal well with multiple zonal isolations.

3-3- Flow regimes of horizontal wells with zonal isolations

3-3-1- Near-Wellbore early radial flow:

For short horizontal wells having dimensionless length (L_D<20) with or without zonal isolations, near-wellbore early radial flow is expected to develop at early time as the fluid flows from all directions into the wellbore as shown in Fig. (3-19). This flow

regime is characterized by a slope equal to $(1/4nL_{pD}L_D)$ on the pressure curve or having the following value on the pressure derivative curve:

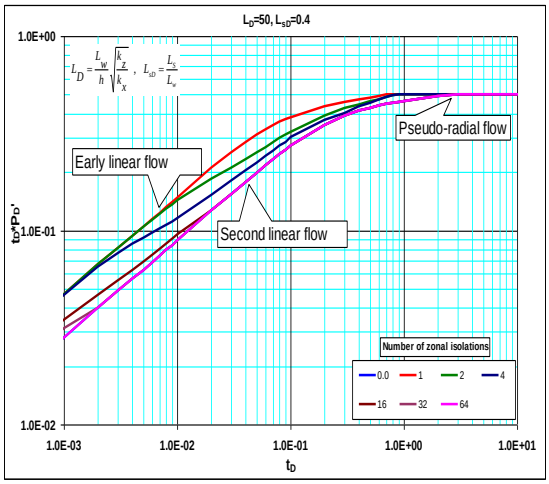

Figure 3-17: Pressure behavior for long horizontal well with multiple zonal isolations.

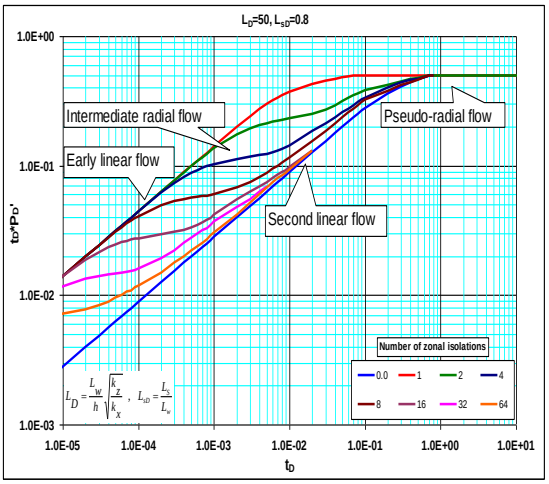

Figure 3-18: Pressure behavior for long horizontal well with multiple zonal isolations.

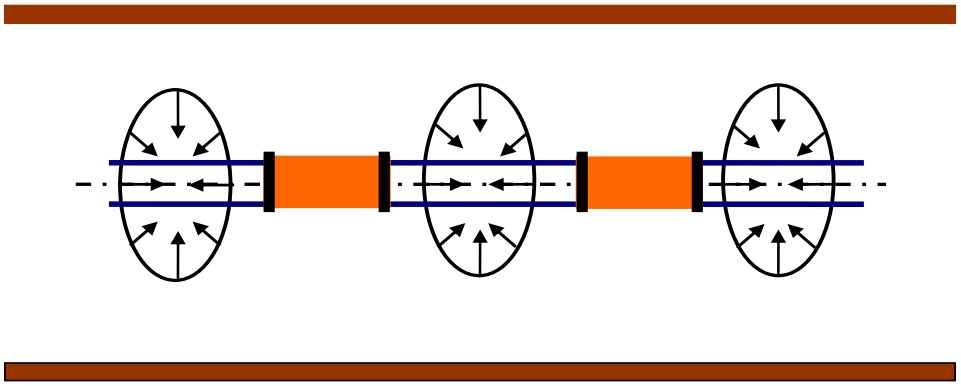

Figure 3-19: Near-Wellbore Early radial flow for horizontal well with zonal isolations.

$$(t_D \times P_D^{'})_{ERF} = \frac{0.5}{2nL_{pD}L_D} \tag{3-23}$$

In field units Eq. 3-23 becomes:

$$(t \times \Delta P')_{ERF} = \frac{35.3q\mu B}{\sqrt{k_z k_y}\, nL_p} \tag{3-24}$$

This equation can be used to calculate $(\sqrt{k_z k_y})$ knowing (n) and (L_p):

$$\sqrt{k_z k_y} = \frac{35.3 q \mu B}{(t \times \Delta P')_{ERF}\, n L_p} \tag{3-25}$$

3-3-2- System early radial flow:

This flow regime is expected to occur when the horizontal wells have an infinite number of zonal isolations in which pressure behavior can be considered similar to the normal horizontal wells shown in Fig. (3-20). Therefore, the governing equation for this type of flow is:

$$(t_D \times P_D^{'})_{SRF} = \frac{0.5}{2 L_D} \tag{3-26}$$

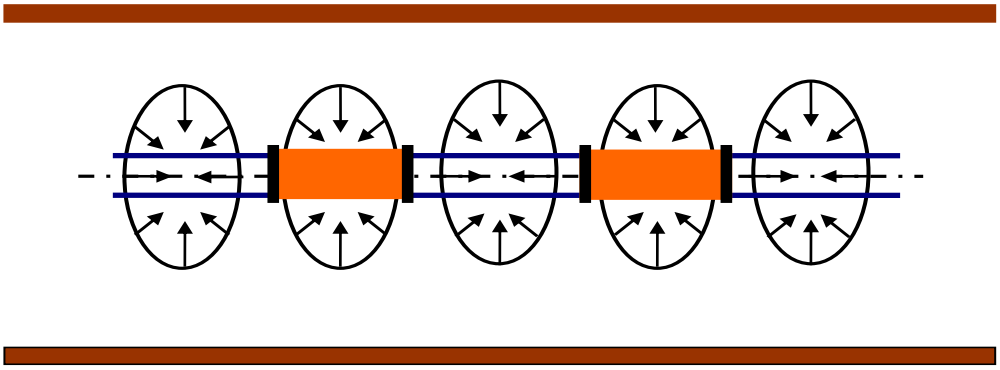

Figure 3-20: System early radial flow for horizontal well with zonal isolations.

In field units Eq. 3-26 becomes:

$$(t \times \Delta P')_{SRF} = \frac{35.3 q \mu B}{\sqrt{k_z k_y}\, L_w} \tag{3-27}$$

This equation can be used to calculate $(\sqrt{k_z k_y})$ knowing (L_w):

$$\sqrt{k_z k_y} = \frac{35.3 q \mu B}{(t \times \Delta P')_{SRF}\, L_w} \tag{3-28}$$

3-3-3 - Intermediate radial Flow:

This flow regime develops for the case of long horizontal wells having multiple long zonal isolations. It represents radial flow around each isolated zone as shown in

Fig. (3-21). This flow regime can be an indictor that the well has serious production problems. Basically the intermediate radial flow is developed in the horizontal plane parallel to the wellbore when there is a long closed section in the perforated zone. This closed section comes from different production problems such as sand production or asphaltic problems. The governing equation for this flow is:

$$(t_D \times P_D')_{IRF} = \frac{0.5}{n} \tag{3-29}$$

In field units, Eq. (3-29) becomes:

$$(t \times \Delta P')_{IRF} = \frac{70.6 q \mu B}{n\sqrt{k_x k_y}\, h} \tag{3-30}$$

This equation can be used to calculate horizontal permeability $\left(\sqrt{k_x k_y}\right)$ knowing the number of closed zones:

$$\sqrt{k_x k_y} = \frac{70.6 q \mu B}{n(t \times \Delta P')_{IRF}\, h} \tag{3-31}$$

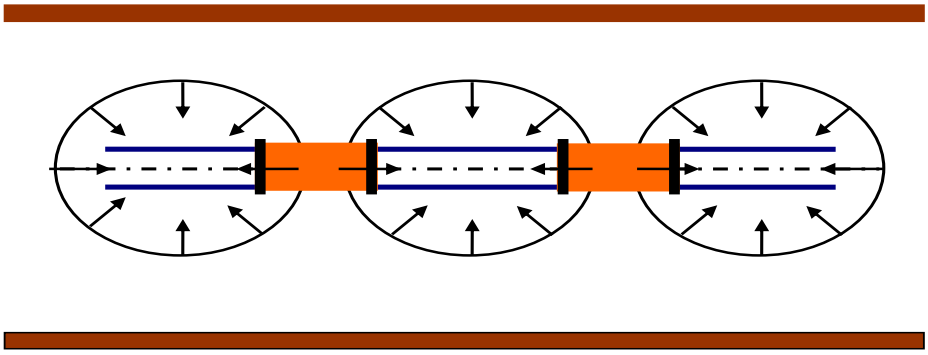

Figure 3-21: Intermediate radial flow for horizontal well with zonal isolations.

3-3-4 - Pseudo-spherical Flow:

This flow regime develops when the length of the perforated zones is extremely short as compared to the height of the formation. Pseudo-spherical flow is expected to

occur at early time as shown in Fig. (3-22). This flow regime is governed by the following equation (Slimani and Tiab 2006):

$$(t_D \times P_D')_{PSF} = \frac{1}{4\sqrt{\pi t_D}} \tag{3-32}$$

$$(t \times \Delta P')_{PSF} = \frac{1226.75 q \mu B L_w}{h\sqrt{t_{PSF}} k_x} \sqrt{\frac{\phi \mu c_t}{k_y}} \tag{3-33}$$

where t_{PSF} and $(t \times \Delta P')_{PSF}$ are the coordinates of any point on the straight line.

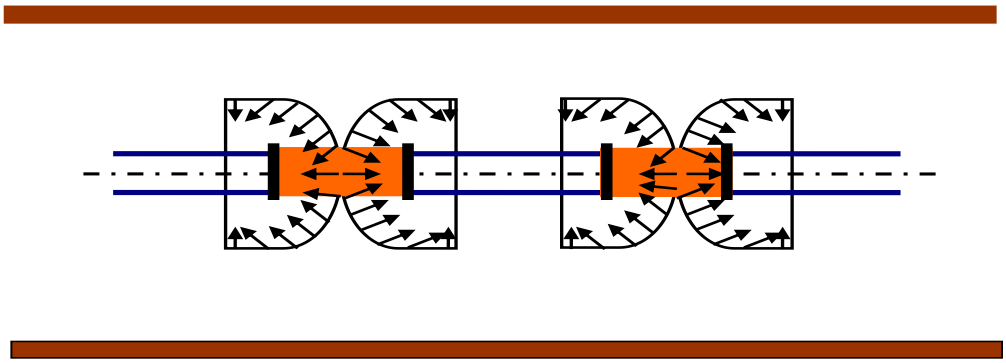

Figure 3-22: Pseudo- spherical flow for horizontal well with zonal isolations.

3-3-5 - Near-Wellbore Early linear flow:

Near-wellbore Early linear flow regime is the dominant flow at early time for long horizontal wellbores (L_D>20) when early radial flow is barely observable. This type of flow develops when both upper and lower boundaries are reached and the flow of fluid becomes normal to the plane of the wellbore as shown in Fig. (3-23). This flow is characterized by a slope of (0.5) on the pressure derivative curve. The governing equation for early linear flow is:

$$(t_D \times \Delta P_D')_{ELF} = \frac{\sqrt{\pi t_D}}{2 n L_{pD}} \tag{3-34}$$

and in field units:

$$(t\times\Delta P')_{ELF}=\frac{2.032qB}{nL_p h}\sqrt{\frac{\mu t_{ELF}}{k_y\phi c_t}} \tag{3-35}$$

This equation can be used to calculate $(\sqrt{k_y})$ knowing (n) and (L_p), by inserting the coordinates (t_{ELF}) and $(t\times\Delta P')_{ELF}$ at any point on the straight line of early linear flow.

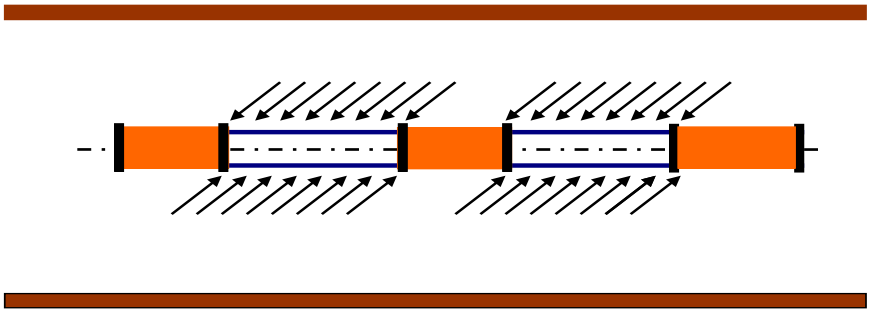

Figure 3-23: Near-Wellbore early linear flow for horizontal well with zonal isolations.

3-3-6- System Early linear flow:

System early linear flow regime occurs for long horizontal wellbores (L_D>20) containing large numbers of zonal isolations. Similar to the early linear flow, this flow is characterized by a slope of (0.5) on the pressure derivative curve. It represents linear flow toward the whole wellbore (isolated zones and perforated zones) as shown in Fig. (3-25). The governing equation for early linear flow is:

$$(t_D\times\Delta P_D')_{SLF}=\frac{\sqrt{\pi t_D}}{2nL_{SD}} \tag{3-36}$$

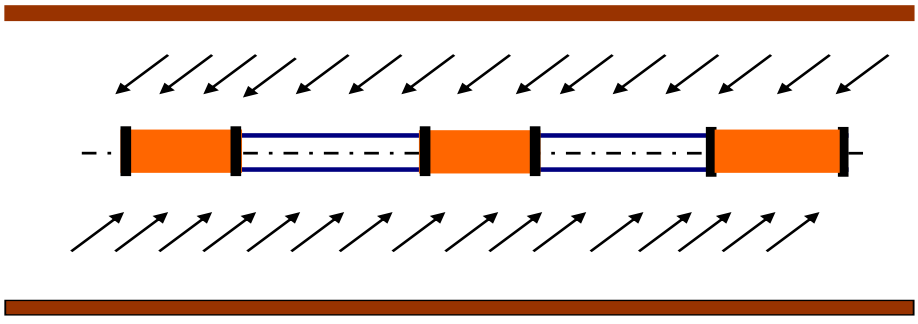

Figure 3-24: System early linear flow for horizontal well with zonal isolations.

and in field units:

$$(t\times\Delta P')_{SLF1hr}=\frac{2.032qB}{hnL_S}\sqrt{\frac{\mu}{k_y\phi c_t}} \tag{3-37}$$

where $(t\times\Delta P')_{SLF1hr}$ is the pressure derivative value at t=1 hr.

3-3-7- Elliptical flow

This flow regime develops before the pseudo-radial flow as shown in Fig. (3-25). Tiab 1994 described this flow regime as a straight line of slope 0.36 on the log-log plot of (t_D*P_D') vs. (t_D). He used multivariate linear regression analysis to derive the relationship between (t_D*P_D') and (t_D). The governing equation for elliptical flow is derived based on multi-regression analysis as shown in Fig. (3-26):

$$(t_D\times P_D')_{EF}=\frac{0.42}{nL_{pD}}\times(t_D)^{0.36} \tag{3-38}$$

In field units:

$$(t\times\Delta P')_{EF}=\frac{3q\mu BL_w^{0.28}}{nL_p\sqrt{k_xk_y}h}\left(\frac{k_xt_{EF}}{\phi\mu c}\right)^{0.36} \tag{3-39}$$

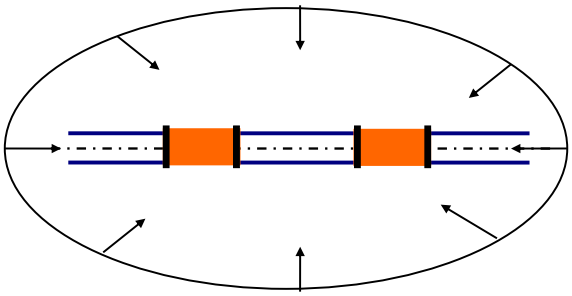

Figure (3-25): Elliptical flow regime for horizontal well with zonal isolations.

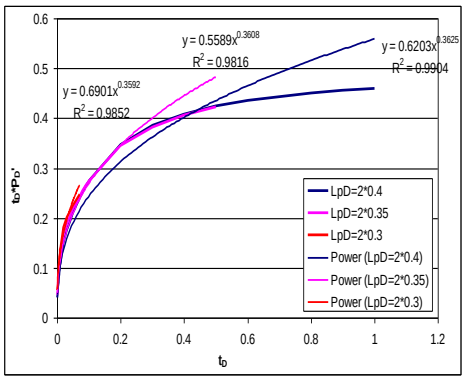

Figure 3-26: Multi-regression analysis for elliptical. flow for horizontal well with zonal isolations.

3-3-8 - Pseudo radial flow:

Pseudo-radial flow appears at late time when the fluid flows from a remote drainage area toward the wellbore as shown in Fig. (3-27). This type of flow is characterized by a horizontal line on the pressure derivative curve with:

$$(t_D \times P_D^{'})_{PRF} = 0.5 \tag{3-40}$$

In field units, Eq. (3-40) becomes:

$$(t \times \Delta P')_{PRF} = \frac{70.6 q \mu B}{\sqrt{k_x k_y}\, h} \tag{3-41}$$

which can be used to calculate:

$$\sqrt{k_x k_y} = \frac{70.6 q \mu B}{(t \times \Delta P')_{PRF}\, h} \tag{3-42}$$

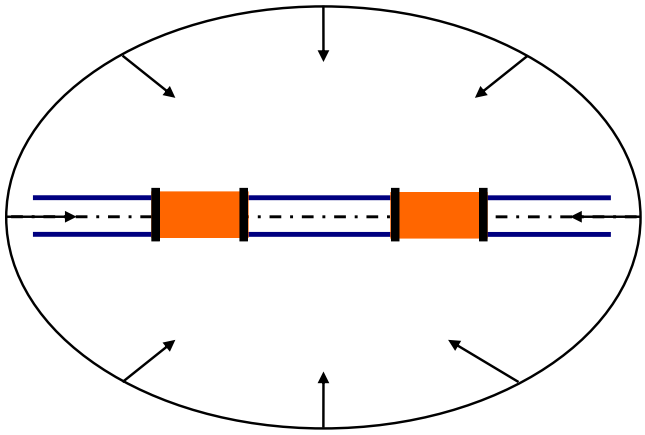

Figure 3-27: Pseudo- radial flow for horizontal well with zonal isolations.

3-4- Intersection Points:

The points of intersection between different lines of flow regimes are very important in the well test interpretation. They can be used to check the results.

3-4-1- The intersection of near-wellbore early linear flow line and pseudo-radial flow line is:

$$t_{PREL} = 1207 \frac{n^2 L_P^2 \phi \mu c_t}{k_x} \quad (3\text{-}43)$$

3-4-2- The point of intersection of system early linear flow line and pseudo-radial flow line is:

$$t_{PRSL} = 1207 \frac{n^2 L_S^2 \phi \mu c_t}{k_x} \quad (3\text{-}44)$$

3-4-3-The intersection of near-wellbore early linear flow line and intermediate radial flow line is:

$$t_{IREL} = 1207 \frac{L_P^2 \phi \mu c_t}{k_x} \quad (3\text{-}45)$$

3-4-4-The point of intersection of system early linear flow line and intermediate radial flow line is:

$$t_{IRSL} = 1207 \frac{L_S^2 \phi \mu c_t}{k_x} \quad (3\text{-}46)$$

3-4-5-The intersection of near-wellbore early linear flow line and near-wellbore early radial flow line is:

$$t_{EREL} = 302 \frac{h^2 \phi \mu c_t}{k_z} \quad (3\text{-}47)$$

3-4-6-The intersection of system early linear flow line and near-wellbore early radial flow line is:

$$t_{ERSL} = 302 \frac{h^2 L_s^2 \phi \mu c_t}{L_p^2 k_z} \quad (3\text{-}48)$$

3-4-7-The intersection of near-wellbore early radial flow line and pseudo-spherical flow line is:

$$t_{ERPS} = 1207 \frac{n^2 L_P^2 L_w^2 k_z \phi \mu c_t}{h^2 k_x^2} \quad (3\text{-}49)$$

3-4-8- The point of intersection of pseudo-radial flow line and pseudo-spherical flow line is:

$$t_{PRPS} = 302 \frac{L_w^2 \phi \mu c_t}{k_x} \quad (3\text{-}50)$$

3-4-9- The point of intersection of pseudo-radial flow line and elliptical flow line is:

$$t_{PREF} = 6155\frac{(nL_p)^{2.8}\phi\mu c_t}{k_x L_w^{0.8}} \tag{3-51}$$

3-4-10- The point of intersection of intermediate radial flow line and elliptical flow line is:

$$t_{IREF} = 6155\frac{(nL_p)^{2.8}\phi\mu c_t}{nk_x L_w^{0.8}} \tag{3-52}$$

3-4-11- The point of intersection of near-wellbore early radial flow line and elliptical flow line is:

$$t_{EREF} = 897.5\frac{\phi\mu c_t}{L_w^{0.8}k_x}\left(h\sqrt{\frac{k_x}{k_z}}\right)^{2.8} \tag{3-53}$$

3-4-12- The point of intersection of near-wellbore early linear flow line and elliptical flow line is:

$$t_{ELEF} = 18.3\frac{L_w^2\phi\mu c_t}{k_x} \tag{3-54}$$

3-4-13- The point of intersection of system early linear flow line and elliptical flow line is:

$$t_{SLEF} = 18.3\frac{L_w^2\phi\mu c_t}{k_x}\left(\frac{L_s}{L_w}\right)^{7.14} \tag{3-55}$$

3-5- Relationships between flow regimes

Many mathematical relationships between various flow regimes' analytical models can be used in pressure transient interpretation to estimate reservoir parameters.

3-5-1- Pseudo-radial and intermediate radial flow regime:

$$\frac{(t_D \times P_D')_{IRF}}{(t_D \times P_D')_{PRF}} = \frac{(t \times \Delta P')_{IRF}}{(t \times \Delta P')_{PRF}} = \frac{1}{n} \tag{3-56}$$

3-5-2-Pseudo-radial and near-wellbore early radial flow regime:

$$\frac{(t_D \times P_D')_{ERF}}{(t_D \times P_D')_{PRF}} = \frac{1}{2nL_{PD}L_D} \tag{3-57}$$

$$\frac{(t \times \Delta P')_{ERF}}{(t \times \Delta P')_{PRF}} = \frac{h}{2nL_P}\sqrt{\frac{k_x}{k_z}} \tag{3-58}$$

3-5-3-Intermediate radial and near-wellbore early radial flow regime:

$$\frac{\left(t_D \times P_D'\right)_{ERF}}{\left(t_D \times P_D'\right)_{IRF}} = \frac{1}{2L_{PD}L_D} \tag{3-59}$$

$$\frac{\left(t \times \Delta P'\right)_{ERF}}{\left(t \times \Delta P'\right)_{IRF}} = \frac{h}{2L_P}\sqrt{\frac{k_x}{k_z}} \tag{3-60}$$

3-5-4-Near-wellbore early radial and system early radial flow regime:

$$\frac{\left(t_D \times P_D'\right)_{ERF}}{\left(t_D \times P_D'\right)_{SRF}} = \frac{1}{nL_{PD}} \tag{3-61}$$

$$\frac{\left(t \times \Delta P'\right)_{ERF}}{\left(t \times \Delta P'\right)_{SRF}} = \frac{h}{nL_P} \tag{3-62}$$

3-5-5-Pseudo-radial and system early radial flow regime:

$$\frac{\left(t_D \times P_D'\right)_{SRF}}{\left(t_D \times P_D'\right)_{PRF}} = \frac{1}{2L_D} \tag{3-63}$$

$$\frac{\left(t \times \Delta P'\right)_{SRF}}{\left(t \times \Delta P'\right)_{PRF}} = \frac{L_w}{2L_P}\sqrt{\frac{k_x}{k_z}} \tag{3-64}$$

3-5-6-Intermediate radial and system early radial flow regime:

$$\frac{\left(t_D \times P_D'\right)_{SRF}}{\left(t_D \times P_D'\right)_{IRF}} = \frac{n}{2L_D} \tag{3-65}$$

$$\frac{\left(t \times \Delta P'\right)_{SRF}}{\left(t \times \Delta P'\right)_{IRF}} = \frac{nL_w}{2L_P}\sqrt{\frac{k_x}{k_z}} \tag{3-66}$$

3-5-7-Near-wellbore early linear and system early linear flow regime:

$$\frac{\left(t_D \times P_D'\right)_{SLF}}{\left(t_D \times P_D'\right)_{ELF}} = \frac{L_{PD}}{L_{SD}} \tag{3-67}$$

$$\frac{\left(t \times \Delta P'\right)_{SLF}}{\left(t \times \Delta P'\right)_{ELF}} = \frac{L_P}{L_S} \tag{3-68}$$

3-6- Skin factor

Pressure behavior of horizontal wells is affected significantly by skin factor. Formation damage due to drilling and completion process, partially penetrating wells, reservoir heterogeneity and anisotropy, as well as the choke effect of fluid flow, may all be involved within the term of skin factor. Skin factor in horizontal wells has different classifications depending on the type of flow regime that can be developed in the vicinity of the wellbore. Generally, most horizontal wells have non-uniform distribution of skin along their lengths and this creates a challenging problem in the interpretation of the pressure transient response. In this study, uniform distribution for the skin factor will be assumed. Figures (3-28), (3-29), and (3-30) show the effect of skin factor on pressure behavior of horizontal wells. It is important to note that the skin factor affects the pressure distribution only and does not affect pressure derivative curves.

3-6-1- Mechanical skin factor

At early time, early radial flow regime may be observed. Therefore, mechanical skin factor (Sm) or average skin factor (Al-Otaibi et al 2005) probably has the dominant effect on pressure behavior at this time period. Therefore, mechanical skin factor can be calculated based on early time approximation model.

$$\Delta P_t = \Delta P_{production} + \Delta P_{skin} \tag{3-69}$$

$$P_D(x_D, y_D, z_D, t_D) = -\frac{1}{4nLpDL_D} Ei\left(-\frac{y_D^2 + z_D^2}{4t_D}\right) + Sm = \frac{1}{4nL_{pD}L_D}\left(\ln\left(\frac{t_D}{y_D^2 + z_D^2}\right) + 0.80907\right) + \frac{(Sm)_{ERF}}{nL_{pD}L_D} \tag{3-70}$$

Since $z_D = 0$, Eq.(3-70) can be written as:

$$P_D(x_D, y_D, z_D, t_D) = \frac{1}{4nL_{pD}L_D}\left(\ln\left(\frac{t_D}{y_D^2}\right) + 0.80907 + 4(Sm)_{ERF}\right) \tag{3-71}$$

In field units, mechanical skin factor can be written as:

$$(Sm)_{ERF} = 0.25\left[\frac{(\Delta P)_{ERF}}{(t\times\Delta P)_{ERF}} - \ln\left(\frac{k_y t_{ERF}}{\phi\mu c_t r_w^2}\right) + 7.43\right] \quad (3\text{-}72)$$

3-6-2- Total skin factor

Total skin factor can be defined as the summation of the mechanical skin factor and the composite skin factor resulting from the partial penetration in the vertical direction, the partial penetration in the horizontal direction, and the effect of the chock flow. Total skin factor can be calculated based on the type of flow regime as follow:

3-6-2-1- From pseudo-radial flow regime

Basically, total skin factor can be calculated from pseudo radial flow which is expected to be dominant at late time using late time approximation given in Eq. (2-44).

$$P_D(x_D, y_D, z_D, t_D) = P_D(x_D, y_D, z_D, t_{D1}) + \frac{1}{2}\ln(\frac{t_D}{t_{D1}}) + S_t \quad (3\text{-}73)$$

Eq. (3-73) can be approximated to the following formula:

$$P_D(x_D, y_D, z_D, t_D) = \frac{1}{2}\ln(t_D) + \frac{S_t}{L_{pD}L_D} = \frac{1}{2}\left[\ln(t_D) + \frac{2S_t}{L_{pD}L_D}\right] \quad (3\text{-}74)$$

In field units, total skin factor can be written as;

$$(S_t)_{PRF} = \frac{0.5L_P}{h}\sqrt{\frac{k_z}{k_x}}\left[\frac{(\Delta P)_{PRF}}{(t\times\Delta P)_{PRF}} - \ln\left(\frac{k_x t_{PRF}}{\phi\mu c_t L_w^2}\right) + 4.659\right] \quad (3\text{-}75)$$

3-6-2-2- From near-wellbore early linear flow regime

In addition, early linear flow regime can be used to calculate total skin factor with some small percentage error due to the approximation of the linear flow model given by Eq. (3-34):

$$(S_t)_{ELF} = \frac{0.0288}{Lp}\sqrt{\frac{k_x}{\phi\mu c_t}}\left[\frac{(\Delta P)_{LF1hr}}{(t\times\Delta P)_{LF1hr}} - 2\right] \quad (3\text{-}76)$$

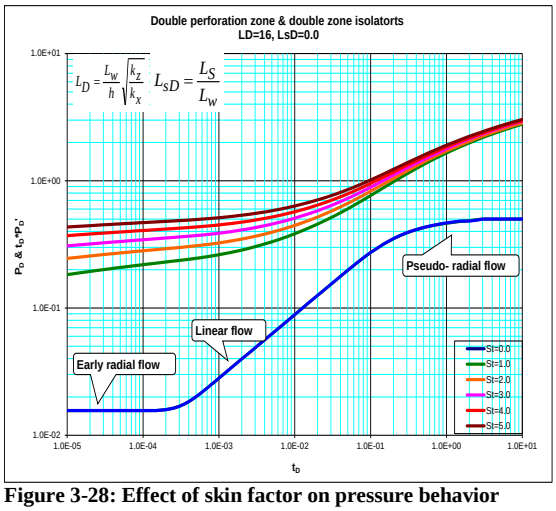

Figure 3-28: Effect of skin factor on pressure behavior of horizontal well without zonal isolations.

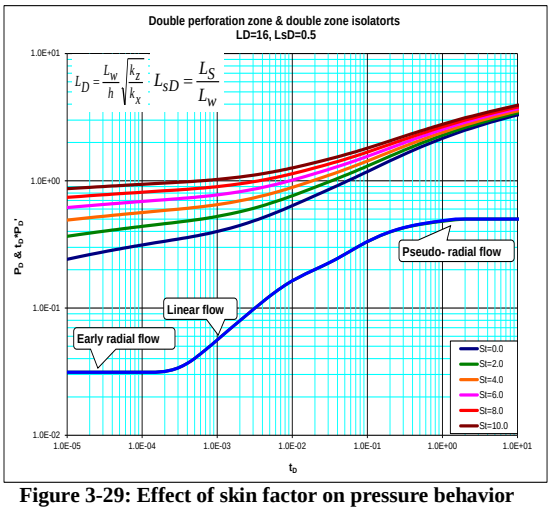

Figure 3-29: Effect of skin factor on pressure behavior of horizontal well with zonal isolations.

3-7- The effect of number and length of zonal isolation on pseudo-skin factor

The dimensionless pressure drop at any point and at any time in a reservoir is created by the production process from a horizontal well consists of two terms. The first is the line source solution and the second is the pseudo-skin function. The pseudo-skin function can be approximated by a constant for large values of dimensionless time, which corresponds to the starting time of pseudo-radial flow, t_{D1}. Therefore when $(t_D \geq t_{D1})$, pseudo-skin factor can be calculated using (Spivak 1988). Malekzadeh and Abdelgawad 1999 considered that pseudo-skin factor is a part of total skin factor if the combined effect of the formation damage and the presence of impermeable barriers and low permeability regions in the vicinity of some sections of the horizontal well are represented by mechanical skin damage. They stated that the total skin factor obtained from the well tests is the summation of mechanical skin factor and pseudo-skin factor. Mathematically, Cinco-Ley (1974) and Spivak (1988) defined pseudo-skin factor as:

$$S(x_D, y_D, z_D, t_D) = P_D(x_D, y_D, z_D, t_{D1}) + 0.5\ln\left(\frac{t_D}{t_{D1}}\right) - 0.5\left[\ln\left(\frac{t_D}{x_D^2 + y_D^2}\right) + 0.80907\right] \qquad (3\text{-}77)$$

When $x_D = 0$, Eq. (3-77) can be written as:

$$S(0, y_D, z_D, t_D) = P_D(0, y_D, z_D, t_{D1}) - 0.5\left[\ln(t_{D1}) + 0.80907\right] + \ln(y_D) \qquad (3\text{-}78)$$

Since the three terms in Eq. (3-78) are constants, the pseudo-skin factor has constant value.

Despite the fact that the zonal-isolation technique seems to be an ideal solution for many serious production problems such as water and gas coning, sand production, and damaged zone separation, it is also a cause of significant increase in the skin factor. This increment depends on the length and number of the zonal isolation. As the length of the zonal isolation increases, the skin factor also increases due to the extra resistance to flow resulting from the existence of the zonal isolations. This skin increment for short horizontal wells is much greater than that for long ones. Figure (3-31) shows the effect of the number and length of zonal isolations on the skin factor of horizontal wells. It can be seen from this figure that the single zonal isolation has a skin factor greater than the skin factor of double or triple zonal isolations for the same length. Skin factor increases slightly with the increase of the number of zonal isolations for long horizontal wells while the skin factor increases significantly for the short horizontal wells.

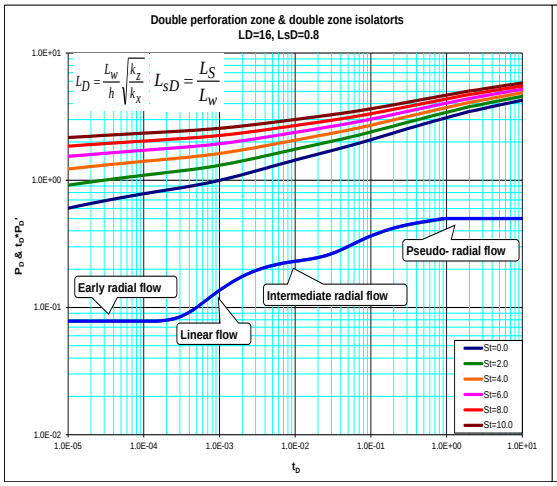

Figure 3-30: Effect of skin factor on pressure behavior of horizontal well with zonal isolations.

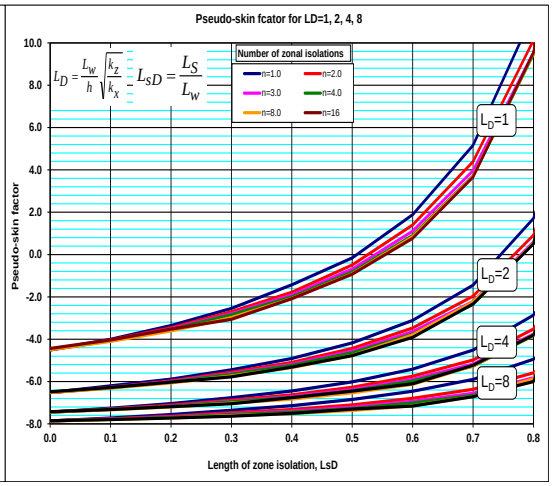

Figure 3-31: Effect of number and length of zonal isolations on pseudo-skin factor.

3-8-Application of Type Curve Matching

As shown on the plots in Appendix A, the pressure and pressure derivatives have different shapes for each combination of length and number of zonal isolation for different wellbore lengths. Different flow regimes are observed for different numbers and lengths of zonal isolations. It is important to note that:

1- Pseudo-spherical flow develops for short perforation section when the length of horizontal wellbore is extremely short and the zonal isolation is extremely long.

2- Intermediate radial flow develops for short perforated sections and long isolated zones in the wellbore.

3- System radial flow develops when the horizontal wellbore contains an infinite number of zonal isolations and an infinite number of perforated sections.

4- Second linear flow develops when the horizontal wellbore contains an infinite number of zonal isolations and an infinite number of perforated sections.

5- Early radial flow develops at early time for short horizontal wells and early linear flow is developed at early time for long horizontal wells.

6- Pseudo-radial flow is dominant at late time.

The following information is associated with each type curve: dimensionless length of horizontal well (L_D), number of zonal isolations (n), Length of zonal isolations (L_{sD}), wellbore radius (y_D). Thus, the following information can be obtained from the type curve matching process: $(P_D)_M$, $(\Delta P)_M$, $(t_D)_M$, $(\Delta t)_M$, $(L_D)_M$, $(n)_M$, $(L_{sD})_M$, $(yD)_M$. The

following steps illustrate how type curve matching is used to determine reservoir characteristics such as: permeability in the three directions and the number and length of zonal isolations.

Step-1 Plot (ΔP vs. t) and ($t \times \Delta P'$ vs. t) on log-log paper.

Step-2 Obtain the best match of the data with one of the type curves.

Step-3 Read from any match point: t_M , ΔP_M , t_{DM} , P_{DM} , L_{DM} , L_{PDM} , L_{sDM} , n_M , y_{DM}.

Step-4 Calculate k_x :

$$k_x = \frac{\phi \mu c_t L_w^2 t_{DM}}{0.0002637 t_M} \tag{3-79}$$

Step-5 Calculate ky :

$$k_y = \frac{1}{k_x}\left[\frac{141.2 q \mu B P_{DM}}{h \Delta P_M}\right]^2 \tag{3-80}$$

Step-6 Calculate k_z :

$$k_z = \frac{L_{DM}^2 h^2 k_x}{L_w^{\ 2}} \tag{3-81}$$

The number and length of the zonal isolations are normally well known prior to running a pressure test. However, this technique can be used to check whether the zonal isolations are performing their functions as expected. This can be done by estimating the number and length of zonal isolations from this technique directly and comparing them with the actual number and length of the existing zonal isolations.

Step-7 Length of perforation zone:

$$L_p = L_{PDM} \times L_w \tag{3-82}$$

Step-8 Length of zonal isolations

$$L_S = L_{SDM} \times L_w \tag{3-83}$$

3-9-Application of TDS technique

This section presents an analytical technique referred to as the *Tiab's Direct Synthesis* (TDS) technique for interpreting log-log plots of pressure and pressure derivatives of a well with zonal isolations. TDS is a powerful technique for the computation of reservoir parameters directly from log-log plots of pressure and pressure derivative data. A well designed pressure transient test in a horizontal well with zonal isolations in an infinite reservoir should yield all the necessary straight lines to calculate the number and length of zonal isolation, permeabilities in all directions. The great advantage of this technique is that it only requires graphing of pressure and pressure derivative on a single log-log plot for direct analysis.

The following step-by-step procedure is for the ideal case where all the necessary straight lines are well defined.

Step 1 - Plot pressure change (ΔP) and pressure derivative (t×ΔP') values versus test time on a log-log graph.

Step 2 - Read the value of $(t\times\Delta P')_{PRF}$ corresponding to the infinite acting pseudo-radial flow line.

Step 3 - Calculate (k_h).

$$k_h = \sqrt{k_x k_y} = \left(\frac{70.6 q \mu B}{h(t \times \Delta P')_{PRF}} \right) \tag{3-84}$$

Step 4 – If the intermediate radial flow develops, read $(t\times\Delta P')_{IRF}$.

Step 5 – Calculate the number of zonal isolations (n) either from Eq. (3-31) or:

$$n = \frac{(t \times \Delta P')_{PRF}}{(t \times \Delta P')_{IRF}} \tag{3-85}$$

Step 6 - Obtain the value of (t×ΔP') at time t = 1 hr from the near-wellbore early linear flow line (extrapolated if necessary), $(t \times \Delta P')_{LF1hr}$.

Step 7 - Calculate $(L_p \sqrt{k_y})$.

$$L_p \sqrt{k_y} = \left(\frac{2.0315 qB}{nh(t \times \Delta P')_{LF1hr}} \right) \sqrt{\frac{\mu}{\phi c_t}} \tag{3-86}$$

Step 8 - Read the value of $(t \times \Delta P')_{SLF1hr}$ corresponding to the system early linear flow line at t=1 hr.

Step 9 - Calculate $(L_S \times \sqrt{k_y})$ using Eq. (3-37).

$$L_s \sqrt{k_y} = \left(\frac{2.032 qB}{hn(t \times \Delta P')_{SLF1hr}} \right) \sqrt{\frac{\mu}{\phi c_t}} \tag{3-87}$$

Step-10- Use the following correlation to calculate the length of isolated and perforated section together:

$$L_p + L_s = \frac{L_w}{n} \tag{3-88}$$

Step-11- Substitute Eq.(3-88) in Eq. (3-87) and (3-86), find the length of L_p and L_s.

Step 12 - Calculate (k_y) using the result of either Step (7) or (9).

Step 13 - Calculate (k_x) using the result of Step (3).

Step 14 – Calculate total length of perforated sections (L_{pt}) :

$$L_{pt} = nL_p \tag{3-89}$$

Step 15 – Calculate total length of isolated sections (L_{st}) :

$$L_{st} = L_w - L_{pt} \tag{3-90}$$

Step 16 - Read the value of $(t\times\Delta P')_{ERF}$ corresponding to the near-wellbore early-radial flow line.

Step 17 - Calculate (k_z).

$$k_z = \frac{1}{k_y}\left(\frac{35.3q\mu B}{nL_P(t\times\Delta P')_{ERF}}\right)^2 \tag{3-91}$$

Step 18 – Calculate mechanical skin factor (Sm):

$$Sm = \frac{0.25h}{nLp}\sqrt{\frac{k_x}{k_z}}\left[\frac{(\Delta P)_{ERF}}{(t\times\Delta P')_{ERF}} - \ln\left(\frac{k_y t_{ERF}}{\phi\mu c_t r_w^2}\right) + 7.43\right] \tag{3-92}$$

Step 19 – Calculate total skin factor (S_t) from Eq. (3-75) based on pseudo-radial flow line data:

$$S_t = \frac{0.5L_P}{h}\sqrt{\frac{k_z}{k_x}}\left[\frac{(\Delta P)_{PRF}}{(t\times\Delta P)_{PRF}} - \ln\left(\frac{k_x t_{PRF}}{\phi\mu c_t L_w^2}\right) + 7.43\right] \tag{3-93}$$

Step 20 – Check the value of total skin factor (S_t) using Eq. (3-76) if applicable:

Step 21 – Calculate the intersection times using Eq. (3-43) through Eq. (3-55) and compare them with those in the plot.

Example-3-1 (short horizontal well):

A pressure drawdown test data of a horizontal well is given in Table (Example 3-1) in Appendix D. Other known reservoir and well data are:

q = 4000 STB/D ϕ = 0.1 μ = 1 cp $c_t = 2\text{x}10^{-6}$ psi^{-1} h = 125 ft

L_w = 4000 ft r_w = 0.566 ft p_i = 5000 psi B = 1.125 bbl/STB

Determine:

1- Formation permeabilities in all directions.

2- Number and length of zonal isolations.

Using type-curve matching and TDS technique.

Solution using type-curve matching

Step-1 Plot (ΔP vs. t) and ($t \times \Delta P'$ vs. t) on log-log paper as shown in Fig. (3-32).

Step-2 Obtain the best match of the data with one of the type curves as shown in Fig. (3-33).

Step-3 Read from any match point: t_M , ΔP_M , t_{DM} , P_{DM} , L_{DM} , L_{PDM} , n_M , y_{DM}.

$$t_M = 100,\ \Delta P_M = 100,\ t_{DM} = 0.066,\ P_{DM} = 0.11,\ L_{DM} = 16,\ L_{PDM} = 0.2,$$
$$L_{sDM} = 0.8, n_M = 2,\ y_{DM} = 0.0001$$

Step-4 Calculate k_x from Eq. (3-79):

$$k_x = \frac{0.1 \times 1 \times 0.000002 \times 4000^2 \times 0.066}{0.0002637 \times 100} = 8$$

Step-5 Calculate ky from Eq. (3-80):

$$k_y = \frac{1}{8}\left[\frac{141.2 \times 4000 \times 1 \times 1.125 \times 0.11}{125 \times 100}\right]^2 = 3.9$$

Step-6 Calculate k_z from Eq. (3-81):

$$k_z = \frac{16^2 \times 125^2 \times 8}{4000^2} = 2$$

The number and length of the zonal isolations are normally well known prior to running a pressure test. However, this technique can be used to check whether the zonal isolations are performing their functions as expected. This can be done by estimating the number and length of zonal isolations from this technique directly and comparing

them with the actual number and length. From the matching point, the number of zonal isolations is two.

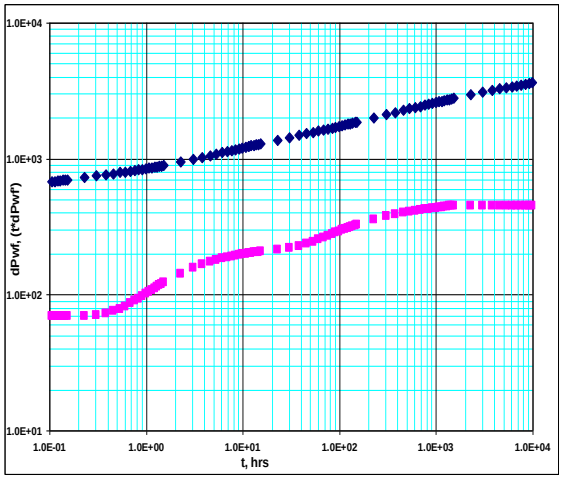

Figure 3-32: Pressure and pressure derivative plot for Example 3-1.

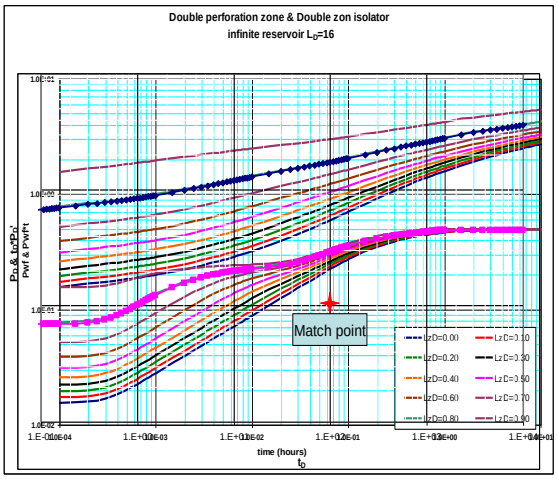

Figure 3-33: Type-curve matching technique for Example 3-1.

Step-7 Length of perforation zone from Eq. (3-82):

$$L_p = 0.2 \times 4000 = 800 \ \ ft$$

Step-8 Length of zonal isolations from Eq. (3-83):

$$L_z = 0.8 \times 4000 = 3200 \ \ ft$$

Solution using TDS

Step 1 - A plot of well pressure change (ΔP) and pressure derivative (t×ΔP') values versus test time is shown in Fig. (3-34).

Step 2 - Read the value of $(t \times \Delta P')_{PR}$ corresponding to the infinite acting pseudo-radial flow line.

$$(t \times \Delta P')_{PR} = 449.3$$

Step 3 - Calculate horizontal permeability (k_h) using Eq. (3-84):

$$k_h = \sqrt{k_x k_y} = \frac{70.6 \times 4000 \times 1 \times 1.125}{125 \times 449.3} = 5.657 \ md$$

Step 4 - Read the value of $(t\times\Delta P')_{IR}$ corresponding to the intermediate radial flow line.

$$(t\times\Delta P')_{IRF}=224.6$$

Step 5 - Calculate (n) the number of the zonal isolations using Eq. (3-30), (3-56), or (3-85):

$$n=\frac{70.6\times 4000\times 1\times 1.125}{224.6\times 125\times 5.657}=2$$

Step 6 - Read the value of $(t\times\Delta P')_{SLF1hr}$ corresponding to the system early linear flow line at t=1 hr.

$$(t\times\Delta P')_{SLF1hr}=25.5$$

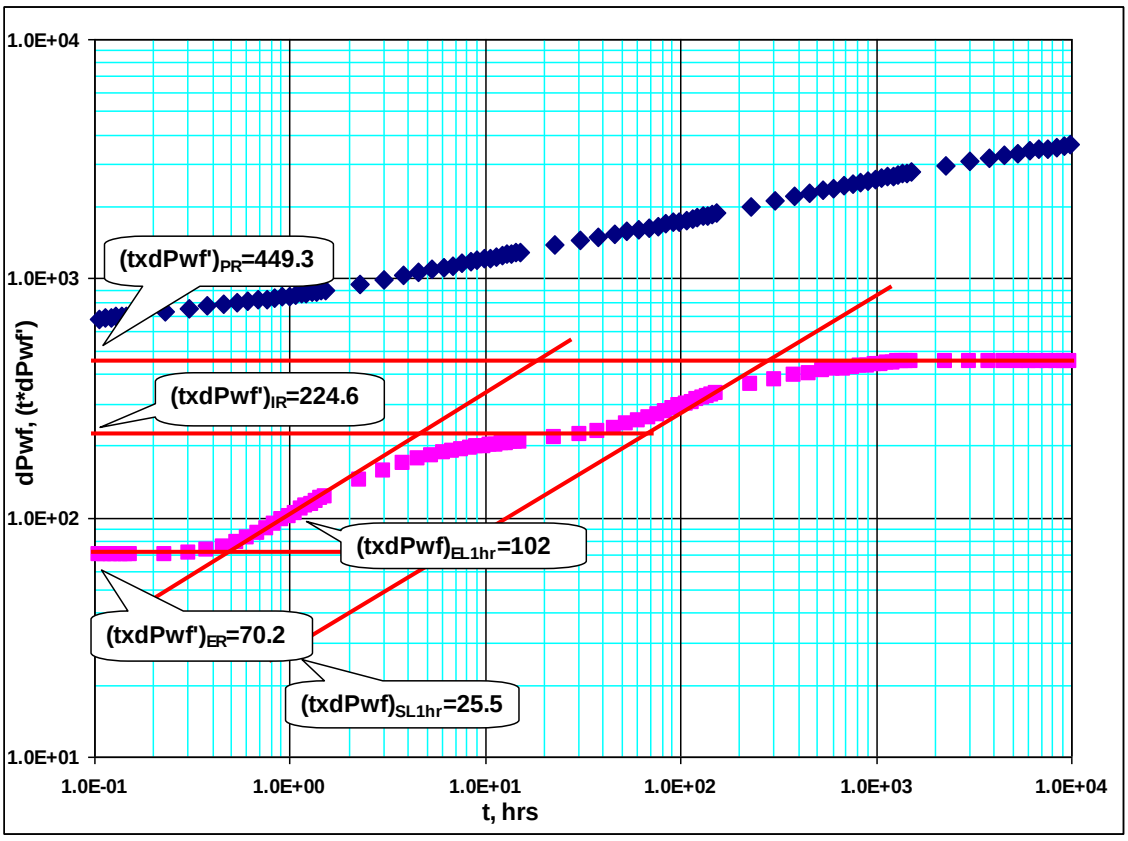

Figure 3-34: TDS technique for example 3-1.

Step 7 - Calculate $(L_S\times\sqrt{k_y})$ using Eq. (3-87).

$$L_S \times \sqrt{k_y} = \left(\frac{2.032 \times 4000 \times 1.125}{125 \times 2 \times 25.5} \right) \sqrt{\frac{1}{0.1 \times 0.000002}} = 3206$$

Step 8 - Read the value of $(t \times \Delta P')_{ELF1hr}$ corresponding to the near-wellbore early linear flow line at t=1 hr.

$$(t \times \Delta P')_{ELF1hr} = 102$$

Step 9 - Calculate $(L_P \times \sqrt{k_y})$ using Eq. (3-86).

$$L_P \times \sqrt{k_y} = \left(\frac{2.032 \times 4000 \times 1.125}{125 \times 2 \times 102} \right) \sqrt{\frac{1}{0.1 \times 0.000002}} = 801$$

Step 10 - Solve for (L_s) and (L_p) from the results of Step-7 and Step-9 taking into accounts that:

$$L_S + L_P = \frac{L_w}{n} = \frac{4000}{2} = 200$$

$$L_S = 1600 \ ft \ \Rightarrow total \ L_S = 2 \times 1600 = 3200 \ ft$$

$$L_P = 400 \ ft \ \Rightarrow total \ L_P = 2 \times 400 = 800 \ ft$$

Step 11 - Calculate (k_y) using the result of either Step (7) or (9).

$$k_y = \left(\frac{801}{400} \right)^2 = 4 \ md$$

Step 12 - Calculate (k_x) using the result of Step (3).

$$k_x = \left(\frac{5.657}{\sqrt{4}} \right)^2 = 8 \ md$$

Step-13- Read the value of $(t \times \Delta P')_{ERF}$ corresponding to the intermediate radial flow line.

$$(t \times \Delta P')_{ERF} = 70.2$$

Step-14- Calculate (k_z) from Eq. (3-91):

$$k_z = \frac{1}{4}\left(\frac{35.3\times 4000\times 1\times 1.125}{2\times 400\times 70.2}\right)^2 = 2$$

Step-15- Read from near-wellbore early radial flow at a certain time the value of pressure and pressure derivative.

$$(t)_{ERF} = 0.1 \quad (\Delta P)_{ERF} = 675 \quad (t\times\Delta P')_{ERF} = 70.2$$

Step-16- Calculate mechanical skin factor from Eq. (3-92).

$$(Sm)_{ERF} = 0.25\left[\frac{675}{70.2} - \ln\left(\frac{4\times 0.1}{0.1\times 1\times 0.000002\times 0.566^2}\right) + 8.24\right] = 0.55$$

Step-17- Read from pseudo-radial flow at a certain time the value of pressure and pressure derivative.

$$(t)_{PRF} = 1618 \quad (\Delta P)_{PRF} = 3662.5 \quad (t\times\Delta P')_{PRF} = 449.3$$

Step-18- Calculate total skin factor from Eq. (3-93).

$$(S_t)_{PRF} = \frac{0.5\times 400}{125}\sqrt{\frac{2}{8}}\left[\frac{3662.5}{449.3} - \ln\left(\frac{8\times 1618}{0.1\times 1\times 0.000002\times 4000^2}\right) + 4.659\right] = 3.6$$

Step-19- Read from linear flow line:

$$(t)_{LF1hr} = 1, \quad (\Delta P)_{LF1hr} = 856, \quad (t\times\Delta P)_{LF1hr} = 102$$

Step-20- calculate total skin factor from eq. (3-76)

$$(S_t)_{ELF} = \frac{0.0288}{400}\sqrt{\frac{8}{0.1\times 1\times 0.000002}}\left[\frac{856}{102} - 2\right] = 2.91$$

Step -21 - Determine the intersection points:

$$t_{PRSL} = 300\,hr, \; t_{PREL} = 19\,hr, \; t_{IRSL} = 73\,hr, \; t_{IREL} = 4.8\,hr, \; t_{EREL} = 0.5, \; t_{ERSL} = 7.5$$

Step -22 – Calculate the intersection points using Eqs. (3-43), (3-44), (3-45), (3-46), (3-47), and (3-48):

$$t_{PREL} = 1207\frac{2^2 \times 400^2 \times 0.1 \times 1 \times 0.000002}{8} = 19.3\ hr$$

$$t_{PRSL} = 1207\frac{2^2 \times 1600^2 \times 0.1 \times 1 \times 0.000002}{8} = 309\ hr$$

$$t_{IREL} = 1207\frac{400^2 \times 0.1 \times 1 \times 0.000002}{8} = 4.8\ hr$$

$$t_{IRSL} = 1207\frac{1600^2 \times 0.1 \times 1 \times 0.000002}{8} = 77\ hr$$

$$t_{ERSL} = 302\frac{125^2 \times 1600^2 \times 0.1 \times 1 \times 0.000002}{400^2 \times 2} = 7.77\ hr$$

$$t_{EREL} = 302\frac{125^2 \times 0.1 \times 1 \times 0.000002}{2} = 0.47\ hr$$

Table (3-1) shows summary of the calculated parameters for Example 3-1 and the input values.

Table (3-1) Summary of results Example 3-1.

Parameter	In-put value	Calculated value by Type-curve matching	Calculated value by TDS technique
k_x	8	8	8
k_y	4	3.9	4
k_z	2	2	2
N	2	2	2
L_p	400	400	400
L_s	1600	1600	1600
$(S_m)_{ERF}$	0.5		0.5
$(S_t)_{PRF}$	3.5		3.6
$(S_t)_{LF}$	3.5		2.91

Example -3-2 (Long horizontal well):

Pressure drawdown test data of a horizontal well is given in Table (Example 3-2) in Appendix F. Other known reservoir and well data are:

q = 1000 STB/D $\phi = 0.1$ $\mu = 1$ cp $c_t = 2x10^{-6}$ psi^{-1} h = 53 ft

L_w = 6000 ft r_w = 0.7 ft p_i = 5000 psi B = 1.25 bbl/STB k_z=10 md

Sm=0.0

Determine:

3- Formation permeabilities in all directions.

4- Number and length of zonal isolations.

Using type-curve matching and TDS technique.

Solution using type-curve matching

Step-1 Plot (ΔP vs. t) and ($t \times \Delta P'$ vs. t) on log-log paper as shown in Fig. (3-35).

Step-2 Obtain the best match of the data with one of the type curves as shown in Fig. (3-36).

Step-3 Read from any match point: t_M , ΔP_M , t_{DM} , P_{DM} ,, L_{PDM} , n_M , y_{DM}.

$t_M = 10,\ \Delta P_M = 10,\ t_{DM} = 0.0073,\ P_{DM} = 0.052,\ L_{PDM} = 0.3,\ L_{sDM} = 0.7, n_M = 4,$
$y_{DM} = 0.0001$

Step-4 Calculate k_x from Eq. (3-79):

$$k_x = \frac{0.1 \times 1 \times 0.000002 \times 6000^2 \times 0.0073}{0.0002637 \times 10} = 20\ md$$

Step-5 Calculate ky from Eq. (3-80):

$$k_y = \frac{1}{20}\left[\frac{141.2\times1000\times1\times1.25\times0.052}{53\times10}\right]^2 = 15\ md$$

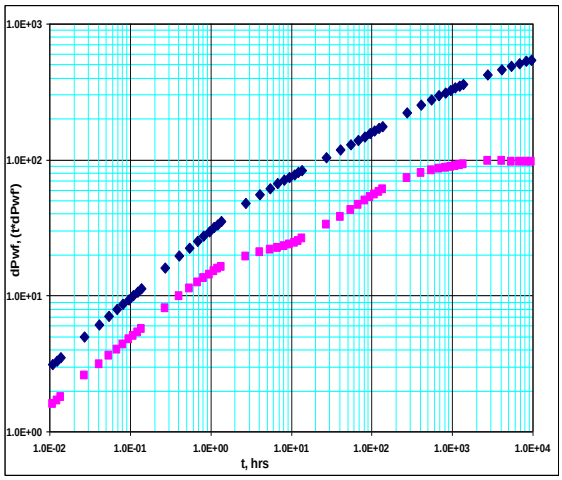

Figure 3-35: Pressure and pressure derivative plot for Example 3-2

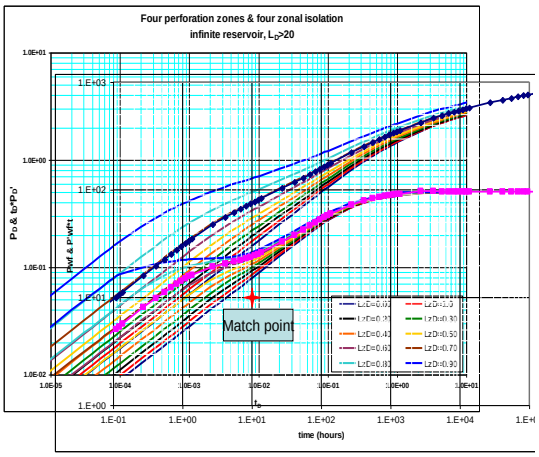

Figure 3-36: Type-curve matching technique for Example 3-2

The number and length of the zonal isolations normally are well known prior to running a pressure test. From the matching point, the number of zonal isolations is 4.

Step-7 Length of perforation zone from Eq. (3-82):

$$L_p = 0.3\times6000 = 1800\ ft$$

Step-8 Length of zonal isolations from Eq. (3-83):

$$L_z = 0.7\times6000 = 4200\ ft$$

Solution using TDS

Step 1 - A plot of well pressure change (ΔP) and pressure derivative (t×ΔP') values versus test time is shown in Fig. (3-37).

Step 2 - Read the value of $(t\times\Delta P')_{PRF}$ corresponding to the infinite acting pseudo-radial flow line.

$$(t\times\Delta P')_{PRF} = 96$$

Step 3 - Calculate horizontal permeability (k_h) using Eq. (3-84):

$$k_h = \sqrt{k_x k_y} = \frac{70.6 \times 1000 \times 1 \times 1.25}{53 \times 96} = 17.32\ md$$

Step 4 - Read the value of $(t \times \Delta P')_{IRF}$ corresponding to the intermediate radial flow line.

$$(t \times \Delta P')_{IRF} = 24$$

Step 5 - Calculate (n) the number of the zonal isolations using Eq. (3-30), (3-56), or (3-85):

$$n = \frac{70.6 \times 1000 \times 1 \times 1.25}{24 \times 53 * 17.32} = 4$$

Step 6 - Read the value of $(t \times \Delta P')_{SLF1hr}$ corresponding to the system early linear flow line at t=1 hr.

$$(t \times \Delta P')_{SLF1hr} = 6.5$$

Step 7 - Calculate $(L_S \times \sqrt{k_y})$ using Eq. (3-87).

$$L_S \times \sqrt{k_y} = \left(\frac{2.032 \times 1000 \times 1.25}{53 \times 4 \times 6.5} \right) \sqrt{\frac{1}{0.1 \times 0.000002}} = 4118$$

Step 8 - Read the value of $(t \times \Delta P')_{ELF1hr}$ corresponding to near-wellbore early linear flow line at t=1 hr.

$$(t \times \Delta P')_{ELF1hr} = 15.3$$

Step 9 - Calculate $(L_P \times \sqrt{k_y})$ using Eq. (3-86).

$$L_P \times \sqrt{k_y} = \left(\frac{2.032 \times 1000 \times 1.25}{53 \times 4 \times 15.3} \right) \sqrt{\frac{1}{0.1 \times 0.000002}} = 1751$$

Step 10 - Solve for (L_s) and (L_p) from the results of Step-7 and Step-9 taking into account that:

$$L_S + L_P = \frac{L_w}{n} = \frac{6000}{4} = 1500$$

$$L_S = 1050\ ft \Rightarrow total\ L_S = 4 \times 1050 = 4200\ ft$$

$$L_P = 450\ ft \Rightarrow total\ L_P = 4 \times 450 = 1800\ ft$$

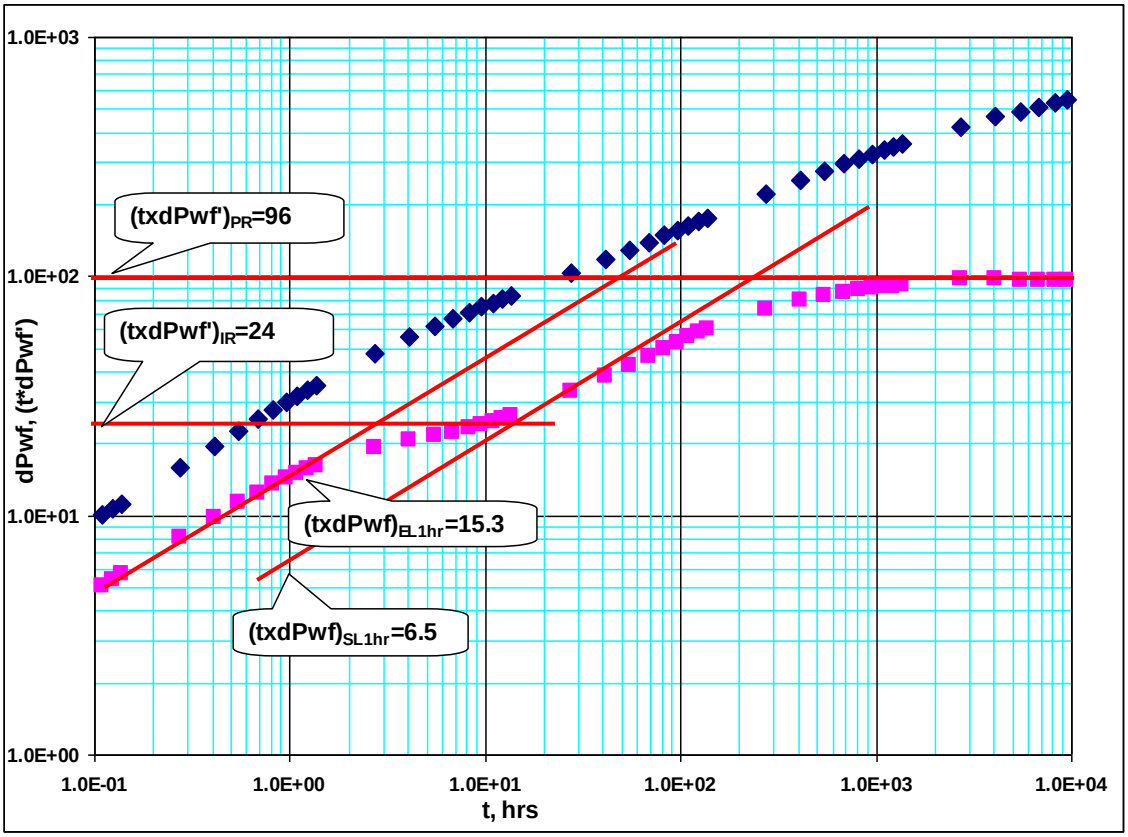

Figure 3-37: TDS technique for example 3-2.

Step 11 - Calculate (k_y) using the result of either Step (7) or (9).

$$k_y = \left(\frac{1751}{450}\right)^2 = 15\ md$$

Step 12 - Calculate (k_x) using the result of step (3).

$$k_x = \left(\frac{17.32}{\sqrt{15}}\right)^2 = 20\ md$$

Step-13- Read from pseudo-radial flow at a certain time the value of pressure and pressure derivative.

$$(t)_{PRF} = 10921 \quad (\Delta P)_{PRF} = 558 \quad (t \times \Delta P')_{PRF} = 496$$

Step-14- Calculate total skin factor from Eq. (3-92).

$$(S_t)_{PRF} = \frac{0.5 \times 450}{53} \sqrt{\frac{10}{20}} \left[\frac{558}{96} - \ln\left(\frac{20 \times 10921}{0.1 \times 1 \times 0.000002 \times 6000^2} \right) + 4.659 \right] = 0.5$$

Step-15- Read from linear flow line:

$$(t)_{LF1} = 1, \quad (\Delta P)_{LF1} = 30, \quad (t \times \Delta P)_{LF1} = 15$$

Step-16- Calculate total skin factor from eq. (3-76):

$$(S_t)_{ELF} = \frac{0.0288}{450} \sqrt{\frac{20}{0.1 \times 1 \times 0.000002}} \left[\frac{31}{15.3} - 2 \right] = 0.02$$

Step-17 - Determine the intersection points:

$$t_{PRSL} = 220\ hr, \ t_{PREL} = 40\ hr, \ t_{IRSL} = 14\ hr, \ t_{IREL} = 2.4\ hr$$

Step 16 – Calculate the intersection points using Eqs. (3-43), (3-44), (3-45), and (3-46):

$$t_{PREL} = 1207 \frac{4^2 \times 450^2 \times 0.1 \times 1 \times 0.000002}{20} = 39\ hr$$

$$t_{PRSL} = 1207 \frac{4^2 \times 1050^2 \times 0.1 \times 1 \times 0.000002}{20} = 213\ hr$$

$$t_{IREL} = 1207 \frac{450^2 \times 0.1 \times 1 \times 0.000002}{20} = 2.44\ hr$$

$$t_{IRSL} = 1207 \frac{1050^2 \times 0.1 \times 1 \times 0.000002}{20} = 13.3\ hr$$

Table (3-2) shows summary of the calculated parameters for Example 3-2 and the input values.

Table (3-2): Summary of results of Example 3-2.

Parameter	In-put value	Calculated value by Type-curve matching	Calculated value by TDS technique
k_x	20	20	20
k_y	15	15	15
N	4	4	4
L_P	450	450	450
L_s	1050	1050	1050
$(S_m)_{ERF}$	0.0		0.0
$(S_t)_{PRF}$	0.5		0.5
$(S_t)_{LF}$	0.5		0.02

3-10- Malfunctioning of zonal isolations

One of the important new applications for well test analysis in this study is the ability to evaluate the performance of the zonal isolations to determine if the they are performing as designed. In addition, well test analysis can be used to detect the locations of unsuccessful zonal isolations. It is well known that the zonal isolations are challenged by harsh environments such high temperature, high pressure, and corrosive fluids as well as stresses caused by production operation and/or unstable formations. Therefore, to maintain effective zonal isolations for the well life by maximizing the asset value and minimizing the risk, they should be designed for all conditions of harsh environments. However, many zonal isolations may not meet the necessary requirements especially when several harsh conditions are found in a single section of the formation that may lead to zonal isolation failure.

Evaluating the performance of the zonal isolation can be considered as the new and important application for the well test analysis. Type-curve matching technique can be used successfully to evaluate the zonal isolators' function and to detect locations of the

failed isolators. Figures (3-38) through (3-44) are a set of type-curve matching plots for single, double, triple, and fourth zonal isolations for L_D=16 with different cases and numbers of failed isolators.

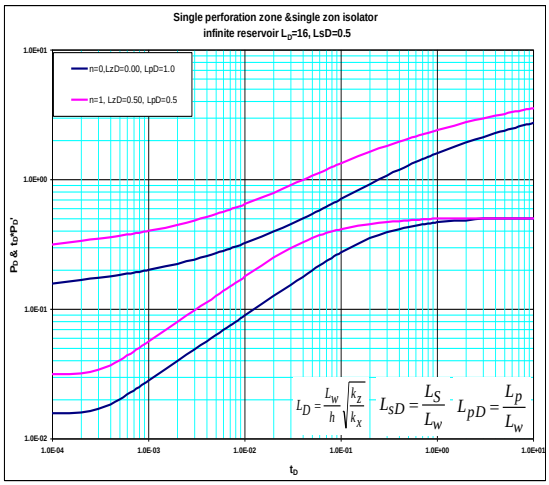

Figure 3-38: Pressure and pressure derivative plot for single failed zonal isolation

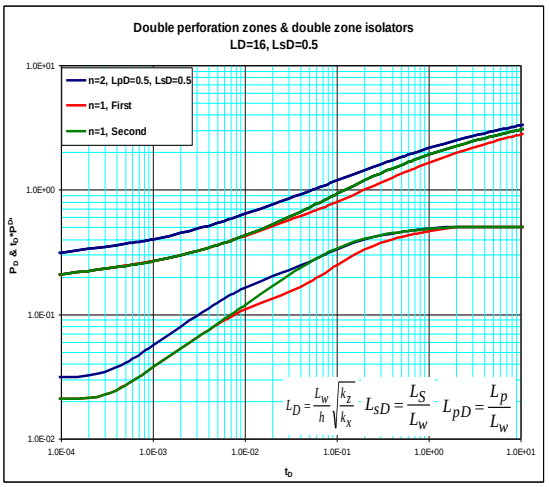

Figure 3-39: Pressure and pressure derivative plot for single failed zonal isolation

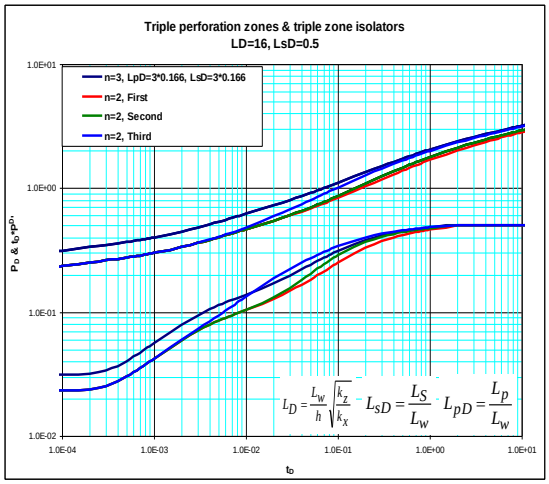

Figure 3-40: Pressure and pressure derivative plot for single failed zonal isolation

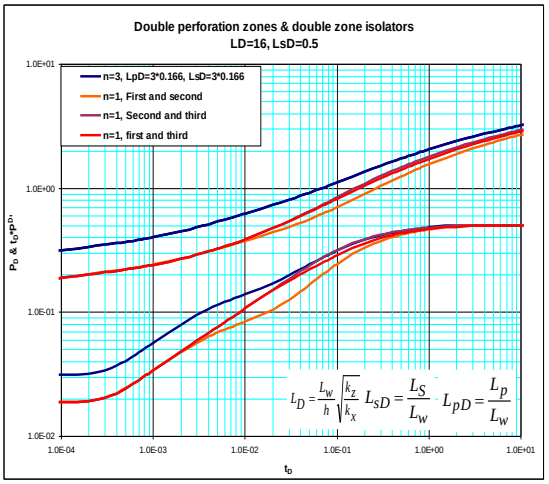

Figure 3-41: Pressure and pressure derivative plot for double failed zonal isolations

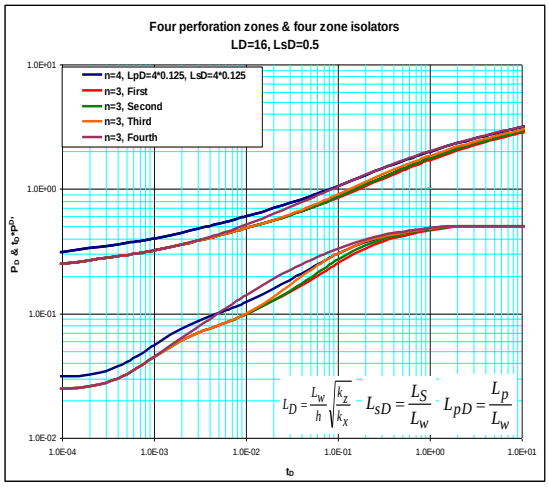

Figure 3-42: Pressure and pressure derivative plot for single failed zonal isolation

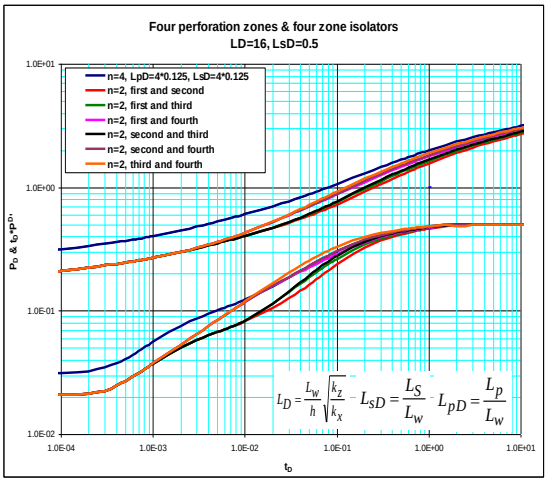

Figure 3-43: Pressure and pressure derivative plot for double failed zonal isolations

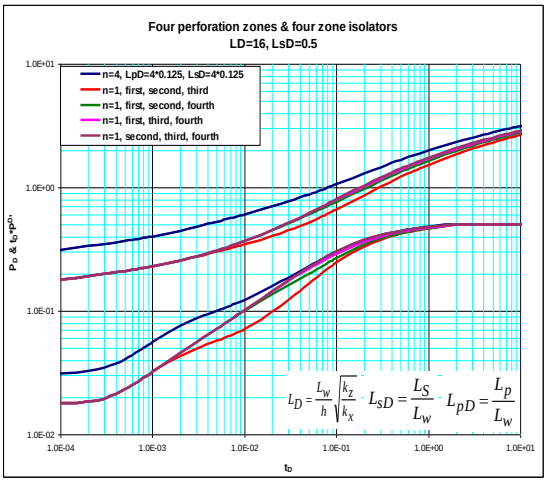

Figure 3-44: Pressure and pressure derivative plot for triple failed zonal isolations.

Example-3-3

A pressure drawdown test of a horizontal well was run to check the performance of zonal isolations. Four zonal isolators have been installed at equal distance starting from the heel of the well. The recorded data is given in Table (Example 3-3) in Appendix F. Other known reservoir and well data are:

q = 1000 STB/D $\quad \phi = 0.1 \quad \mu = 1$ cp $\quad c_t = 2\text{x}10^{-6}$ psi^{-1} $\quad h = 79$ ft

$L_w = 4000$ ft $\quad r_w = 0.462$ ft $\quad p_i = 5000$ psi $\quad B = 1.25$ bbl/STB

Solution

Step-1 Plot (ΔP vs. t) and ($t \times \Delta P'$ vs. t) on log-log paper as shown in Fig. (3-45).

Step-2 Obtain the best match of the data with one of the type curves as shown in Fig. (3-46).

Step-3 Read from any match point: t_M , ΔP_M , t_{DM} , P_{DM} ,, L_{PDM} , n_M , y_{DM}.

$t_M = 100,\ \Delta P_M = 10,\ t_{DM} = 0.165,\ P_{DM} = 0.077,\ L_{PDM} = 0.5,\ L_{sDM} = 0.5, n_M = 3,$
$y_{DM} = 0.0001,\ \ L_{DM} = 16$

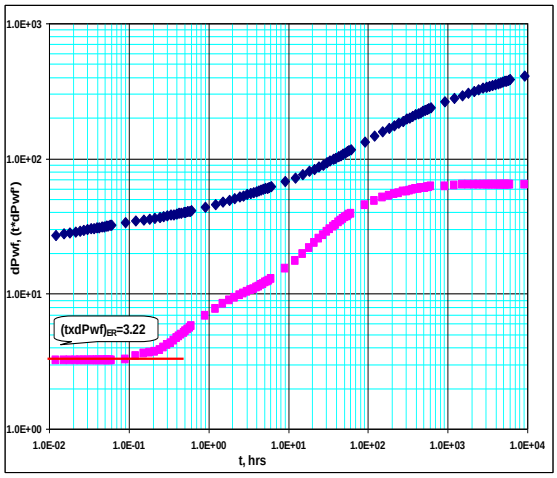

Figure 3-45: Pressure and pressure derivative plot for Example 3-3

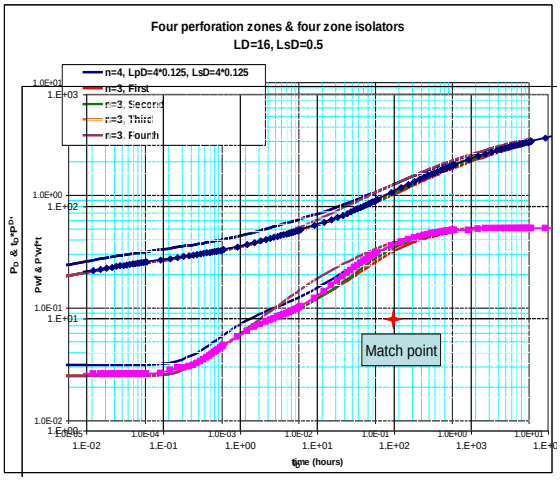

Figure 3-46: Type-curve matching for Example 3-3

From type curve matching, it can be seen that the well has lost the third zonal isolation. Therefore, there are only three working zonal isolations. The location of the failed one is at (3000 ft) from the heel of the well. Other reservoir parameters can be determined as follows:

Step-4 Calculate k_x from Eq. (3-79):

$$k_x = \frac{0.1 \times 1 \times 0.000002 \times 4000^2 \times 0.165}{0.0002637 \times 100} = 20\ md$$

Step-5 Calculate ky from Eq. (3-80):

$$k_y = \frac{1}{20}\left[79\frac{141.2\times1000\times1\times1.25\times0.077}{53\times10}\right]^2 = 15\ md$$

Step-6 Calculate k_z from Eq. (3-81):

$$k_z = \frac{16^2\times79^2\times20}{4000^2} = 2\ md$$

To check the result obtained from the type-curve matching, the following steps can be done:

Step-7- Read the value of $(t\times\Delta P')_{ER}$ corresponding to the early radial flow line from Fig. (3-45).

$$(t\times\Delta P')_{ER} = 3.22$$

Step-8- calculate the value of $(t\times\Delta P')_{ER}$ corresponding to the early radial flow line for the horizontal well with four zonal isolations using Eq. (3-24).

$$(t\times\Delta P')_{ER} = \frac{35.3\times1000\times1\times1.25}{\sqrt{2\times15}\times4\times500} = 4$$

Step-9- The ratio of the calculated value of $(t\times\Delta P')_{ER}$ from step-8 and the one obtained from the plot in step-7, which is (1.25), indicates the perforated sections have been increased by one (from four to five) and similarly the isolated sections have been decreased by one (from four to three).

Table (3-3) shows summary of the calculated parameters for Example 3-1 and the input values.

Table (3-3) Summary of results of Example 3-3.

Parameter	In-put value	Calculated value by Type-curve matching
k_x	20	20
k_y	25	25
k_z	2	2
n (working)	4	4
n (not working)	1 (The third)	1 (The third)
Location of non-working zonal isolation	3000 ft from the heel	3000 ft from the heel

4- MATHEMATICAL MODELS FOR MULTIPLE INCLINED HYDRAULIC FRACTURES

The hydraulic fracturing process can be defined as the process of generating a fracture or fracture system in a formation by injecting fracturing fluid under pressure higher than the tensile strength of the formation through a wellbore in order to overcome in-situ stresses and to cause rock's failure in the porous medium.

The hydraulic fractures are propagated approximately perpendicular to the axis of the minimum horizontal principal stress. Therefore, horizontal hydraulic fractures are expected to occur at shallow depth where the vertical (overburden pressure) is the least principal stress as shown in Fig. (4-1), while vertical hydraulic fractures usually occur where the depth is great and the least stress is one of the horizontal stress components as shown in Fig. (4-2).

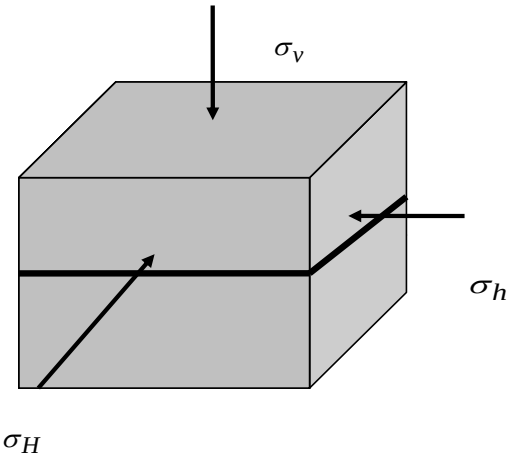

Figure 4-1: Horizontal fracture for $\sigma_v < \sigma_h < \sigma_H$

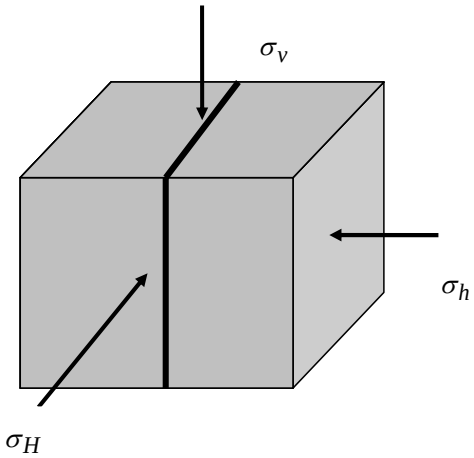

Figure 4-2: Vertical fracture for $\sigma_h < \sigma_H < \sigma_v$

Hubbert et al. (1957) stated that for tectonically relaxed layers characterized by normal fault, the least principal stress should be horizontal, thus the fractures should propagate in the vertical direction with the injection pressure less than the overburden

pressure. In the areas of active tectonic compression such as thrust fault, the least principal stress should be vertical and equal to the pressure of the overburden. The fractures in this case should propagate in the horizontal direction with injection pressure equal to or greater than the overburden. However, experiments conducted by Hubbert et al., that simulated tectonic movements, only considered the case where the movements are uniform vertically and horizontally and thus, there were no shear stresses involved. This is not always the case in actual field situations where reservoirs may contain complex stress fields due to geological structure, pore pressure and tectonic movements.

4-1-State of in-situ stress

Economides et al 1989, explained that the in-situ stress underground is affected by the following components:

- **Overburden pressure:** Represents the amount of pressure from the overlying rock layers.
- **Tectonic Stresses:** Formed by large crustal movements and introduced additional directional components which can be added to the stress components already described.
- **Topographical Effects:** The computed overburden stress will not, in general, be the same as the true vertical stress where there is a significant topography. Some times, vertical stress increases with depth at a rate greater than the overburden due to extra loading by the surrounding topography.
- **Other Stresses:** Other factors affecting the in-situ stress include rock types, thermal effect, change of layers' volume due to chemical processes, and presence of faulting.

- **Induced Stresses:** Drilling of a borehole and injection of fluid such as water in water flooding process, can also alter the in-situ stress.

4-2- Inclined Hydraulic Fractures

Several researches and studies have indicated that hydraulic fractures are not necessary to propagate truly vertical or horizontal due to the effect of the in-situ stress distribution. In realty, it is difficult to control the orientation of the hydraulic fractures as a result of the difficulty of controlling the parameters that affect the propagation direction. Some of these parameters relate to the formation rock properties while others relate to the stresses. Daneshy (1970) showed through a series of experiments on different rock types that the appearance of a vertical fracture at the wellbore is not sufficient evidence to ensure a vertical fracture. He asserted that the fracture can change direction once it gets sufficiently away from the wellbore according to the least principal stress. He also investigated theoretically and experimentally inclined fractures. In this study, he confirmed that inclined fractures often intersect the borehole along two diametrically opposite axial lines, thus giving it the appearance of a vertical fracture. The fractures then changed their orientation as they extend away from the wellbore until they become perpendicular to the least compressive in-situ principal stress.

Wright et al 1995, explained that the production process may lead to fractures reorientation due to the change in the in-situ stress distribution. They stated that the inclination angle of a vertical fracture from the vertical axis increases with the continuous production as shown in Fig. (4-3). Therefore a dip angle of more than (35) degree is not rare as it was thought before.

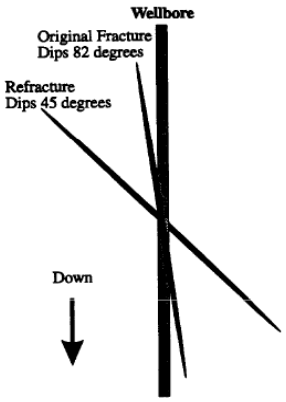

Figure 4-3: Effect of depletion production on hydraulic fracture orientation (Wright et al 1995).

4-3- Models Derivation

In this chapter, several analytical models for the pressure behavior of a horizontal well intersected by multiple-inclined hydraulic fractures will be introduced. Both longitudinal and transverse fractures will be considered for both the deviation from the vertical axis and the deviation from the horizontal axis where the horizontal well is assumed to extend. The following facts would be important to be noticed:

- The flow from the reservoir to the wellbore sections between fractures is negligible as compared with the flow from the reservoir to the fracture plane.
- Fluid flows from the reservoir to the well through planar and totally penetrating vertical fractures.
- A first approximation of the behavior of the system is the uniform flux fracture case. It is assumed that fluid enters the fractures at a uniform rate per unit area of the fracture face.
- In the analysis, flow through the fractures is considered and the flow through the matrix is ignored. This is a reasonable assumption since multiple fractures are

typically created in very low permeability formations and the wells are very often cased and perforated. Moreover, fractures are initiated at the perforations.

The following assumptions are important for the derivation of the model:

1- The reservoir is homogenous, having constant and uniform thickness with two impermeable layers at the top and bottom of the formation.

2- Constant porosity and permeability in each direction, but the formation is anisotropic.

3- Gravitational and frictional effects are negligible.

4- The well is extending in the midpoint of the formation height (symmetrical).

5- Single phase fluid of small and constant compressibility, constant viscosity, and formation volume factor, flows from the reservoir to the fractures.

6- Reservoir pressure is initially constant.

$$P\big|_{t=0} = P_i \tag{4-1}$$

7- The pressure at the outer boundaries of the reservoir is assumed to be constant and equal to the initial reservoir pressure.

$$P_e = P_i \tag{4-2}$$

8- The pressure at the upper and lower impermeable boundaries is assumed to be constant so that:

$$\left.\frac{\partial P}{\partial Z}\right|_{Z=0} = 0 \tag{4-3}$$

$$\left.\frac{\partial P}{\partial Z}\right|_{Z=h} = 0 \tag{4-4}$$

9- Considering the problem of production from an infinite reservoir. Diffusivity equation can be written as:

$$\eta_x \frac{\delta^2 \Delta P}{\delta x_D{}^2} + \eta_y \frac{\delta^2 \Delta P}{\delta y_D{}^2} + \eta_z \frac{\delta^2 \Delta P}{\delta z_D{}^2} = \frac{\delta \Delta P}{\delta t_D} \tag{4-5}$$

Many techniques have been used to solve the diffusivity equation for different applications in the petroleum industry such as the study of the pressure transient behavior in porous media. Two commonly used solutions for this equation can be found in the literature. An early solution, treated by Carslaw and Jaeger, was derived based on the use of Lord Kelvin's point source solution for solving heat conduction problem. The second one was introduced by Gringarten and Ramey in 1973 based on the use of the Green's function method. Many instantaneous source solutions for different configurations (point source, line source, plane source, slab source) have been developed based on the two solutions.

4-3-1-Transverse fractures

Consider a horizontal well with multiple-inclined transverse hydraulic fractures in an infinite, homogenous, isotropic or anisotropic $\left(k = k_x = \sqrt{k_{yz}}\right)$ formation, horizontal slab reservoir as shown in fig. (4-4). Each fracture is considered as a single plane of length ($2x_f$), width (w), height (h_f), and an angle of inclination from the vertical direction (θ_v). The spacing between fractures is (D). If we assume that all fluid withdrawal will be through the fractures, and further, that the fractures are fully penetrating the formation, the fractures can be simulated as inclined plane sources. The unsteady state pressure drop created by these planes at any point (x_m, y_m, z_m) is:

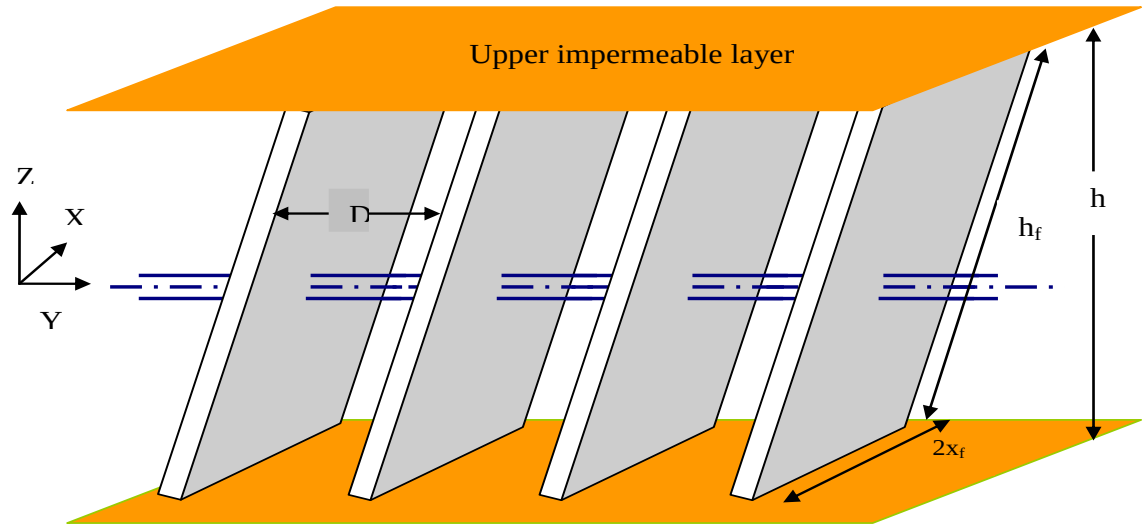

Figure 4-4: Horizontal well intersected by multiple-inclined transverse hydraulic fractures.

$$P(x_m, y_m, z_m, t, \theta, z_f, h_f, x_f, h) = \frac{q}{\phi c}\int_0^t S_{xyz}(x_m, y_m, z_m, t-\tau, \theta, z_f, h_f, x_f, h)d\tau \qquad (4\text{-}6)$$

Where (S_{xyz}) is the instantaneous source function for an inclined plane source in an infinite slab reservoir. q is the fluid withdrawal per unit fracture surface area per unit time.

$$q = \frac{Q}{2nx_f h_f} \qquad (4\text{-}7)$$

The source function (S_{xyz}) can be obtained using Newman product method. This method proposed that the instantaneous uniform flux source function for a three dimensional flow problem can be obtained as the product of instantaneous source function for a one dimensional flow problem. Therefore:

$$S_{xyz}(x_m, y_m, z_m, t, \theta_v, z_f, h_f, x_f, h) = S_{yz}(y_m, z_m, t, \theta_v, z_f, h_f, h) * S_x(x_m, t, x_f) \qquad (4\text{-}8)$$

S_{yz} is the instantaneous source function for an inclined plane source in an infinite slab reservoir. S_x is the instantaneous source function for an infinite slab source in an

infinite reservoir in the direction of X-axis as shown in Fig. (4-5). S_x can be estimated based on half fracture length as follows:

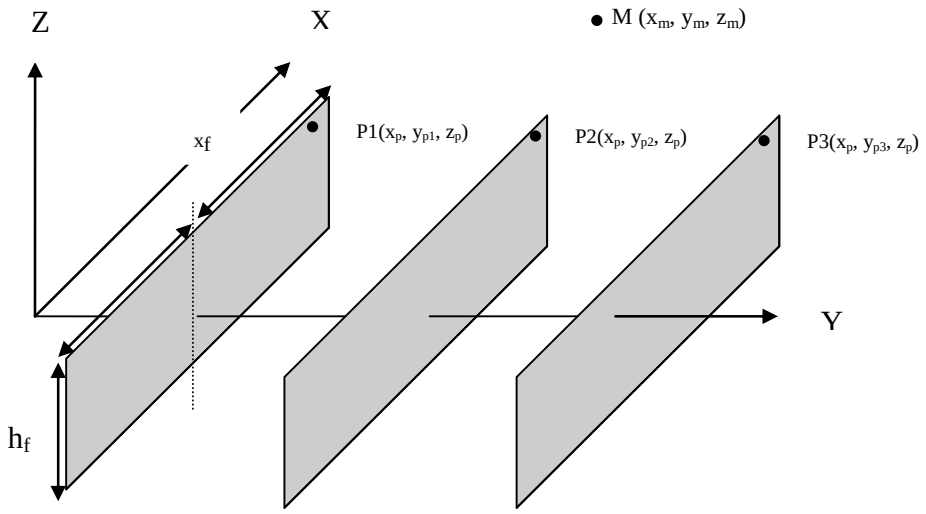

Figure 4-5: The monitoring point and the source points for multiple- inclined transverse hydraulic fractures.

$$S_x = \frac{1}{2\sqrt{\pi\eta t}} e^{-\frac{(x_m - x')^2}{4\eta t}} = \frac{1}{2\sqrt{\pi\eta t}} \int_{-x_f}^{x_f} e^{-\frac{(x_m - x - x_p)}{4\eta t}} dx_p = \frac{1}{2}\left[erf\left(\frac{x_m - x + x_f}{2\sqrt{\eta t}} \right) - erf\left(\frac{x_m - x - x_f}{2\sqrt{\eta t}} \right) \right] \quad (4\text{-}9)$$

S_{yz} can be derived as follows:

$$S_{yz}\left(y_m, z_m, t, \phi_v, h, h_f\right) = \frac{1}{4\eta\pi t} e^{-\frac{d^2}{4\eta t}} \quad (4\text{-}10)$$

Where d is the distance, in the (YZ) plane normal to the hydraulic fractures propagation, between the monitoring point (M) and the production points (P1, P2, P3) as shown in Fig. (4-6).

$$S_{yz}\left(y_m, z_m, t, \phi_v, h, h_f\right) = \frac{1}{4\eta\pi t} \int_{-\frac{h_f}{2}\cos(\phi_v)}^{\frac{h_f}{2}\cos(\phi_v)} \left[e^{-\frac{(P_1M)^2}{4\eta t}} + e^{-\frac{(P_2M)^2}{4\eta t}} + e^{-\frac{(P_3M)^2}{4\eta t}} \right] dh_f \qquad (4\text{-}11)$$

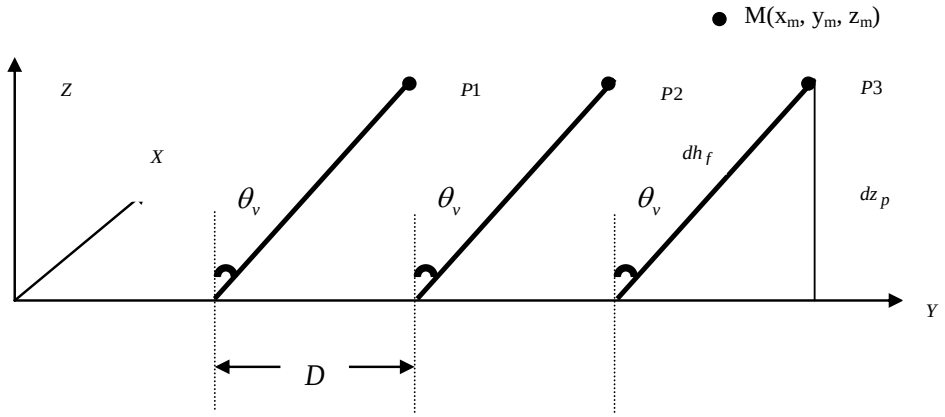

Figure 4-6: Schematic diagram for horizontal well intersected by multiple- inclined transverse hydraulic fractures.

The distance between the monitoring point and each production point can be calculated as shown in Fig. (4-7) as follows:

$$(P_1M)^2 = (y_m - y - D - zp \times \tan(\theta_v))^2 + (z_m - (z + z_p))^2 \qquad (4\text{-}12)$$

Similarly:

$$(P_2M)^2 = (y_m - y - 2D - zp \times \tan(\theta_v))^2 + (z_m - (z + z_p))^2 \qquad (4\text{-}13)$$

$$(P_3M)^2 = (y_m - y - 3D - zp \times \tan(\theta_v))^2 + (z_m - (z + z_p))^2 \qquad (4\text{-}14)$$

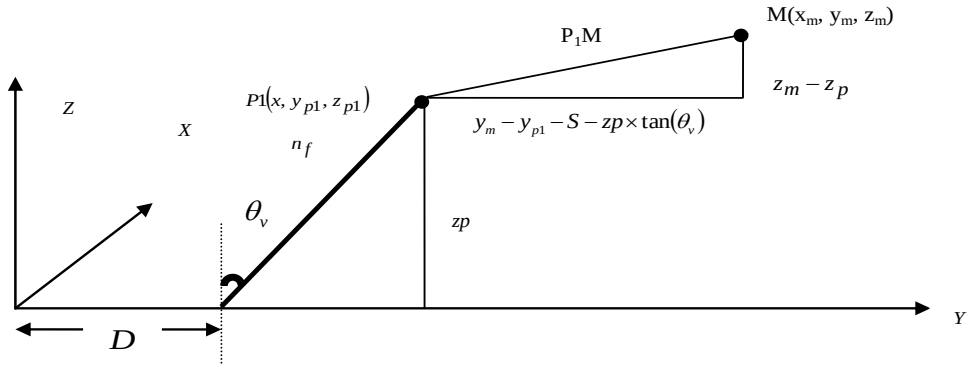

Figure 4-7: The distance between the monitoring point and production points.

The distances between the monitoring point and the images as shown in Fig. (4-8) are:

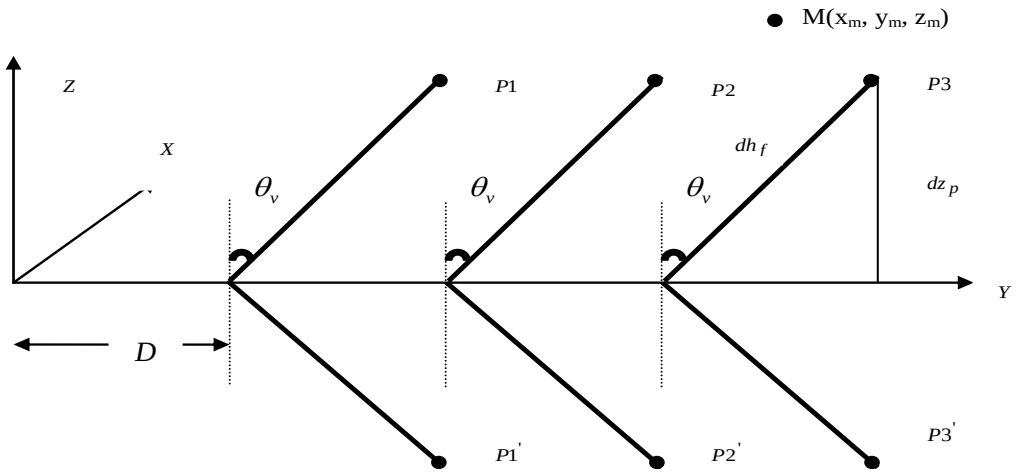

Figure 4-8: Superposition principles for multiple-inclined fractures.

$$\left(P_1^{'}M\right)^2=\left(y_m-y-D+zp\times\tan(\theta_v)\right)^2+\left(z_m-(z_p-z)\right)^2 \tag{4-15}$$

Similarly:

$$\left(P_2^{'}M\right)^2=\left(y_m-y-2D+zp\times\tan(\theta_v)\right)^2+\left(z_m-(z_p-z)\right)^2 \tag{4-16}$$

$$\left(P_3^{'}M\right)^2=\left(y_m-y-3D+zp\times\tan(\theta_v)\right)^2+\left(z_m-(z_p-z)\right)^2 \tag{4-17}$$

and;

$$dh_f=\frac{dz_p}{\cos(\theta_v)} \tag{4-18}$$

Eq. (4-11) can be written as follows:

$$S_{yz}=\frac{1}{4\eta\pi t\cos(\theta_v)}\int_{-\frac{h_f}{2}\cos(\theta_v)}^{\frac{h_f}{2}\cos(\theta_v)}\left\{\left[e^{-\frac{\left[y_m-\left(y+D+z_p\tan(\theta_v)\right)\right]^2+\left[z_m-(z+z_p)\right]^2}{4\eta t}}+e^{-\frac{\left[y_m-\left(y+D-z_p\tan(\theta_v)\right)\right]^2+\left[z_m-(z_p-z)\right]^2}{4\eta t}}\right]+\left[e^{-\frac{\left[y_m-\left(y+2D+z_p\tan(\theta_v)\right)\right]^2+\left[z_m-(z+z_p)\right]^2}{4\eta t}}+e^{-\frac{\left[y_m-\left(y+2D-z_p\tan(\theta_v)\right)\right]^2+\left[z_m-(z_p-z)\right]^2}{4\eta t}}\right]+\left[e^{-\frac{\left[y_m-\left(y+3D+z_p\tan(\theta_v)\right)\right]^2+\left[z_m-(z+z_p)\right]^2}{4\eta t}}+e^{-\frac{\left[y_m-\left(y+3D-z_p\tan(\theta_v)\right)\right]^2+\left[z_m-(z_p-z)\right]^2}{4\eta t}}\right]\right\}dz_p \tag{4-19}$$

For (n) number of fractures, Eq. (4-19) can be written as:

$$S_{yz}=\frac{1}{4\eta\pi t\cos(\theta_v)}\sum_{n=1}^{n=\infty}\int_{-\frac{h_f}{2}\cos(\theta_v)}^{\frac{h_f}{2}\cos(\theta_v)}\left[e^{-\frac{\left[y_m-\left(y+nD+z_p\tan(\theta_v)\right)\right]^2+\left[z_m-(z+z_p)\right]^2}{4\eta t}}+e^{-\frac{\left[y_m-\left(y+nD-z_p\tan(\theta_v)\right)\right]^2+\left[z_m-(z_p-z)\right]^2}{4\eta t}}\right]dz_p \quad (4\text{-}20)$$

Applying superposition theory:

$$S_{yz}=\frac{1}{4\eta\pi t\cos(\theta_v)}\sum_{n=1}^{n=\infty}\sum_{N=-\infty}^{N=\infty}\int_{-\frac{h_f}{2}\cos(\theta_v)}^{\frac{h_f}{2}\cos(\theta_v)}\left[e^{-\frac{\left[y_m-\left(y+nD+z_p\tan(\theta_v)\right)\right]^2+\left[z_m+2Nh-(z+z_p)\right]^2}{4\eta t}}+e^{-\frac{\left[y_m-\left(y+nD-z_p\tan(\theta_v)\right)\right]^2+\left[z_m+2Nh-(z_p-z)\right]^2}{4\eta t}}\right]dz_p \quad (4\text{-}21)$$

The two exponential terms in Eq. (4-21) can be solved as follows:

$$e^{-\frac{\left[y_m-\left(y+nD+z_p\tan(\theta_v)\right)\right]^2+\left[z_m+2Nh-(z+z_p)\right]^2}{4\eta t}}=\left[\frac{z_p}{\cos(\theta_v)}-\sin(\theta_v)(y_m-y-nD)-\cos(\theta_v)(z_m-z+2Nh)\right]^2+\left[\cos(\theta_v)(y_m-y-nD)-\sin(\theta_v)(z_m-z+2Nh)\right]^2 \quad (4\text{-}22)$$

$$e^{-\frac{\left[y_m-\left(y+nD-z_p\tan(\theta_v)\right)\right]^2+\left[z_m+2Nh-(z_p+z)\right]^2}{4\eta t}}=\left[\frac{z_p}{\cos(\theta_v)}+\sin(\theta_v)(y_m-y-nD)-\cos(\theta_v)(z_m+z+2Nh)\right]^2+\left[\cos(\theta_v)(y_m-y-nD)+\sin(\theta_v)(z_m+z+2Nh)\right]^2 \quad (4\text{-}23)$$

therefore Eq. (4-21) can be written as:

$$S_{yz}=\frac{1}{4\pi\eta t\cos(\theta_v)}\sum_{n=1}^{n=\infty}\sum_{N=-\infty}^{N=\infty}\left\{\left[e^{-\frac{\left[\cos(\theta_v)(y_m-y-nD)-\sin(\phi_v)(z_m-z+2Nh\right]^2}{4\eta t}}\int_{-\frac{h_f}{2}\cos(\theta_v)}^{\frac{h_f}{2}\cos(\theta_v)}e^{-\frac{\left[\frac{z_p}{\cos(\theta_v)}-\sin(\theta_v)(y_m-y-nD)-\cos(\theta_v)(z_m-z+2Nh)\right]^2}{4\eta t}}\right]+\left[e^{-\frac{\left[\cos(\theta_v)(y_m-y-nD)+\sin(\theta_v)(z_m+z+2Nh)\right]^2}{4\eta t}}\int_{-\frac{h_f}{2}\cos(\theta_v)}^{\frac{h_f}{2}\cos(\theta_v)}e^{-\frac{\left[\frac{z_p}{\cos(\theta_v)}+\sin(\theta_v)(y_m-y-nD)-\cos(\theta_v)(z_m+z+2Nh)\right]^2}{4\eta t}}\right]\right\}dz_p \quad (4\text{-}24)$$

Integrating for (z_p), Eq.(4-24) becomes:

$$S_{yz}=\frac{1}{4\sqrt{\pi\eta t}}\sum_{n=1}^{n=\infty}\sum_{N=-\infty}^{N=\infty}\left\{\begin{array}{l}\left[\begin{array}{l}e^{-\frac{[\cos(\theta_v)(y_m-y-nD)-\sin(\theta_v)(z_m-z+2Nh)]^2}{4\eta t}}\\ \left[erf\left(\frac{h_f/2-\sin(\theta_v)(y_m-y-nD)-\cos(\theta_v)(z_m-z+2Nh)}{2\sqrt{\eta t}}\right)\right.\\ \left.-erf\left(\frac{-h_f/2-\sin(\theta_v)(y_m-y-nD)-\cos(\theta_v)(z_m-z+2Nh)}{2\sqrt{\eta t}}\right)\right]\end{array}\right]+\\ \left[\begin{array}{l}e^{-\frac{[\cos(\theta_v)(y_m-y-nD)+\sin(\theta_v)(z_m+z+2Nh)]^2}{4\eta t}}\\ \left[erf\left(\frac{h_f/2+\sin(\theta_v)(y_m-y-nD)-\cos(\theta_v)(z_m+z+2Nh)}{2\sqrt{\eta t}}\right)\right.\\ \left.-erf\left(\frac{-h_f/2+\sin(\theta_v)(y_m-y-nD)-\cos(\theta_v)(z_m+z+2Nh)}{2\sqrt{\eta t}}\right)\right]\end{array}\right]\end{array}\right\} \quad (4\text{-}25)$$

Substitute Eqs. (4-7), (4-9), and (4-25) in Eq. (4-6), the pressure drop can be found as follows:

$$\Delta P=\frac{q}{16nx_f h_f\phi c\sqrt{\pi\eta}}\int_0^t\frac{1}{\sqrt{t}}\left[erf\left(\frac{x_m-x+x_f}{2\sqrt{\eta t}}\right)-erf\left(\frac{x_m-x-x_f}{2\sqrt{\eta t}}\right)\right]$$
$$\sum_{n=1}^{n=\infty}\sum_{N=-\infty}^{N=\infty}\left\{\begin{array}{l}\left[\begin{array}{l}e^{-\frac{[\cos(\theta_v)(y_m-y-nD)-\sin(\theta_v)(z_m-z+2Nh)]^2}{4\eta t}}\\ \left[erf\left(\frac{h_f/2-\sin(\theta_v)(y_m-y-nD)-\cos(\theta_v)(z_m-z+2Nh)}{2\sqrt{\eta t}}\right)\right.\\ \left.-erf\left(\frac{-h_f/2-\sin(\theta_v)(y_m-y-nD)-\cos(\theta_v)(z_m-z+2Nh)}{2\sqrt{\eta t}}\right)\right]\end{array}\right]+\\ \left[\begin{array}{l}e^{-\frac{[\cos(\theta_v)(y_m-y-nS)+\sin(\theta_v)(z_m+z+2Nh)]^2}{4\eta t}}\\ \left[erf\left(\frac{h_f/2+\sin(\theta_v)(y_m-y-nD)-\cos(\theta_v)(z_m+z+2Nh)}{2\sqrt{\eta t}}\right)\right.\\ \left.-erf\left(\frac{-h_f/2+\sin(\theta_v)(y_m-y-nD)-\cos(\theta_v)(z_m+z+2Nh)}{2\sqrt{\eta t}}\right)\right]\end{array}\right]\end{array}\right\}dt \quad (4\text{-}26)$$

In dimensionless form, the final model for pressure response of horizontal wells intersected by multiple-inclined fully penetrating transverse hydraulic fractures is:

$$P_D = \frac{\sqrt{\pi}\cos(\theta_v)}{8n}\int_0^{t_D}\frac{1}{\sqrt{\tau_D}}\left[erf\left(\frac{x_D+1}{2\sqrt{\tau}}\right)-erf\left(\frac{x_D-1}{2\sqrt{\tau}}\right)\right]$$

$$\sum_{n=1}^{n=\infty}\sum_{N=-\infty}^{N=\infty}\left\{\left[\begin{array}{l} e^{-\frac{\left[\cos(\theta_v)(y_D-nD_D)-\sin(\theta_v)(z_D-z_{fD}+2Nh_D\right]^2}{4\tau}} \\ \left[erf\left(\frac{h_{fD}/2-\sin(\theta_v)(y_D-nD_D)-\cos(\theta_v)(z_D-z_{fD}+2Nh_D)}{2\sqrt{\tau}}\right)\right. \\ \left.-erf\left(\frac{-h_{fD}/2-\sin(\theta_v)(y_D-nD_D)-\cos(\theta_v)(z_D-z_{fD}+2Nh_D)}{2\sqrt{\tau}}\right)\right] \end{array}\right]+\right.$$

$$\left.\left[\begin{array}{l} e^{-\frac{\left[\cos(\theta_v)(y_D-nD_D)+\sin(\theta_v)(z_D+z_{fD}+2Nh_D)\right]^2}{4\tau}} \\ \left[erf\left(\frac{h_{fD}/2+\sin(\theta_v)(y_D-nD_D)-\cos(\theta_v)(z_D+z_{fD}+2Nh_D)}{2\sqrt{\tau}}\right)\right. \\ \left.-erf\left(\frac{-h_{fD}/2+\sin(\theta_v)(y_D-nD_D)-\cos(\theta_v)(z_D+z_{fD}+2Nh_D)}{2\sqrt{\tau}}\right)\right] \end{array}\right]\right\}d\tau$$

(4-27)

where:

$$x_D = \frac{x_m - x}{x_f} \tag{4-28}$$

$$y_D = \frac{y_m - y}{x_f} \tag{4-29}$$

$$z_D = \frac{z_m}{x_f} \tag{4-30}$$

$$h_{fD} = \frac{h_f}{x_f} \tag{4-31}$$

$$z_{fD} = \frac{z}{x_f} \tag{4-32}$$

$$h_D = \frac{h}{x_f} \tag{4-33}$$

$$D_D = \frac{D}{x_f} \tag{4-34}$$

$$t_D = \frac{0.0002637\,kt}{\phi\,\mu\,c\,x_f^2} \tag{4-35}$$

$$P_D = \frac{2\pi kh\Delta P}{q\mu} \tag{4-36}$$

$$k = k_x = k_{yz} \tag{4-37}$$

$$k_{yz} = \sqrt{k_y k_z} \tag{4-38}$$

To solve the above model given in Eq. (4-27), two long time approximations should be done based on the fluid flow dynamics and flow regimes in late time. The first one is the approximation for the instantaneous source function for an infinite slab source in an infinite reservoir S_x given by Eq. (4-9). The second one is the approximation for the instantaneous source function for an inclined plane source in an infinite slab reservoir S_{yz} given in Eq. (4-25).

Eq. (4-27) can be redefined as follows:

$$P_D = \frac{1}{2}\int_0^{t_D} X(x_D,\tau)\times YZ(y_D,z_D,\tau,\theta_v,z_{fD},h_{fD},h_D)\,d\tau \tag{4-39}$$

where:

$$X(x_D,\tau_D) = \frac{\sqrt{\pi}}{2\sqrt{t_D}}\left[erf\left(\frac{x_D+1}{2\sqrt{t_D}}\right) - erf\left(\frac{x_{D-1}}{2\sqrt{t_D}}\right)\right] \tag{4-40}$$

$$YZ=\frac{\cos(\theta_v)}{2n}\int_0^{t_D}\sum_{n=1}^{n=\infty}\sum_{N=-\infty}^{N=\infty}\left\{\begin{array}{l}\left[\begin{array}{l}e^{-\frac{\left[\cos(\theta_v)(y_D-nD_D)-\sin(\theta_v)(z_D-z_{fD}+2Nh_D)\right]^2}{4\tau}}\\ \left[\begin{array}{l}erf\left(\dfrac{h_{fD}/2-\sin(\theta_v)(y_D-nD_D)-\cos(\theta_v)(z_D-z_{fD}+2Nh_D)}{2\sqrt{\tau}}\right)\\ -erf\left(\dfrac{-h_{fD}/2-\sin(\theta_v)(y_D-nD_D)-\cos(\theta_v)(z_D-z_{fD}+2Nh_D)}{2\sqrt{\tau}}\right)\end{array}\right]\end{array}\right]+\\ \left[\begin{array}{l}e^{-\frac{\left[\cos(\theta_v)(y_D-nD_D)+\sin(\theta_v)(z_D+z_{fD}+2Nh_D)\right]^2}{4\tau}}\\ \left[\begin{array}{l}erf\left(\dfrac{h_{fD}/2+\sin(\theta_v)(y_D-nD_D)-\cos(\theta_v)(z_D+z_{fD}+2Nh_D)}{2\sqrt{\tau}}\right)\\ -erf\left(\dfrac{-h_{fD}/2+\sin(\theta_v)(y_D-nD_D)-\cos(\theta_v)(z_D+z_{fD}+2Nh_D)}{2\sqrt{\tau}}\right)\end{array}\right]\end{array}\right]\end{array}\right\}d\tau \tag{4-41}$$

The error functions in Eq. (4-40) can be approximated as follows:

$$erf\left(\frac{x_{D+1}}{2\sqrt{t_D}}\right)=\frac{2}{\pi}\sum_{n=0}^{n=\infty}\frac{(-1)^n}{n!}\frac{\left(\dfrac{x_{D+1}}{2\sqrt{t_D}}\right)^{2n+1}}{(2n+1)}=\frac{x_{D+1}}{\sqrt{t_D}}-\frac{(x_D+1)^3}{12t_D^{3/2}}+\frac{(x_D+1)^5}{160t_D^{5/2}}-.....+.....\cong\frac{x_D+1}{\sqrt{t_D}} \tag{4-42}$$

Since:

$$\frac{x_D+1}{\sqrt{t_D}}\geq\frac{100(x_D+1)^3}{12t_D^{3/2}} \tag{4-43}$$

therefore:

$$t_D\geq\frac{25}{3}(xD+1) \tag{4-44}$$

Similarly:

$$erf\left(\frac{x_D}{2\sqrt{t_D}}-1\right)=\frac{2}{\pi}\sum_{n=0}^{n=\infty}\frac{(-1)^n}{n!}\frac{\left(\dfrac{x_{D11}}{2\sqrt{t_D}}\right)^{2n+1}}{(2n+1)}=\frac{x_{D11}}{\sqrt{t_D}}-\frac{(x_D-1)^3}{12t_D^{3/2}}+\frac{(x_D-1)^5}{160t_D^{5/2}}-.....+.....\cong\frac{x_D-1}{\sqrt{t_D}} \tag{4-45}$$

and

$$t_D \geq \frac{25}{3}(xD-1) \tag{4-46}$$

Substitute Eqs. (4-43) and (4-45) in Eq. (4-40):

$$X(x_D, t_D) = \frac{\sqrt{\pi}}{4}\left[erf\left(\frac{x_D+1}{2\sqrt{t_D}}\right) - erf\left(\frac{x_D-1}{2\sqrt{t_D}}\right)\right] = \frac{1}{t_D} \tag{4-47}$$

while:

$$YZ = \frac{\cos(\theta_v)}{2n}\int_0^{t_D}\sum_{n=1}^{n=\infty}\sum_{N=-\infty}^{N=\infty}\left\{\begin{array}{l} \left[e^{-\frac{\left[\cos(\theta_v)(y_D-nD_D)-\sin(\theta_v)(z_D-z_{fD}+2Nh_D)\right]^2}{4\tau}} \right. \\ \left[erf\left(\frac{h_{fD}/2-\sin(\theta_v)(y_D-nD_D)-\cos(\theta_v)(z_D-z_{fD}+2Nh_D)}{2\sqrt{\tau}}\right)\right. \\ \left.\left. -erf\left(\frac{-h_{fD}/2-\sin(\theta_v)(y_D-nD_D)-\cos(\theta_v)(z_D-z_{fD}+2Nh_D)}{2\sqrt{\tau}}\right)\right]\right] + \\ \left[e^{-\frac{\left[\cos(\theta_v)(y_D-nD_D)+\sin(\theta_v)(z_D+z_{fD}+2Nh_D)\right]^2}{4\tau}} \right. \\ \left[erf\left(\frac{h_{fD}/2+\sin(\theta_v)(y_D-nD_D)-\cos(\theta_v)(z_D+z_{fD}+2Nh_D)}{2\sqrt{\tau}}\right)\right. \\ \left.\left. -erf\left(\frac{-h_{fD}/2+\sin(\theta_v)(y_D-nD_D)-\cos(\theta_v)(z_D+z_{fD}+2Nh_D)}{2\sqrt{\tau}}\right)\right]\right] \end{array}\right\} d\tau = 1 \tag{4-48}$$

$$t_D \geq \frac{25}{3}\left[\frac{h_{fD}}{2} - \sin(\theta_v)(y_D-nD_D) - \cos(\theta_v)(z_D-z_{fD}+2h_D)\right]^2 \tag{4-49}$$

$$t_D \geq \frac{25}{3}\left[-\frac{h_{fD}}{2} - \sin(\theta_v)(y_D-nD_D) - \cos(\theta_v)(z_D-z_{fD}+2h_D)\right]^2 \tag{4-50}$$

$$t_D \geq \frac{25}{3}\left[\frac{h_{fD}}{2} + \sin(\theta_v)(y_D-nD_D) - \cos(\theta_v)(z_D+z_{fD}+2h_D)\right]^2 \tag{4-51}$$

$$t_D \geq \frac{25}{3}\left[\frac{h_{fD}}{2} + \sin(\theta_v)(y_D-nD_D) - \cos(\theta_v)(z_D+z_{fD}+2h_D)\right]^2 \tag{4-52}$$

$$t_D \geq 25\left[\cos(\theta_v)(y_D-nD_D) - \sin(\theta_v)(z_D-z_{fD}+2h_D)\right]^2 \tag{4-53}$$

$$t_D \geq 25\left[\cos(\theta_v)(y_D-nD_D) + \cos(\theta_v)(z_D+z_{fD}+2h_D)\right]^2 \tag{4-54}$$

The long time approximation can be written based on Eq. (4-39) as:

$$P_D = \frac{q}{2nx_f h_f \theta \mu} \int_0^{t_{D1}} X(x_D, t_D) \times YZ(y_D, z_D, t_D, \phi_v, z_{fD}, h_{fD}, h_D) + \frac{1}{2} \int_{t_{D1}}^{t_D} \frac{1}{\tau_D} d\tau_D$$
$$= P_D(x_D, y_D, z_D, z_{wD}, L_D, t_{D1}) + \frac{1}{2} \ln\left(\frac{t_D}{t_{D1}}\right) \tag{4-55}$$

and the proper time for this approximation is:

$$t_{D1} \geq \begin{bmatrix} \frac{25}{3}(xD+1) \\ \frac{25}{3}(xD-1) \\ \frac{25}{3}\left[\frac{h_{fD}}{2} - \sin(\theta_v)(y_D - nD_D) - \cos(\theta_v)(z_D - z_{fD} + 2h_D)\right]^2 \\ \frac{25}{3}\left[-\frac{h_{fD}}{2} - \sin(\theta_v)(y_D - nD_D) - \cos(\theta_v)(z_D - z_{fD} + 2h_D)\right]^2 \\ \frac{25}{3}\left[\frac{h_{fD}}{2} + \sin(\theta_v)(y_D - nD_D) - \cos(\theta_v)(z_D + z_{fD} + 2h_D)\right]^2 \\ \frac{25}{3}\left[\frac{h_{fD}}{2} + \sin(\theta_v)(y_D - nD_D) - \cos(\theta_v)(z_D + z_{fD} + 2h_D)\right]^2 \\ 25\left[\cos(\theta_v)(y_D - nD_D) - \sin(\theta_v)(z_D - z_{fD} + 2h_D)\right]^2 \\ 25\left[\cos(\theta_v)(y_D - nD_D) + \cos(\theta_v)(z_D + z_{fD} + 2Nh_D)\right]^2 \end{bmatrix} \tag{4-56}$$

4-3-2- Longitudinal fractures

Consider a horizontal well with multiple-inclined longitudinal hydraulic fractures in an infinite, homogenous, isotropic or anisotropic $\left(k = k_y = \sqrt{k_{xz}}\right)$, horizontal slab reservoir as shown in fig. (4-9). Each fracture is considered as a single plane of length ($2x_f$), width (w), height (h_f), and an angle of inclination from the vertical direction (θ_v). The spacing between fractures is (D). If we assume that all fluid withdrawal will be through the fractures, and that the fractures are fully penetrating the formation, the fractures can be simulated as inclined plane sources. The unsteady state pressure drop

created by these planes at any point can be found using same procedures of transverse fractures:

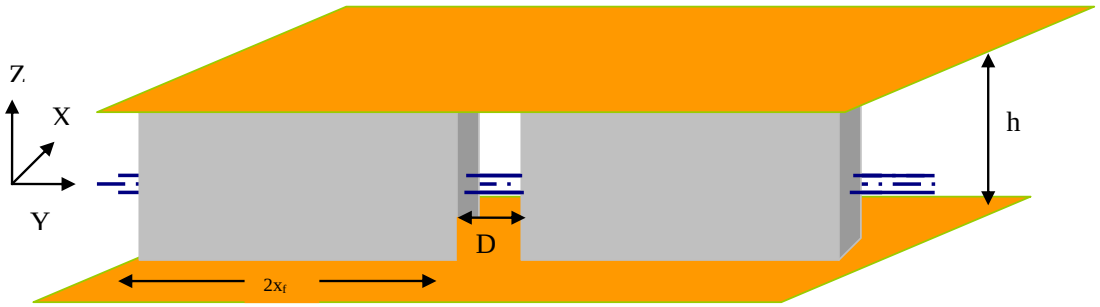

Figure 4-9: Horizontal well intersected by multiple-inclined longitudinal hydraulic fractures.

The source function (S_{xyz}) in this case is;

$$S_{xyz}(x_m, y_m, z_m, t, \theta_v, z_f, h_f, x_f, h) = S_{xz}(y_m, z_m, t, \theta_v, z_f, h_f, h) * S_y(x_m, t, x_f) \qquad (4\text{-}57)$$

Where (S_{xz}) is the instantaneous source function for an inclined plane source in an infinite slab reservoir. S_y is the instantaneous source function for an infinite slab source in an infinite reservoir in the direction of Y-axis as shown in Fig. (4-10). S_y can be estimated based on half fracture length as follows:

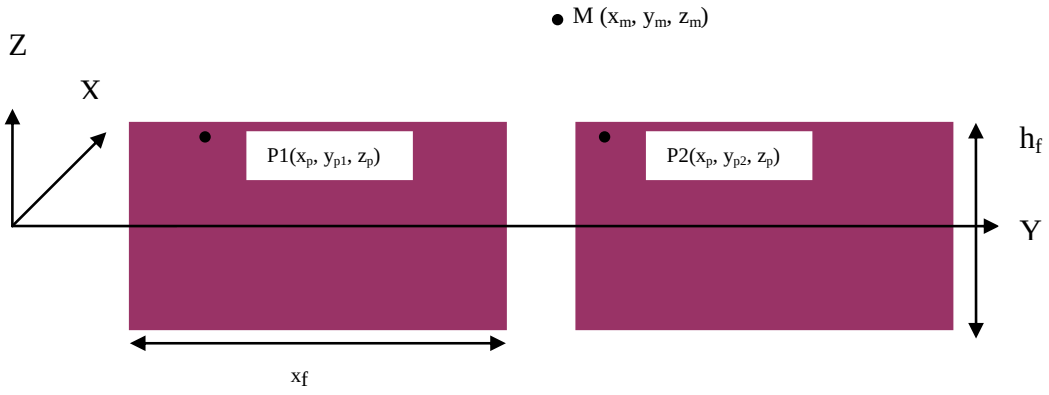

Figure 4-10: The monitoring point and the source point for multiple- inclined longitudinal hydraulic fractures.

$$S_y = \frac{1}{2\sqrt{\pi\eta t}} e^{-\frac{(y_m - y')^2}{4\eta t}} = \frac{1}{2\sqrt{\pi\eta t}} \left[\int_{y}^{y+2x_f} e^{-\frac{(y_m - y_p)}{4\eta t}} dy_p + \int_{y+2xf+D}^{y+4x_f+D} e^{-\frac{(y_m - y_p)}{4\eta t}} dy_p + ... \right]$$
$$= \frac{1}{2} \sum_{n=1}^{n=\infty} \left[erf\left(\frac{y_m - y - (n-1)D - 2(n-1)x_f}{2\sqrt{\eta t}} \right) - erf\left(\frac{y_m - y - (n-1)D - 2nx_f}{2\sqrt{\eta t}} \right) \right] \quad (4\text{-}58)$$

S_{xz} can be derived as follows:

$$S_{xz}\left(y_m, z_m, t, \phi_v, h, h_f\right) = \frac{1}{4\eta\pi t} e^{-\frac{d^2}{4\eta t}} \quad (4\text{-}59)$$

Where d is the distance, in the (XZ) plane normal to the hydraulic fractures propagation, between the monitoring point (M) and the production points (P1, P2, P3,…). The distance in this case will be the same for all fractures and can be determined as follows:

$$d^2 = \left(x_m - x - z_p \times \tan(\theta_v)\right)^2 + \left(z_m - (z + z_p)\right)^2 \quad (4\text{-}60)$$

The distance between the monitoring point and the images is:

$$d^2 = \left(x_m - x + zp \times \tan(\theta_v)\right)^2 + \left(z_m - (z_p - z)\right)^2 \quad (4\text{-}61)$$

therefore:

$$S_{xz} = \frac{1}{4\eta\pi t \cos(\theta_v)} \int_{-\frac{h_f}{2} cso(\theta_v)}^{\frac{h_f}{2}\cos(\theta_v)} \left[e^{-\frac{\left[x_m - (x + z_p \tan(\theta_v)\right]^2 + \left[z_m - (z + z_p)\right]^2}{4\eta t}} + e^{-\frac{\left[x_m - (x - z_p \tan(\theta_v))\right]^2 + \left[z_m - (z_p - z)\right]^2}{4\eta t}} \right] dz_p \quad (4\text{-}62)$$

Applying superposition theory:

$$S_{xz} = \frac{1}{4\eta\pi t \cos(\theta_v)} \sum_{N=1}^{N=\infty} \int_{-\frac{h_f}{2} cso(\theta_v)}^{\frac{h_f}{2}\cos(\theta_v)} \left[e^{-\frac{\left[x_m - (x + z_p \tan(\theta_v)\right]^2 + \left[z_m + 2Nh - (z + z_p)\right]^2}{4\eta t}} + e^{-\frac{\left[x_m - (x - z_p \tan(\theta_v)\right]^2 + \left[z_m + 2Nh - (z_p - z)\right]^2}{4\eta t}} \right] dz_p \quad (4\text{-}63)$$

The two exponential terms in Eq. (4-63) can be solved and integrated for (z_p). Therefore, Eq. (4-63) becomes:

$$S_{xz}=\frac{1}{4\sqrt{\pi\eta t}}\sum_{N=-\infty}^{N=\infty}\left\{\begin{array}{l}\left[\begin{array}{l}e^{-\frac{[\cos(\theta_v)(x_m-x)-\sin(\theta_v)(z_m-z+2Nh]^2}{4\eta t}}\\ \left[\begin{array}{l}erf\left(\frac{h_f/2-\sin(\theta_v)(x_m-x)-\cos(\theta_v)(z_m-z+2Nh)}{2\sqrt{\eta t}}\right)\\ -erf\left(\frac{-h_f/2-\sin(\theta_v)(x_m-x)-\cos(\theta_v)(z_m-z+2Nh)}{2\sqrt{\eta t}}\right)\end{array}\right]\end{array}\right]+\\ \left[\begin{array}{l}e^{-\frac{[\cos(\theta_v)(x_m-x)+\sin(\theta_v)(z_m+z+2Nh)]^2}{4\eta t}}\\ \left[\begin{array}{l}erf\left(\frac{h_f/2+\sin(\theta_v)(x_m-x)-\cos(\theta_v)(z_m+z+2Nh)}{2\sqrt{\eta t}}\right)\\ -erf\left(\frac{-h_f/2+\sin(\theta_v)(x_m-x)-\cos(\theta_v)(z_m+z+2Nh)}{2\sqrt{\eta t}}\right)\end{array}\right]\end{array}\right]\end{array}\right\} \quad (4\text{-}64)$$

In dimensionless form, the final model for pressure response of horizontal wells intersected by multi-inclined fully penetrating longitudinal hydraulic fractures is:

$$P_D=\frac{\sqrt{\pi}\cos(\theta_v)}{8n}\int_0^{t_D}\frac{1}{\sqrt{\tau_D}}\sum_{n=1}^{n=\infty}\left[erf\left(\frac{y_D-(n-1)D_D-2(n-1)}{2\sqrt{\tau}}\right)-erf\left(\frac{y_D-(n-1)D_D-2n}{2\sqrt{\tau}}\right)\right]$$

$$\sum_{N=-\infty}^{N=\infty}\left\{\begin{array}{l}\left[\begin{array}{l}e^{-\frac{[x_D\cos(\theta_v)-\sin(\theta_v)(z_D-z_{fD}+2Nh_D]^2}{4\tau}}\\ \left[\begin{array}{l}erf\left(\frac{h_{fD}/2-x_D\sin(\theta_v)-\cos(\theta_v)(z_D-z_{fD}+2Nh_D)}{2\sqrt{\tau}}\right)\\ -erf\left(\frac{-h_{fD}/2-x_D\sin(\theta_v)-\cos(\theta_v)(z_D-z_{fD}+2Nh_D)}{2\sqrt{\tau}}\right)\end{array}\right]\end{array}\right]+\\ \left[\begin{array}{l}e^{-\frac{[x_D\cos(\theta_v)+\sin(\theta_v)(z_D+z_{fD}+2Nh_D)]^2}{4\tau}}\\ \left[\begin{array}{l}erf\left(\frac{h_{fD}/2+x_D\sin(\theta_v)-\cos(\theta_v)(z_D+z_{fD}+2Nh_D)}{2\sqrt{\tau}}\right)\\ -erf\left(\frac{-h_{fD}/2+x_D\sin(\theta_v)-\cos(\theta_v)(z_D-z_{fD}+2Nh_D)}{2\sqrt{\tau}}\right)\end{array}\right]\end{array}\right]\end{array}\right\}d\tau \quad (4\text{-}65)$$

To solve the model given in Eq. (4-65), the two long time approximations should be done based on the fluid flow dynamics and flow regimes in late time. Eq. (4-65) can be redefined as follows:

$$P_D = \frac{1}{2}\int_0^{t_D} Y(y_D,\tau)\times XZ(x_D,z_D,\tau,\theta_v,z_{fD},h_{fD},h_D)d\tau \tag{4-66}$$

where:

$$Y(y_D,\tau_D) = \frac{\sqrt{\pi}}{2\sqrt{t_D}}\left[erf\left(\frac{y_D-(n-1)D_D-2(n-1)}{2\sqrt{t_D}}\right)-erf\left(\frac{y_D-(n-1)D_D-2n}{2\sqrt{t_D}}\right)\right] \tag{4-67}$$

$$XZ = \frac{\cos(\theta_v)}{2n}\int_0^{t_D}\sum_{N=-\infty}^{N=\infty}\left\{\begin{array}{l}\left[\begin{array}{l} e^{-\frac{\left[x_D\cos(\theta_v)-\sin(\theta_v)(z_D-z_{fD}+2Nh_D)\right]^2}{4\tau}} \\ \left[erf\left(\frac{h_{fD}/2-x_D\sin(\theta_v)-\cos(\theta_v)(z_D-z_{fD}+2Nh_D)}{2\sqrt{\tau}}\right)\right. \\ \left.-erf\left(\frac{-h_{fD}/2-x_D\sin(\theta_v)-\cos(\theta_v)(z_D-z_{fD}+2Nh_D)}{2\sqrt{\tau}}\right)\right]\end{array}\right]+ \\ \left[\begin{array}{l} e^{-\frac{\left[x_D\cos(\theta_v)+\sin(\theta_v)(z_D+z_{fD}+2Nh_D)\right]^2}{4\tau}} \\ \left[erf\left(\frac{h_{fD}/2+x_D\sin(\theta_v)-\cos(\theta_v)(z_D+z_{fD}+2Nh_D)}{2\sqrt{\tau}}\right)\right. \\ \left.-erf\left(\frac{-h_{fD}/2+x_D\sin(\theta_v)-\cos(\theta_v)(z_D-z_{fD}+2Nh_D)}{2\sqrt{\tau}}\right)\right]\end{array}\right]\end{array}\right\}d\tau \tag{4-68}$$

Similar to what it has been done for transverse hydraulic fractures starting from Eq. (4-42) through (4-48), the late time approximation model can be written as follows:

$$\begin{aligned} P_D &= \frac{q}{2nx_f h_f\theta\mu}\int_0^{t_{D1}} X(x_D,t_D)\times YZ(y_D,z_D,t_D,\phi_v,z_{fD},h_{fD},h_D)+\frac{1}{2}\int_{t_{D1}}^{t_D}\frac{1}{\tau_D}d\tau_D \\ &= P_D(x_D,y_D,z_D,z_{wD},L_D,t_{D1})+\frac{1}{2}\ln\left(\frac{t_D}{t_{D1}}\right) \end{aligned} \tag{4-69}$$

and the proper time for this approximation is:

$$t_{D1} \geq \begin{bmatrix} \frac{25}{3}\left(y_D - (n-1)D_D - 2(n1-)\right) & \frac{25}{3}\left(y_D - (n-1)D_D - 2n\right) \\ \frac{25}{3}\left[\frac{h_{fD}}{2} - x_D \sin(\theta_v) - \cos(\theta_v)(z_D - z_{fD} + 2h_D)\right]^2 & \frac{25}{3}\left[-\frac{h_{fD}}{2} - x_D \sin(\theta_v) - \cos(\theta_v)(z_D - z_{fD} + 2h_D)\right]^2 \\ \frac{25}{3}\left[\frac{h_{fD}}{2} + x_D \sin(\theta_v) - \cos(\theta_v)(z_D + z_{fD} + 2h_D)\right]^2 & \frac{25}{3}\left[\frac{h_{fD}}{2} + x_D \sin(\theta_v) - \cos(\theta_v)(z_D + z_{fD} + 2h_D)\right]^2 \\ 25\left[x_D \cos(\theta_v) - \sin(\theta_v)(z_D - z_{fD} + 2h_D)\right]^2 & 25\left[x_D \cos(\theta_v) + \cos(\theta_v)(z_D + z_{fD} + 2h_D)\right]^2 \end{bmatrix}$$

(4-70)

4-3-2- Deviation from horizontal wellbore (Semi-transverse fractures)

Consider a horizontal well with multiple-inclined hydraulic fractures in an infinite, homogenous, isotropic or anisotropic ($k = k_x = \sqrt{k_{yz}}$) formation, horizontal slab reservoir as shown in fig. (4-9). Each fracture is considered as a single plane of length ($2x_f$), width (w), height (h_f), and an angle of inclination from the vertical direction (θ_v) and an angle of deviation from the horizontal wellbore axis (θ_h) as shown in Fig. (4-11). The spacing between fractures is (D). If we assume that all fluid withdrawal will be through the fractures, and that the fractures are fully penetrating the formation, the fractures can be simulated as inclined plane sources. The source function (S_{xyz}) in this case is;

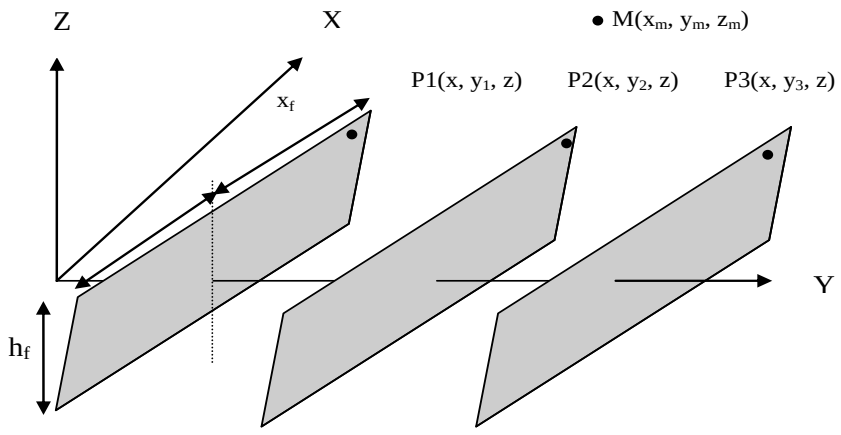

Figure 4-11: Horizontal well intersected by deviated hydraulic fractures.

$$S_{xyz}(x_m, y_m, z_m, t, \theta_v, z_f, h_f, x_f, h) = S_{yz}(y_m, z_m, t, \theta_v, z_f, h_f, h) \times S_x(x_m, t, x_f) \quad (4\text{-}71)$$

Where (S_{yz}) is the instantaneous source function for an inclined plane source in an infinite slab reservoir. S_x is the instantaneous source function for an infinite slab source in an infinite reservoir in the direction parallel to the hydraulic fractures. S_x can be estimated based on half fracture length as follow:

$$S_x = \frac{1}{2\sqrt{\pi\eta t}} e^{-\frac{(x_m - x')^2}{4\eta t}} = \frac{1}{2\sqrt{\pi\eta t}} \int_{-x_f}^{x_f} e^{-\frac{(x_m - x - x_p)}{4\eta t}} dx_p = \frac{1}{2}\left[erf\left(\frac{x_m - x + x_f \sin(\theta_h)}{2\sqrt{\eta t}}\right) - erf\left(\frac{x_m - x - x_f \sin(\theta_h)}{2\sqrt{\eta t}}\right)\right] \quad (4\text{-}72)$$

S_{yz} can be derived as follows:

$$S_{yz}\left(y_m, z_m, t, \theta_v, h, h_f\right) = \frac{1}{4\eta\pi t} \int_{-\frac{h_f}{2}\cos(\theta_v)}^{\frac{h_f}{2}\cos(\theta_v)} \left[e^{-\frac{(P_1M)^2}{4\eta t}} + e^{-\frac{(P_2M)^2}{4\eta t}} + e^{-\frac{(P_3M)^2}{4\eta t}} \right] dh_f \quad (4\text{-}73)$$

The distance between the monitoring point and each production point (PM) can be calculated as shown in Fig. (4-12) as follows:

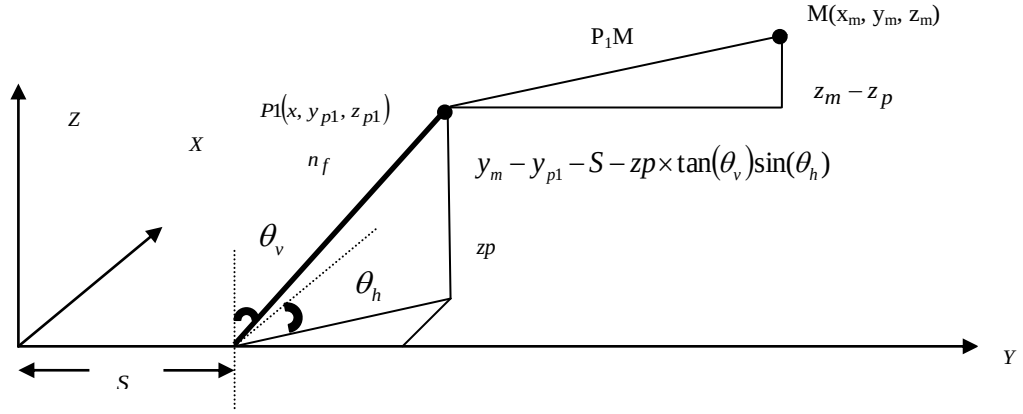

Figure 4-12: The distance between the monitoring point and production points for deviated hydraulic fractures.

$$(P_1M)^2 = \left(y_m - y - S - zp \times \tan(\theta_v)\sin(\theta_h)\right)^2 + \left(z_m - (z + z_p)\right)^2 \quad (4\text{-}74)$$

$$(P_2M)^2 = (y_m - y - 2S - zp \times \tan(\theta_v)\sin(\theta_h))^2 + (z_m - (z + z_p))^2 \quad (4\text{-}75)$$

$$(P_3M)^2 = (y_m - y - 3S - zp \times \tan(\theta_v)\sin(\theta_h))^2 + (z_m - (z + z_p))^2 \quad (4\text{-}76)$$

The distances between the monitoring point and the images are:

$$(P_1'M)^2 = (y_m - y - S + zp \times \tan(\theta_v)\sin(\theta_h))^2 + (z_m - (z_p - z))^2 \quad (4\text{-}77)$$

$$(P_2'M)^2 = (y_m - y - 2S + zp \times \tan(\theta_v)\sin(\theta_h))^2 + (z_m - (z_p - z))^2 \quad (4\text{-}78)$$

$$(P_3'M)^2 = (y_m - y - 3S + zp \times \tan(\theta_v)\sin(\theta_h))^2 + (z_m - (z_p - z))^2 \quad (4\text{-}79)$$

Assume that:

$$\tan(\theta) = \tan(\theta_v)\sin(\theta_h) \quad (4\text{-}80)$$

Eq. (4-73) can be written for (n) numbers of fractures as follows:

$$S_{yz} = \frac{1}{4\eta\pi t\cos(\theta_v)} \sum_{n=1}^{n=\infty} \int_{-\frac{h_f}{2}\cos(\theta_v)}^{\frac{h_f}{2}\cos(\theta_v)} \left[e^{-\frac{[y_m - (y+nD+z_p\tan(\theta))]^2 + [z_m - (z+z_p)]^2}{4\eta t}} + e^{-\frac{[y_m - (y+nD-z_p\tan(\theta))]^2 + [z_m - (z_p - z)]^2}{4\eta t}} \right] dz_p \quad (4\text{-}81)$$

Applying superposition theory:

$$S_{yz} = \frac{1}{4\eta\pi t\cos(\theta_v)} \sum_{n=1}^{n=\infty} \sum_{N=-\infty}^{N=\infty} \int_{-\frac{h_f}{2}\cos(\theta_v)}^{\frac{h_f}{2}\cos(\theta_v)} \left[e^{-\frac{[y_m - (y+nD+z_p\tan(\theta))]^2 + [z_m + 2Nh - (z+z_p)]^2}{4\eta t}} + e^{-\frac{[y_m - (y+nD-z_p\tan(\theta))]^2 + [z_m + 2Nh - (z_p - z)]^2}{4\eta t}} \right] dz_p \quad (4\text{-}82)$$

Solving the two exponential terms in Eq. (4-82) and integrating for (z_p), Eq. (4-82) becomes:

$$S_{yz}=\frac{1}{4\sqrt{\pi\eta t}}\sum_{n=1}^{n=\infty}\sum_{N=-\infty}^{N=\infty}\left\{\begin{array}{l}\left[\begin{array}{l}e^{\frac{-[\cos(\theta)(y_m-y-nD)-\sin(\theta)(z_m-z+2Nh]^2}{4\eta t}}\\ \left[\begin{array}{l}erf\left(\dfrac{\frac{h_f}{2\cos(\theta)}\cos(\theta_v)-\sin(\theta)(y_m-y-nD)-\cos(\theta)(z_m-z+2Nh)}{2\sqrt{\eta t}}\right)\\ -erf\left(\dfrac{-\frac{h_f}{2\cos(\theta)}\cos(\theta_v)-\sin(\theta)(y_m-y-nD)-\cos(\theta)(z_m-z+2Nh)}{2\sqrt{\eta t}}\right)\end{array}\right]\end{array}\right]+\\ \left[\begin{array}{l}e^{\frac{-[\cos(\theta)(y_m-y-nS)+\sin(\theta)(z_m+z+2Nh)]^2}{4\eta t}}\\ \left[\begin{array}{l}erf\left(\dfrac{\frac{h_f}{2\cos(\theta)}\cos(\theta_v)+\sin(\theta)(y_m-y-nD)-\cos(\theta)(z_m+z+2Nh)}{2\sqrt{\eta t}}\right)\\ -erf\left(\dfrac{-\frac{h_f}{2\cos(\theta)}\cos(\theta_v)+\sin(\theta)(y_m-y-nD)-\cos(\theta)(z_m+z+2Nh)}{2\sqrt{\eta t}}\right)\end{array}\right]\end{array}\right]\end{array}\right\} \tag{4-83}$$

Substitute Eqs. (4-7), (4-72), and (4-83) in Eq. (4-6), the pressure drop in dimensionless form can be found as follows:

$$P_D=\frac{\sqrt{\pi}\cos(\theta_v)}{8n}\int_0^{t_D}\frac{1}{\sqrt{\tau_D}}\left[erf\left(\frac{x_D+\sin(\theta_h)}{2\sqrt{\tau}}\right)-erf\left(\frac{x_D-\sin(\theta_h)}{2\sqrt{\tau}}\right)\right]$$

$$\sum_{n=1}^{n=\infty}\sum_{N=-\infty}^{N=\infty}\left\{\begin{array}{l}\left[\begin{array}{l}e^{\frac{-[\cos(\theta)(y_D-nD_D)-\sin(\theta)(z_D-z_{fD}+2Nh_D)]^2}{4\tau}}\\ \left[\begin{array}{l}erf\left(\dfrac{\frac{h_{fD}cso(\theta_v)}{2\cos(\theta)}-\sin(\theta)(y_D-nD_D)-\cos(\theta)(z_D-z_{fD}+2Nh_D)}{2\sqrt{\tau}}\right)\\ -erf\left(\dfrac{-\frac{h_{fD}cso(\theta_v)}{2\cos(\theta)}-\sin(\theta)(y_D-nD_D)-\cos(\theta)(z_D-z_{fD}+2Nh_D)}{2\sqrt{\tau}}\right)\end{array}\right]\end{array}\right]+\\ \left[\begin{array}{l}e^{\frac{-[\cos(\theta)(y_D-nD_D)+\sin(\theta)(z_D+z_{fD}+2Nh_D)]^2}{4\tau}}\\ \left[\begin{array}{l}erf\left(\dfrac{\frac{h_{fD}\cos(\theta_v)}{2\cos(\theta)}+\sin(\theta)(y_D-nD_D)-\cos(\theta)(z_D+z_{fD}+2Nh_D)}{2\sqrt{\tau}}\right)\\ -erf\left(\dfrac{-\frac{h_{fD}\cos(\phi_v)}{2\cos(\phi)}+\sin(\phi)(y_D-nS_D)-\cos(\phi)(z_D+z_{fD}+2Nh_D)}{2\sqrt{\tau}}\right)\end{array}\right]\end{array}\right]\end{array}\right\}d\tau \tag{4-84}$$

The long time approximation for this model can be written as:

$$P_D = \frac{q}{2nx_f h_f \theta \mu} \int_0^{t_{D1}} X(x_D, t_D) \times YZ(y_D, z_D, t_D, \phi_v, z_{fD}, h_{fD}, h_D) + \frac{1}{2} \int_{t_{D1}}^{t_D} \frac{1}{\tau_D} d\tau_D$$
$$= P_D(x_D, y_D, z_D, z_{wD}, L_D, t_{D1}) + \frac{1}{2} \ln\left(\frac{t_D}{t_{D1}}\right) \tag{4-85}$$

and the proper time for this approximation is:

$$t_{D1} \geq \begin{bmatrix} \frac{25}{3}\left(xD + \sin(\theta_h)\right) \\ \frac{25}{3}\left(xD - \sin(\theta_h)\right) \\ \frac{25}{3}\left[\frac{h_{fD}\cos(\theta_v)}{2\cos(\theta)} - \sin(\phi)(y_D - nD_D) - \cos(\theta)(z_D - z_{fD} + 2h_D)\right]^2 \\ \frac{25}{3}\left[-\frac{h_{fD}\cos(\theta_v)}{2\cos(\theta)} - \sin(\phi)(y_D - nD_D) - \cos(\theta)(z_D - z_{fD} + 2h_D)\right]^2 \\ \frac{25}{3}\left[\frac{h_{fD}\cos(\theta_v)}{2\cos(\theta)} + \sin(\phi)(y_D - nD_{SD}) - \cos(\theta)(z_D + z_{fD} + 2h_D)\right]^2 \\ \frac{25}{3}\left[\frac{h_{fD}\cos(\theta_v)}{2\cos(\theta)} + \sin(\phi)(y_D - nD_D) - \cos(\theta)(z_D + z_{fD} + 2h_D)\right]^2 \\ 25\left[\cos(\theta)(y_D - nD_D) - \sin(\theta)(z_D - z_{fD} + 2h_D)\right]^2 \\ 25\left[\cos(\theta)(y_D - nD_D) + \cos(\theta)(z_D + z_{fD} + 2Nh_D)\right]^2 \end{bmatrix} \tag{4-86}$$

4-4-Model for anisotropic formation $\left(k_x \neq k_{yz}\right)$

The same models, given in Eqs. (4-27), (4-65), and (4-84), can be used for anisotropic formation with the following definitions:

4-4-1- Transverse and semi-transverse fractures $\left(k_y \neq k_{xz}\right)$:

$$y_D = \frac{y_m - y}{x_f} \sqrt{\frac{k_x}{k_{yz}}} \tag{4-87}$$

$$z_D = \frac{z_m}{x_f} \sqrt{\frac{k_x}{k_{yz}}} \tag{4-88}$$

$$h_{fD} = \frac{h_f}{x_f} \sqrt{\frac{k_x}{k_{yz}}} \tag{4-89}$$

$$z_{fD} = \frac{z}{x_f}\sqrt{\frac{k_x}{k_{yz}}} \tag{4-90}$$

$$h_D = \frac{h}{x_f}\sqrt{\frac{k_x}{k_{yz}}} \tag{4-91}$$

$$D_D = \frac{D}{x_f}\sqrt{\frac{k_x}{k_{yz}}} \tag{4-92}$$

$$t_D = \frac{0.0002637\, k_x t}{\phi \mu c x_f^2} \tag{4-93}$$

$$P_D = \frac{2\pi\sqrt{k_x k_{yz}}\, h \Delta P}{q\mu} \tag{4-94}$$

$$k_{yz} = \sqrt{k_y k_z} \tag{4-95}$$

4-4-2- Longitudinal fractures $(k_x \neq k_{yz})$:

$$y_D = \frac{y_m - y}{x_f}\sqrt{\frac{k_x}{k_y}} \tag{4-96}$$

$$z_D = \frac{z_m}{x_f}\sqrt{\frac{k_x}{k_z}} \tag{4-97}$$

$$h_{fD} = \frac{h_f}{x_f}\sqrt{\frac{k_x}{k_z}} \tag{4-98}$$

$$z_{fD} = \frac{z}{x_f}\sqrt{\frac{k_x}{k_z}} \tag{4-99}$$

$$h_D = \frac{h}{x_f}\sqrt{\frac{k_x}{k_z}} \tag{4-100}$$

$$D_D = \frac{D}{x_f}\sqrt{\frac{k_x}{k_y}} \tag{4-101}$$

$$t_D = \frac{0.0002637\,k_x t}{\phi\,\mu\,c\,x_f^2} \tag{4-102}$$

$$P_D = \frac{2\pi\sqrt{k_y k_{xz}}\,h\Delta P}{q\mu} \tag{4-103}$$

$$k_{xz} = \sqrt{k_x k_z} \tag{4-104}$$

4-5- Models validation

Two previous models have been considered to check the validity of the suggested model in this study for multiple-inclined hydraulic fractures. The first case is for multiple-vertical hydraulic fractures where the suggested model can be developed to represent this case as:

$$\phi_v = 0.0, \quad \phi_h = 90, \quad \phi = 0.0$$

Therefore Eq. (4-84) can be written as:

$$P_D = \frac{\sqrt{\pi}}{8n}\int_0^{t_D}\frac{1}{\sqrt{\tau_D}}\left[erf\left(\frac{x_D+1}{2\sqrt{\tau}}\right)-erf\left(\frac{x_D-1}{2\sqrt{\tau}}\right)\right]$$
$$\sum_{n=1}^{n=\infty}\sum_{N=-\infty}^{N=\infty}\left\{\left[e^{-\frac{[(y_D-nD_D)-(z_D-z_{fD}+2Nh_D)]^2}{4\tau}}\left[erf\left(\frac{\frac{h_{fD}}{2}-(y_D-nD_D)-(z_D-z_{fD}+2Nh_D)}{2\sqrt{\tau}}\right)-erf\left(\frac{-\frac{h_{fD}}{2}-(y_D-nD_D)-(z_D-z_{fD}+2Nh_D)}{2\sqrt{\tau}}\right)\right]\right]+\left[e^{-\frac{[(y_D-nD_D)+(z_D+z_{fD}+2Nh_D)]^2}{4\tau}}\left[erf\left(\frac{\frac{h_{fD}}{2}+(y_D-nD_D)-(z_D+z_{fD}+2Nh_D)}{2\sqrt{\tau}}\right)-erf\left(\frac{-\frac{h_{fD}}{2}+(y_D-nS_D)-(z_D+z_{fD}+2Nh_D)}{2\sqrt{\tau}}\right)\right]\right]\right\}d\tau \tag{4-105}$$

The solution for Eq. (4-105) is identical to the solution obtained from the model introduced by Ozkan (1988) as shown in Fig. (4-13).

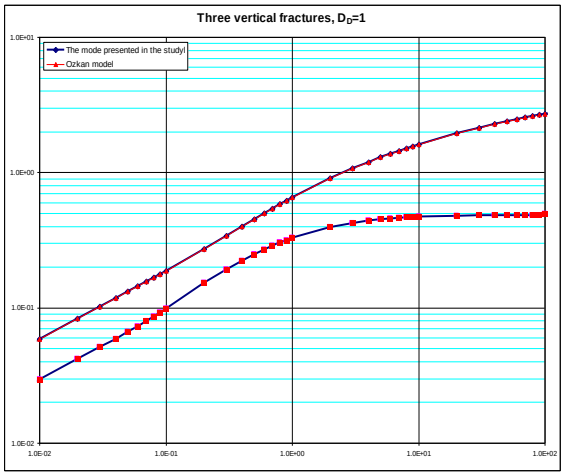

Figure 4-13: The result of three vertical fractures using the new model and Ozkan's model.

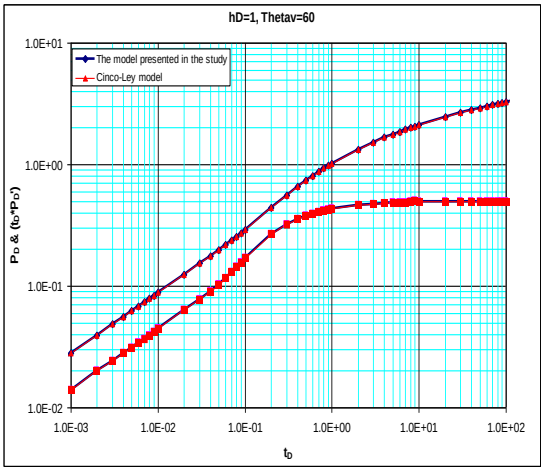

Figure 4-14: The result of single inclined fractures using the new model and Cinco-Ley's model.

The second case is for the solution of a single inclined fracture where $(n=1)$ and:

$$\phi_h = 90, \quad \phi = \phi_v$$

therefore Eq. (4-84) can be written as:

$$P_D = \frac{\sqrt{\pi}\cos(\theta_v)}{8n}\int_0^{t_D}\frac{1}{\sqrt{\tau_D}}\left[erf\left(\frac{x_D+1}{2\sqrt{\tau}}\right)-erf\left(\frac{x_D-1}{2\sqrt{\tau}}\right)\right]$$
$$\sum_{n=1}^{n=\infty}\sum_{N=-\infty}^{N=\infty}\left\{\left[e^{-\frac{[y_D\cos(\theta_v)-\sin(\theta_v)(z_D-z_{fD}+2Nh_D)]^2}{4\tau}}\left[erf\left(\frac{\frac{h_{fD}}{2}-y_D\sin(\theta_v)-\cos(\theta_v)(z_D-z_{fD}+2Nh_D)}{2\sqrt{\tau}}\right)-erf\left(\frac{-\frac{h_{fD}}{2}-y_D\sin(\theta_v)-\cos(\theta_v)(z_D-z_{fD}+2Nh_D)}{2\sqrt{\tau}}\right)\right]\right]+\left[e^{-\frac{[y_D\cos(\theta_v)+\sin(\theta_v)(z_D+z_{fD}+2Nh_D)]^2}{4\tau}}\left[erf\left(\frac{\frac{h_{fD}}{2}+y_D\sin(\theta_v)-\cos(\theta_v)(z_D+z_{fD}+2Nh_D)}{2\sqrt{\tau}}\right)-erf\left(\frac{-\frac{h_{fD}}{2}+y_D\sin(\phi_v)-\cos(\phi_v)(z_D+z_{fD}+2Nh_D)}{2\sqrt{\tau}}\right)\right]\right]\right\}d\tau \quad (4\text{-}106)$$

The model represented by Eq. (4-106) is identical to the model introduced by Cinco-Ley (1974) as shown in Fig. (4-13).

5- PRESSURE TRANSIENT ANALYSIS FOR HORIZONTAL WELLS WITH MULTIPLE-INCLINED HYDRAULIC FRACTURES

The pressure behaviors and flow regimes are expected to be changeable depending on different parameters such as number of fractures, inclination angle, and the spacing between them for the same reservoir properties.

5-1- Pressure behavior

Two responses can be identified based on the spacing or the distance between fractures.

5-1-1- Short spacing (D_D<5)

Because of the short spacing between fractures, the interference between them is expected to occur shortly after the linear flow period. The following cases can be identified:

1- For a small number of hydraulic fractures (less than five) and small inclination angle $(\theta_v \leq 45)$, linear, elliptical and pseudo-radial flow regimes are observed as shown in Fig. (5-1)

2- For a small number of hydraulic fractures (less than five) and high inclination angle $(\theta_v \geq 45)$, linear, transition and pseudo radial flow regimes are observed as shown in Fig. (5-1).

3- For a large number of hydraulic fractures (more than five) and small inclination angle $(\theta_v \leq 45)$, linear, elliptical, transition and pseudo-radial flow regimes are observed such as in Fig. (5-2).

4- For a large number of hydraulic fractures (more than five) and high inclination angle ($\theta_v \geq 45$), linear, transition and pseudo radial flow regimes are observed as shown in Fig. (5-2). The transition flow in this case is lasting longer than the transition flow for short spacing.

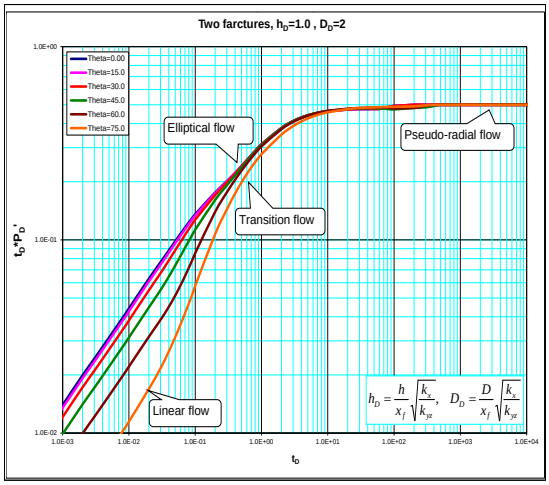

Figure 5-1: Pressure behavior of two inclined transverse hydraulic fractures.

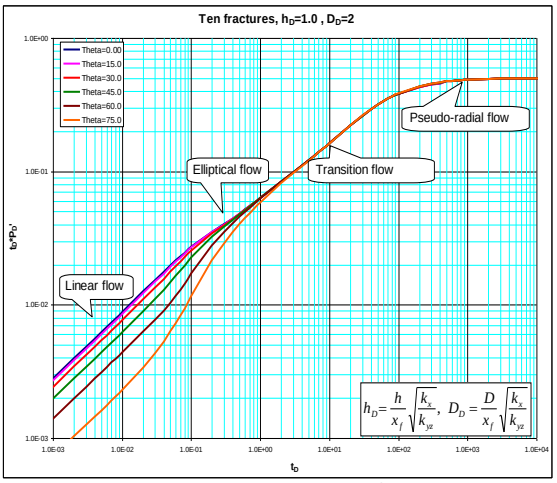

Figure 5-2: Pressure behavior of ten inclined transverse hydraulic fractures.

5-1-2- Long spacing (D_D>5)

Because of the long spacing between fractures, the interference between them requires long time period to occur after the linear flow. Therefore, intermediate radial flow, which represents radial flow around each fracture, is expected to develop. The following cases can be identified:

1- For a small number of hydraulic fractures (less than five) and small inclination angle ($\theta_v \leq 45$), linear, early radial, transition and pseudo-radial flow regimes are observed as shown in Fig. (5-3)

2- For a small number of hydraulic fractures (less than five) and high inclination angle ($\theta_v \geq 45$), linear, transition, early radial, transition and pseudo radial flow regimes are observed as shown in Fig. (5-3).

3- For a large number of hydraulic fractures (more than five) and small inclination angle $(\theta_v \leq 45)$, linear, early radial, transition and pseudo-radial flow regimes are observed such as in Fig. (5-4).

4- For a large number of hydraulic fractures (more than five) and high inclination angle $(\theta_v \geq 45)$, linear, transition, early radial, transition and pseudo radial flow regimes are observed as shown in Fig. (5-4). the transition flow in this case is lasting longer than the transition flow for short spacing.

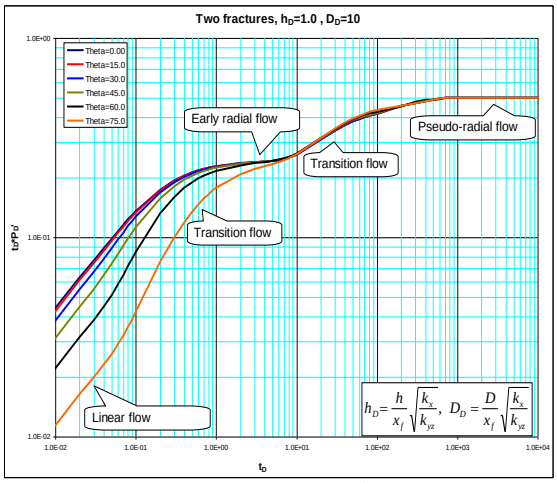

Figure 5-3: Pressure behavior of two inclined transverse hydraulic fractures.

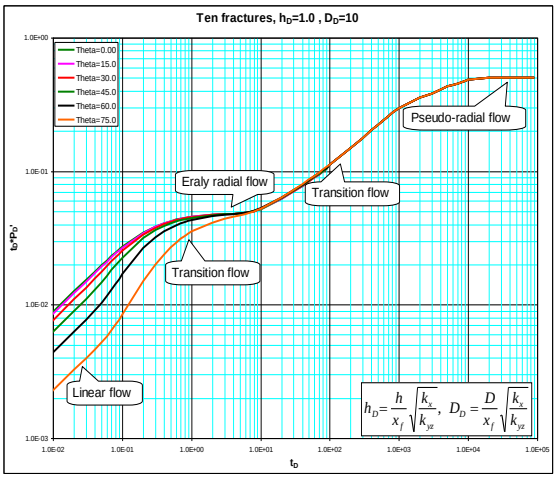

Figure 5-4: Pressure behavior of ten inclined transverse hydraulic fractures.

For longitudinal hydraulic fractures, the response is similar to the transverse hydraulic fractures. The differences between the longitudinal and transverse fractures occur in the anisotropic formations when there is a difference between the permeability in the X-direction (k_x) and Y-direction (k_y).

1- For small spacing (D_D=1), Linear, transition, and pseudo-radial flow are developed for both small and large inclination angle as shown in Fig. (5-5).

2- For moderate spacing (D_D=5), Linear, transition, elliptical and pseudo-radial flow are developed for both small and large inclination angle such as shown in Fig.(5-6).

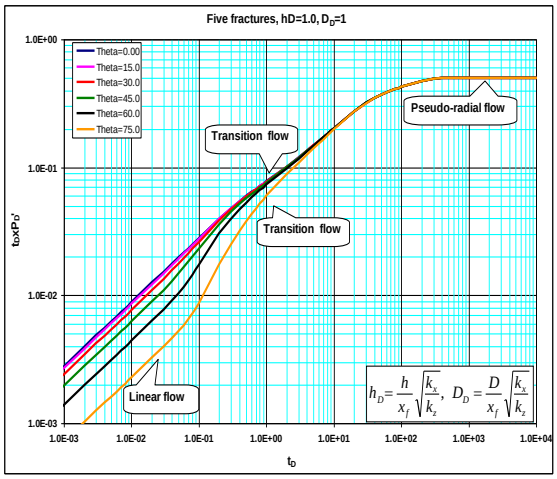

Figure 5-5: Pressure behavior of five inclined longitudinal hydraulic fractures.

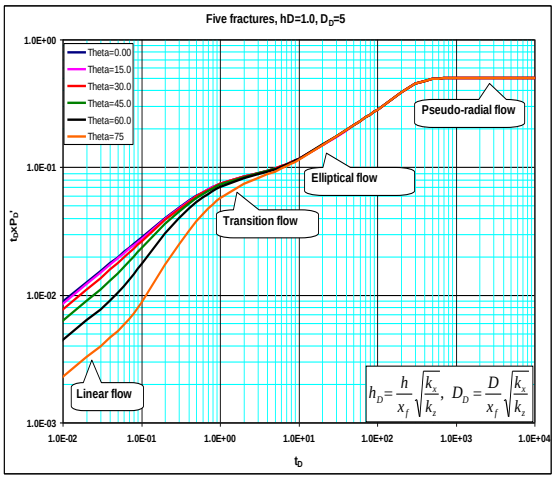

Figure 5-6: Pressure behavior of five inclined longitudinal hydraulic fractures.

For semi-transverse fractures, the deviation from the horizontal wellbores has two different impacts: the first for $(\theta_h \le 45)$ in which the pressure drop increases slightly as the deviation angle increases. The second for $(\theta_h \ge 45)$ in which the pressure drop decreases slightly with the increasing of the deviation angle. The following cases for five hydraulic fractures can be identified based on spacing, vertical inclination angle and the deviation from the horizontal wellbore.

1- Short spacing (D_D=1) and five vertical fractures $(\theta_v = 0)$: Linear, transition and pseudo-radial flow regimes are developed for both small and large deviation angle as shown in Fig. (5-7).

2- Short spacing (D_D=1) and five inclined fractures $(\theta_v = 60)$: Linear, transition and pseudo-radial flow regimes are developed for both small and large deviation angle from the wellbore as shown in Fig. (5-8).

3- Long spacing (D_D=5) and five vertical fractures $(\phi_v = 0)$: Linear, transition, early radial, transition and pseudo-radial flow regimes are developed for both small and large deviation angle from the wellbore such as in Fig. (5-9).

4- Long spacing (D_D=5) and five inclined fractures $(\theta_v = 60)$: Linear, transition and pseudo-radial flow regimes are developed for both small and large deviation angle from the wellbore such as in Fig. (5-10).

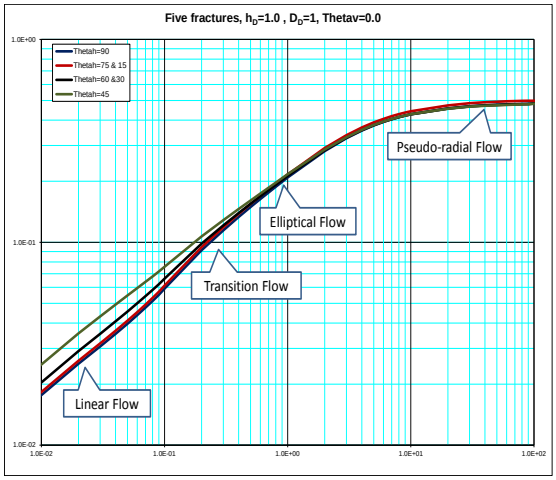

Figure 5-7: Pressure behavior of five semi-transverse inclined hydraulic fractures.

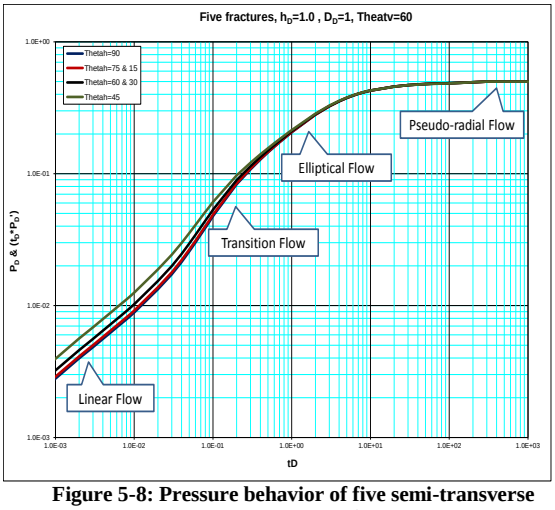

Figure 5-8: Pressure behavior of five semi-transverse inclined hydraulic fractures.

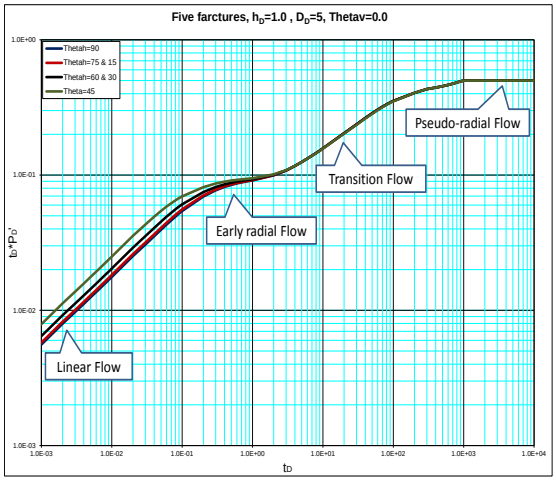

Figure 5-9: Pressure behavior of five semi-transverse inclined hydraulic fractures.

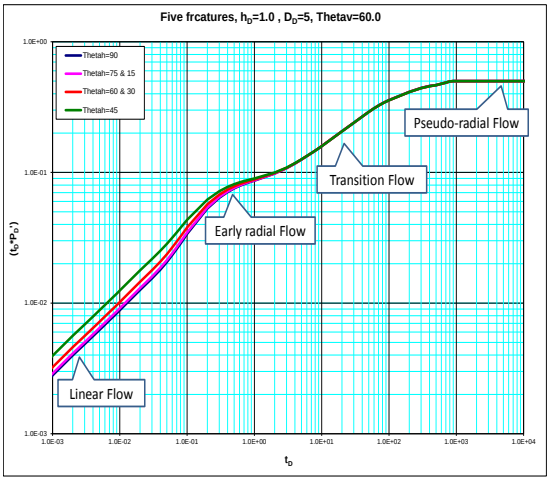

Figure 5-10: Pressure behavior of five semi-transverse inclined hydraulic fractures.

5-2- Flow regimes

5-2-1-Linear flow regime

At early time, reservoir fluid flows linearly and directly from the formations to the individual fractures as shown in Fig. (5-11). Each fracture behaves independently from the others. The flow regime is recognized by straight line with slope of (0.5) in the log-log plots for both dimensionless pressure and pressure derivative with dimensionless time.

5-2-1-1-For isotropic and anisotropic formation $\left(k = k_x = k_{xy}\right)$

- The governing equations for transverse and longitudinal hydraulic fractures are:

$$P_D = \frac{\sqrt{\pi t_D}\cos(\theta_v)}{n} \tag{5-1}$$

$$\left(\Delta P\right)_{ELF} = \frac{4.063qB\cos(\theta_v)}{nhx_f}\sqrt{\frac{\mu t}{k\phi c_t}} \tag{5-2}$$

or;

$$\left(t_D \times P_D'\right)_{ELF} = \frac{\sqrt{\pi t_D}\cos(\theta_v)}{2n} \tag{5-3}$$

$$\left(t \times \Delta P\right)_{ELF} = \frac{2.032qB\cos(\theta_v)}{nhx_f}\sqrt{\frac{\mu t}{k\phi c_t}} \tag{5-4}$$

The governing equations for semi-transverse hydraulic fractures are:

$$P_D = \frac{\sqrt{\pi t_D}\cos(\theta_v)}{n\sin(\theta_h)} \tag{5-5}$$

$$\left(\Delta P\right)_{ELF} = \frac{4.063qB\cos(\theta_v)}{nhx_f\sin(\theta_h)}\sqrt{\frac{\mu t}{k\phi c_t}} \tag{5-6}$$

or;

$$\left(t_D \times P_D'\right)_{ELF} = \frac{\sqrt{\pi t_D}\cos(\theta_v)}{2n\sin(\theta_h)} \tag{5-7}$$

$$\left(t \times \Delta P\right)_{ELF} = \frac{2.032qB\cos(\theta_v)}{nhx_f \sin(\theta_h)}\sqrt{\frac{\mu t}{k\phi c_t}} \tag{5-8}$$

5-2-1-2-For anisotropic formation $\left(k_x \neq k_{yz}\right)$:

-The governing equation for transverse and longitudinal hydraulic fractures is:

$$\left(\Delta P\right)_{ELF} = \frac{4.063qB\cos(\theta_v)}{nhx_f}\sqrt{\frac{\mu t}{k_{yz}\phi c_t}} \tag{5-9}$$

or;

$$\left(t \times \Delta P\right)_{ELF} = \frac{2.032qB\cos(\theta_v)}{nhx_f}\sqrt{\frac{\mu t}{k_{yz}\phi c_t}} \tag{5-10}$$

The governing equation for semi-transverse hydraulic fractures is:

$$\left(\Delta P\right)_{ELF} = \frac{2.032qB\cos(\theta_v)}{nhx_f \sin(\theta_h)}\sqrt{\frac{\mu t}{k_{yz}\phi c_t}} \tag{5-11}$$

or;

$$\left(t \times \Delta P\right)_{ELF} = \frac{1.16qB\cos(\theta_v)}{nhx_f \sin(\theta_h)}\sqrt{\frac{\mu t}{k_{yz}\phi c_t}} \tag{5-12}$$

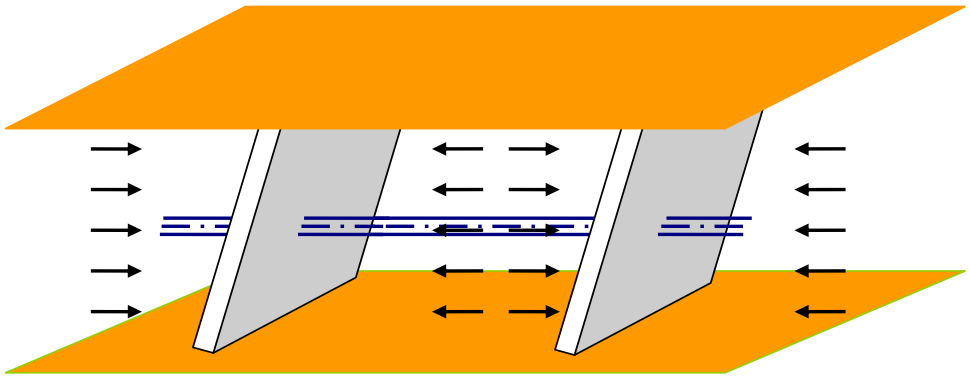

Figure 5-11: Linear flow regime of multiple-inclined hydraulic fractures.

Generally, in all cases (transverse, semi-transverse, and longitudinal fractures), the following correlation is applicable:

$$P_D = 2 \times (t_D \times P_D') \tag{5-13}$$

5-2-2-Pseudo-radial flow

Pseudo-radial flow regime is the dominant flow for all cases at late time when reservoir fluids flow in the XY plane radially toward the fractures such as shown in Fig. (5-12). This flow is characterized by constant value (0.5) for the dimensionless pressure derivative curves on log-log plot of dimensionless pressure and dimensionless time. The governing equation for this flow is:

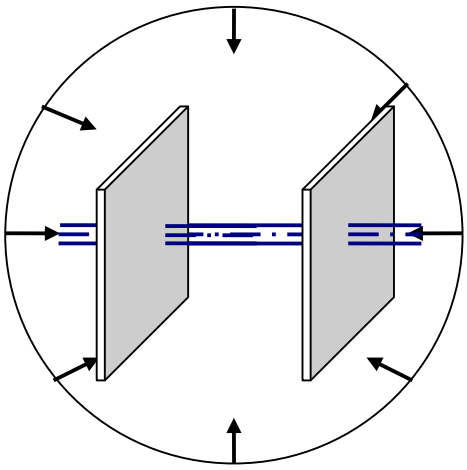

Figure 5-12: Pseudo- radial flow regime for multiple inclined hydraulic fracture.

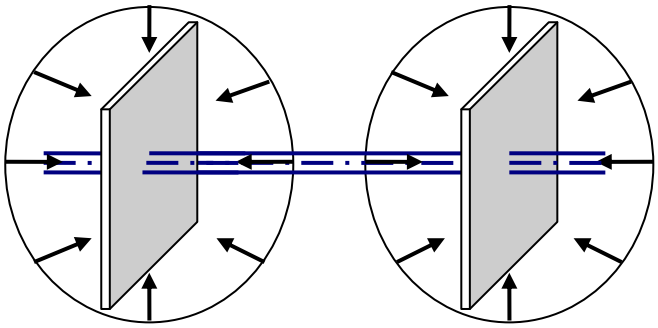

Figure 5-13: Early radial flow regime for multiple-inclined hydraulic fractures.

$$(t_D \times P_D')_{PRF} = 0.5 \tag{5-14}$$

$$(t \times \Delta P)_{PRF} = \frac{70.6qB}{kh} \tag{5-15}$$

And for anisotropic formation $(k_x \neq k_{xy})$:

$$(t \times \Delta P)_{PRF} = \frac{70.6qB}{\sqrt{k_x k_{yz}}h} \tag{5-16}$$

5-2-3-Early radial flow

Early radial flow regime represents the radial flow around each fracture. Typically, this flow is expected to be observed when the spacing between fractures is long enough. In this flow, reservoir fluids flow radially in XY plane toward each individual fractures such as shown in Fig. (5-13). The governing equations for this flow are:

$$\left(t_D \times P_D'\right)_{ERF} = \frac{0.5}{n} \tag{5-17}$$

$$\left(t \times \Delta P\right)_{ERF} = \frac{70.6qB}{nkh} \tag{5-18}$$

And for anisotropic formation $\left(k_x \neq k_{xy}\right)$:

$$\left(t \times \Delta P\right)_{ERF} = \frac{70.6qB}{n\sqrt{k_x k_{yz}}h} \tag{5-19}$$

5-2-4- Elliptical flow regime

Elliptical flow regime indicates elliptical flow toward the fracture such as shown in Fig. (5-14). This flow regime was described initially by Tiab (1994). It often occurs in the case of infinite conductivity fractures. However, it can be seen in a few cases of uniform flux fractures. This type of flow depends on the number of fractures and spacing between them as shown in Fig. (5-15). Neither the inclination angle from the vertical axis $\left(\theta_v\right)$ nor the deviation angle from the horizontal wellbore $\left(\theta_h\right)$ have an impact on this flow as shown in Fig. (5-16). Multivariate linear regression analysis is used to derive the governing equation for this flow regime:

$$\left(t_D \times P_D'\right)_{EF} = \frac{t_D^{0.366}}{nD_D^{0.6}} \tag{5-20}$$

$$\left(t\times\Delta P\right)_{EF}=\frac{7q\mu B}{nD^{0.6}hk^{0.64}x_f^{0.12}}\left(\frac{t}{\phi\mu c_t}\right)^{0.36} \tag{5-21}$$

And for anisotropic formation $\left(k_x\neq k_{xy}\right)$:

$$\left(t\times\Delta P\right)_{EF}=\frac{7q\mu B}{nD^{0.6}hx_f^{0.12}k_x^{0.14}\sqrt{k_{yz}}}\left(\frac{t}{\phi\mu c_t}\right)^{0.36} \tag{5-22}$$

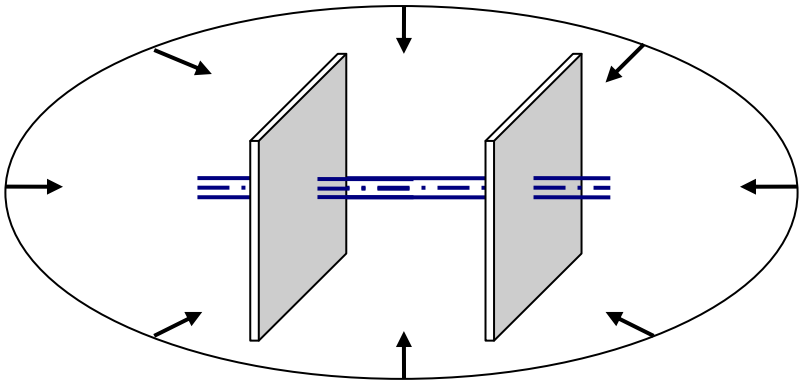

Figure 5-14: Elliptical flow regime for multiple-inclined hydraulic farctures.

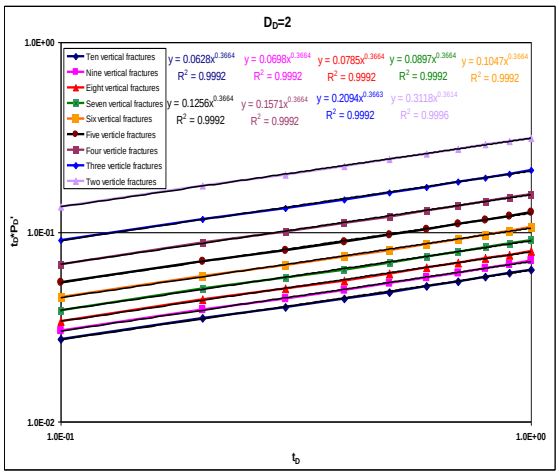

Figure 5-15: Multivariate regression analysis for elliptical flow regime (transverse and longitudinal fractures).

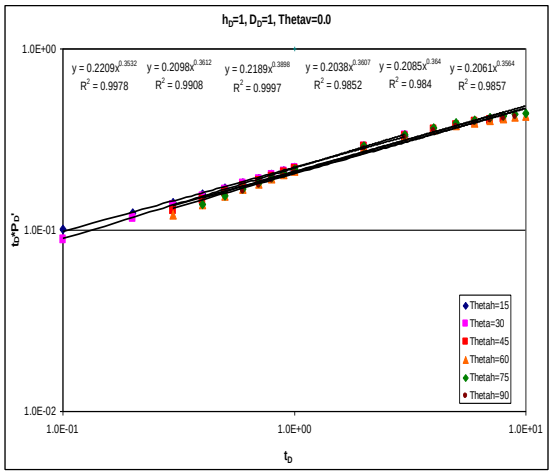

Figure 5-16: Multivariate regression analysis for elliptical flow regime (semi-transverse fractures).

5-3- Intersection Points:

The points of intersection between different lines of flow regimes are very important in the well test interpretation. They can be used to check the results.

5-3-1- The point of intersection of linear flow line and pseudo-radial flow line is:

-For transverse and longitudinal fractures acting in isotropic and anisotropic formation $\left(k = k_x = k_{yz}\right)$:

$$t_{PREL} = 1207 \frac{n^2 x_f^2 \phi \mu c_t}{k \cos^2(\theta_v)} \tag{5-23}$$

-For semi-transverse fractures acting in isotropic and anisotropic formation $\left(k = k_x = k_{yz}\right)$:

$$t_{PREL} = 1207 \frac{n^2 x_f^2 \phi \mu c_t}{k} \frac{\sin^2(\theta_h)}{\cos^2(\theta_v)} \tag{5-24}$$

-For transverse, longitudinal fractures, and semi-transverse fractures acting in an anisotropic formation $\left(k_x \neq k_{yz}\right)$, k_x should be used instead of k in Eqs. (5-23) and (5-24).

5-3-2- The point of intersection of linear flow line and early radial flow line is:

-For transverse and longitudinal fractures acting in isotropic and anisotropic formation $\left(k = k_x = k_{yz}\right)$:

$$t_{EREL} = 1207 \frac{x_f^2 \phi \mu c_t}{k \cos^2(\theta_v)} \tag{5-25}$$

-For semi-transverse fractures acting in isotropic and anisotropic formation $\left(k = k_x = k_{yz}\right)$:

$$t_{EREL} = 1207 \frac{x_f^2 \phi \mu c_t}{k} \frac{\sin^2(\theta_h)}{\cos^2(\theta_v)} \tag{5-26}$$

-For transverse, longitudinal fractures and semi-transverse fractures acting in an anisotropic formation $(k_x \neq k_{yz})$, k_x should be used instead of k in Eqs. (5-25) and (5-26).

5-3-3-The point of intersection of elliptical flow line and pseudo-radial flow line is:

-For transverse and longitudinal fractures acting in isotropic and anisotropic formation $(k = k_x = k_{yz})$:

$$t_{PREF} = 570.7\left(\frac{nD^{0.6}}{x_f^{0.6}}\right)^{1/0.36}\left(\frac{\phi\mu c_t x_f^2}{k}\right) \tag{5-27}$$

-For transverse and longitudinal fractures acting in an anisotropic formation $(k_x \neq k_{yz})$:

$$t_{PREF} = 570.7\left(\frac{nD^{0.6}}{x_f^{0.6}}\right)^{1/0.36}\left(\frac{\phi\mu c_t x_f^2}{k_x}\right) \tag{5-28}$$

5-3-4-The point of intersection of elliptical flow line and early radial flow line is:

-For transverse and longitudinal fractures acting in isotropic and anisotropic formation $(k = k_x = k_{yz})$:

$$t_{EREF} = 570.7\left(\frac{D^{0.6}}{x_f^{0.6}}\right)^{1/0.36}\left(\frac{\phi\mu c_t x_f^2}{k}\right) \tag{5-29}$$

-For transverse and longitudinal fractures acting in an anisotropic formation $(k_x \neq k_{yz})$:

$$t_{EREF} = 570.7\left(\frac{D^{0.6}}{x_f^{0.6}}\right)^{1/0.36}\left(\frac{\phi\mu c_t x_f^2}{k_x}\right) \tag{5-30}$$

5-4-Pseudo-skin factor

Pseudo-skin factor was defined by Cinco-Ley et al 1975 as the difference in the wellbore dimensionless pressure for a fully penetrating inclined hydraulic fracture $P_{fD}(t_D, \theta_w, h_D)$ and a vertical fracture $P_{fD}(t_D)$. Mathematically, it is:

$$S = P_{fD}(t_D, \theta_w, h_D) - P_{fD}(t_D) \tag{5-31}$$

Gringarten et al 1974 introduced the equation for dimensionless pressure of a well intercepting a uniform flux vertical fracture at its center as:

$$P_{fD}(t_D) = \frac{1}{2}\left[\ln(t_D) + 2.80907\right] \tag{5-32}$$

Therefore, late time pseudo-skin factor can be found as:

$$S = \frac{1}{2}\int_0^{t_{D1}} Y(y_D, \tau) \times Z(x_D, z_D, \tau, \theta_w, z_{wD}, h_{wD}, h_D) d\tau - \frac{1}{2}\left[\ln(t_{D1}) + 2.80907\right] \tag{5-33}$$

In general, the pseudo-skin factor decreases with the inclination angle from the vertical axis and the deviation from the wellbore. For the same number of longitudinal and transverse fractures, the pseudo-skin factor decreases when the spacing between fractures increases and when the inclination angle (ϕ_v) increases as shown in Fig. (5-17). For the same number of semi-transverse fractures, the pseudo-skin factor increases as the deviation from the wellbore increases and the spacing between fractures increases as shown in Fig. (5-18). Appendix-D shows the tables of pseudo-skin factor.

Even though skin factor has not been included in all above models, the equivalent skin factor can be determined based on the single fracture solution using the early radial flow line when it is well developed. The equivalent skin factor model for transverse fractures is:

$$\bar{s} = 0.5\left[\frac{(\Delta P)_{ERF}}{(t \times \Delta P')_{ERF}} - \ln\left(\frac{k_x t_{ERF}}{\phi \mu c_t r_w^2}\right) + 7.43\right] \tag{5-34}$$

and for longitudinal fractures is:

$$\bar{s} = 0.5\left[\frac{(\Delta P)_{ERF}}{(t \times \Delta P')_{ERF}} - \ln\left(\frac{k_y t_{ER}}{\phi \mu c_t r_w^2}\right) + 7.43\right] \tag{5-35}$$

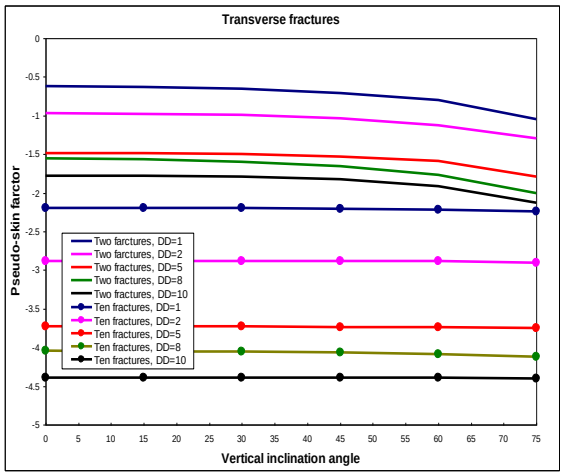

Figure 5-17: Pseudo-skin factor for transverse hydraulic fractures

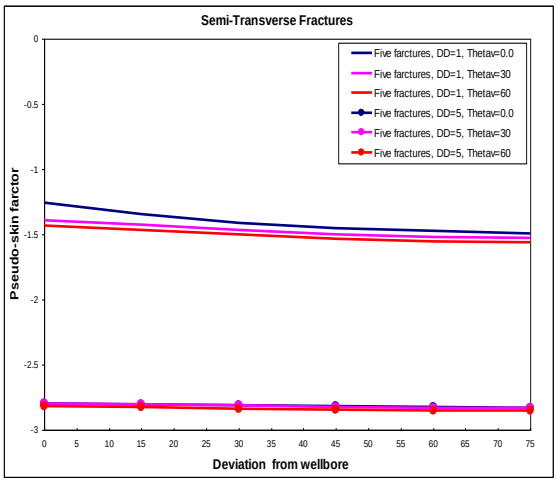

Figure 5-18: Pseudo-skin factor for semi-transverse hydraulic fractures

while total skin factor can be determined from pseudo-radial flow as:

$$s = 0.5\left[\frac{(\Delta P)_{PRF}}{(t \times \Delta P')_{PRF}} - \ln\left(\frac{k t_{ERF}}{\phi \mu c_t r_w^2}\right) + 7.43\right] \tag{5-36}$$

5-5-Appliction of Type Curve Matching

As shown on the plots in Appendix (B), the pressure and pressure derivative have different shapes for each combination of number of fractures, spacing between fractures, inclination angle from the vertical axis, and deviation from the wellbore. Type-curve matching can provide a quick estimation for reservoir and fractures parameters.

The following information is associated with each type curve: dimensionless spacing between fractures (D_D), number of fractures (n), and inclination angle (ϕ_v). Thus, the following information can be obtained from the type curve matching process: $(P_D)_M$, $(\Delta P)_M$, $(t_D)_M$, $(\Delta t)_M$, $(\phi_v)_M$, $(h_D)_M$, $(D)_M$, $(s)_M$, $(n)_M$. The following steps illustrate how type curve matching is used to determine reservoir characteristics such as: permeability, inclination angle, spacing, pseudo-skin factor, fracture half length, and number of fractures.

Step-1 Plot (ΔP vs. t) and ($t \times \Delta P'$ vs. t) on log-log paper.

Step-2 Obtain the best match of the data with one of the type curves.

Step-3 Read from any match point: $t_M, \Delta P_M, t_{DM}, P_{DM}, h_{DM}, D_{DM}, \phi_{vM}, n_M, s_M$.

Step-4 Calculate half fracture length (x_f).

$$x_f = h \times h_D \tag{5-37}$$

Step-5 Calculate k_x:

$$k_x = \frac{\phi \mu c_t x_f^2 t_{DM}}{0.0002637 t_M} \tag{5-38}$$

Step-6 Calculate (k_{yz}):

$$\sqrt{k_{yz}} = \frac{141.2 quBP_{DM}}{\sqrt{k_x} h \Delta P_M} \tag{5-39}$$

Step-7 Calculate $\left(k_y\right)$.

$$k_y = \frac{k_{yz}^2}{k_z} \tag{5-40}$$

Step-8 Number of fractures can be determined directly as:

$$n = n_M \tag{5-41}$$

Step-9 Inclination angle can be determined directly as:

$$\phi\nu = \phi_{\nu M} \tag{5-42}$$

Step-10 Spacing between fractures can be calculated as:

$$D = x_f \times D_M \tag{5-43}$$

Step-11 Pseudo-skin factor can be determined directly as:

$$S = S_M \tag{5-44}$$

5-6-Application of TDS technique

TDS is a powerful technique for computation of reservoir parameters directly from log-log plots of pressure and pressure derivative data. A well designed pressure transient test in multiple-inclined hydraulically fractured horizontal wells should yield all the necessary straight lines to calculate number of fractures, the inclination angle, spacing between fractures, and permeability. The great advantage of this technique is that it only requires graphing of pressure and pressure derivative on a single log-log plot for direct analysis.

The following step-by-step procedure is for the ideal case where all the necessary straight lines are well defined.

Step 1 - Plot pressure change (ΔP) and pressure derivative ($t \times \Delta P'$) values versus test time on a log-log graph.

Step 2 - Read the value of $(t \times \Delta P')_{PRF}$ corresponding to the infinite acting pseudo-radial flow line.

Step 3 - Calculate (k_x) for isotropic or anisotropic formation $\left(k = k_x = k_{yz}\right)$ or $\left(\sqrt{k_x k_{yz}}\right)$ for anisotropic formation $\left(k_x \neq k_{yz}\right)$:

$$k = k_x = k_{yz} = \left(\frac{70.6 q \mu B}{h(t \times \Delta P')_{PRF}} \right) \tag{5-45}$$

$$\sqrt{k_x k_{yz}} = \frac{70.6 q B}{(t \times \Delta P'')_{PRF}\, h} \tag{5-46}$$

Step 4- Calculate k_y :

$$k_y = \frac{k_{yz}}{k_z} = \frac{k_x}{k_z} \tag{5-47}$$

Step 5 – If the early radial flow is developed, read $(t \times \Delta P')_{ER}$.

Step 6 – Calculate number of fractures (n) :

$$n = \frac{(t \times \Delta P')_{PRF}}{(t \times \Delta P')_{ERF}} \tag{5-48}$$

Step 7 - Obtain the value of (t×ΔP') at time t = 1 hr from the elliptical flow line (extrapolated if necessary), $(t \times \Delta P')_{EF1hr}$.

Step 8 - Calculate (D).

-For transverse and longitudinal fractures acting in isotropic and anisotropic formation $\left(k = k_x = k_{yz}\right)$:

$$D = \left[\frac{7 q \mu B}{n x_f^{0.12} h k^{0.64} (t \times \Delta P)_{EF\,1hr}} \left(\frac{1}{\phi \mu c_t} \right)^{0.36} \right]^{1/0.6} \tag{5-49}$$

-For transverse and longitudinal fractures acting in anisotropic formation $\left(k_x \neq k_{yz}\right)$:

$$D=\left[\frac{7q\mu B}{nhx_f^{0.12}k_x^{0.14}\sqrt{k_{yz}}\left(t\times\Delta P'\right)_{EF1hr}}\left(\frac{t}{\phi\mu c_t}\right)^{0.36}\right]^{1/0.6} \tag{5-50}$$

Step 9 - Obtain the value of (t×ΔP') at time t = 1 hr from the linear flow line (extrapolated if necessary), $(t\times\Delta P')_{ELF1hr}$.

Step 10 - Calculate (ϕ_v).

-For transverse and longitudinal fractures acting in isotropic and anisotropic formation $\left(k=k_x=k_{yz}\right)$:

$$\theta_v=\cos^{-1}\left(\frac{nhx_f\left(t\times\Delta P\right)_{ELF1hr}}{2.032qB}\sqrt{\frac{k\phi c_t}{\mu}}\right) \tag{5-51}$$

-For semi-transverse fractures acting in isotropic and anisotropic formation $\left(k=k_x=k_{yz}\right)$:

$$\theta_h=\sin^{-1}\left(\frac{2.032qB}{nhx_f\left(t\times\Delta P'\right)_{ELF1hr}\cos(\theta_v)}\sqrt{\frac{\mu}{k\phi c_t}}\right) \tag{5-52}$$

-For transverse and longitudinal fractures acting in anisotropic formation $\left(k_x\neq k_{yz}\right)$:

$$\theta_v=\cos^{-1}\left(\frac{nhx_f\left(t\times\Delta P\right)_{ELF1hr}}{2.032qB}\sqrt{\frac{k_{yz}\phi c_t}{\mu}}\right) \tag{5-53}$$

-For semi-transverse fractures acting in anisotropic formation $\left(k_x\neq k_{yz}\right)$:

$$\theta_h=\sin^{-1}\left(\frac{2.032qB}{nhx_f\left(t\times\Delta P'\right)_{ELF1hr}\cos(\theta_v)}\sqrt{\frac{\mu}{k_{yz}\phi c_t}}\right) \tag{5-54}$$

Step 11 – From early radial flow line, read the value of $\left(t\times\Delta P'\right)_{ER}$ and $\left(\Delta P\right)_{ER}$ at a certain time $\left(t_{ER}\right)$.

Step-12- Calculate the equivalent skin factor $(\bar{s})$ from Eq. (5-34):

Step 13 – From pseudo radial flow line, read the value of $(t \times \Delta P')_{PRF}$ and $(\Delta P)_{PRF}$ at a certain time (t_{PRF}).

Step-14- Calculate the total skin factor (s) from Eq. (5-36):

Step 15 – Calculate the intersection times using Eq. (5-23) through Eq. (5-32) and compare them with those in the plot.

Example -5-1

Pressure drawdown test data of a hydraulically fractured horizontal well is given in Table (Example 5-1) of Appendix (F). Other known reservoir and well data are:

q = 200 STB/D ϕ = 0.07 μ = 0.75 cp $c_t = 1.5 \times 10^{-6}$ psi^{-1} h = 80 ft

x_f = 80 ft r_w = 0.5 ft p_i = 6000 psi B = 1.15 bbl/STB k_z=0.1 md

Determine:

1- Formation permeability.

2- Number of fractures.

3- Spacing between fractures.

4- Inclination angle.

1- Solution using type-curve matching:

Step-1 Plot (ΔP vs. t) and ($t \times \Delta P'$ vs. t) on log-log paper as shown in Fig. (5-19).

Step-2 Obtain the best match of the data with one of the type curves as shown in Fig. (5-20).

Step-3 Read from any match point:

$$t_M = 10,\ \Delta P_M = 10,\ t_{DM} = 1.3,\ P_{DM} = 0.0082,\ h_{DM} = 1,\ D_{DM} = 8,\ \phi_{vM} = 45,\ n_M = 7,\ s_M = -3.612$$

Step-4 Calculate half fracture length (x_f) from Eq. (5-37).

$$x_f = 80 \times 1 = 80 \ ft$$

Step-5 Calculate k_x from Eq. (5-38):

$$k_x = \frac{0.07 \times 0.75 \times 0.0000015 \times 80^2 \times 1.3}{0.0002637 \times 10} = 0.25 \ md$$

Step-6 Calculate (k_{yz}) from Eq. (5-39):

$$\sqrt{k_{yz}} = \frac{141.2 \times 200 \times 0.75 \times 1.15 \times 0.0082}{\sqrt{0.25} \times 80 \times 10} = 0.5$$

Step-7 Calculate $\left(k_y\right)$ from Eq. (5-40).

$$k_y = \frac{k_{yz}^2}{k_z} = \frac{0.5^2}{0.1} = 2.5 \ md$$

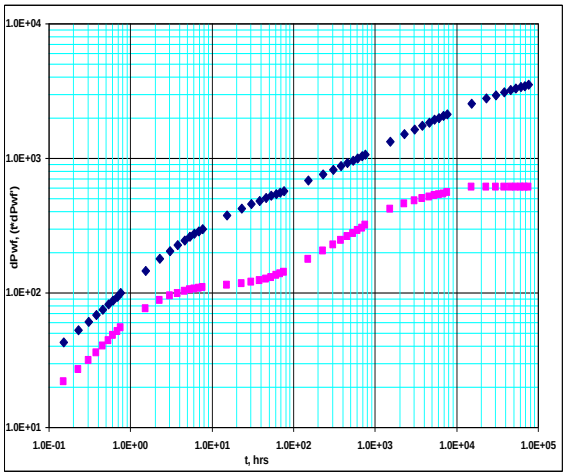

Figure 5-19: Pressure and pressure derivative plot Example 5-1.

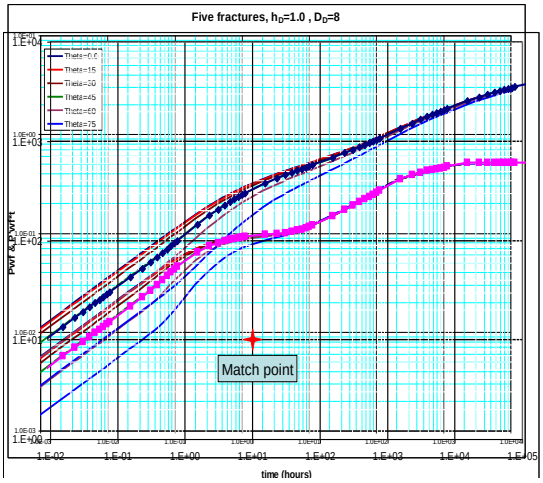

Figure 5-20: Type-curve matching plot for Example 5-1.

Step-8 Number of fractures from Eq. (5-41):

$$n = 5 \ fractures$$

Step-9 Inclination angle from Eq. (5-42):

$$\phi\nu = 45$$

Step-10 Spacing between fractures from Eq. (5-43):

$$D = x_f \times D_M = 80 \times 8 = 640 \ ft$$

Step-11 Pseudo-skin factor directly as in Eq. (5-44):

$$s = -3.612$$

2- Solution using TDS:

Step 1 - Plot pressure change (ΔP) and pressure derivative (t×ΔP') values versus test time on a log-log graph as shown in Fig. (5-21).

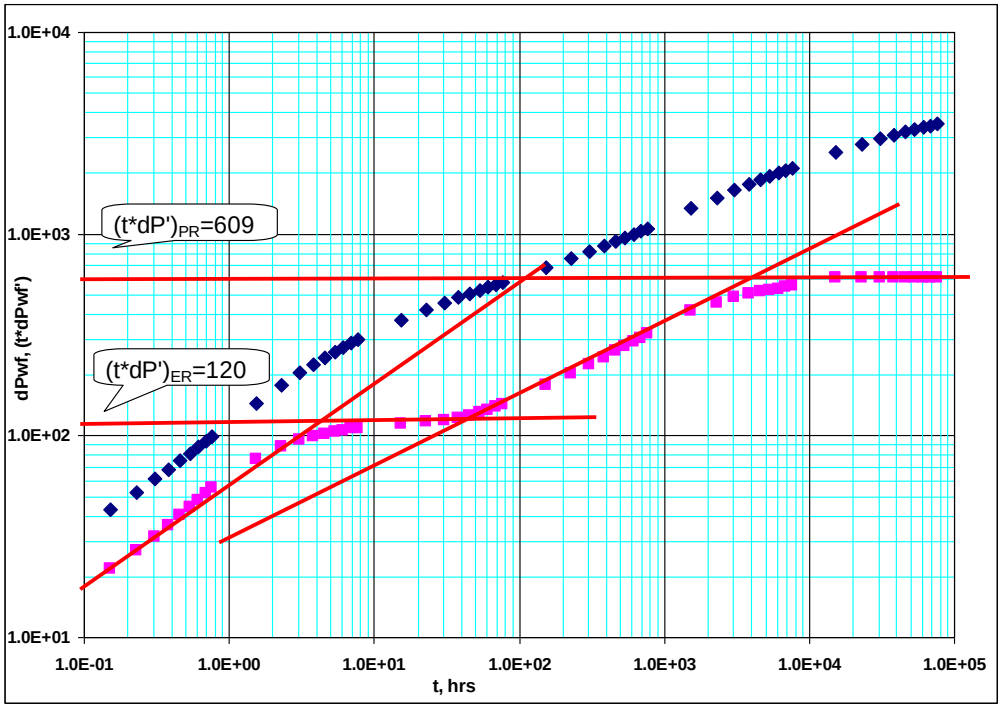

Figure 5-21: TDS technique for example 5-1.

Step 2 - Read the value of $(t \times \Delta P')_{PRF}$ corresponding to the infinite acting pseudo-radial flow line.

$$(t \times \Delta P')_{PRF} = 609.$$

Step 3 - Calculate (k_x) from Eq. (5-45).

$$k = k_x = k_{yz} = \left(\frac{70.6 q \mu B}{h(t \times \Delta P')_{PRF}} \right) = \frac{70.6 \times 200 \times 0.75 \times 1.15}{80 \times 609} = 0.25 \ md$$

Step-4- Calculate k_y from Eq. (5-47):

$$k_y = \frac{0.25}{0.1} = 2.5\ md$$

Step 4 – If the early radial flow is developed, read $(t\times\Delta P')_{ERF}$.

$$\left(t \times \Delta P'\right)_{ERF} = 120$$

Step 5 – Calculate number of fractures (n) from Eq. (5-48):

$$n = \frac{609}{120} = 5\ farctures$$

Step 6 - Obtain the value of (t×ΔP') at time t = 1 hr from the elliptical flow line (extrapolated if necessary), $(t\times\Delta P')_{EF1hr}$.

$$\left(t \times \Delta P'\right)_{EF1hr} = 32$$

Step 7 - Calculate (D) from Eq. (5-49).

$$D = \left[\frac{7\times 200\times 0.75\times 1.15}{5\times 80^{0.12}\times 80\times 0.25^{0.64}\times 32}\left(\frac{1}{0.07\times 0.75\times 0.0000015}\right)^{0.36}\right]^{1/0.6} = 650\ ft$$

Step 8 - Obtain the value of (t×ΔP') at time t = 1 hr from linear flow line (extrapolated if necessary), $(t\times\Delta P')_{ELF1hr}$.

$$\left(t \times \Delta P'\right)_{ELF1hr} = 55$$

Step 9 - Calculate (ϕ_v) from Eq. (5-51).

$$\theta_v = \cos^{-1}\left(\frac{5\times 80\times 80\times 55}{2.032\times 200\times 1.15}\sqrt{\frac{0.25\times 0.07\times 0.0000015}{0.75}}\right) = 45$$

Step 10 – Calculate the intersection times using Eq. (5-23) through Eq. (5-32) and compare them with those in the plot.

-From the plot, $t_{PREL} = 120\ hrs,\ t_{EREL} = 4.6\ hrs,\ t_{PREF} = 4000\ hrs,\ t_{EREF} = 4.3\ hrs$

-The calculated values:

1- The intersection point between linear flow and pseudo-radial flow from Eq. (5-23)

$$t_{PREL} = 1207\frac{5^2 \times 80^2 \times 0.07 \times 0.75 \times 0.0000015}{0.25 \times \cos^2(45)} = 121\ hrs$$

2- The intersection point between linear flow and early radial flow from Eq. (5-25)

$$t_{EREL} = 1207\frac{x_f^2 \phi \mu c_t}{k\cos(\theta_v)} = 1207\frac{80^2 \times 0.07 \times 0.75 \times 0.0000015}{0.25 \times \cos^2(45)} = 4.9\ hrs$$

3- The intersection point between elliptical flow and pseudo-radial flow from Eq. (5-27).

$$t_{PREF} = 570.7\left(\frac{5 \times 640^{0.6}}{80^{0.6}}\right)^{1/0.36}\frac{0.07 \times 0.75 \times 0.0000015 \times 80^2}{0.25} = 3220\ hrs$$

4- The intersection point between elliptical flow and pseudo-radial flow from Eq. (5-29).

$$t_{EREF} = 570.7\left(\frac{640^{0.6}}{80^{0.6}}\right)^{1/0.36}\frac{0.07 \times 0.75 \times 0.0000015 \times 80^2}{0.25} = 37\ hrs$$

Table (5-1) summarizes the input data and the resulted value for Example 5-1.

Table 5-1: Summary of results of Example 5-1.

Parameter	In-put value	Calculated value by Type-curve matching	Calculated value by TDS technique
k_x, md	0.25	0.25	0.25
k_y, md	2.5	2.5	2.5
n	5	5	5
x_f, ft	80	80	
D, ft	640	640	650
θ_v	45	45	45

Example -5-2

Pressure drawdown test data of a hydraulically fractured horizontal well is given in Table (Example 5-2) in Appendix (F). No indication for vertical deviation. Other known reservoir and well data are:

q = 500 STB/D ϕ = 0.05 μ = 0.5 cp $c_t = 1.0 \times 10^{-6}$ psi^{-1} h = 100 ft

x_f = 100 ft r_w = 0.5 ft p_i = 10000 psi B = 1.15 bbl/STB k_z=0.4 md

Determine:

5- Formation permeability.

6- Number of fractures.

7- Spacing between fractures.

8- Deviation angle from the wellbore.

1- Solution using type-curve matching:

Step-1 Plot (ΔP vs. t) and ($t \times \Delta P'$ vs. t) on log-log paper as shown in Fig. (5-22).

Step-2 Obtain the best match of the data with one of the type curves as shown in Fig. (5-23).

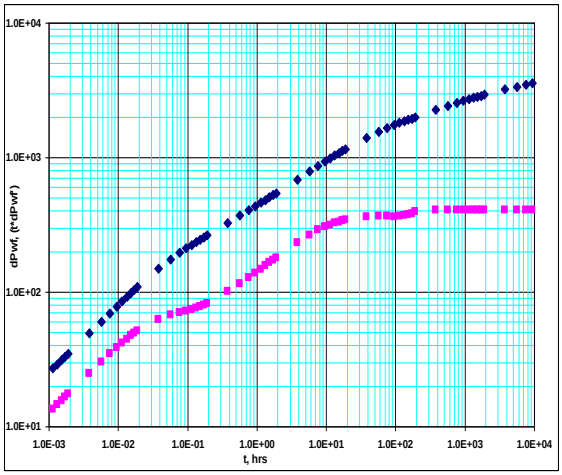

Figure 5-22: Pressure and pressure derivative plot Example 5-2.

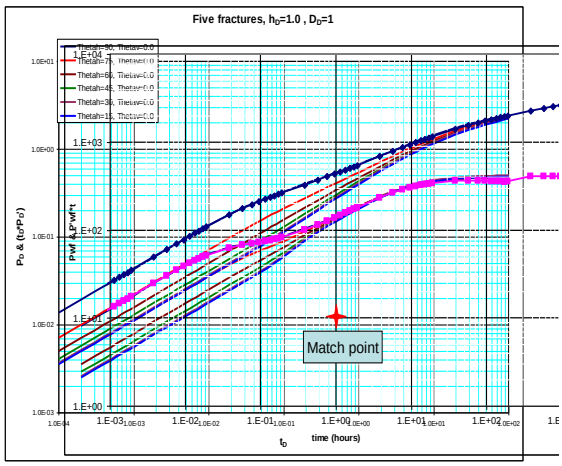

Figure 5-22: Type-curve matching plot for Example 5-2.

Step-3 Read from any match point:

$t_M = 1, \Delta P_M = 10, t_{DM} = 0.53, P_{DM} = 0.0123, h_{DM} = 1, D_{DM} = 1, \theta_{hM} = 15, \phi_{vM} = 0, n_M = 5,$
$s_M = -1.255$

Step-4 Calculate half fracture length (x_f) from Eq. (5-37).

$x_f = 100 \times 1 = 100 \ ft$

Step-5 Calculate k_x from Eq. (5-38):

$$k_x = \frac{0.05 \times 0.5 \times 0.000001 \times 100^2 \times 0.53}{0.0002637 \times 1} = 0.5 \ md$$

Step-6 Calculate (k_{yz}) from Eq. (5-39):

$$\sqrt{k_{yz}} = \frac{141.2 \times 500 \times 0.5 \times 1.15 \times 0.0123}{\sqrt{0.5} \times 100 \times 10} = 0.706$$

Step-7 Calculate $\left(k_y\right)$ from Eq. (5-40).

$$k_y = \frac{k_{yz}^2}{k_z} = \frac{0.706^2}{0.4} = 1.24 \ md$$

Step-8 Number of fractures from Eq. (5-41):

$n = 5 \ fractures$

Step-9 Inclination angle from Eq. (5-42):

$\theta\nu = 0$

Step-10 Deviation angle from wellbore:

$\theta_h = 15$

Step-11 Spacing between fractures from Eq. (5-43):

$D = x_f \times D_{DM} = 100 \times 1 = 100 \ ft$

Step-12 Pseudo-skin factor from Eq. (5-44):

$s = -1.255$

2- Solution using TDS:

Step 1 - Plot pressure change (ΔP) and pressure derivative (t×ΔP') values versus test time on a log-log graph as shown in Fig. (5-24).

Step 2 - Read the value of $(t\times\Delta P')_{PRF}$ corresponding to the infinite acting pseudo-radial flow line.

$(t\times\Delta P')_{PRF} = 406.$

Step 3 - Calculate (k_x) from Eq. (5-45).

$$k = k_x = k_{yz} = \left(\frac{70.6q\mu B}{h(t\times\Delta P')_{PRF}}\right) = \frac{70.6\times 500\times 0.5\times 1.15}{100\times 406} = 0.5\, md$$

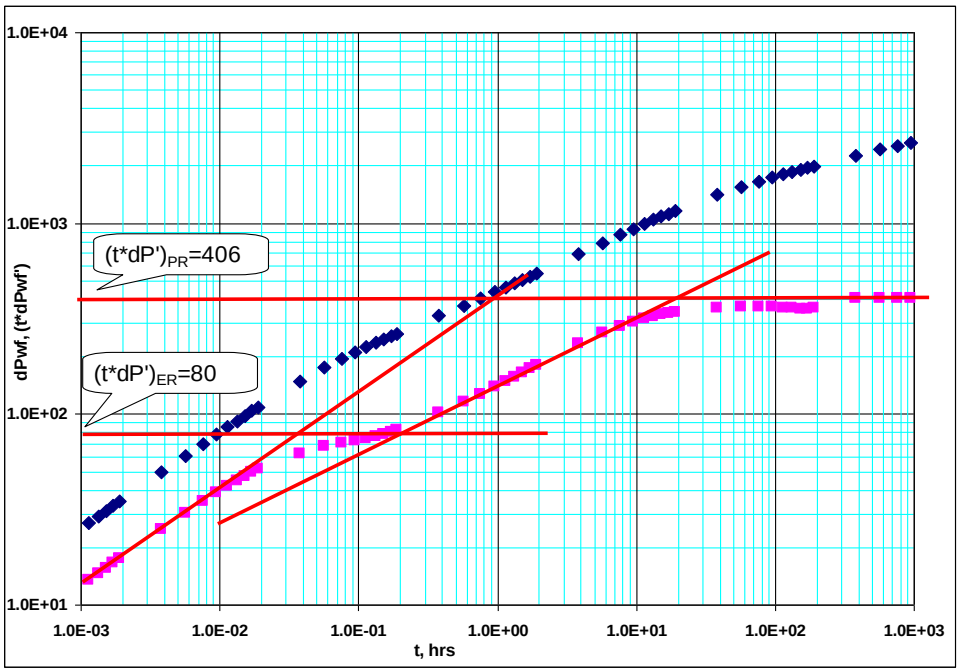

Figure 5-24: TDS technique for example 5-2.

Step-4- Calculate k_y from Eq. (5-47):

$$k_y = \frac{0.5}{0.4} = 1.25\, md$$

Step 4 – If the early radial flow is developed, read $(t\times\Delta P')_{ER}$.

$$(t\times\Delta P')_{ER}=80$$

Step 5 – Calculate number of fractures (n) from Eq. (5-48):

$$n=\frac{406}{8}=5\ \ farctures$$

Step 6 - Obtain the value of (t×ΔP') at time t = 1 hr from the elliptical flow line of slope (0.36) (extrapolated if necessary), $(t\times\Delta P')_{EF1hr}$.

$$(t\times\Delta P')_{EF1hr}=130$$

Step 7 - Calculate (D) from Eq. (5-49).

$$D=\left[\frac{7\times500\times0.5\times1.15}{5\times100^{0.12}\times100\times0.5^{0.64}\times130}\left(\frac{1}{0.05\times0.5\times0.000001}\right)^{0.36}\right]^{1/0.6}=95\ \ ft$$

Step 8 - Obtain the value of (t×ΔP') at time t = 1 hr from linear flow line (extrapolated if necessary), $(t\times\Delta P')_{ELF1hr}$.

$$(t\times\Delta P')_{ELF1hr}=400$$

Step 9 - Calculate (θ_h) from Eq. (5-52).

$$\theta_h=\sin^{-1}\left(\frac{2.032\times500\times1.15}{5\times100\times100\times400\times\cos(0)}\sqrt{\frac{0.5}{0.5\times0.05\times0.000001}}\right)=15$$

Step 10 – Calculate the intersection times using Eq. (5-23) through Eq. (5-32) and compare them with those in the plot.

-From the plot, $t_{PREL}=0.95\ hrs,\ t_{EREL}=0.038\ hrs,\ t_{PREF}=20\ hrs,\ t_{EREF}=0.2\ hrs$

-The calculated values:

1- The intersection point between linear flow and pseudo-radial flow from Eq. (5-24).

$$t_{PREL} = 1207 \frac{100^2 \times 5^2 \times 0.05 \times 0.5 \times 0.000001}{0.5} \frac{\sin^2(15)}{\cos^2(0)} = 1\ hr$$

2- The intersection point between linear flow and early radial flow lines from Eq. (5-26).

$$t_{PREL} = 1207 \frac{100^2 \times 0.05 \times 0.5 \times 0.000001}{0.5} \frac{\sin^2(14)}{\cos^2(0)} = 0.04\ hrs$$

3- The intersection point between elliptical flow and pseudo-radial flow lines from Eq. (5-27).

$$t_{PREF} = 570.7 \left(\frac{5 \times 95^{0.6}}{100^{0.6}} \right)^{1/0.36} \left(\frac{0.05 \times 0.5 \times 0.000001 \times 100^2}{0.5} \right) = 22\ hrs$$

4- The intersection point between elliptical flow and pseudo-radial flow from Eq. (5-29).

$$t_{EREF} = 570.7 \left(\frac{95^{0.6}}{100^{0.6}} \right)^{1/0.36} \left(\frac{0.05 \times 0.5 \times 0.000001 \times 100^2}{0.5} \right) = 0.26\ hrs$$

Table (5-2) summarizes the input data and the resulted value for Example 5-2.

Table 5-2: Summary of results of Example 5-2.

Parameter	In-put value	Calculated value by Type-curve matching	Calculated value by TDS technique
k_x , md	0.5	0.5	0.5
k_y , md	1.25	1.24	1.25
n	5	5	5
x_f , ft	100	100	
D , ft	100	100	95
θ_h	15	15	15

5-7- Hydraulic fractures malfunction

The hydraulic fracturing process is an excellent stimulation process for both unconventional and conventional hydrocarbon resources. This process always requires

great attention in order to assert the objectives such as creating multiple-hydraulic fractures and maintaining that they remain open. The successful fracturing treatment requires expensive completion process where the zonal isolations are required and the well may cased and cemented. However, there are several parameters may increase the risk of an unsuccessful fracturing process. These parameters can be classified under three general categories. The first category is the fracturing process itself (type of fracturing fluid and the additives). The second category is the type of formation and the degree of complexity. The third category is the completion process. Therefore, it is necessary to evaluate the performance of the hydraulic fractures.

This study introduces new and important application for the well test analysis. Well test analysis can be used as an excellent tool for the purpose of evaluating the performance of hydraulic fractures and determining locations of the fractures that do not perform as designed. Type-curve matching is the recommended technique for the interpretation process of the well test data of hydraulically fractured well. By using this technique, it is possible to know if one or more hydraulic fractures are not working properly (closed). Using the same technique, it is also possible to determine the locations of the malfunction hydraulic fractures.

Figures (5-25), (5-26), (5-27), (5-28), (5-29), (5-30), (5-31) and (5-32) represent pressure behavior of three, four, five, six, seven, eight, nine and ten vertical hydraulic fractures respectively when one fracture is not working properly (closed).

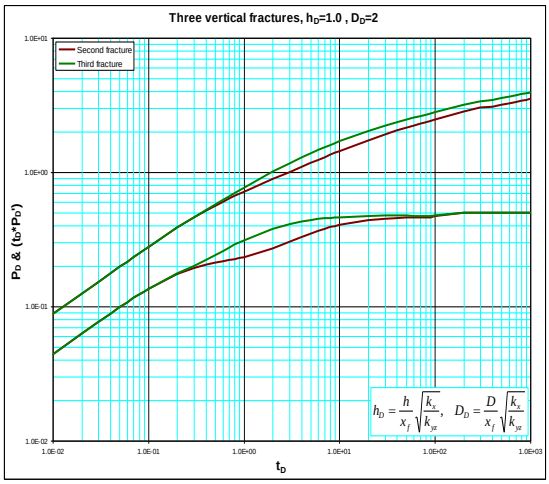

Figure 5-25: Pressure behavior of three vertical fractures with one malfunction fracture.

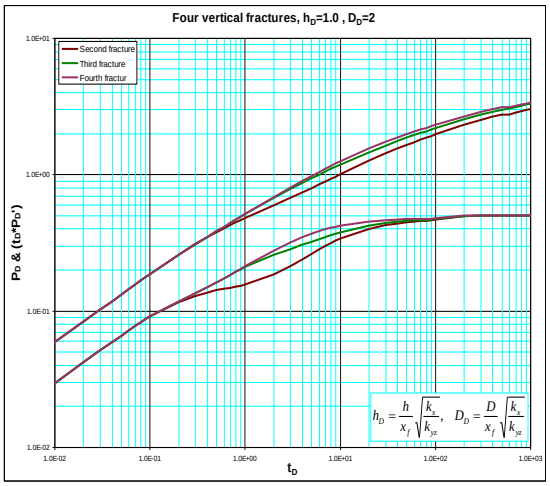

Figure 5-26: Pressure behavior of four vertical fractures with one malfunction fracture.

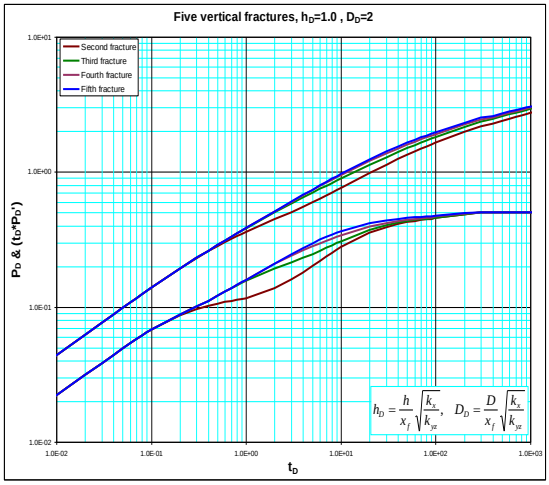

Figure 5-27: Pressure behavior of five vertical fractures with one malfunction fracture.

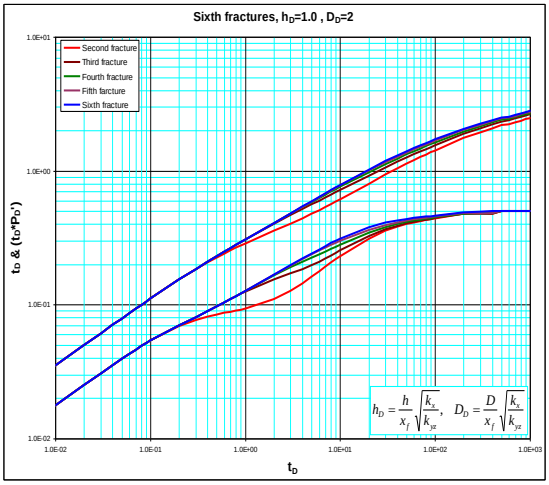

Figure 5-28: Pressure behavior of six vertical fractures with one malfunction fracture.

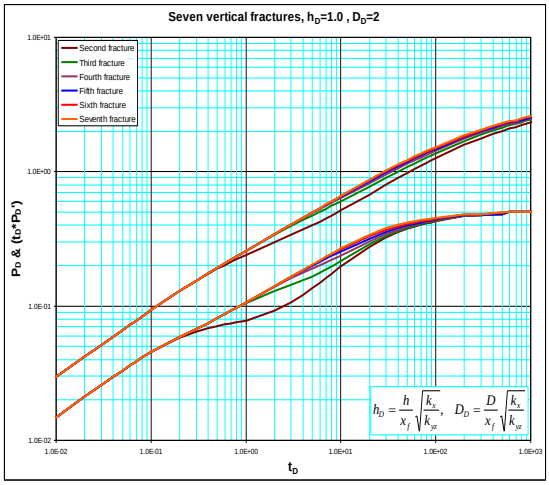

Figure 5-29: Pressure behavior of seven vertical fractures with one malfunction fracture.

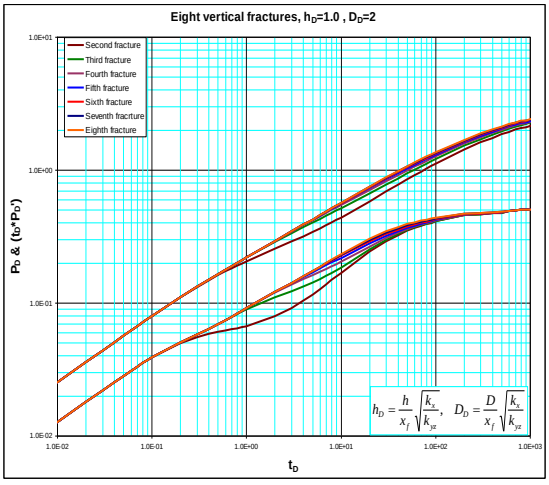

Figure 5-30: Pressure behavior of eight vertical fractures with one malfunction fracture.

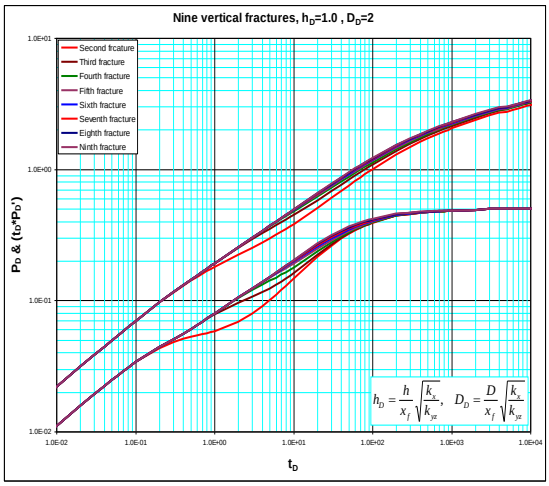

Figure 5-31: Pressure behavior of nine vertical fractures with one malfunction fracture.

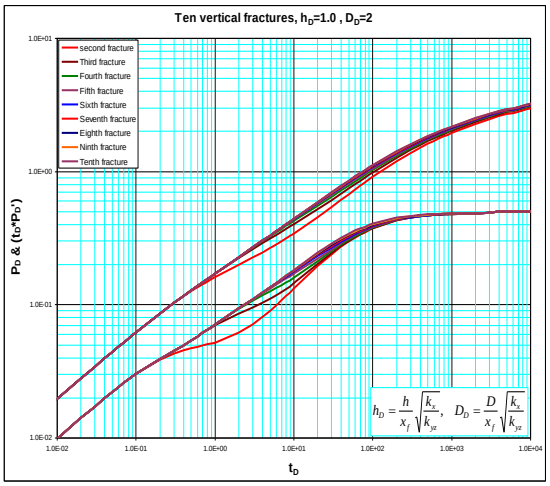

Figure 5-32: Pressure behavior of ten vertical fractures with one malfunction fracture.

For short spacing hydraulic fractures, the interference between fractures is expected to occur after short production time. Therefore, there will not be enough time for the intermediate radial flow to develop. Based on this fact, the development of this flow can be used as an indication of the existence of long spacing between fractures in addition to the existence of malfunctioning fractures. Fig.(5-33) shows the development of the intermediate radial flow when a system of eight vertical fractures looses two or more fractures.

For large spacing between fractures, the interference between fractures is expected to occur after a long period of time. Therefore, there will be enough time for the intermediate radial to be observed as a result of the radial flow toward each individual fracture. The impact of losing one or more hydraulic fractures can be represented by developing clear intermediate radial flow that lasts for a long period of time as shown in Fig. (5-34). In this case, it is difficult to decide whether the intermediate radial flow is developed by the originally designed long spacing fractures or because of the long spacing of malfunctioning fractures. However, the situation can be figured out by knowing the number of fractures that have been originally fractured and the ratio

between the pseudo-radial and intermediate radial flow. The number of existing hydraulic fractures can be found from this ratio and compared to the real member of fractures.

Example -5-3

Pressure drawdown test data has been done to evaluate the performance of a horizontal well intersected by six vertical hydraulic fractures. The test data is given in Table (Example 5-3) in Appendix (F). Other known reservoir and well data are:

$q = 100$ STB/D $\quad \phi = 0.1$ $\quad \mu = 1.5$ cp $\quad c_t = 2.5\text{x}10^{-5}$ psi^{-1} $\quad h = 50$ ft

$x_f = 50$ ft $\quad r_w = 0.5$ ft $\quad p_i = 8000$ psi $\quad B = 1.25$ bbl/STB $\quad k = 0.5$ md

$D = 100$ ft

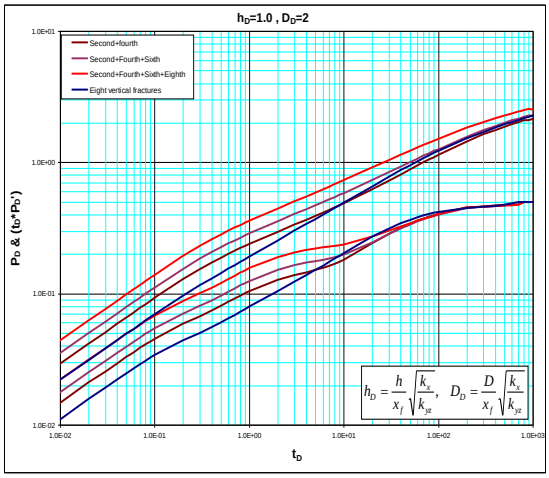

Figure 5-33: Eight vertical hydraulic fractures system with malfunctioning fractures

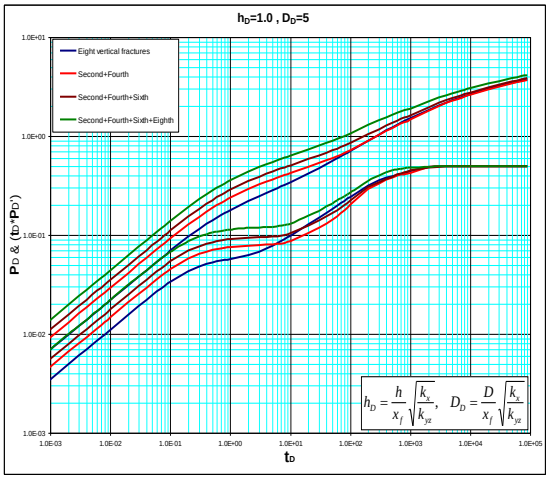

Figure 5-34: Eight vertical hydraulic fractures system with malfunctioning fractures

Solution using type-curve matching:

Step-1 Plot (ΔP vs. t) and ($t \times \Delta P'$ vs. t) on log-log paper as shown in Fig. (5-35).

Step-2 Obtain the best match of the data with one of the type curves as shown in Fig. (5-36).

From type-curve matching, it can be seen that only one hydraulic fracture is not working properly (closed) which is the third ones. Based on the spacing between fractures, the location of the malfunction fractures is (200 ft) from the heel of the horizontal well.

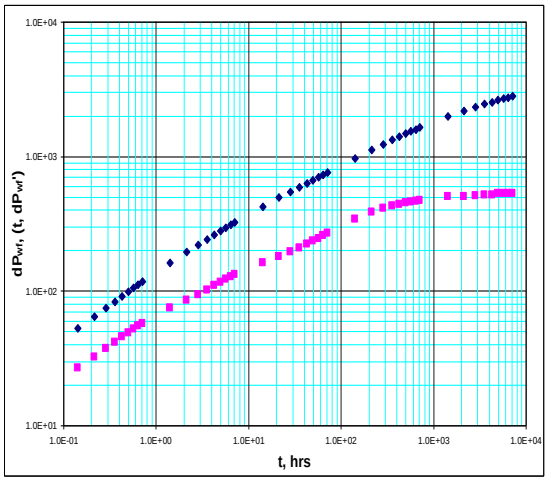

Figure 5-35: Pressure and pressure derivative plot Example 5-3.

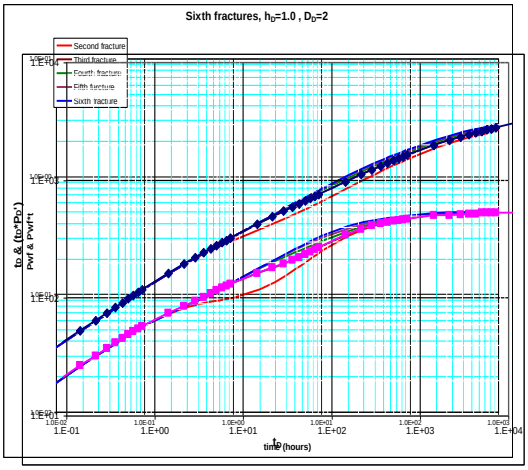

Figure 5-36: Type-curve matching plot for Example 5-3.

6- MATHEMATICAL MODELS FOR PARTIALLY PENETRATING MULTIPLE HYDRAULIC FRACTURES

Even though hydraulic fracturing process has been a common application in the petroleum industry during the last two decades, the final output of this process is significantly affected by several factors. The successful process has to produce maximum actual production from the total reserve in the formation. Fracture dimensions (half fracture length, fracture width, and fracture height) are of great importance in the performance as are the orientation of the fractures as well as the rock and fluid properties. Typically, it is preferred that the fracture height be equal to the formation height, where fully-penetrating fractures can be produced. Unfortunately, the fractures can not always penetrate totally the formation where partially penetrating fractures may be produced. Partially penetrating hydraulic fractures are undesirable stimulation process due to the possibility of reducing the expected production rate of the fractured formation. However, fully penetrating fractures in a reservoir with water and oil in contact may lead to an early or immediate water production. Therefore, partially penetrating fractures may be the only way to prevent the production of unwanted water.

6-1- Models Derivation

In this chapter, an analytical model for the pressure behavior of a horizontal well intersecting with partially penetrating multiple hydraulic fractures will be introduced. The same facts and assumptions that have been mentioned in item (4-3) for the derivation of the multiple-inclined hydraulic fractures model are necessary to be followed for the derivation of the partially penetrating hydraulic fractures models also.

Consider a horizontal well with partially penetrating vertical transverse hydraulic fractures in an infinite, homogenous, isotropic or anisotropic, horizontal slab reservoir as shown in fig. (6-1). Each fracture is considered as a single plane of length ($2x_f$), width (w), height (h_f). The spacing between fractures is (D). If we assume that all fluid withdrawal will be through the fractures, the fractures are partially penetrating the formation, the fractures can be simulated as inclined plane sources. The unsteady state pressure drop created by these planes at any point (x_m, y_m, z_m) is:

$$P(x_m, y_m, z_m, t, z_f, h_f, x_f, h) = \frac{q}{\phi c}\int_0^t S_{xyz}(x_m, y_m, z_m, t-\tau, z_f, h_f, x_f, h)d\tau \qquad (6\text{-}1)$$

S_{xyz} is the instantaneous source function for an inclined plane source in an infinite slab reservoir and (q) is the fluid withdrawal per unit fracture surface area per unit time.

$$q = \frac{Q}{2nx_f h_f} \qquad (6\text{-}2)$$

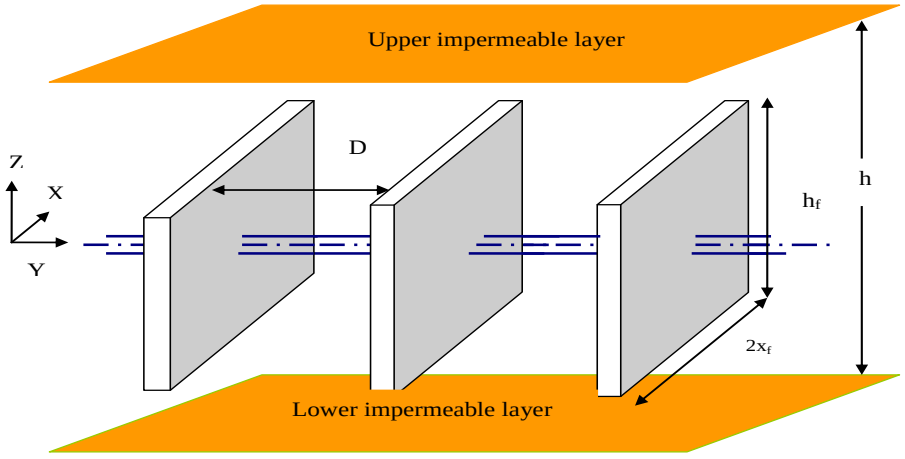

Figure 6-1: Horizontal well intersected by partially penetrating multiple hydraulic fractures.

The source function (S_{xyz}) can be obtained using the Newman product method. This method proposed that the instantaneous uniform flux source function for a three dimensional flow problem is the product of the instantaneous source function for a one dimensional flow problem. Therefore;

$$S_{xyz}(x_m, y_m, z_m, t, z_f, h_f, x_f, h) = S_x(x,t) \times S_y(y,t) \times S_z(z,t) \tag{6-3}$$

S_x is the instantaneous source function for an infinite slab source in an infinite reservoir in the direction of X-axis. S_y is the instantaneous source function for an inclined plane source in an infinite slab reservoir in the Y-direction. S_z is the instantaneous source function for an inclined plane source in an infinite slab reservoir in the vertical direction as shown in Fig. (6-2). S_x can be estimated based on half fracture length as follow:

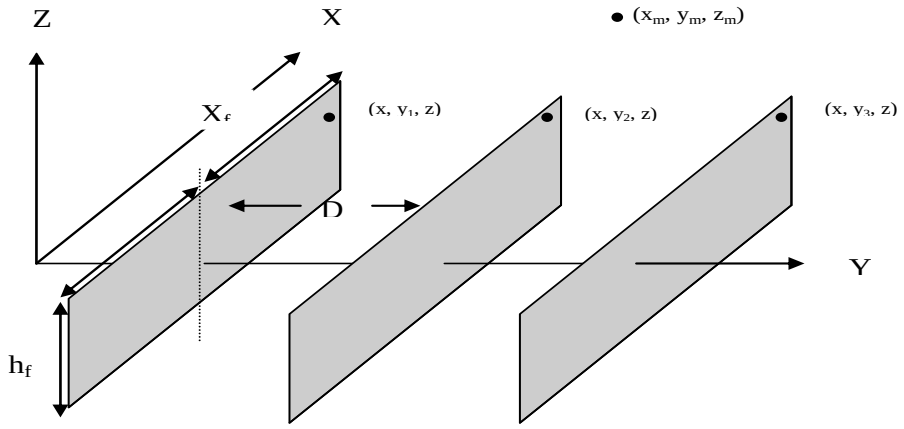

Figure 6-2: The monitoring point and the source point of partially penetrating multiple transverse hydraulic fractures.

$$S_x = \frac{1}{2\sqrt{\pi\eta_x t}} e^{-\frac{(x_m - x')^2}{4\eta_x t}} = \frac{1}{2\sqrt{\pi\eta_x t}} \int_{-x_f}^{x_f} e^{-\frac{(x_m - x - x_p)}{4\eta_x t}} dx_p = \frac{1}{2}\left[erf\left(\frac{x_m - x + x_f}{2\sqrt{\eta_x t}}\right) - erf\left(\frac{x_m - x - x_f}{2\sqrt{\eta_x t}}\right)\right] \tag{6-4}$$

$$= \frac{1}{2}\left[erf\left(\frac{x_D + 1}{2\sqrt{t_D}}\right) - erf\left(\frac{x_D - 1}{2\sqrt{t_D}}\right)\right]$$

S_y can be derived as follow:

$$S_y = \frac{1}{2\sqrt{\pi\eta_y t}} e^{-\frac{(y_m - y')^2}{4\eta t}} = \frac{1}{2\sqrt{\pi\eta_y t}} \sum_{n=1}^{n=\infty} e^{-\frac{(ym-y-nD)^2}{4\eta_y t}} = \frac{\sqrt{n_x/\eta_y}}{2\sqrt{\pi t_D}} \sum_{n=1}^{n=\infty} e^{-\frac{(y_D - nD_D)^2}{4t_D}} \quad (6\text{-}5)$$

S_z represents the instantaneous source function that is affected by the height of the formation and the height of fractures as shown in Fig. (6-3). Gringarten and Ramey 1973 presented the solution for this source function as:

$$S_z = \frac{h_f}{h}\left[1 + \frac{4h}{\pi h_f}\sum_{N=1}^{N=\infty}\frac{1}{N} e^{-\frac{N^2\pi^2\eta_z t}{h^2}} \sin\left(N\pi\frac{h_f}{2h}\right)\cos\left(N\pi\frac{z_f}{h}\right)\cos\left(N\pi\frac{z}{h}\right)\right] \quad (6\text{-}6)$$

Substitute Eqs. (6-4), (6-5), and (6-6) in Eq. (6-3) first and then substitute Eqs. (6-3) and (6-2) in Eq. (6-1) gives:

$$\Delta P = \frac{qh_f}{8nx_f h_f \phi ch\sqrt{\pi\eta_y}} \int_0^t \frac{1}{\sqrt{t}}\left[erf\left(\frac{x_m - x + x_f}{2\sqrt{\eta_x t}}\right) - erf\left(\frac{x_m - x - x_f}{2\sqrt{\eta_x t}}\right)\right] \times \sum_{n=1}^{n=\infty} e^{-\frac{(ym-y-nD)^2}{4\eta_y t}} \times \left[1 + \frac{4h}{\pi h_f}\sum_{N=1}^{N=\infty}\frac{1}{N} e^{-\frac{N^2\pi^2\eta_z t}{h^2}} \sin\left(N\pi\frac{h_f}{2h}\right)\cos\left(N\pi\frac{z_f}{h}\right)\cos\left(N\pi\frac{z}{h}\right)\right] dt \quad (6\text{-}7)$$

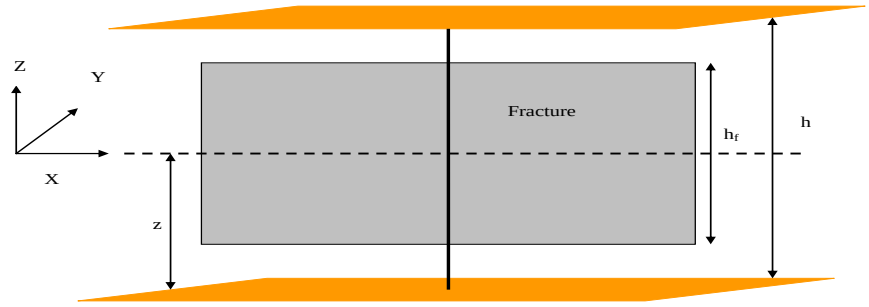

Figure 6-3: Schematic diagram of partial penetrating hydraulic fracture.

In dimensionless form, the final model for pressure response of horizontal wells intersecting by multiple partially penetrating vertical hydraulic fractures is:

$$P_D = \frac{\sqrt{\pi}}{4n}\int_0^{t_D}\frac{1}{\sqrt{t_D}}\left[erf\left(\frac{x_D+1}{2\sqrt{t_D}}\right)-erf\left(\frac{x_D-1}{2\sqrt{t_D}}\right)\right]\times\sum_{n=1}^{n=\infty}e^{-\frac{(y_D-nD_D)^2}{4t_D}}\times \left[1+\frac{4}{\pi h_{hfD}}\sum_{N=1}^{N=\infty}\frac{1}{N}e^{-N^2\pi^2 h_{xfD}^2 t_D}\sin\left(N\pi\frac{h_{hfD}}{2}\right)\cos\left(N\pi z_{fD}\right)\cos\left(N\pi z_{hfD}\right)\right]dt \quad (6\text{-}8)$$

where:

$$x_D = \frac{x_m - x}{x_f} \quad (6\text{-}9)$$

$$y_D = \frac{y_m - y}{x_f}\sqrt{\frac{k_x}{k_y}} \quad (6\text{-}10)$$

$$z_{fD} = \frac{z_f}{h} \quad (6\text{-}11)$$

$$h_{xfD} = \frac{x_f}{h}\sqrt{\frac{k_z}{k_x}} \quad (6\text{-}12)$$

$$z_{hfD} = \frac{z}{h} \quad (6\text{-}13)$$

$$h_{hfD} = \frac{h_f}{h} \quad (6\text{-}14)$$

$$D_D = \frac{D}{x_f}\sqrt{\frac{kx}{k_y}} \quad (6\text{-}15)$$

$$t_D = \frac{0.0002637\,k_x t}{\phi\mu c x_f^2} \quad (6\text{-}16)$$

$$P_D = \frac{2\pi\sqrt{k_x k_y}\,h\Delta P}{q\mu} \quad (6\text{-}17)$$

To solve the above model given in Eq. (6-8), three long time approximations should be done based on the fluid flow dynamics and flow regimes in late time. The first approximation is for instantaneous source function S_x given by Eq. (6-4).

$$erf\left(\frac{x_{D+1}}{2\sqrt{t_D}}\right)=\frac{2}{\pi}\sum_{n=0}^{n=\infty}\frac{(-1)^n}{n!}\frac{\left(\frac{x_{D+1}}{2\sqrt{t_D}}\right)^{2n+1}}{(2n+1)}=\frac{x_{D+1}}{\sqrt{t_D}}-\frac{(x_D+1)^3}{12t_D^{3/2}}+\frac{(x_D+1)^5}{160t_D^{5/2}}-.....+.....\cong\frac{x_D+1}{\sqrt{t_D}} \quad (6\text{-}18)$$

and:

$$erf\left(\frac{x_D-1}{2\sqrt{t_D}}\right)=\frac{2}{\pi}\sum_{n=0}^{n=\infty}\frac{(-1)^n}{n!}\frac{\left(\frac{x_{D11}}{2\sqrt{t_D}}\right)^{2n+1}}{(2n+1)}=\frac{x_{D11}}{\sqrt{t_D}}-\frac{(x_D-1)^3}{12t_D^{3/2}}+\frac{(x_D-1)^5}{160t_D^{5/2}}-.....+.....\cong\frac{x_D-1}{\sqrt{t_D}} \quad (6\text{-}19)$$

therefore:

$$t_D\geq\frac{25}{3}(xD+1) \quad (6\text{-}20)$$

and:

$$t_D\geq\frac{25}{3}(xD-1) \quad (6\text{-}21)$$

The second approximation is for the instantaneous source function S_y given in Eq. (6-5).

$$S_y=\frac{\sqrt{n_x/\eta_y}}{2\sqrt{\pi t_D}}\sum_{n=1}^{n=\infty}e^{-\frac{(y_D-nD_D)^2}{4t_D}}=\frac{\sqrt{n_x/\eta_y}}{2\sqrt{\pi t_D}}\left[1-\frac{(y_D-nD_D)^2}{4t_D}+\frac{(y_D-nD_D)^4}{32t_D^2}-....\right] \quad (6\text{-}22)$$

The exponential expansion can be approximated by its first term:

$$\frac{100(y_D-nD_D)^2}{4t_D}\leq 1 \quad (6\text{-}23)$$

therefore:

$$t_D\geq 25(y_D-nD_D)^2 \quad (6\text{-}24)$$

The third approximation for the instantaneous source function S_z is given in Eq. (6-6).

$$S_z = \frac{h_f}{h}\left[1+\frac{4h}{\pi h_f}\sum_{N=1}^{N=\infty}\frac{1}{N}e^{-\frac{N^2\pi^2\eta_z t}{h^2}}\sin\left(N\pi\frac{h_f}{2h}\right)\cos\left(N\pi\frac{z_f}{h}\right)\cos\left(N\pi\frac{z}{h}\right)\right]= \\ \frac{h_f}{h}+\frac{4}{\pi}\sum_{N=1}^{N=\infty}\frac{1}{N}e^{-\frac{N^2\pi^2\eta_z t}{h^2}}\sin\left(N\pi\frac{h_f}{2h}\right)\cos\left(N\pi\frac{z_f}{h}\right)\cos\left(N\pi\frac{z}{h}\right) \tag{6-25}$$

Since:

$$\frac{4}{\pi}e^{-\pi^2 h_{xfD}^2 t_D} \le 0.01 \tag{6-26}$$

therefore:

$$t_D \ge \frac{5}{\pi^2 h_{xfD}^2} \tag{6-27}$$

The long time approximation can be written as:

$$P_D = \frac{q}{2nx_f h_f \theta\mu}\int_0^{t_{D1}} X(x_D,t_D)\times YZ(y_D,z_D,t_D,\phi_v,z_{fD},h_{fD},h_D)+\frac{1}{2}\int_{t_{D1}}^{t_D}\frac{1}{\tau_D}d\tau_D \\ = P_D(x_D,y_D,z_D,z_{wD},L_D,t_{D1})+\frac{1}{2}\ln\left(\frac{t_D}{t_{D1}}\right) \tag{6-28}$$

and the proper time for this approximation is:

$$t_{D1} \ge \begin{bmatrix} \frac{25}{3}(xD+1) \\ \frac{25}{3}(xD-1) \\ 25(y_D-nD_D)^2 \\ \frac{5}{\pi^2 h_{xfD}^2} \end{bmatrix} \tag{6-29}$$

6-2-Partially penetrating multiple inclined transverse hydraulic fractures

For partially penetrating multiple inclined fractures as shown in Fig. (6-4), the model for pressure behavior can be derived using the same method as for the partially

penetrating multiple vertical fractures, except the instantaneous source function in the vertical direction should be as:

$$S_z = \frac{h_f \cos(\theta_v)}{h}\left[1+\frac{4h}{\pi h_f \cos(\theta_v)}\sum_{N=1}^{N=\infty}\frac{1}{N}e^{-\frac{N^2\pi^2\eta_z t}{h^2}}\sin\left(N\pi\frac{h_f\cos(\theta_v)}{2h}\right)\cos\left(N\pi\frac{z_f}{h}\right)\cos\left(N\pi\frac{z}{h}\right)\right] \quad (6\text{-}30)$$

Therefore the pressure model becomes:

$$\Delta P = \frac{qh_f}{8nx_f h_f \phi ch\sqrt{\pi\eta_y}}\int_0^t \frac{1}{\sqrt{t}}\left[erf\left(\frac{x_m - x + x_f}{2\sqrt{\eta_x t}}\right) - erf\left(\frac{x_m - x - x_f}{2\sqrt{\eta_x t}}\right)\right]\times\sum_{n=1}^{n=\infty}e^{-\frac{(ym-y-nD)^2}{4\eta_y t}} \quad (6\text{-}31)$$
$$\times\left[1+\frac{4h}{\pi h_f\cos(\theta_v)}\sum_{N=1}^{N=\infty}\frac{1}{N}e^{-\frac{N^2\pi^2\eta_z t}{h^2}}\sin\left(N\pi\frac{h_f\cos(\theta_v)}{2h}\right)\cos\left(N\pi\frac{z_f}{h}\right)\cos\left(N\pi\frac{z}{h}\right)\right]dt$$

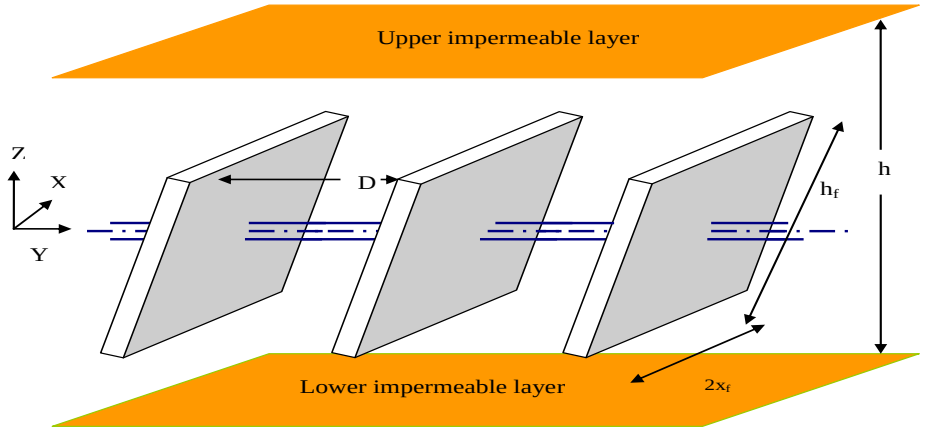

Figure 6-4: Horizontal well intersected by partially penetrating multiple inclined hydraulic fractures.

In dimensionless form, the model becomes:

$$P_D = \frac{\sqrt{\pi}}{4n}\int_0^{t_D}\frac{1}{\sqrt{t_D}}\left[erf\left(\frac{x_D+1}{2\sqrt{t_D}}\right)-erf\left(\frac{x_D-1}{2\sqrt{t_D}}\right)\right]\times\sum_{n=1}^{n=\infty}e^{-\frac{(y_D-nD_D)^2}{4t_D}}\times \quad (6\text{-}32)$$
$$\left[1+\frac{4}{\pi h_{hfD}\cos(\theta_v)}\sum_{N=1}^{N=\infty}\frac{1}{N}e^{-N^2\pi^2 h_{xfD}^2 t_D}\sin\left(N\pi\frac{h_{hfD}\cos(\theta_v)}{2}\right)\cos\left(N\pi z_{fD}\right)\cos\left(N\pi z_{hfD}\right)\right]dt$$

7- PRESSURE TRANSIENT ANALYSIS FOR HORIZONTAL WELLS INTERSECTED BY PARTIALLY PENETRATING MULTIPLE INCLINED HYDRAULIC FRACTURES

The penetration ratio (the ratio of the fracture's height to the formation's height) has significant influences on the pressure behaviors and flow regimes. Several analytical models will be introduced in this chapter for six flow regimes. A set of type-curve matching plots have been presented to reflect the compound effects of the penetration ratio, the number of fractures, the spacing between fractures as well as fracture dimensions and inclination angle from the vertical axis. Three new flow regimes can be observed for the partially penetrating fractures. These are in addition to the early linear (First linear) flow, intermediate radial (early radial for fully penetrating fractures), elliptical flow, and pseudo-radial flow. The first of these three new regimes is the second linear flow. This regime represents the flow toward the fractures plane in the XZ plane after the pressure behavior is affected by the upper and lower boundary. The second regime is the early radial that represents the radial flow in the YZ plane toward the fracture before the boundaries are reached. The third regime is the third linear flow that represents the linear flow toward the fractures in the YZ plane.

7-1- Pressure behavior

The following responses are easy to identify based on different penetration ratios.

7-1-1- Large penetration ratio (h_{hfD}>0.5)

Because of the penetration ratio, the pressure behavior in this case tends to be similar to the fully penetrating fractures where other factors such as the number of

fractures, spacing between them, fracture dimensions, and inclination angle have the main influences.

7-1-1-1- Short half fracture length (h_{xfD}<10)

1- For a small number of hydraulic fractures (less than five) and short spacing, first linear, transition, second linear, transition and pseudo-radial flow are observed as shown in Figs. (7-1) and (7-2).

2- For a small number of hydraulic fractures (less than five) and long spacing, first linear, transition, second linear, intermediate radial, transition and pseudo radial flow are observed as shown in Figs. (7-3) and (7-4).

3- For a large number of hydraulic fractures (more than five) and small spacing, first linear, transition, second linear, third linear, transition and pseudo-radial flow regimes are observed such as in Figs. (7-5) and (7-6).

4- For a large number of hydraulic fractures (more than five) and long spacing, first linear, transition, second linear, intermediate radial, elliptical, transition and pseudo radial flow regimes are observed as shown in Figs. (7-7) and (7-8).

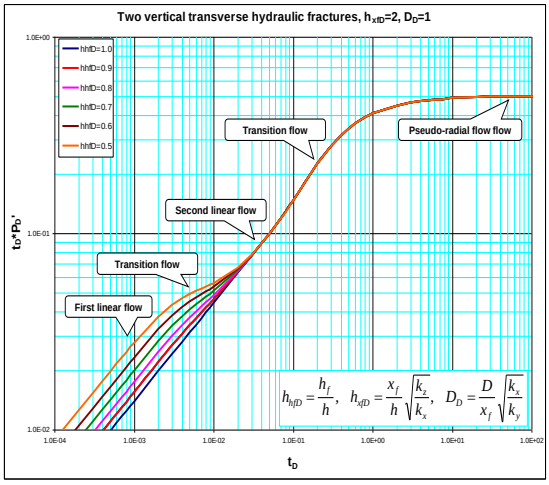

Figure 7-1: Pressure behavior of two partially penetrating vertical hydraulic fractures.

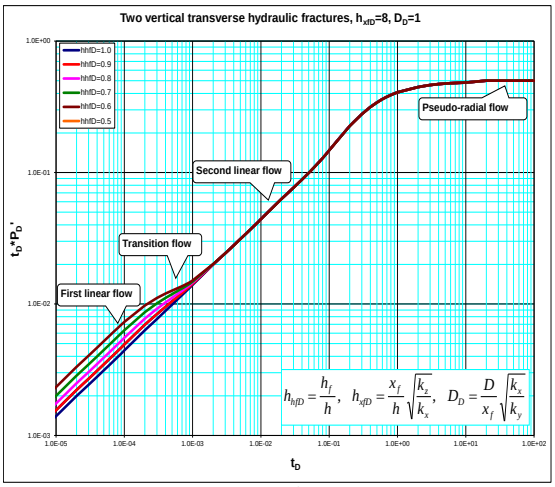

Figure 7-2: Pressure behavior of two partially penetrating vertical hydraulic fractures.

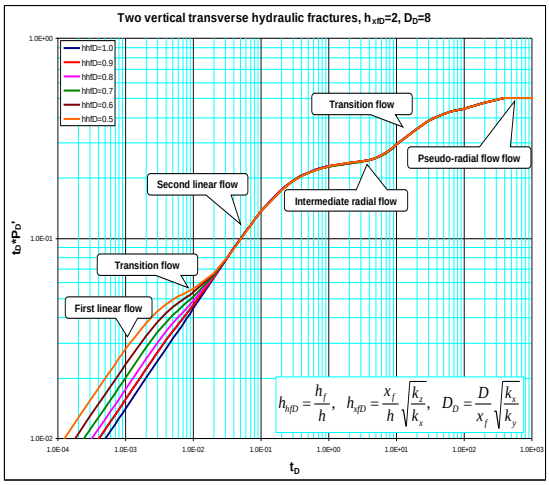

Figure 7-3: Pressure behavior of two partially penetrating vertical hydraulic fractures.

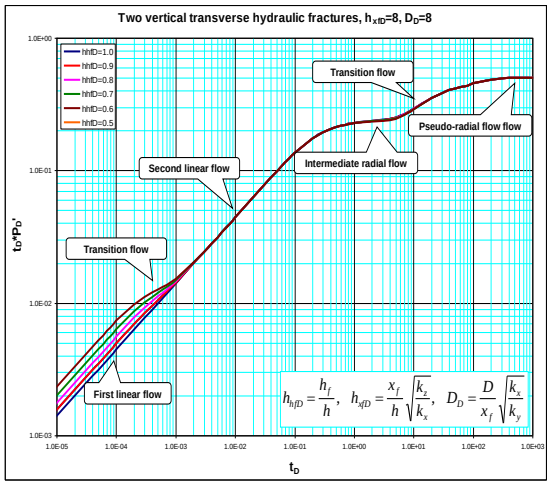

Figure 7-4: Pressure behavior of two partially penetrating vertical hydraulic fractures.

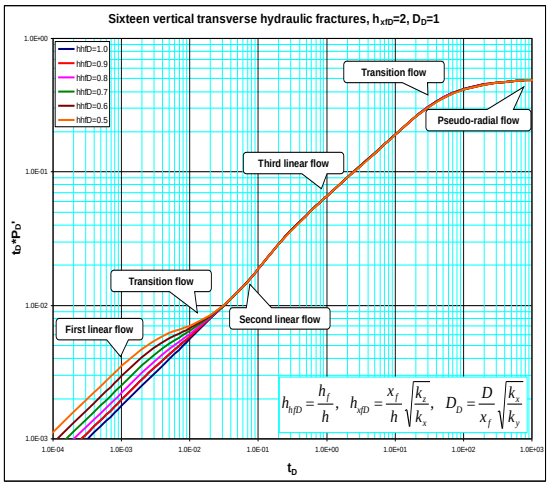

Figure 7-5: Pressure behavior of sixteen partially penetrating vertical hydraulic fractures.

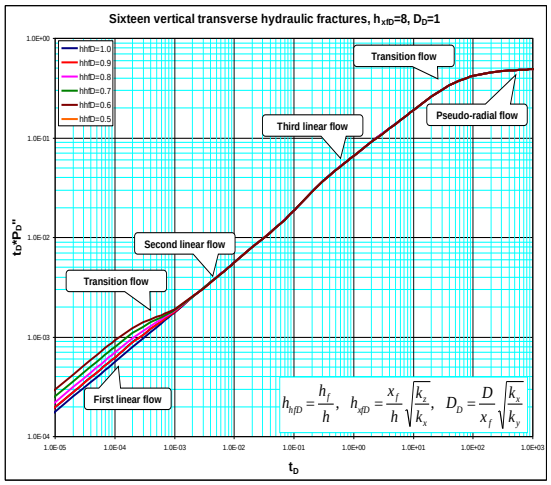

Figure 7-6: Pressure behavior of sixteen partially penetrating vertical hydraulic fractures.

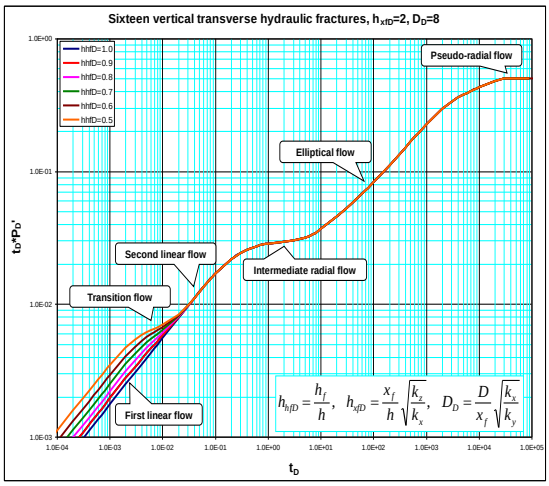

Figure 7-7: Pressure behavior of sixteen partially penetrating vertical hydraulic fractures.

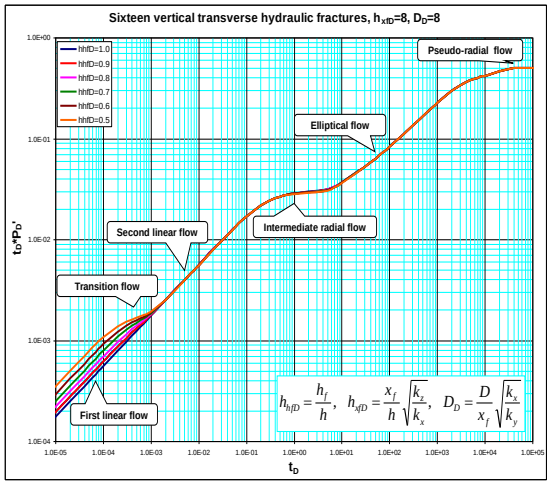

Figure 7-8: Pressure behavior of sixteen partially penetrating vertical hydraulic fractures.

7-1-1-2- Long half fracture length (h_{xfD}>10)

1- For a small number of hydraulic fractures (less than five) and short spacing, first linear, transition, second linear, transition and pseudo-radial flow regimes are observed as shown in Figs. (7-9) and (7-10).

2- For a small number of hydraulic fractures (less than five) and long spacing, first linear, transition, second linear, intermediate radial, transition and pseudo radial flow regimes are observed as shown in Figs. (7-11) and (7-12).

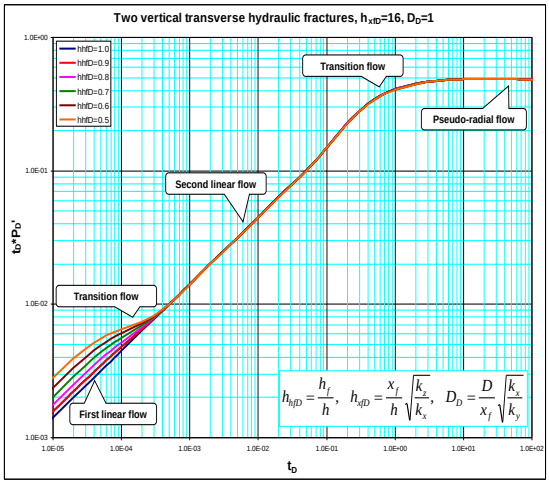

Figure 7-9: Pressure behavior of two partially penetrating vertical hydraulic fractures.

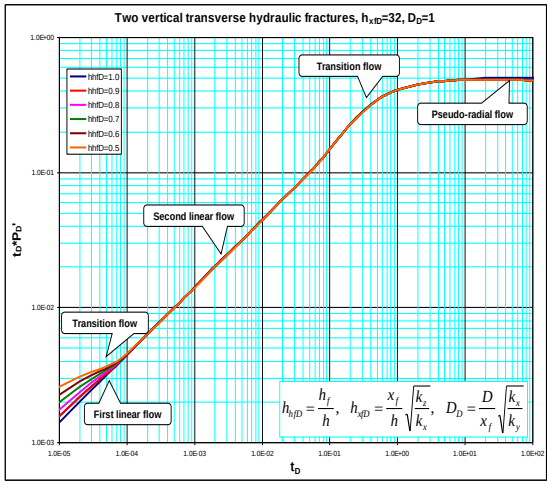

Figure 7-10: Pressure behavior of two partially penetrating vertical hydraulic fractures.

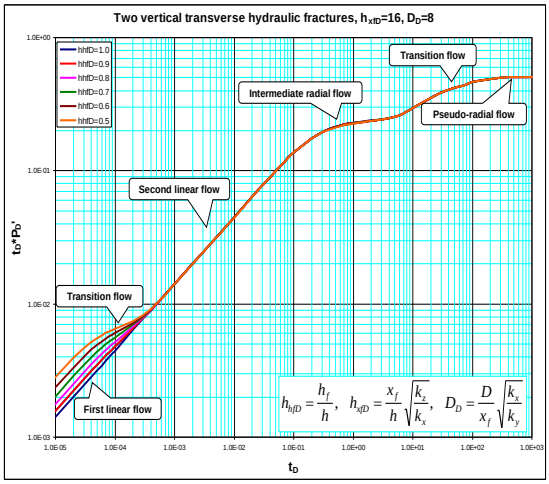

Figure 7-11: Pressure behavior of two partially penetrating vertical hydraulic fractures.

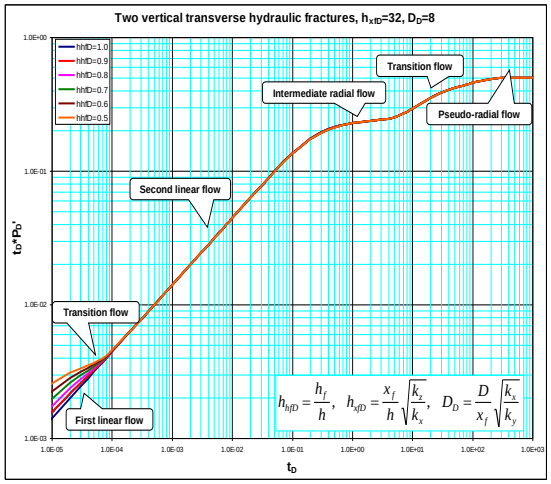

Figure 7-12: Pressure behavior of two partially penetrating vertical hydraulic fractures.

3- For a large number of hydraulic fractures (more than five) and small spacing, first linear flow is not observed. Therefore, second linear, third linear, transition and pseudo-radial flow regimes are the only flow regimes that are observed such as in Figs. (7-13) and (7-14).

4- For a large number of hydraulic fractures (more than five) and long spacing, first linear flow also is not observed. Second linear, intermediate radial, elliptical, transition and pseudo radial flow regimes are observed as shown in Figs. (7-15) and (7-16).

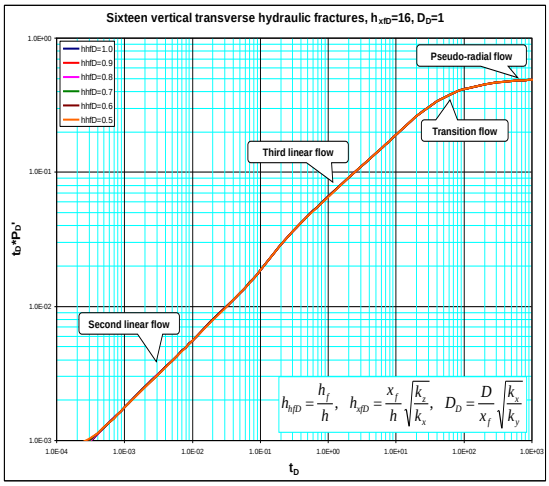

Figure 7-13: Pressure behavior of sixteen partially penetrating vertical hydraulic fractures.

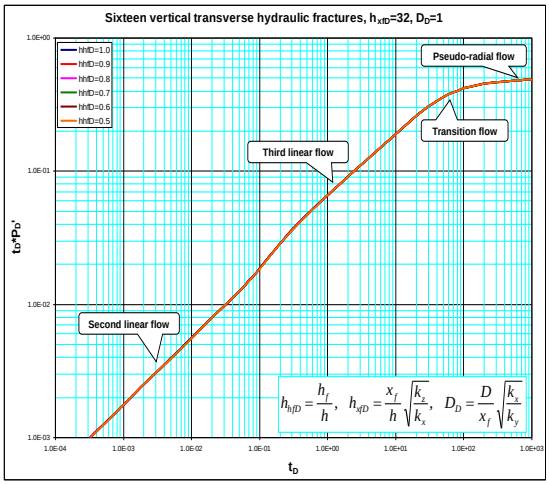

Figure 7-14: Pressure behavior of sixteen partially penetrating vertical hydraulic fractures.

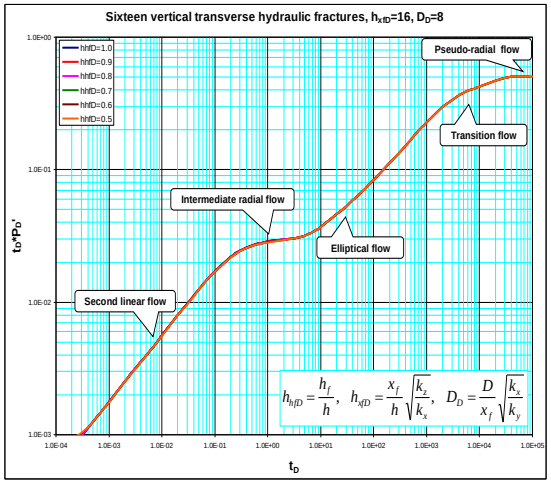

Figure 7-15: Pressure behavior of sixteen partially penetrating vertical hydraulic fractures.

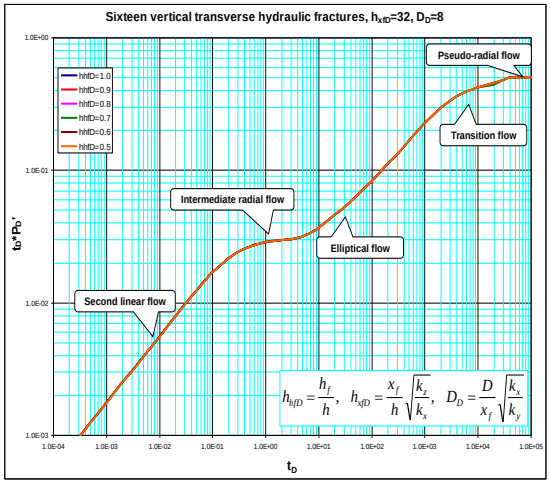

Figure 7-16: Pressure behavior of sixteen partially penetrating vertical hydraulic fractures

7-1-2- Small penetration ratio (h_{hfD}<0.5)

Because of the small penetration ratio, the pressure behavior at early time tends to develop a new early radial flow regime where the flow of fluid takes place in the YZ plane.

7-1-2-1- Short half fracture length (h_{xfD}<10)

1- For a small number of hydraulic fractures (less than five) and short spacing, first linear, transition, early radial, second linear for h_{xfD}>5 or transition for h_{xfd}<5 and pseudo-radial flow regimes are observed as shown in Figs. (7-17) and (7-18).

2- For a small number of hydraulic fractures (less than five) and long spacing, first linear, early radial, second linear, transition, intermediate radial, transition and pseudo radial flow regimes are observed as shown in Figs. (7-19) and (7-20).

3- For a large number of hydraulic fractures (more than five) and small spacing, first linear, early radial, second linear, third linear, transition and pseudo-radial flow regimes are observed for h_{xfD}<5 such as in Fig. (7-21). While for h_{xfD}>5, first linear flow can't be observed such as in Figs. (7-22).

4- For a large number of hydraulic fractures (more than five) and long spacing, first radial, early radial, second linear, intermediate radial, elliptical, transition and pseudo radial flow regimes are observed foe h_{xfD}<5 as shown in Fig. (7-23). While for h_{xfD}>5, first linear flow can't be observed as shown in Fig. (7-24).

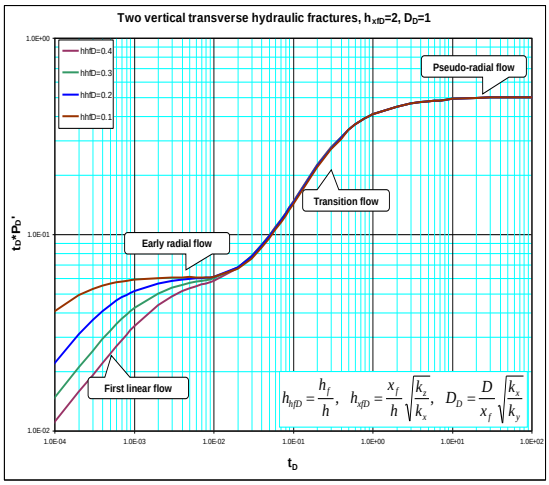

Figure 7-17: Pressure behavior of two partially penetrating vertical hydraulic fractures.

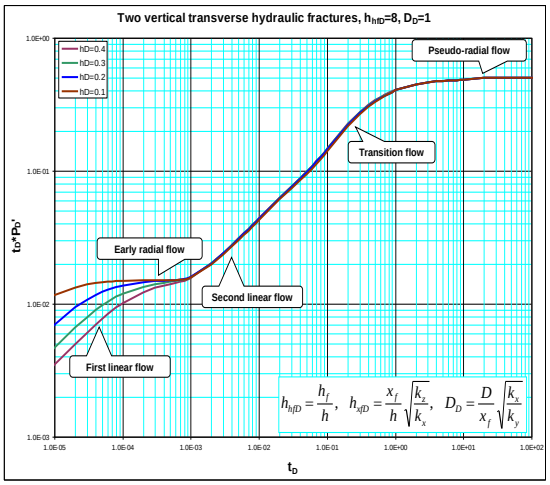

Figure 7-18: Pressure behavior of two partially penetrating vertical hydraulic fractures.

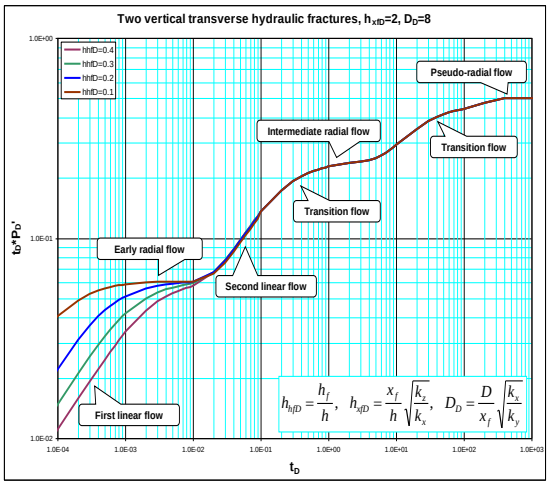

Figure 7-19: Pressure behavior of two partially penetrating vertical hydraulic fractures.

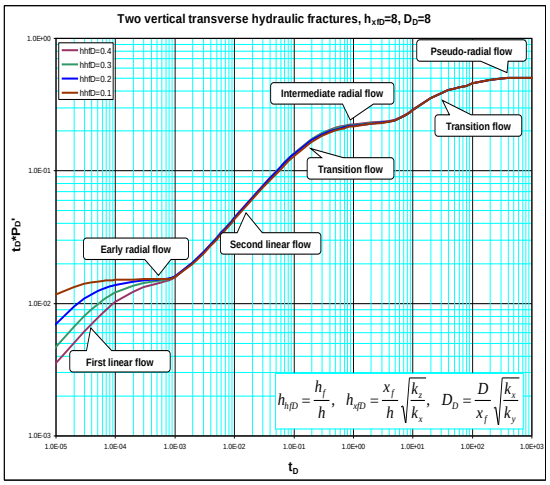

Figure 7-20: Pressure behavior of two partially penetrating vertical hydraulic fractures.

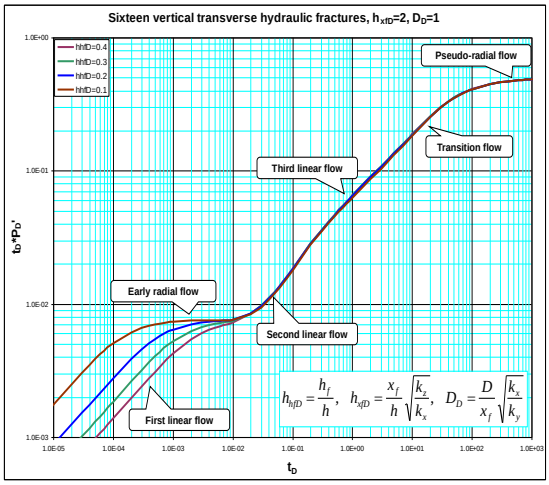

Figure 7-21: Pressure behavior of sixteen partially penetrating vertical hydraulic fractures.

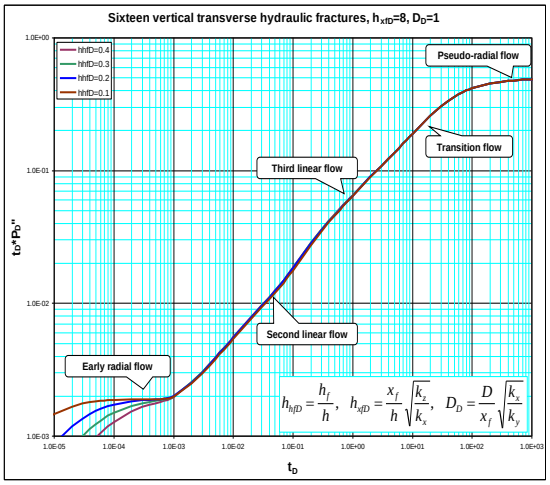

Figure 7-22: Pressure behavior of sixteen partially penetrating vertical hydraulic fractures.

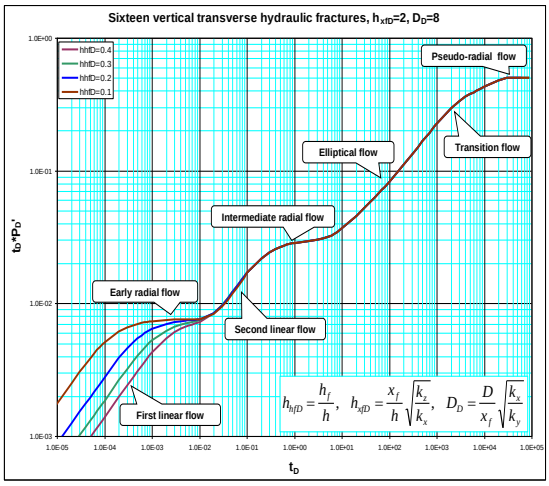

Figure 7-23: Pressure behavior of sixteen partially penetrating vertical hydraulic fractures.

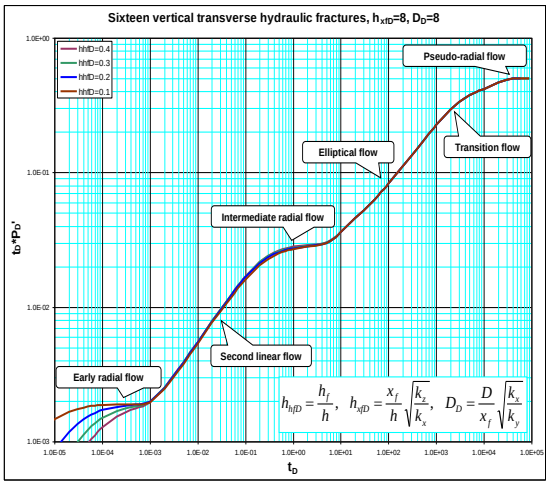

Figure 7-24: Pressure behavior of sixteen partially penetrating vertical hydraulic fractures.

7-1-1-2- Long half fracture length (h_{xfD}>10)

1- For a small number of hydraulic fractures (less than five) and short spacing, first linear flow can not be observed. Early radial, second linear, transition and pseudo-radial flow regimes are observed as shown in Figs. (7-25) and (7-26). The behavior in these two cases is similar to the horizontal wells with short to moderate wellbore length.

2- For a small number of hydraulic fractures (less than five) and long spacing, first linear flow can not be observed. Early radial, second linear, transition, intermediate radial, transition and pseudo radial flow regimes are observed as shown in Figs. (7-27) and (7-28).

3- For a large number of hydraulic fractures (more than five) and small spacing, neither first linear flow nor early radial flow can be observed. Second linear, third linear, transition and pseudo-radial flow are the only flow regimes that are observed such as in Figs. (7-29) and (7-30). The behavior in these two cases is similar to a single vertical hydraulic fracture.

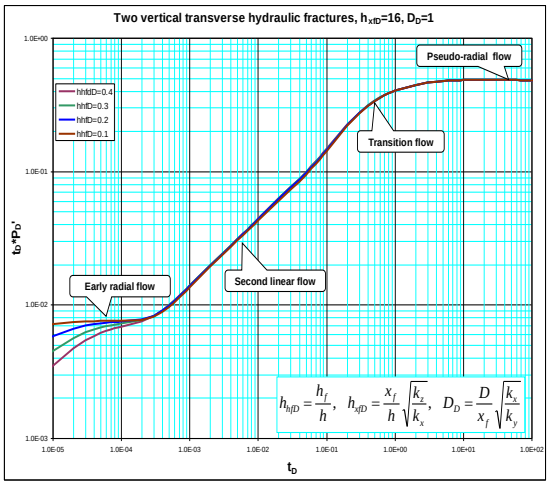

Figure 7-25: Pressure behavior of two partially penetrating vertical hydraulic fractures.

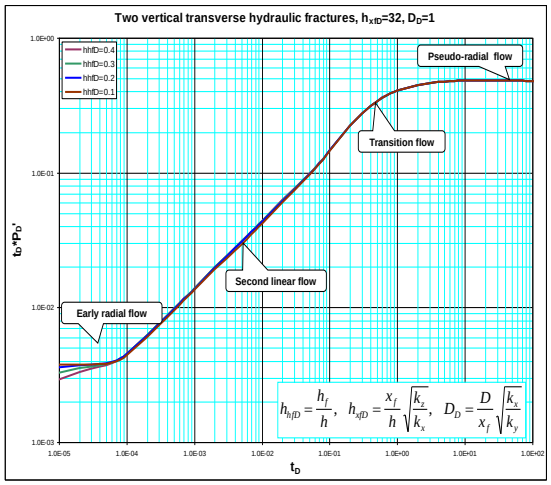

Figure 7-26: Pressure behavior of two partially penetrating vertical hydraulic fractures.

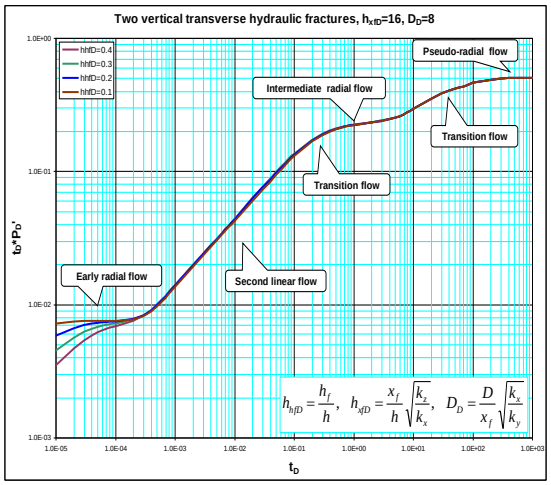

Figure 7-27: Pressure behavior of two partially penetrating vertical hydraulic fractures.

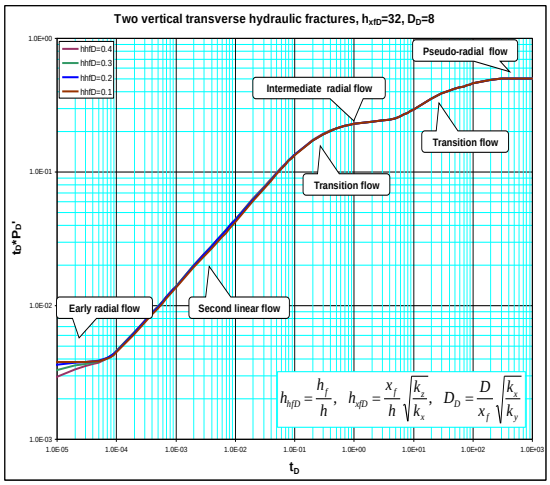

Figure 7-28: Pressure behavior of two partially penetrating vertical hydraulic fractures.

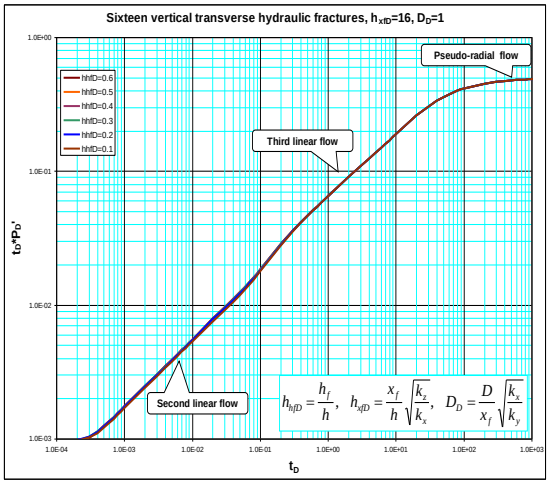

Figure 7-29: Pressure behavior of sixteen partially penetrating vertical hydraulic fractures.

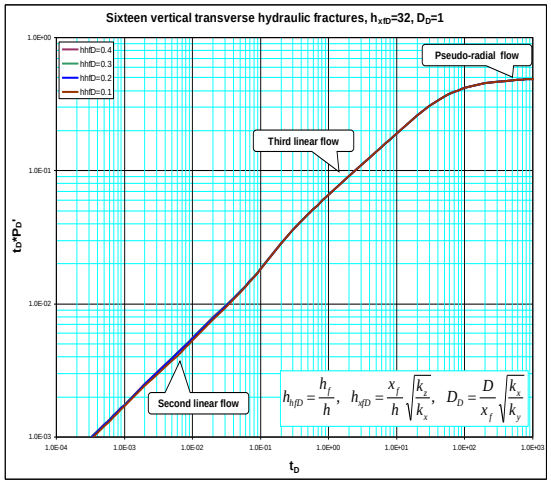

Figure 7-30: Pressure behavior of sixteen partially penetrating vertical hydraulic fractures.

4- For a large number of hydraulic fractures (more than five) and long spacing, neither first linear flow nor early radial flow can be observed also. Second linear, intermediate radial, elliptical, transition and pseudo radial flow regimes are observed as shown in Figs. (7-31) and (7-32). The behavior in these two cases is similar to multiple hydraulic fractures.

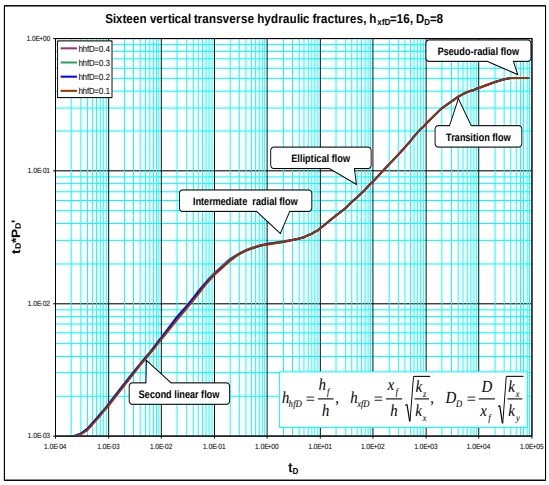

Figure 7-31: Pressure behavior of sixteen partially penetrating vertical hydraulic fractures.

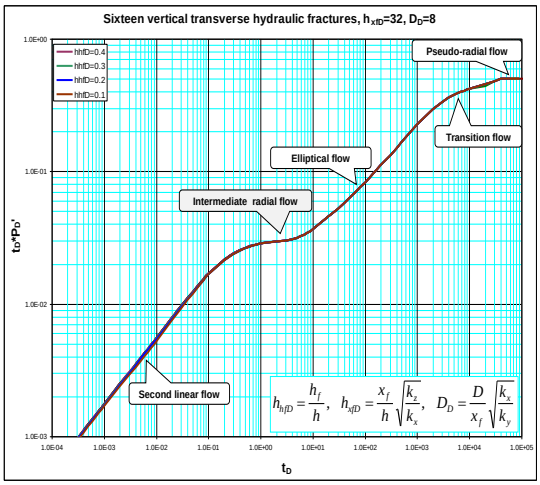

Figure 7-32: Pressure behavior of sixteen partially penetrating vertical hydraulic fractures

7-2- Effect of inclination angle

The inclination angle from the vertical axis (θ_v) has a similar effect on pressure behavior of partially penetrating hydraulic fractures as the penetration ratio. It can be explained by the reduction in the fracture height which leads to a reduction in the penetration ratio, when the fractures are inclined from the vertical direction. As fractures propagate in inclined directions rather than the vertical one, the probability for partially penetrating fractures to occur is high. Figures (7-33) and (7-34) represent pressure behaviors for two partially penetrating inclined hydraulic fractures for different inclination angles. While Figures (7-35) and (7-36) represent pressure behaviors of ten partially penetrating inclined hydraulic fractures for different inclination angles. For all

cases, the early radial flow develops when the inclination angle from the vertical direction increases.

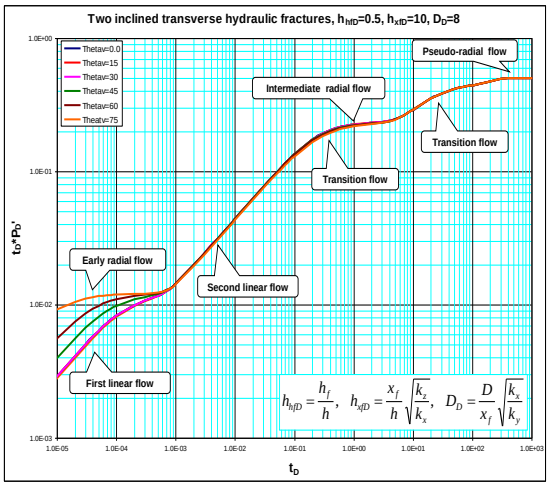

Figure 7-33: Pressure behavior of two partially penetrating inclined hydraulic fractures.

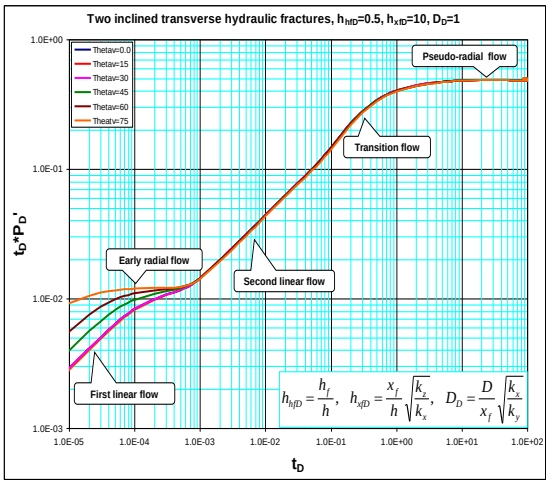

Figure 7-34: Pressure behavior of two partially penetrating inclined hydraulic fractures.

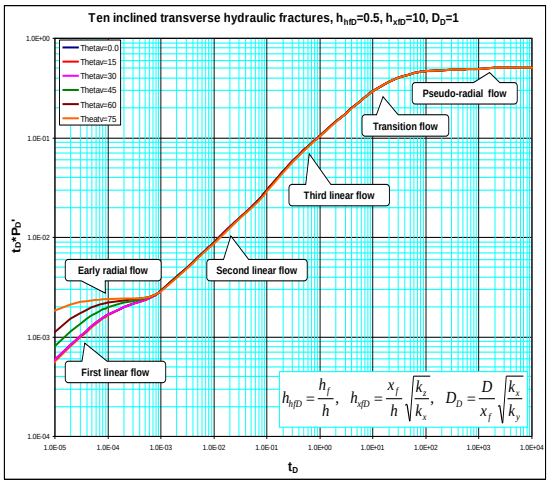

Figure 7-35: Pressure behavior of ten partially penetrating inclined hydraulic fractures.

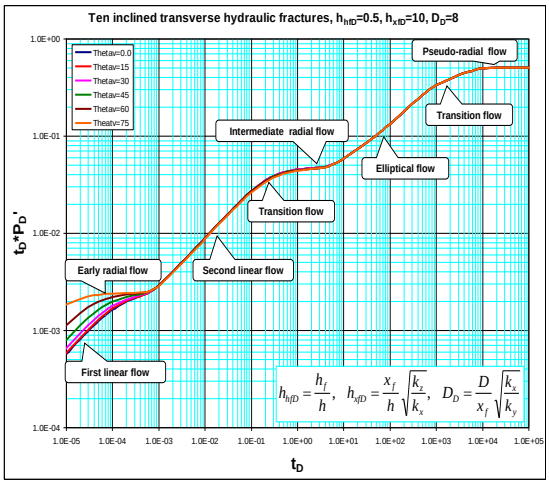

Figure 7-36: Pressure behavior of ten partially penetrating inclined hydraulic fractures.

7-3- Flow regimes

7-3-1- First linear flow regime

At early time, reservoir fluid flows linearly and directly from the formation to the individual fractures in the XZ plane as shown in Fig. (7-37). Each fracture behaves independently from the others. The flow regime is represented by straight line with a slope of (0.5) in the log-log plots for both dimensionless pressure and pressure

derivative with dimensionless time. The governing equations for linear flow regime in the case of transverse hydraulic fractures are:

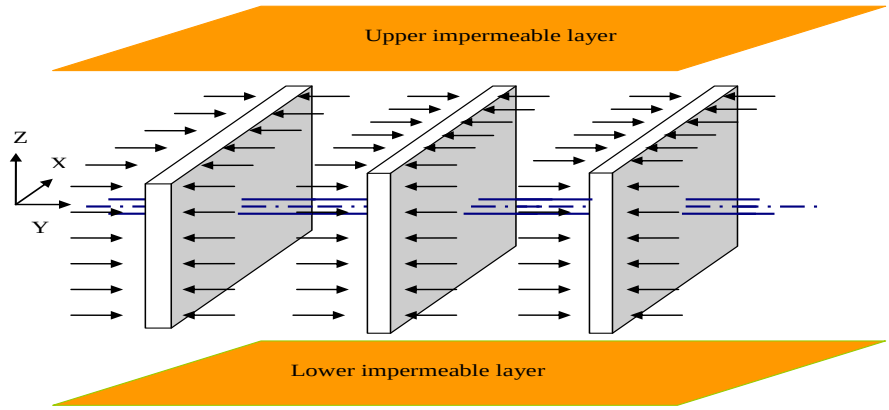

Figure 7-37: First linear flow regime for partially penetrating multiple hydraulic fractures.

$$\left(P_D\right)_{FLF} = \frac{\sqrt{\pi t_D}}{n h_{hfD} \cos(\theta_v)} \tag{7-1}$$

$$\left(\Delta P\right)_{FLF} = \frac{4.063 qB}{n h_f x_f \cos(\theta_v)} \sqrt{\frac{\mu t}{k_y \phi c_t}} \tag{7-2}$$

or;

$$\left(t_D \times P_D'\right)_{FLF} = \frac{\sqrt{\pi t_D}}{2 n h_{hfD} \cos(\theta_v)} \tag{7-3}$$

$$\left(t \times \Delta P\right)_{FLF} = \frac{2.032 qB}{n h_f x_f \cos(\theta_v)} \sqrt{\frac{\mu t}{k_y \phi c_t}} \tag{7-4}$$

where;

$$\left(P_D\right)_{FLF} = 2 \times \left(t_D \times P_D'\right)_{FLF} \tag{7-5}$$

7-3-2- Early radial flow regime

Early radial flow regime represents the radial flow around each fracture in the YZ plane. Typically, this flow is observed when the penetratation ratio is small (h_{hfD}<0.5)

and the spacing between fractures is long (D_D>5). In this flow, reservoir fluids flow radially in YZ plane toward each individual fractures such as shown in Fig. (7-38). The governing equations for this flow are:

$$\left(t_D \times P_D'\right)_{ERF} = \frac{0.5}{2nh_{xfD}} \tag{7-6}$$

$$\left(t \times \Delta P\right)_{ERF} = \frac{35.3q\mu B}{nx_f\sqrt{k_y k_z}} \tag{7-7}$$

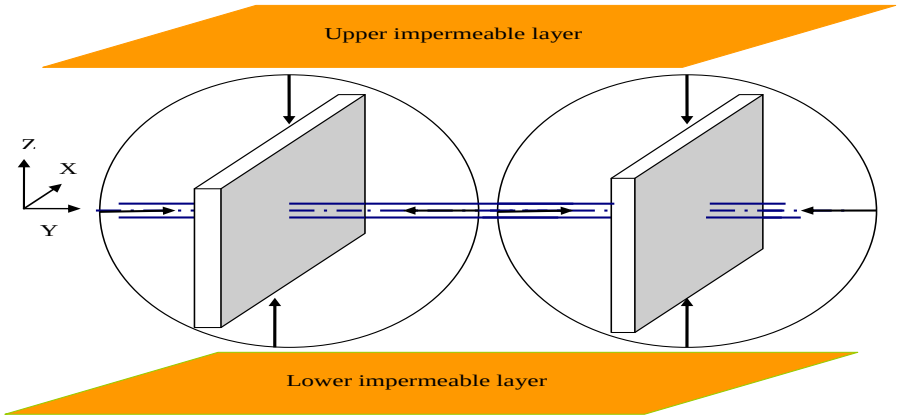

Figure 7-38: Early radial flow regime for partially penetrating multiple hydraulic fractures.

7-3-3- Second linear flow regime

When the pressure pulse reaches the upper and lower boundary, reservoir fluid continues flowing linearly and directly from the formation to the fractures in the XZ plane as shown in Fig. (7-39). The flow regime is represented by straight line with a slope of (0.5) in the log-log plots for pressure derivative with dimensionless time. The governing equations for a second linear flow regime in case of transverse hydraulic fractures are:

$$\left(t_D \times P_D'\right)_{SLF} = \frac{\sqrt{\pi t_D}}{2n} \tag{7-8}$$

$$\left(t \times \Delta P\right)_{SLF} = \frac{2.032qB}{nhx_f}\sqrt{\frac{\mu t}{k_y \phi c_t}} \tag{7-9}$$

It is important to notice that:

$$(P_D)_{SLF} \neq 2\times(t_D \times P_D')_{SLF} \tag{7-10}$$

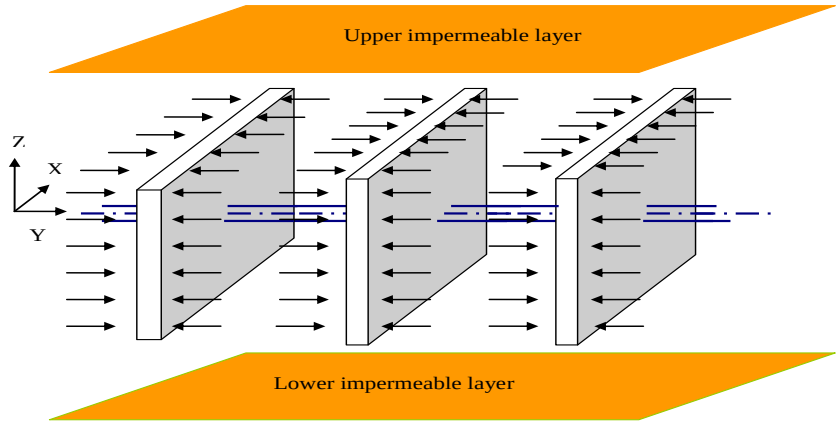

Figure 7-39: Second linear flow regime for partially penetrating multiple hydraulic fractures .

7-3-4- Third linear flow regime

A Third linear flow regime develops for short spacing, large number of hydraulic fractures and large half fracture length. In this case, pressure behavior can be considered similar to the pressure behavior of long horizontal wells. The flow takes place in the YZ plane toward the fractures as shown in Fig. (7-40). This flow is represented by a straight line of a slope (0.5) in the log-log plot of dimensionless pressure derivative with dimensionless time. The governing equations for a third linear flow regime is:

$$(P_D)_{TLF} = \frac{1.2\sqrt{\pi t_D}}{nD_D} \tag{7-11}$$

In field units:

$$(\Delta P)_{TLF} = \frac{4.88qB}{nhD}\sqrt{\frac{\mu t}{k_x \phi c_t}} \tag{7-12}$$

and:

$$\left(t_D \times P_D'\right)_{TLF} = \frac{1.2\sqrt{\pi t_D}}{2nD_D} \tag{7-13}$$

In field units:

$$\left(t \times \Delta P\right)_{TLF} = \frac{2.44qB}{nhD}\sqrt{\frac{\mu t}{k_x \phi c_t}} \tag{7-14}$$

where:

$$P_D = 2 \times \left(t_D \times P_D'\right) \tag{7-15}$$

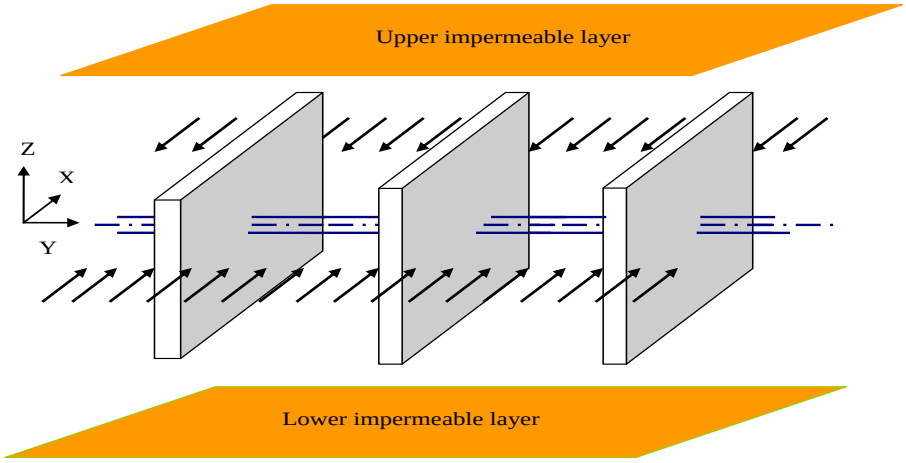

Figure 7-40: Third linear flow regime for partially penetrating multiple hydraulic fractures.

7-3-5-Intermediate radial flow regime

Intermediate radial flow regimes develope for long spacing between fractures when there is sufficient time for reservoir fluid to flow radially in the XY plan to each individual fracture as shown in Fig. (7-41). The governing equation for this flow regime is:

$$\left(t_D \times P_D'\right)_{IRF} = \frac{0.5}{n} \tag{7-16}$$

In dimensionless units:

$$\left(t \times \Delta P\right)_{IRF} = \frac{70.6qB}{n\sqrt{k_x k_y}h} \tag{7-17}$$

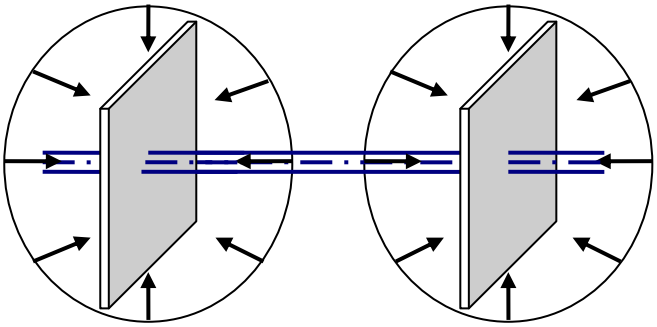

Figure 7-41: Intermediate radial flow regime for partially pentrating multiple hydraulic fractures.

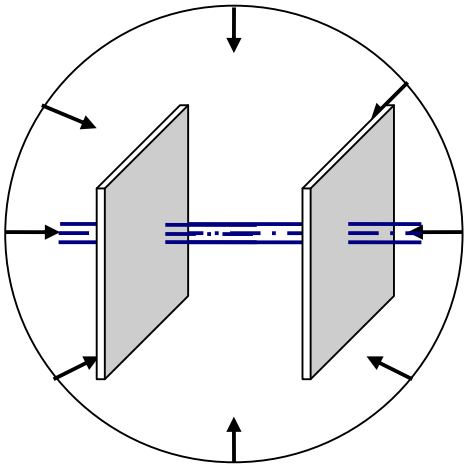

Figure 7-42: Pseudo-radial flow regime for partially penetrating multiple hydraulic fractures.

7-3-6-Pseudo-radial flow

Pseudo-radial flow regime is the dominant flow for all cases at late time when reservoir fluids flow in the XY plane radially toward the fractures such as shown in Fig. (7-42). This flow is characterized by constant value (0.5) for the dimensionless pressure derivative curves on log-log plot of dimensionless pressure and dimensionless time. The governing equation for this flow are:

$$\left(t_D \times P_D'\right)_{PRF} = 0.5 \tag{7-18}$$

$$\left(t \times \Delta P\right)_{PRF} = \frac{70.6qB}{\sqrt{k_x k_y}h} \tag{7-19}$$

7-3-7- Elliptical flow regime

An elliptical flow regime indicates elliptical flow toward the fractures such as shown in Fig. (5-43). Multivariate linear regression analysis is used to derive the governing equation for this flow regime:

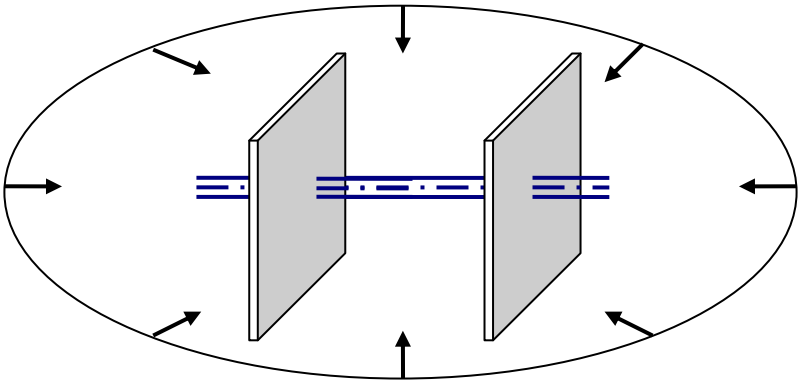

Figure 7-43: Elliptical flow regime for partially penetrating multiple hydraulic fractures.

$$\left(t_D \times P_D'\right)_{EF} = \frac{2t_D^{0.366}}{nD_D} \tag{7-20}$$

$$\left(t \times \Delta P\right)_{EF} = 13.835 \frac{q\mu B x_f^{0.28}}{nDhk_x}\left(\frac{k_x t}{\phi\mu c_t}\right)^{0.36} \tag{7-21}$$

7-4- Intersection Points:

The points of intersection between different lines of flow regimes are very important in the well test interpretation. They can be used to check the results.

7-4-1- The point of intersection of first linear flow line and pseudo-radial flow line is:

$$t_{PRFL} = 1207 \frac{n^2 h_f^2 x_f^2 \phi\mu c_t \cos^2(\theta_v)}{k_x h^2} \tag{7-22}$$

7-4-2- The point of intersection of first linear flow line and intermediate radial flow line is:

$$t_{IRFL} = 1207 \frac{h_f^2 x_f^2 \phi\mu c_t \cos^2(\theta_v)}{k_x h^2} \tag{7-23}$$

7-4-3- The point of intersection of first linear flow line and early radial flow line is:

$$t_{ERFL} = 302 \frac{h_f^2 \phi\mu c_t \cos^2(\theta_v)}{k_z} \tag{7-24}$$

7-4-4- The point of intersection of second linear flow line and pseudo-radial flow line is:

$$t_{PRSL} = 1207 \frac{n^2 x_f^2 \phi \mu c_t}{k_x} \quad (7\text{-}25)$$

7-4-5- The point of intersection of second linear flow line and intermediate radial flow line is:

$$t_{IRSL} = 1207 \frac{x_f^2 \phi \mu c_t}{k_x} \quad (7\text{-}26)$$

7-4-6- The point of intersection of second linear flow line and early radial flow line is:

$$t_{ERSL} = 302 \frac{h^2 \phi \mu c_t}{k_z} \quad (7\text{-}27)$$

7-4-7- The point of intersection of third linear flow line and pseudo-radial flow line is:

$$t_{PRTL} = 838.7 \frac{n^2 D^2 \phi \mu c_t}{k_y} \quad (7\text{-}28)$$

7-4-8- The point of intersection of third linear flow line and intermediate radial flow line is:

$$t_{IRTL} = 838.7 \frac{D^2 \phi \mu c_t}{k_y} \quad (7\text{-}29)$$

7-4-9- The point of intersection of third linear flow line and early radial flow line is:

$$t_{ERSL} = 209.7 \frac{D^2 h^2 k_x \phi \mu c_t}{x_f^2 k_y k_z} \quad (7\text{-}30)$$

7-5- Relationships between flow regimes

Many mathematical relationships between flow regimes' analytical models can be used in pressure transient interpretation to estimate reservoir and fractures parameters.

5-5-1- Pseudo-radial and intermediate radial flow regime:

$$\frac{(t_D \times P_D')_{IRF}}{(t_D \times P_D')_{PRF}} = \frac{(t \times \Delta P')_{IRF}}{(t \times \Delta P')_{PRF}} = \frac{1}{n} \quad (7\text{-}31)$$

7-5-2-Pseudo-radial and early radial flow regime:

$$\frac{(t_D \times P_D')_{ERF}}{(t_D \times P_D')_{PRF}} = \frac{1}{2nh_{xfD}} \tag{7-32}$$

$$\frac{(t \times \Delta P')_{ERF}}{(t \times \Delta P')_{PRF}} = \frac{h}{2nx_f}\sqrt{\frac{k_x}{k_z}} \tag{7-33}$$

7-5-3-Intermediate radial and early radial flow regime:

$$\frac{(t_D \times P_D')_{ERF}}{(t_D \times P_D')_{IRF}} = \frac{1}{2h_{xfD}} \tag{7-34}$$

$$\frac{(t \times \Delta P')_{ERF}}{(t \times \Delta P')_{IRF}} = \frac{h}{2x_f}\sqrt{\frac{k_x}{k_z}} \tag{7-35}$$

7-5-4-Second linear and first linear flow regime:

$$\frac{(t_D \times P_D')_{SLF}}{(t_D \times P_D')_{FLF}} = h_{hfD}\cos(\theta_v) \tag{7-36}$$

$$\frac{(t \times \Delta P')_{SLF}}{(t \times \Delta P')_{FLF}} = \frac{h_f \cos(\theta_v)}{h} \tag{7-37}$$

7-5-5-Third linear and first linear flow regime:

$$\frac{(t_D \times P_D')_{TLF}}{(t_D \times P_D')_{FLF}} = \frac{1.2h_{hfD}}{D_D} \tag{7-38}$$

$$\frac{(t \times \Delta P')_{TLF}}{(t \times \Delta P')_{FLF}} = \frac{1.2h_f x_f}{hD}\sqrt{\frac{k_y}{k_x}} \tag{7-39}$$

3-5-6-Seond linear and third linear flow regime:

$$\frac{(t_D \times P_D')_{SLF}}{(t_D \times P_D')_{TLF}} = \frac{D_D}{1.2} \tag{7-40}$$

$$\frac{(t \times \Delta P')_{SLF}}{(t \times \Delta P')_{TLF}} = \frac{D}{1.2x_f}\sqrt{\frac{k_x}{k_y}} \tag{7-41}$$

Fig. (7-42) shows a few of the above important relationships between flow regimes.

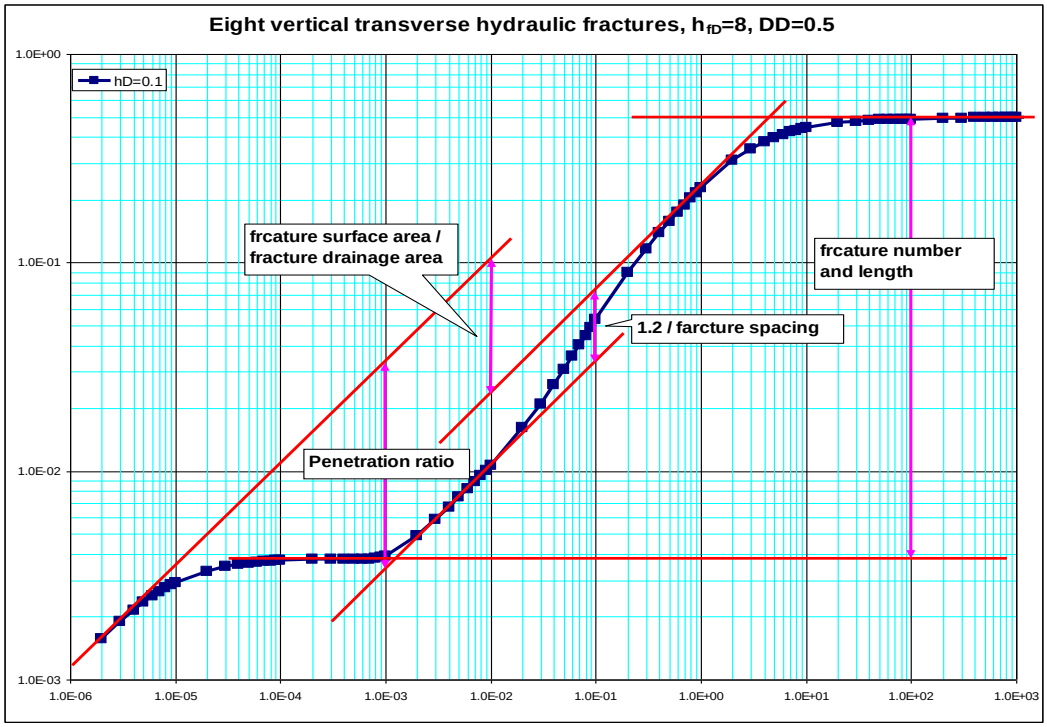

Figure 7-44: Relationships between flow regimes for partially penetrating multiple hydraulic fractures.

7-6-Pseudo-skin factor

In general, pseudo-skin factor increases as the penetration ratio increases. For the same number of longitudinal and transverse fractures, the pseudo-skin factor decreases when the spacing between fractures increases and when the ratio of the half fracture length to the fracture height (h_{xfD}) increases. Similar to the fully penetrating multiple hydraulic fractures, pseudo skin factor for partially penetrating fractures decreases significantly with the increase of the number of fractures for the same penetration ratio, same spacing and same (h_{xfD}). Appendix-E shows the tables of pseudo-skin factor for partially penetrating hydraulic fractures.

7-7-Appliction of Type Curve Matching

As shown on the plots in Appendix (C), the pressure and pressure derivative have different shapes for each combination of penetration rate, half fracture length, number

of fractures, spacing between fractures, and inclination angle from the vertical axis. Type-curve matching can provide a quick estimation for reservoir and fractures parameters.

The following information is associated with each type curve: penetration rate (h_{hfD}), half fracture length to fracture height ratio (h_{xfD}), dimensionless spacing between fractures (D_D), number of fractures (n), and inclination angle (ϕ_v). Thus, the following information can be obtained from the type curve matching process: $(P_D)_M$, $(\Delta P)_M$, $(t_D)_M$, $(\Delta t)_M$, $(\phi_v)_M$, $(h_{xfD})_M$, $(D)_M$, $(h_{hfD})_M$, $(n)_M$. The following steps illustrate how type curve matching is used to determine reservoir characteristics such as: permeability, inclination angle, spacing, pseudo-skin factor, fracture half length, and number of fractures.

Step-1 Plot (ΔP vs. t) and ($t \times \Delta P'$ vs. t) on log-log paper.

Step-2 Obtain the best match of the data with one of the type curves.

Step-3 Read from any match point: t_M , ΔP_M , t_{DM} , P_{DM} , h_{hxfDM} , D_{DM} , ϕ_{vM} , n_M , h_{hfDM} .

Step-4 Calculate k_x :

$$k_x = \frac{\phi \mu c_t x_f^2 t_{DM}}{0.0002637 t_M} \tag{7-42}$$

Step-5 Calculate (k_y) :

$$k_y = \frac{1}{k_x}\left[\frac{141.2 quBP_{DM}}{h\Delta P_M}\right]^2 \tag{7-43}$$

Step-6 Determine penetration ratio:

$$Penetration\ ratio = \frac{h_f}{h} = h_{hfDM} \tag{7-44}$$

Step-7 Calculate the height of fractures:

$$h_f = h_{hfDM} \times h \tag{7-45}$$

Step-8 Calculate the half fracture length:

$$x_f = h_{xfDM} \times h \times \sqrt{\frac{k_x}{k_z}} \tag{7-46}$$

Step-9 Calculate the spacing between fractures:

$$D = D_{DM} \times x_f \sqrt{\frac{k_y}{k_x}} \tag{7-47}$$

Step-10 Number of fractures can be determined directly as:

$$n = n_M \tag{7-48}$$

Step-11 Inclination angle can be determined directly as:

$$\phi\nu = \phi_{vM} \tag{7-49}$$

7-8-Application of TDS technique

TDS is a powerful technique for computation of reservoir parameters directly from log-log plots of pressure and pressure derivative data. A well-designed pressure transient test in a horizontal well with partially penetrating hydraulic fractures should yield all the necessary straight lines to calculate penetrating ratio, number of fractures, the inclination angle, spacing between fractures, and permeability.

The following procedure is for the ideal case where all the necessary straight lines are well defined.

Step 1 - Plot pressure change (ΔP) and pressure derivative ($t \times \Delta P'$) values versus test time on a log-log graph.

Step 2 - Read the value of $(t \times \Delta P')_{PRF}$ corresponding to the infinite acting pseudo-radial flow line.

Step 3 - Calculate $(k_x k_y)$:

$$k_x k_y = k_h = \left(\frac{70.6 q \mu B}{h(t \times \Delta P')_{PRF}} \right)^2 \tag{7-50}$$

Step 4 – If the intermediate radial flow is developed, read $(t \times \Delta P')_{IRF}$.

Step 5 – Calculate number of fractures (n) :

$$n = \frac{(t \times \Delta P')_{PRF}}{(t \times \Delta P')_{IRF}} \tag{7-51}$$

Step 6 - Obtain the value $(t \times \Delta P')_{EF}$ at time t_{EF} from the elliptical flow line .

Step 7 - Calculate $(\frac{k_x^{0.64}}{x_f^{0.28}})$ if the spacing between fractures is known.

$$\frac{k_x^{0.64}}{x_f^{0.28}} = 13.835 \frac{q \mu B}{n D h (t \times \Delta P')_{EF}} \left[\frac{t_{EF}}{\phi \mu c_t} \right]^{0.36} \tag{7-52}$$

Step 8 - Obtain the value $(t \times \Delta P')_{SLF}$ at time t_{SLF} from the second linear flow line.

Step 9 - Calculate $(x_f \sqrt{k_y})$:

$$x_f \sqrt{k_y} = \frac{2.032 q B}{n h (t \times \Delta P')_{SLF}} \sqrt{\frac{\mu t_{SLF}}{\phi c_t}} \tag{7-53}$$

Step 10- Solve Eqs. (7-50), (7-52), and (7-53) to calculate $(k_x), (k_y), (x_f)$:

Step 11 - Read the value $(t \times \Delta P')_{ERF}$ corresponding to the early radial flow line.

Step 12- Calculate (k_z):

$$k_z = \frac{1}{k_y} \left[\frac{35.3 q \mu B}{n x_f (t \times \Delta P')_{ERF}} \right]^2 \tag{7-54}$$

Step 13 - Read the value of $(t\times\Delta P')_{FLF}$ corresponding to a certain time t_{FLF} from the first linear flow line.

Step 14- Calculate $\left(h_f\right)$ if the inclination angle is known:

$$h_f = \frac{2.032qB}{nx_f\left(t\times\Delta P'\right)_{FLF}\cos(\theta_v)}\sqrt{\frac{\mu t_{FLF}}{k_y\phi c_t}} \tag{7-55}$$

Step 15 – Calculate the penetration ratio:

$$Penetration\ ratio = \frac{h_f}{h} \tag{7-56}$$

Step 16 – Calculate the intersection times using Eq. (7-22) through Eq. (7-30) and compare them with those in the plot.

Example -7-1

Pressure drawdown test data of a hydraulically fractured horizontal well, extending in homogenous isotropic reservoir, is given in Table (Example 7-1) of Appendix (F). Other known reservoir and well data are:

q = 500 STB/D ϕ = 0.04 μ = 0. 5 cp $c_t = 1.0\text{x}10^{-6}$ psi^{-1} h = 40 ft

r_w = 0.5 ft p_i = 5000 psi B = 1.1 bbl/STB

Determine:

1-Formation permeability.

2-Number of fractures.

3-Fracture half length.

4-Fracture height and penetration ratio.

5-Spacing between fractures.

6-Inclination angle.

1- Solution using type-curve matching:

Step-1 Plot (ΔP vs. t) and ($t \times \Delta P'$ vs. t) on log-log paper as shown in Fig. (7-45).

Step-2 Obtain the best match of the data with one of the type curves as shown in Fig. (7-46).

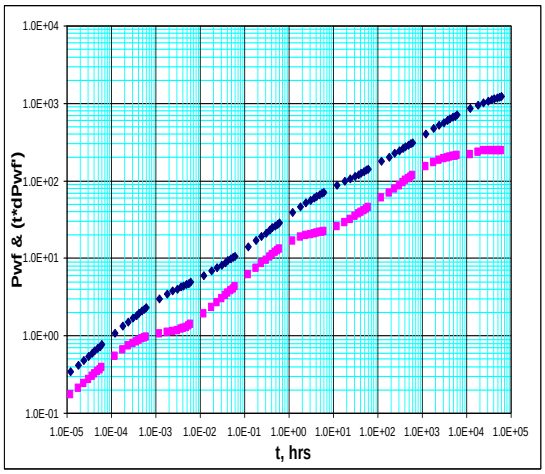

Figure 7-45: Pressure and pressure derivative plot Example 7-1.

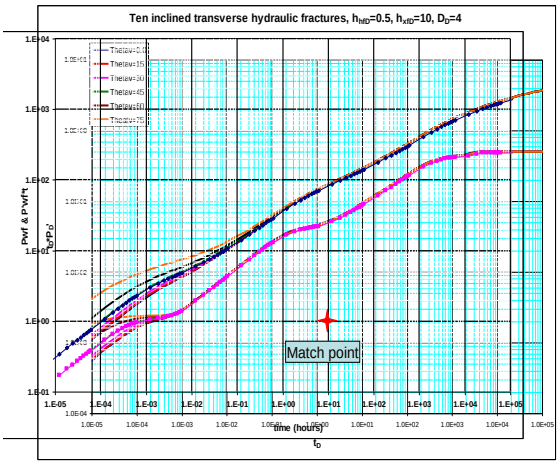

Figure 7-46: Type-curve matching plot for Example 7-1.

Step-3 Read from any match point:

$t_M = 10,\ \Delta P_M = 1,\ t_{DM} = 1.7,\ P_{DM} = 0.002, h_{hfDM} = 0.5,\ D_{DM} = 4,\ \phi_{vM} = 45, n_M = 10, s_M = -3.46$

$h_{xfDM} = 10$

Step-4 Calculate half fracture length (x_f) from Eq. (7-46).

$$x_f = 10 \times 40 = 400 \ ft$$

Step-5 Calculate k from Eq. (7-42):

$$k = \frac{0.04 \times 0.5 \times 0.000001 \times 400^2 \times 1.7}{0.0002637 \times 10} = 2 \ md$$

Step-6 Number of fractures:

$$n = n_M = 10 \ fractures$$

Step-7 Penetration ratio:

$$\frac{h_f}{h} = h_{hfD} = 0.5$$

Step-8 Calculate fracture height from eq. (7-45):

$$h_f = 0.5 \times 40 = 20 \ ft.$$

Step-9 Inclination angle:

$$\phi\nu = 45$$

Step-10 Spacing between fractures from Eq. (7-47):

$$D = x_f \times D_{DM} = 400 \times 4 = 1600 \ ft$$

Step-11 Pseudo-skin factor:

$$s = -3.46$$

2- Solution using TDS:

Step 1 - Plot pressure change (ΔP) and pressure derivative (t×ΔP') values versus test time on a log-log graph as shown in Fig. (7-47).

Step 2 - Read the value of $(t \times \Delta P')_{PRF}$ corresponding to the infinite acting pseudo-radial flow line.

$$(t \times \Delta P')_{PRF} = 242$$

Step 3 - Calculate (k) from Eq. (7-50).

$$k = \frac{70.6 \times 500 \times 0.5 \times 1.1}{40 \times 242} = 2 \ md$$

Step 4 – At a certain time, read $(t \times \Delta P')_{TLF}$ from third linear flow line and $(t \times \Delta P')_{SLF}$ from second linear flow line.

$$t = 1, \quad (t \times \Delta P')_{TLF} = 60, \quad (t \times \Delta P')_{SLF} = 28$$

Step 5 – Calculate number of fractures (n) from Eq. (7-51):

$$n = \frac{242}{24} = 10 \ farctures$$

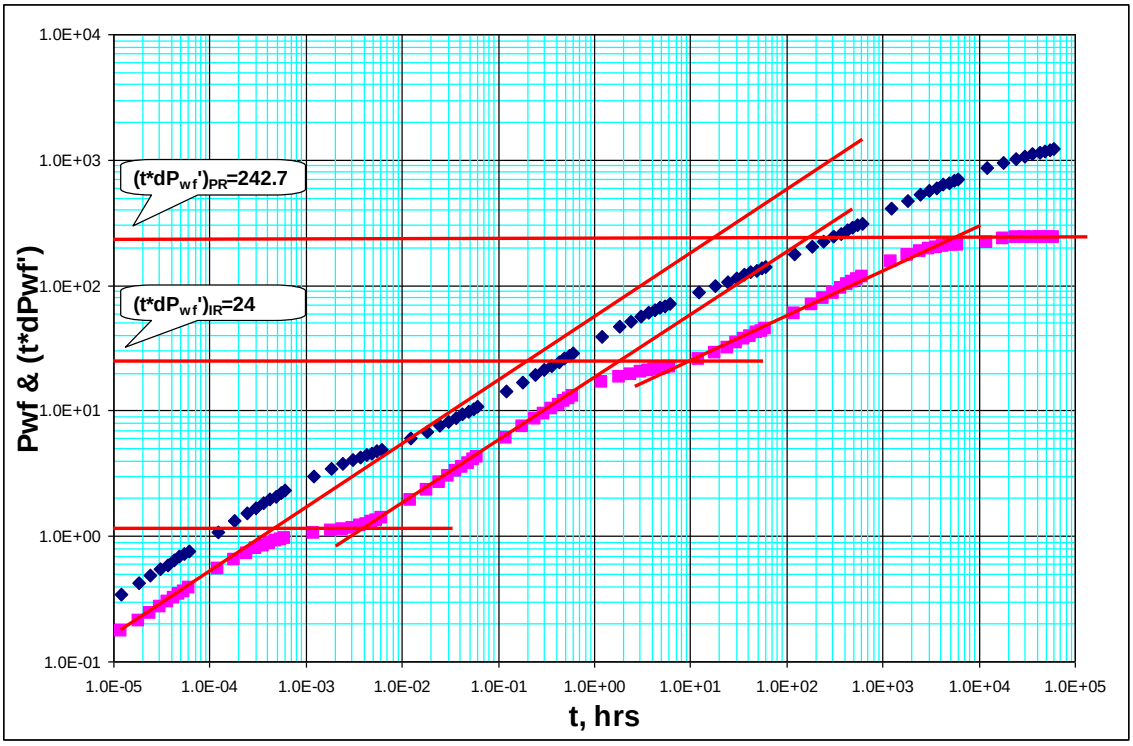

Figure 7-47: Pressure and pressure derivative plot for example 7-1.

Step 6 - Obtain the value of $(t\times\Delta P')_{SLF}$ at time t_{SLF} from the second linear flow line.

$$(t \times \Delta P')_{SLF} = 6.0744 \ \ at \ \ t_{SLF} = 0.12135$$

Step 7 - Calculate (x_f) from Eq. (7-53).

$$x_f = \frac{2.032 \times 500 \times 1.1}{10 \times 40 \times 6.0744} \sqrt{\frac{0.5 \times 0.012135}{2 \times 0.04 \times 0.000001}} = 400 \ ft$$

Step 8 - Obtain the value $(t\times\Delta P')_{EF}$ at time t_{EF} from the elliptical flow line .

$$(t \times \Delta P')_{EF} = 35 \ \ at \ \ t_{EF} = 30$$

Step 8 - Calculate (D) from Eq. (7-52).

$$D = 13.835 \frac{500 \times 0.5 \times 1.1 \times 400^{0.28}}{10 \times 40 \times 35 \times 2^{0.64}} \left[\frac{30}{0.04 \times 0.5 \times 0.000001} \right]^{0.36} = 1760 \ ft$$

Step 9 - Read the value $(t\times\Delta P')_{FLF}$ corresponding to a certain time t_{FLF} from the first linear flow line.

$$\left(t\times\Delta P'\right)_{FLF}=0.3636 \quad at \;\; t_{FLF}=0.0000546$$

Step 10- Calculate $\left(h_f\cos(\theta_v)\right)$ from Eq. (7-55):

$$h_f\cos(\theta_v)=\frac{2.032\times500\times1.1}{10\times400\times0.3636}\sqrt{\frac{0.5\times0.0000546}{2\times0.04\times0.000001}}=14.4$$

Step 11 – To calculate $\left(\theta_v\right)$, determine the three intersection points of the first linear flow with the pseudo-radial, intermediate radial and early radial from the plot.

$$t_{PRFL}=18, \quad t_{IRFL}=0.18, \quad t_{ERFL}=0.00045$$

Step 12- Calculate t_{PRFL} from Eqs. (7-22):

$$t_{PRFL}=1207\frac{10^2\times400^2\times0.04\times0.5\times0.000001\times14.4^2}{2\times40^2}=25$$

Step 13- Calculate $\left(\theta_v\right)$:

$$\theta_v=\cos^{-1}(\frac{18}{25})=44$$

Step 14- Calculate $\left(h_f\right)$:

$$h_f=\frac{14.4}{\cos(44)}=20 \;\; ft$$

Step 15- Calculate penetration ratio:

$$\frac{h_f}{h}=\frac{20}{40}=0.5$$

Step 16- Check the calculated values of $\left(\theta_v\right) and \left(h_f\right)$ using the intersection points of the first linear flow line and the intermediate and early radial flow lines from Eqs. (7-23) and (7-24):

$$t_{IRFL} = 1207\frac{400^2 \times 0.04 \times 0.5 \times 0.000001 \times 14.4^2}{2 \times 40^2} = 0.25$$

$$\theta_v = \cos^{-1}(\frac{0.18}{0.25}) = 44$$

$$t_{ERFL} = 302\frac{0.04 \times 0.5 \times 0.000001 \times 14.4^2}{2} = 0.000626$$

$$\theta_v = \cos^{-1}(\frac{0.00045}{0.000626}) = 44$$

Table (7-1) summarizes the input data and the resulted value for Example 7-1.

Table 7-1: Summary of results of Example 7-1.

Parameter	In-put value	Calculated value by Type-curve matching	Calculated value by TDS technique
k, md	2	2	2
x_f , ft	400	400	400
n	10	10	10
Penetrating ratio	0.5	0.5	0.5
h_f , ft	20	20	20
θ_v	45	45	44
D, ft	1600	1600	1760

Example -7-2

Pressure drawdown test data of a hydraulically fractured horizontal well is given in Table (Example 7-2) in Appendix (F). Sixteen vertical hydraulic fractures have been designed with a half fracture length (310 ft). Other known reservoir and well data are:

q = 100 STB/D ϕ = 0.04 μ = 0.8 cp $c_t = 1.0x10^{-6}$ psi^{-1} h = 10 ft

r_w = 0.5 ft p_i = 10000 psi B = 1.1 bbl/STB

Determine:

1-Formation permeabilities.

2-Fracture height and penetration ratio.

3-Spacing between fractures.

1- Solution using type-curve matching:

Step-1 Plot (ΔP vs. t) and ($t \times \Delta P'$ vs. t) on log-log paper as shown in Fig. (7-48).

Step-2 Obtain the best match of the data with one of the type curves as shown in Fig. (7-49).

Step-3 Read from any match point:

$t_M = 1,\ \Delta P_M = 1,\ t_{DM} = 0.13,\ P_{DM} = 0.0007, h_{hfDM} = 0.3,\ D_{DM} = 0.5, n_M = 16, s_M = -2.09$

$h_{xfDM} = 8$

Step-4 Calculate k_x from Eq. (7-42):

$$k_x = \frac{0.04 \times 0.8 \times 0.000001 \times 310^2 \times 0.13}{0.0002637 \times 1} = 1.5\ md$$

Step-5 Calculate (k_z) from Eq. (7-46).

$$k_z = \left(\frac{8 \times 10}{310}\right)^2 \times 1.5 = 0.1\ md$$

Step-6 Calculate (k_y) from Eq. (7-43).

$$k_y = \frac{1}{1.5}\left[\frac{141.2 \times 100 \times 0.8 \times 1.1 \times 0.0007}{10 \times 1}\right]^2 = 0.5\ md$$

Step-7 Number of fractures:

$n = n_M = 16\ fractures$

Step-8 Penetration ratio:

$$\frac{h_f}{h} = h_{hfD} = 0.3$$

Step-9 Calculate fracture height from eq. (7-45):

$h_f = 0.3 \times 10 = 3\ ft.$

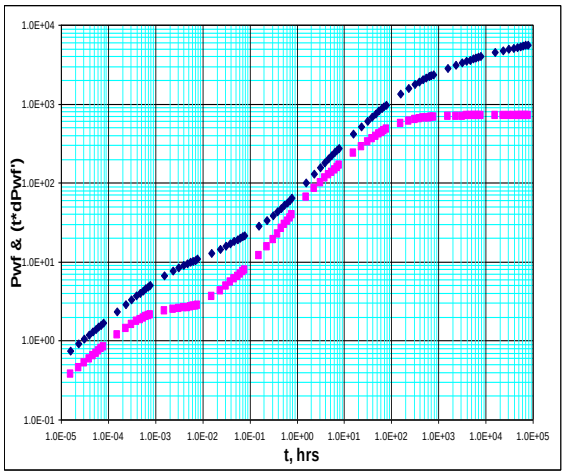

Figure 7-48: Pressure and pressure derivative plot Example 7-2.

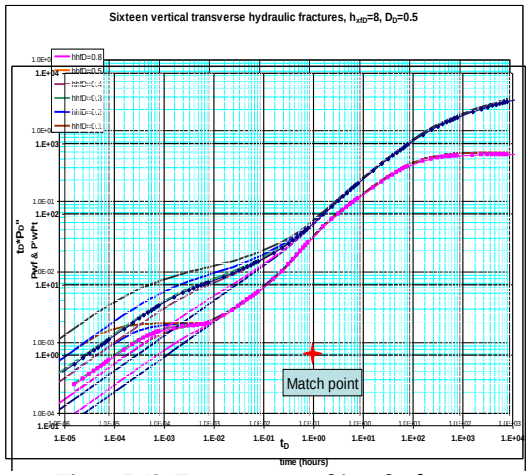

Figure 7-49: Type-curve matching plot for Example 7-2.

Step-10 Spacing between fractures from Eq. (7-47):

$$D = 310 \times 0.5 \times \sqrt{\frac{0.5}{1.5}} = 89.5 \ ft$$

Step-11 Pseudo-skin factor:

$$s = -3.46$$

2- Solution using TDS:

Step 1 - Plot pressure change (ΔP) and pressure derivative (t×ΔP') values versus test time on a log-log graph as shown in Fig. (7-50).

Step 2 - Read the value of $(t \times \Delta P')_{PRF}$ corresponding to the infinite acting pseudo-radial flow line.

$$(t \times \Delta P')_{PRF} = 717.4$$

Step 3 - Calculate $(k_x k_y)$ from Eq. (7-52).

$$k_h = k_x k_y = \left(\frac{70.6 \times 100 \times 0.8 \times 1.1}{10 \times 717.4} \right)^2 = 0.75$$

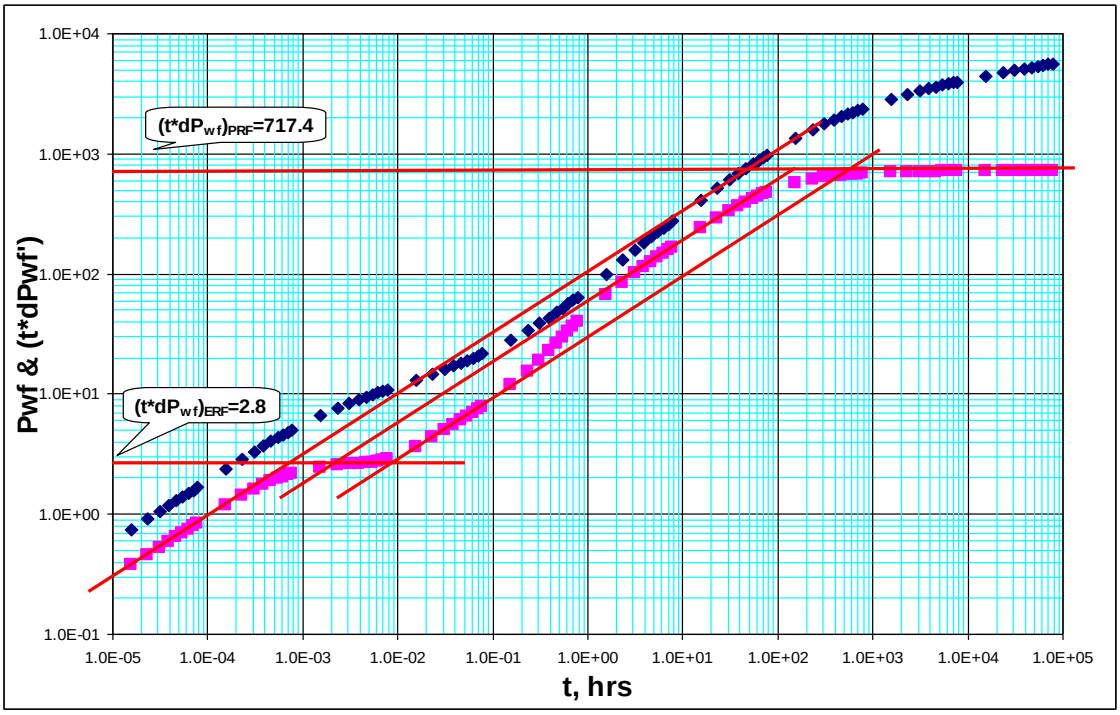

Figure 7-50: Pressure and pressure derivative plot for example 7-2.

Step 4- Read $(t\times\Delta P')_{SLF}$ at a certain time t_{SLF} from the second linear flow line.

$$t_{SLF}=0.054 \qquad (t\times\Delta P')_{SLF}=6.56$$

Step 5- Calculate k_y from Eq. (7-53):

$$k_y=\left(\frac{2.032\times100\times1.1}{310\times16\times10\times6.56}\right)^2\frac{0.8\times0.054}{0.04\times0.000001}=0.5\,md$$

Step-6 Calculate k_x from the result of Step-3:

$$k_x=\frac{0.75}{0.5}=1.5\,md$$

Step 7- If the early radial flow is developed, read $(t\times\Delta P')_{ERF}$.

$$\left(t\times\Delta P'\right)_{ERF}=2.8$$

Step 8- Calculate number of fractures (k_z) from Eq. (7-54):

$$k_z=\frac{1}{0.5}\left[\frac{35.3\times100\times0.8\times1.1}{16\times310\times2.8}\right]^2=0.1\,md$$

Step 9- Obtain the value of $(t\times\Delta P')_{FLF}$ at a certain time t_{FLF} from first linear flow line.

$$(t\times\Delta P')_{FLF}=0.7,\ t_{FLF}=0.000054$$

Step 10- Calculate the height of fractures from eq. (7-55):

$$h_f=\frac{2.032\times100\times0.8\times1.1}{16\times310\times0.7}\sqrt{\frac{0.8\times0.000054}{0.5\times0.04\times0.000001}}=3\ ft$$

Step 11- Obtain the value $(t\times\Delta P')_{TLF}$ at time t_{TLF} from first linear flow line.

$$(t\times\Delta P')_{TLF}=237.5,\ t_{FLF}=15.5$$

Step 12 - Calculate (D) from Eq. (7-13).

$$D=\frac{2.44\times100\times1.1}{16\times10\times237.5}\sqrt{\frac{0.8\times15.5}{1.5\times0.04\times0.000001}}=101\ ft$$

Step 13 – Determine the intersection point time of different flow regimes from the plot:

$$t_{PRFL}=57\ hrs,\ t_{PRSL}=635\ hrs,\ t_{PPRTL}=140\ hrs,\ t_{ERFL}=0.00087\ hrs,\ t_{ERSL}=0.0097\ hrs,\ t_{ERTL}=0.0021\ hrs$$

Step 14 – Calculate the intersection times using Eq. (7-22) through Eq. (7-30) and compare them with those determined from the plot in Step-14.

$$t_{PRFL}=57\ hrs,\ t_{PRSL}=633\ hrs,\ tP_{PRTL}=140\ hrs,\ t_{ERFL}=0.00087\ hrs,\ t_{ERSL}=0.0097\ hrs,\ t_{ERTL}=0.0021\ hrs$$

Table (7-2) summarizes the input data and the resulted value for Example 7-2.

Table 7-2: Summary of results of Example 7-2.

Parameter	In-put value	Calculated value by Type-curve matching	Calculated value by TDS technique
k_x, md	1.5	1.5	1.5
k_y, md	0.5	0.5	0.5
k_z, md	0.1	0.1	0.1
Penetrating ratio	0.3	0.3	0.3
h_f, ft	3	3	3
n	16	16	
D, ft	89.5	89.5	101

SUMMURY AND CONCLUSIONS

Open-Hole Horizontal Well:

The completion of the horizontal wells is of great importance in terms of fluids deliverability and production management. Low cost and simplicity is the two factors recognize the open hole completion. However, the difficulties in the maintenance and control are the other two parameters control this type of completion. Pressure transient analysis for the open hole horizontal wells is governing by:

1- Early radial flow regime develops at early time in the case of short and moderate length horizontal wells. However, this flow regime cannot be observed for long horizontal wells.
2- Linear flow and pseudo-radial radial flow can be observed for both short and long horizontal wells.
3- The pressure behavior of a long horizontal well is similar to the pressure behavior of vertical hydraulic fracture.

Zonal Isolation:

Horizontal wells with multiple zonal isolations have become a common completion technique in the oil and gas industry. Sand problems, damaged zones, and water or gas coning are the main reasons for using isolators to maintain or improve oil and gas recovery. However, the use of isolators affects pressure behavior of the horizontal wells and changes the flow regimes that may develop in the vicinity of the wellbore. In addition, zonal isolations technique leads to an increase of the skin factor significantly.

Pressure transient analysis is used to investigate the effects of the isolators on both pressure behavior and flow regimes of horizontal wells. Several analytical solutions

have been developed in this study. These models were used for different applications such as: reservoir characterization and for the evaluation of the isolators performance.

1- Zonal isolation can be a practical solution for different formation problems such as water cresting, gas coning and sand or asphaltic production, however, it has great impact on the skin factor.

2- The main influence of zonal isolation is observed on early flow regimes of the horizontal wellbore, such as early radial and early linear flow regimes.

3- Well test analysis is the most effective tool to evaluate the performance of the zonal isolations.

4- The development of intermediate radial flow can be used as an indication of serious problems, such as damaged perforated sections, that may lead to the complete loss of the well, depending of the nature of the problem.

5- System radial flow and system linear flow can only be developed for the cases where the horizontal well contains multiple zonal isolators.

Hydraulic fractures:

Hydraulic fracturing is an important stimulation technique that has been widely used in conventional and unconventional oil and gas reservoirs all over the world. The technique involves the creation of multiple hydraulic fractures to overcome wellbore damage, and to improve oil and gas productivity in low permeability reservoirs. Depending on the stresses orientation relative to the wellbore, the fractures may be transverse or longitudinal, vertical or inclined, fully penetrating or partially penetrating the formations.

For hydraulically fractured horizontal wells, well test analysis is commonly used to

determine reservoir parameters and to estimate well productivity. Many factors, such as vertical permeability or the vertical anisotropy, inclination angle from the vertical direction, the spacing between fractures, and the penetration ratio (the ratio of the fractures height to the formation height) can be estimated from pressure transient data. The performance of the hydraulic fractures can be evaluated and the location of the damaged fractures can be determined by the well test.

1- Both the inclination from the vertical direction and the deviation from the horizontal wellbore have a significant effect on pressure behavior of the hydraulically fractured horizontal well.
2- Both transverse and longitudinal hydraulic fractures have the same pressure response and flow regimes if the formation is isotropic. Different behaviors are expected for anisotropic formations.
3- Early radial flow can be used as an indication of long spacing between fractures or as an indication of non-functioning hydraulic fractures.
4- An early radial flow regime is expected to be observed for the case of the partially penetrating hydraulic fractures where the fluid flows radially in the normal plane to the wellbore.
5- A third linear flow regime is developed for short spacing partially penetrating hydraulic fractures where the fluid flows linearly in a parallel plane to the wellbore.
6- For small penetrating ratio and large number of hydraulic fractures, the pressure behavior is similar to the behavior of long horizontal wells.

RECOMMENDATIONS

1- The wellbore storage and skin factors should be included for the models of horizontal wells with either zonal isolations or hydraulic fractures.

2- The infinite conductivity solution should be investigated and compared to the uniform flux solution.

3- Zonal isolation models have been derived for no-flow isolated sections. It is more realistic to assume different flow rates from these sections toward the wellbore.

4- Finite conductivity solution can be studied for both fully and partially penetrating fractures.

NOMENCLATURES

B Oil formation volume factor, RB/STB

D Spacing between fractures, ft

D_D Dimensionless spacing

h Formation height, ft

h_f Fracture height, ft

c_t Total compressibility, psi^{-1}

k_x Permeability in the X-direction, md

k_y Permeability in the Y-direction, md

k_z Permeability in the Z-direction, md

L_D Dimensionless wellbore length

L_p Length of perforated section, ft

L_s Length of isolated section, ft

L_w Wellbore length, ft

n Number of perforated section or hydraulic fractures

ΔP_t Total pressure drop, psi

ΔP_i Pressure drop of single perforated interval or single hydraulic fracture, psi

P_D Dimensionless pressure

q_t Total flow rate, STB/D

q_i Flow rate from single perforated section or single hydraulic facture, STB/D

r_w Wellbore radius, ft

t Time, hr

t_D Dimensionless time

$(t_D \times P_D')$ Dimensionless pressure derivative

x_f Half fracture length, ft

x_w X-Cartesian coordinates of the production point

y_w Y-Cartesian coordinates of the production point

z_w Z-Cartesian coordinates of the production point

x' The position in the X-direction of any single production interval

y' The position in the Y-direction of any single production interval

z' The position in the X-direction of any single production interval

GREEK SYMBOLS

ϕ Porosity

μ Viscosity, cp

η Diffusivity coefficient, ft^2/sec

η_x Diffusivity coefficient in the X-direction, ft^2/sec

η_y Diffusivity coefficient in the Y-direction, ft^2/sec

η_z Diffusivity coefficient in the Z-direction, ft^2/sec

τ Dummy variable of time

θ_v Inclination angle from vertical direction

θ_h Deviation from horizontal direction

SUBSCRIPTS

ERF early radial flow

IRF intermediate radial flow

SRF system radial flow

PRF pseudo radial flow

ELF early linear flow

EF elliptical flow

FLF first linear flow

SLF second linear flow

TLF third linear flow

PSF pseudo-spherical flow

REFERNCES

Al-Kobaisi M., Ozkan E. and Kazemi, H."A hybrid numerical analytical model of finite conductivity vertical fractures intercepted by a horizontal well.", SPE 92040-MS Paper presented at the SPE International Petroleum Conference, Puebla, Mexico, 8-9 November, 2004.

Allison, D., Folds, D., Harless, D., Howell, M., and Vargus, G.: "Optimization Open Hole Completion Techniques for Horizontal Foam drilled Wells." SPE 125642-MS paper presented at the 2009 SPE Eastern Regional Meeting, West Virginia, 23-25 September, 2009.

Al-Otabi, A.M. and Ozkan, E.: "Interpretation of Skin Effect from Pressure Transient Tests in Horizontal Wells." SPE 93296-MS Paper presented at the 14th SPE Middle East Oil and Gas Show and Conference, Bahrain, 12-15 March, 2005.

Barker, B. J., Ramey, H. and Henery, J.: "Transient flow to finite conductivity fractures." SPE 7489 –MS Paper presented at 53rd SPE Annual Technical Conference and Exhibition, Dallas, TX, 1-3 October, 1978.

Brooks, R. T. and Steven S.: "Improvement in Completing and Testing Multi-Zone Open-hole Carbonate Formations" SPE 119426-MS Paper presented at the 2009 SPE Middle East Oil and Gas Show and Conference, Bahrain, 15-18 March 2009.

Brown, M., Ozkan, E., Raghavan, R. and Kazemi, H.: "Practical Solution for Pressure Transient Response of fractured Horizontal Wells in Unconventional Reservoirs" SPE 125043-MS Paper presented at the SPE Annual Technical Conference and Exhibition, New Orleans, Louisiana, 4-7 October, 2009.

Cinco-Ley, H.: "Unsteady-State Pressure Distribution Created by a Slanted Well or a Well with an Inclined Fracture," PhD dissertation, Stanford University (1974).

Cinco-Ley, H. and Meng H.Z.: "Pressure transient analysis of wells with finite conductivity vertical fractures in double porosity reservoirs." SPE 18172-MS Paper presented at the SPE 63rd Annual Technical Conferences and Exhibition, Houston, TX, 2-5 October, 1988.

Cinco-Ley, H., Ramey, H. and Miller, F. G.: "Unsteady-State Pressure Distribution Created by a Well with an Inclined Fracture." SPE 5591-MS Paper presented at the 50th SPE Annual Fall Meeting, Dallas, TX, 28 September-1 October, 1975.

Cinco-Ley, H. and Samaniego-V, F. “Transient Pressure Analysis: finite conductivity fracture case versus damaged fracture case.” SPE 10179-MS Paper presented at the SPE 56th Annual Technical Conference and Exhibition, San Antonio, TX, 5-7 October, 1981.

Clonts, M.D., and Ramey, H.: “Pressure Transient Analysis for Wells with Horizontal drainholes.” SPE 15116-MS Paper presented at the SPE 56th California Regional Meeting, Oakland, California, 2-4 April, 1986.

Daneshy, A. A.: “A Study of Inclined Hydraulic Fractures.” SPE 4062-MS Paper presented at the SPE 47th Annual Fall Meeting, San Antonio, TX, 8-11 October, 1972.

Daneshy, A. A.: “True and Apparent Direction of Hydraulic Fractures.” SPE 3226-MS Paper presented at the Fifth Conference on Drilling and Rock Mechanics, Austin, TX, 5-6 January, 1970.

Daviau, F., Mouronval, G., Bourdarot, G., and Curutchet, P.: “Pressure Analysis for Horizontal Wells.” SPE Formation Evaluation Journal, December 1988, pp 716-724.

Del Rio, C., Boucher, A., Salazar, F., Milne, A., and Robles, M.: “Temporary Zonal Isolation Minimizes Reservoir damage During Workover Operation in Ecuador.” SPE 143771-MS Paper presented at the SPE European Formation Damage Conference, Noordwijk, Netherlands, 7-10 June 2011.

Dinh, A. V. and Tiab, D., “ Transient pressure analysis of a well with an inclined hydraulic fracture using Tiab’s direct synthesis technique.” SPE 120545-MS Paper presented at the SPE Production and Operation Symposium, Oklahoma City, 4-8 April, 2009.

Dinh, A. V. and Tiab, D., “ Transient pressure analysis of a well with an inclined hydraulic fracture using type curve matching.” SPE 120540-MS Paper presented at the SPE Production and Operation Symposium, Oklahoma City, 4-8 April, 2009.

East, L. E., Kenneth, W. M., Tucker J., Covington R. and Duell A.: “Improved Zonal Isolation Through the use of Sealants before Primary cementing Operation.” IADC/SPE 59131 Paper presented at the 2000 IADC/SPE Drilling Conference, New Orleans, 23-25 February, 2000.

Economides, M.: “Horizontal Wells: Completion & Evaluation,” PE307 Petroleum Engineering manual.

Economides, M. J. and Nolte, K. G.: “Reservoir Stimulation”, 2nd Ed., Prentice Hall, Eaglewood Cliffs, New Jersey, 1989.

Frick, T.P., Brand, C.W. and Schlager, B.: "Horizontal Well Testing of Isolated Segments." SPE 29959-PA Paper presented at the Annual SPE International Meeting on Petroleum Engineering, Beijing, China, 14-17 November, 1995.

Giger, F. M.: "Horizontal Wells Production Techniques in Heterogeneous Reservoirs." SPE 13710-MS Paper presented at the Middle East Oil Technical Conference, Bahrain, 11-14 March, 1985.

Gomez J., Passos A. and Melo, A.: "Cement Zonal isolation to Control Salt and CO2 in Brazilian Ultra Deep Water Presalt Well of Santos Basin." SPE 143772-MS Paper presented at the Brazil Offshore Conference and Exhibition, Macae, Brazil, 14-17 June 2011.

Goode, P.A., and Kuchuk, F.J.: "Inflow Performance of Horizontal Wells." SPE Reservoir Engineering Journal, August, 1991, pp 319-323.

Goode, P. A. and Thambynaygam, R.K.M.: "Pressure Drawdown and buildup Analysis of Horizontal Wells in Anisotropic Media," SPE Formation evaluation, December, 1987.

Gringarten, A. C. and Ramey, H. : "The Use of Source and Green's Function in Solving Unsteady-Flow Problem in Reservoir." SPE Journal, October 1973, pp. 285-295.

Guo, G., and Evans, R.D.: "An Economic Model for Assessing the Feasibilty of exploiting Naturally Fractured Reservoirs by Horizontal Well technology." SPE 26676-MS Paper presented at the 68th Annual Technical Conference, Houston, TX, 3-6 October, 1993.

Hashemi, A., Nicolas L. M., and Gringarten, A.C.: "Well test Analysis of Horizontal Wells in Gas-condensate reservoirs." SPE 89905-PA Paper presented at the SPE Annual Technical Conference, Houston, TX, 26-29 September, 2004.

Henriksen, K.H., Augustine, J. and Wood, E.: "Integration of New Open Hole Zonal Isolation Technology Contributes to Improved Reserve Recovery and Revision in Industry Best Practice." SPE 97614-MS Paper presented at the 2005 SPE International Improved Oil Recovery Conference, Kuala Lumpur, Malaysia, 5-6 December, 2005.

Howard, G. C. and Fast, C. R.: "Hydraulic Fracturing" Monograph Vol. 2 of the Henry L. Doherty series, SPE of AIME, Dallas, TX, 1970.

Hubbert, M. K. and Willis, G. D.: "Mechanics of Hydraulic Fracturing." Trans, AIME (1957) Vol. 210, 153-168.

Joshi, S.D.: “Augmentation of Well Productivity Using Slant and Horizontal Wells,” SPE 15375-MS Paper presented at the 61st Annual Technical Conference, New Orleans, LA, 5-8October, 1986.

Kelbie G. M. and Garfield G. L.: “Isolating Water Production at the Source Utilizing Through-Tubing Inflatable Technology.” SPE 102759-MS Paper presented at the 2006 SPE International Oil and Gas Conference, Beijing, China, 5-7 December, 2006.

Kuchuk F. and Habusky T.: “Pressure behavior of horizontal wells with multiple fractures.” SPE 27971-MS Paper presented at the Tulsa University Centennial Petroleum Engineering Symposium, Tulsa, OK, 29-31 August. 1994.

Kuchuk, F., Goode, P.A., Wilkinson, D.J. and Thambynayagam, R.K.: “Pressure-Transient behavior of Horizontal wells with and without gas Cap or aquifer.” SPE Formation Evaluation Journal, March 1991, pp 86-94.

Lee, J., Rollings, J. B., and Spivey, J. P.: “Pressure Transient Testing”, SPE Textbook Series, vol. 9. Society of Petroleum Engineers, Richardson, Texas, USA. 2003.

Leif L., Hegre T.M.: “Pressure transient analysis of multifractured horizontal wells.” SPE 28389-MS Paper presented at the SPE 69th Annual Technical Conference and Exhibition, New Orleans, LA, 25-28 September, 1994.

Malekzadeh, D., and Abdelgawad, A.: “Analytical and statistical Analysis of Pseudo-Skin factors for Horizontal Wells.” JCPT, October 1999, Vol. 38, No. 10.

Maddox, B., Wharton, M., Hinkie, R., Farabee, M. and Ely, J.: “Cementless Multi-Zone Horizontal Completion Yields Three-Fold Increase.” IADC/SPE 112774-MS Paper presented at the 2008 IADC/SPE Drilling conference in Orlando, 4-6 March 2008.

Odeh, A.S., and Babu, D.K.: “Transient Flow Behavior of Horizontal wells: Pressure Drawdown and Buildup analysis.” SPE Formation Evaluation Journal, March, 1990, pp 7-15.

Olarewaju J., Lee, W.J.: “Pressure behavior of layered and dual porosity reservoirs in the presence of wellbore effects.” SPE Formation Evaluation Journal, September 1989, pp 397-405.

Ozkan E.: “Performance of horizontal wells” Ph.D. dissertation, University of Tulsa, 1988.

Poe B. D. and Elbel J.L.: "Pressure transient behavior of a finite conductivity fracture in infinite acting and bounded reservoirs." SPE 28392-MS Paper presented at the SPE 69th Annual Technical Conference and Exhibition, New Orleans, LA, 25-28 September, 1994.

Raghavan, R.: "An analysis of horizontal wells intercepted by multiple fractures." SPE Journal, Vol. 2, Sepember 1997: pp 235-245.

Rentano, A. and Muhammed, Y.: "Impact of Completion Technique on Horizontal Well Productivity." SPE 54302-MS Paper presented at the 1999 SPE Asia and Pacific Oil and Gas conference, Jakarta, 20-22 April 1999.

Robison, C.E., Mashaw, H.R. and Welch, W.R.: "Zone Isolation of Horizontal Wells by Coiled-Tubing-Actuated Tools." OTC 7354-MS Paper presented at the 25th annual offshore technical conference in Houston, TX, 3-5 May 1993.

Rodriguez, F., Cinco-Ley, H. and Samaniego-V, F.: "Evaluation of fracture asymmetry of finite-Conductivity fractured Wells." SPE Production Evaluation Journal, May 1992, PP 233-239.

Rodriguez, F., and Cinco-Ley, H: "Partially penetrating fracture: Pressure Transient analysis of an infinite Conductivity Fractures." SPE 12743-MS Paper presented at SPE California Regional Meeting, 11-13 April, 1984.

Rosa, A.J and Carvalho, R.S.: "A Mathematical Model for Pressure Evaluation in an infinite-Conductivity Horizontal well." SPE Formation Evaluation Journal, December, 1989, pp 559-566.

Slimani, K. and Tiab, D.: "Pressure transient Analysis of Partially Penetrating Wells in a Naturally Fractured Reservoir" SPE 104059-MS Paper presented at the first international oil conference and exhibition, Mexico, 31 Aug.-2 Sep. 2006.

Spivak, D.: "Pressure Analysis for Horizontal Wells," Ph.D. Dissertation, Louisiana Tech University, May 1988.

Tiab, D.: "Analysis of Pressure Derivative Data of Hydraulic Fractured Wells by the Tiab's Direct Synthesis Technique." Journal of Petroleum Science and Engineering, 49 (2005).

Tiab, D.: "Analysis of Pressure Derivative without Type-Curve Matching: Vertically Fractured Wells in Closed Systems." Journal of Petroleum Science and Engineering, 11 (1994) 323-333. This paper

was originally presented as SPE 26138 at the 1993 SPE Western Regional Meeting, May 26-28, Anchorage, Alaska.

Tiab, D. and Puthigai, S.K.: "Pressure Derivative Type-Curves for a Vertically Fractured Well". SPE Formation Evaluation journal, March 1988, pp 156-158.

Thompson, L.G., and Temeng, K.O.: "Automatic Type-Curve matching for Horizontal wells" SPE 25507-MS Paper presented at the production operation symposium, Oklahoma City, March 21-23, 1993.

Valko P. and Economides M.J.: "Performance of a longitudinally fractured horizontal well", SPE Journal, March1996, pp 11-19.

Wan, J. and Aziz, K.: "Multiple hydraulic fractures in horizontal wells." SPE 54627-MS Paper presented at the SPE Western Regional Meeting, Anchorage, Alake, 26-28 December, 1999.

Wong D. and Harrington A.: "application of the pressure derivative function in the pressure transient testing of fractured wells." SPE Formation Evaluation Journal, October 1986, pp 470-480.

Wright, C. A. and Conant, R. A.: "Hydraulic Fracture Reorientation in Primary and Secondary Recovery from Low Permeability Reservoirs." SPE 30484-MS Paper presented at the SPE Annual Technical Conference, Dallas, TX, 22-25 October, 1995.

Wright, C. A., Davis, Minner, W. A.,E. J., Ward, J. F., and Weijers, L.: "Surface Tiltmeter Fracture Mapping Reaches New Depths – 10000 Feet, and Beyond." SPE 39919-MS Paper presented at the SPE Rocky Mountain Regional/Low-Permeability Reservoir Symposium and Exhibition, Denver, Colorado, 5-8 April 1998.

Zerzar, A. and Bettam, Y., "Interpretation of multiple hydraulically fractured horizontal wells in closed systems.", SPE 84888-MS, Paper presented at the SPE International Improved Oil Recovery Conference in Asia Pacific, Kuala Lumpur, Malaysia, 20-21 October, 2003.

APPENDIXES

APPENDIX-A: Plots for horizontal wells with zonal isolations.

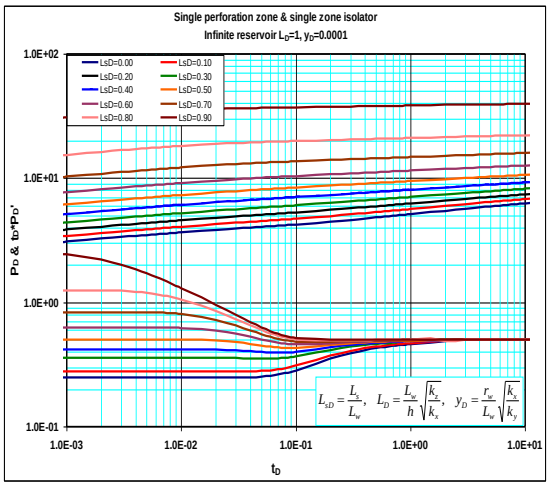

Figure A-1: Pressure and pressure derivative plot.

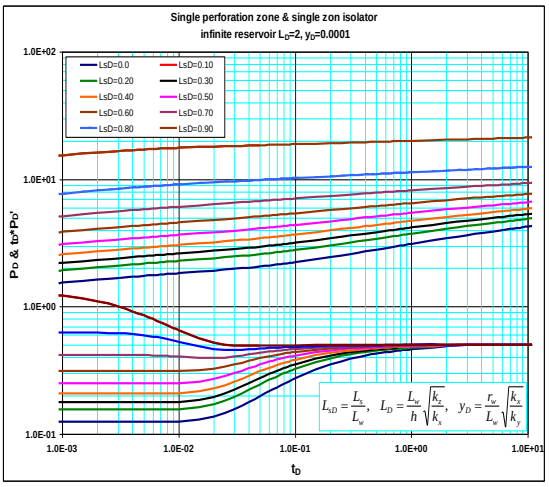

Figure A-2: Pressure and pressure derivative plot.

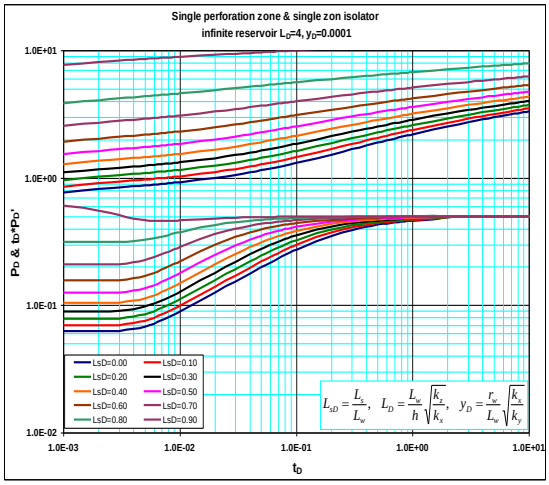

Figure A-3: Pressure and pressure derivative plot.

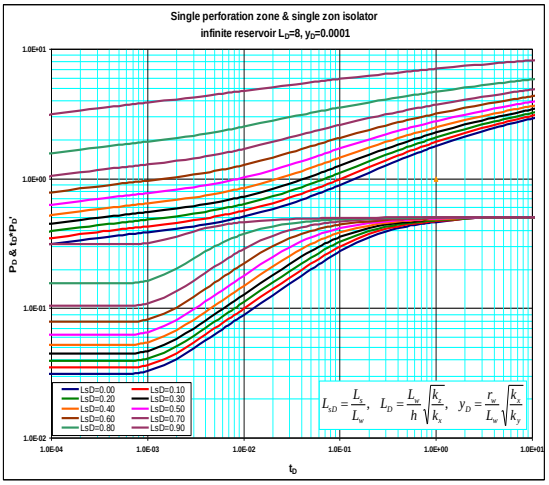

Figure A-4: Pressure and pressure derivative plot.

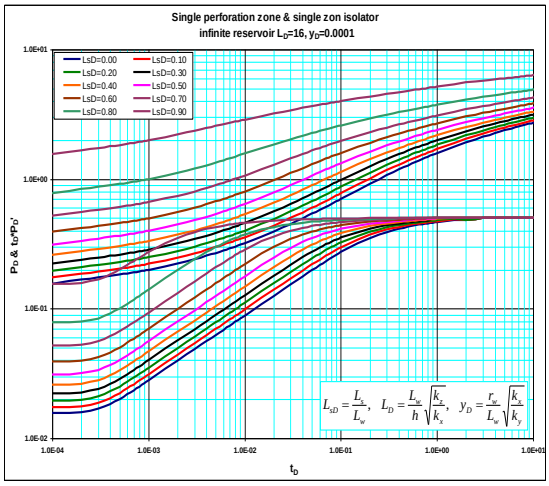

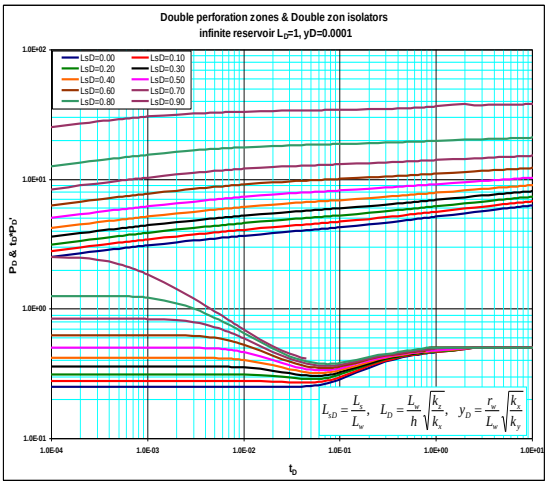

Figure A-5: Pressure and pressure derivative plot.

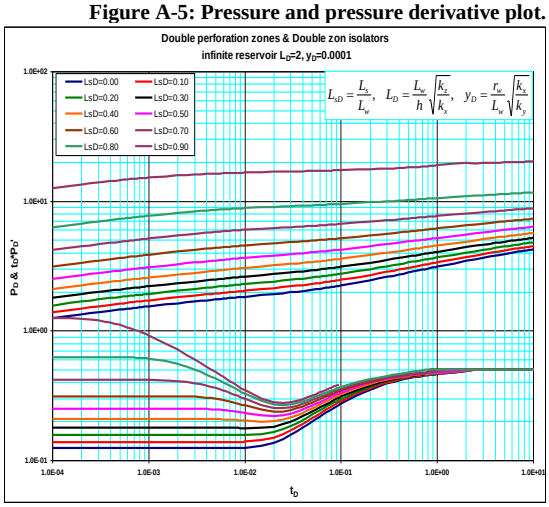

Figure A-6: Pressure and pressure derivative plot.

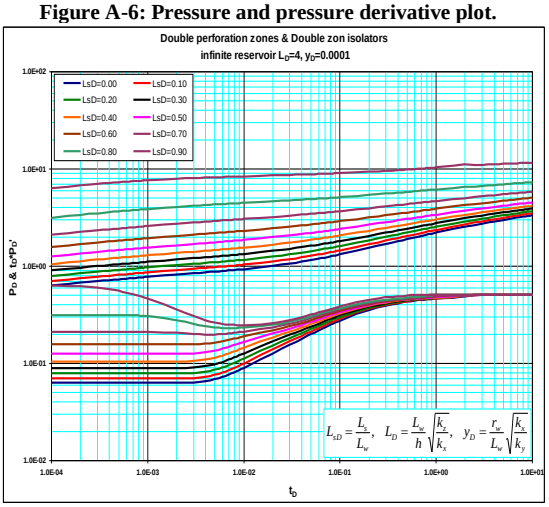

Figure A-7: Pressure and pressure derivative plot.

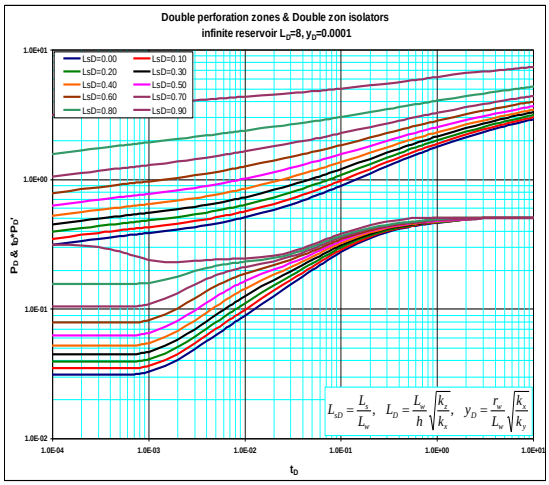

Figure A-8: Pressure and pressure derivative plot.

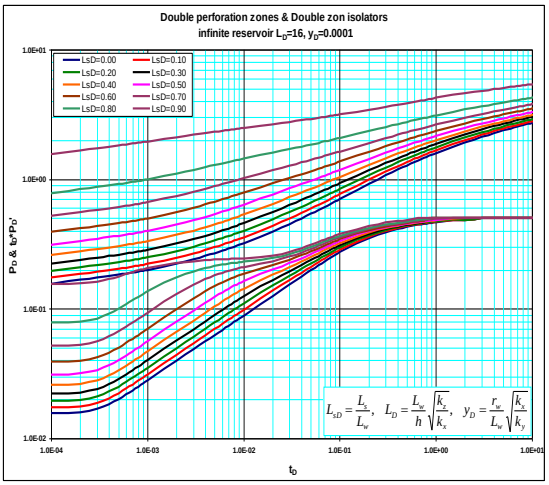

Figure A-9: Pressure and pressure derivative plot.

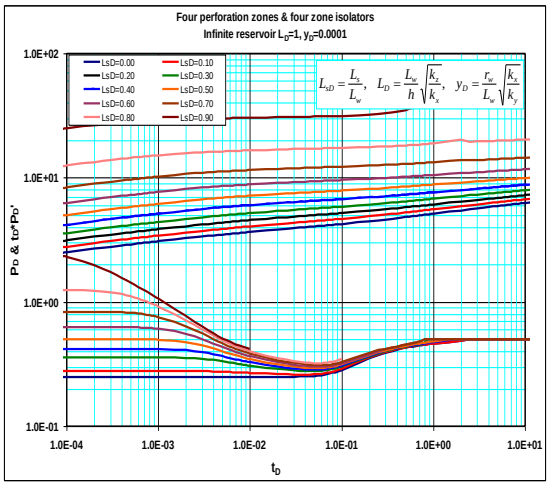

Figure A-10: Pressure and pressure derivative plot.

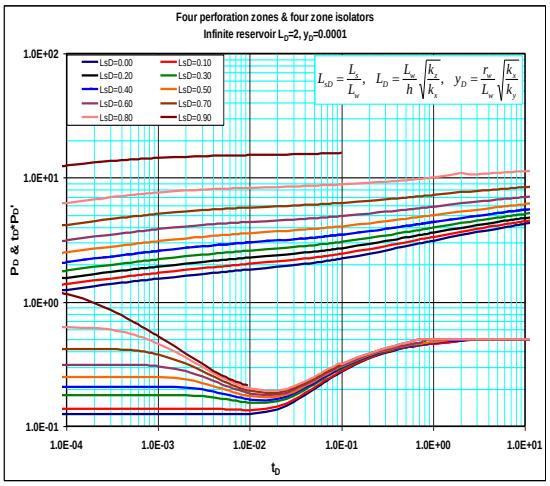

Figure A-11: Pressure and pressure derivative plot.

Figure A-12: Pressure and pressure derivative plot.

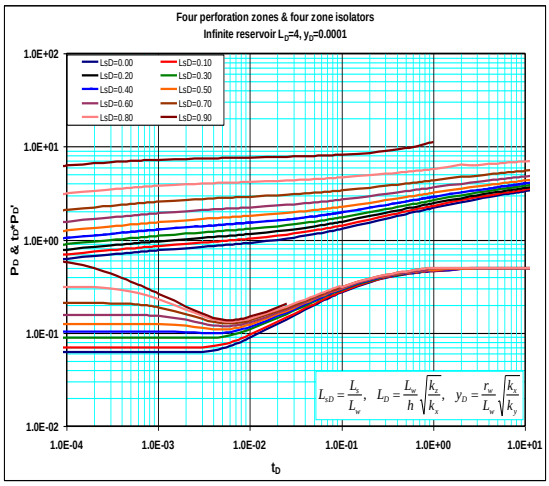

Figure A-13: Pressure and pressure derivative plot.

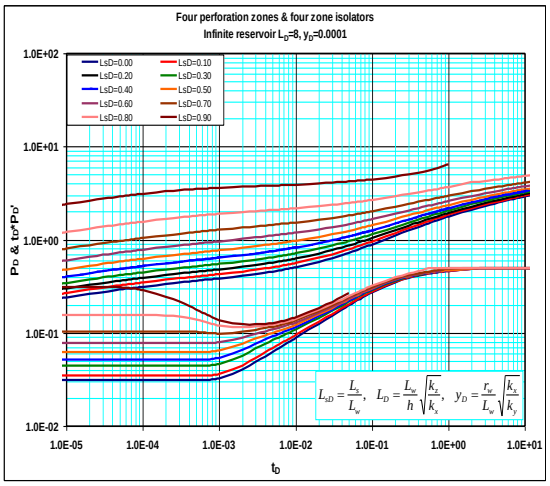

Figure A-14: Pressure and pressure derivative plot.

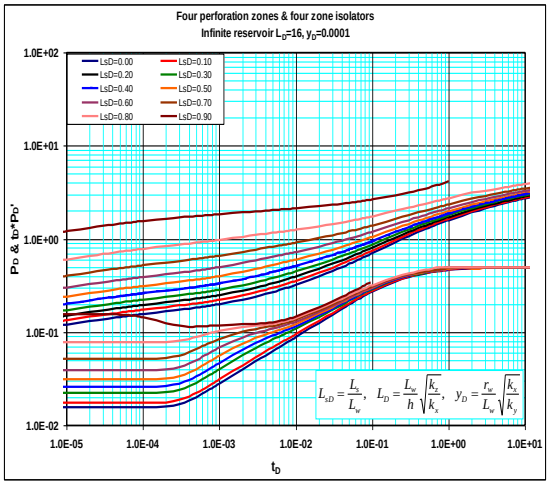

Figure A-15: Pressure and pressure derivative plot.

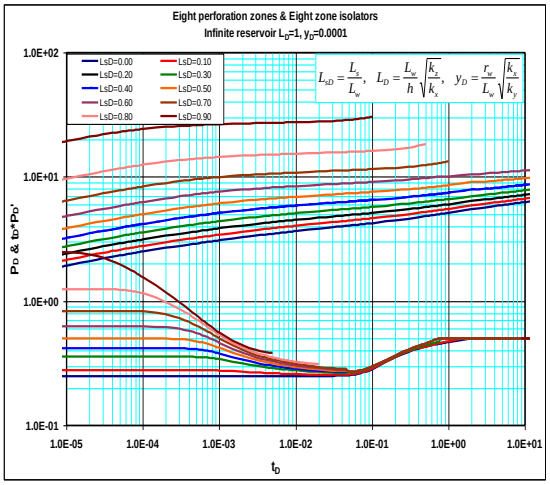

Figure A-16: Pressure and pressure derivative plot.

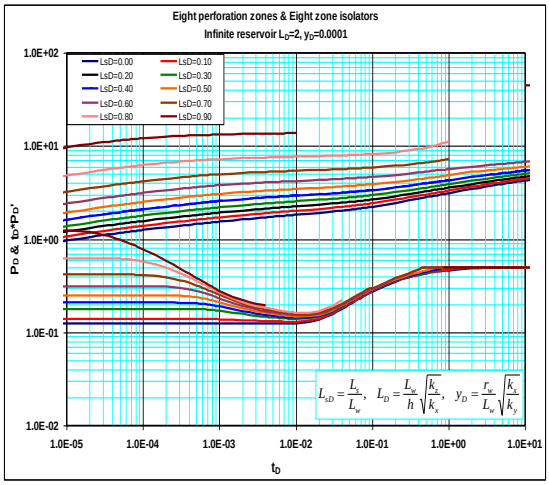

Figure A-17: Pressure and pressure derivative plot.

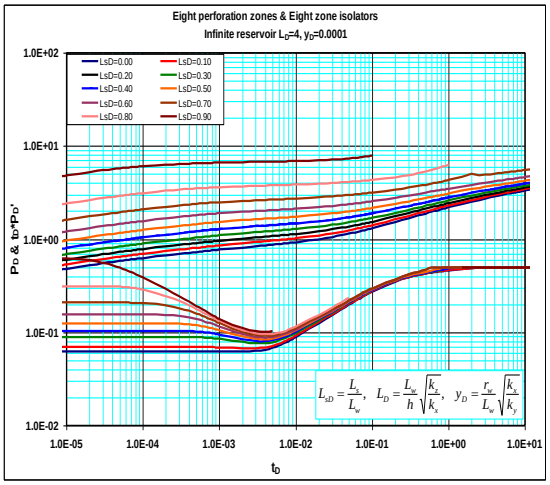

Figure A-18: Pressure and pressure derivative plot.

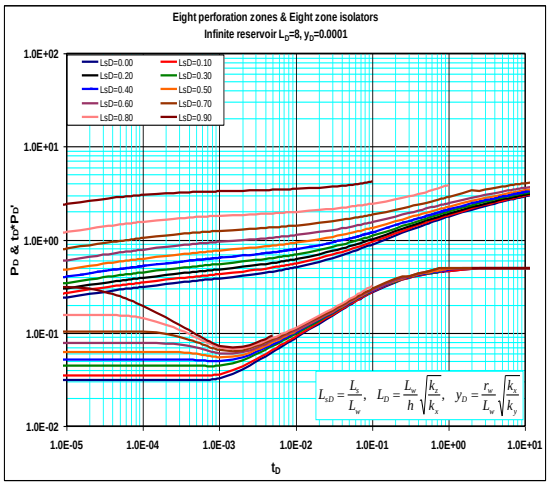

Figure A-19: Pressure and pressure derivative plot.

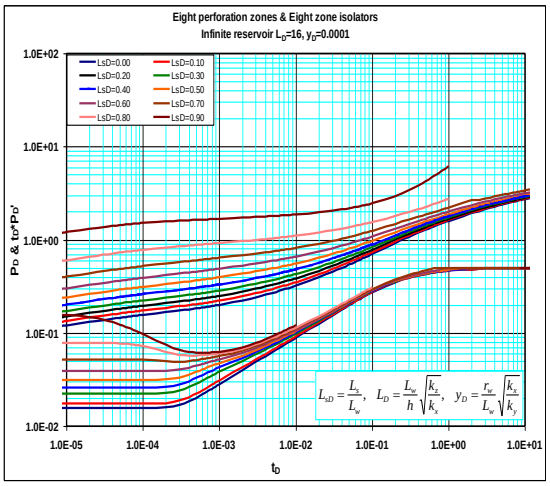

Figure A-20: Pressure and pressure derivative plot.

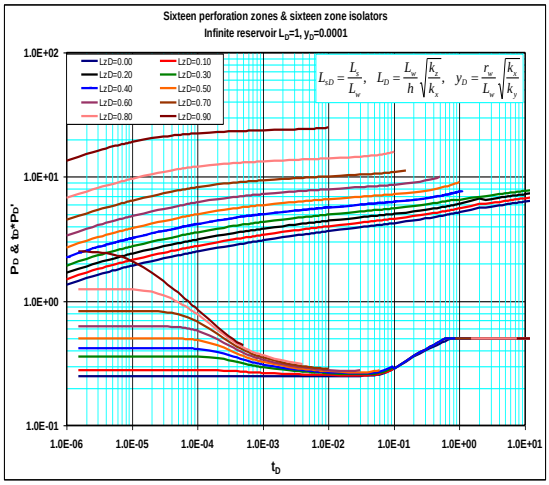

Figure A-21: Pressure and pressure derivative plot.

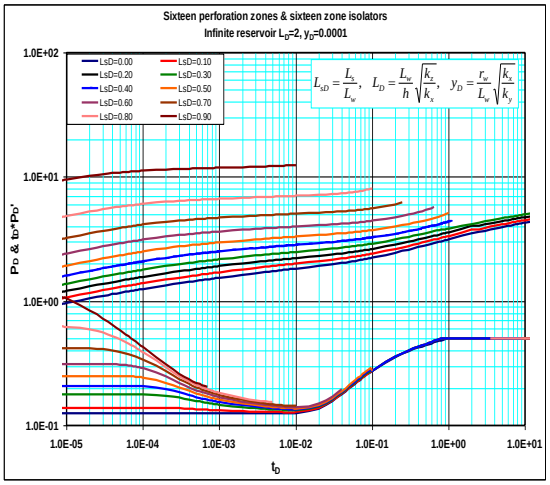

Figure A-22: Pressure and pressure derivative plot.

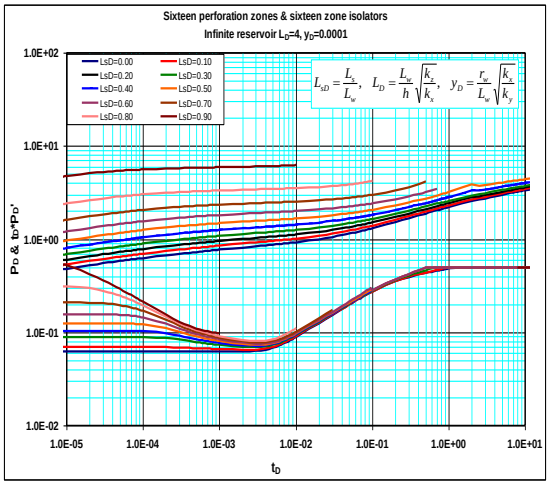

Figure A-23: Pressure and pressure derivative plot.

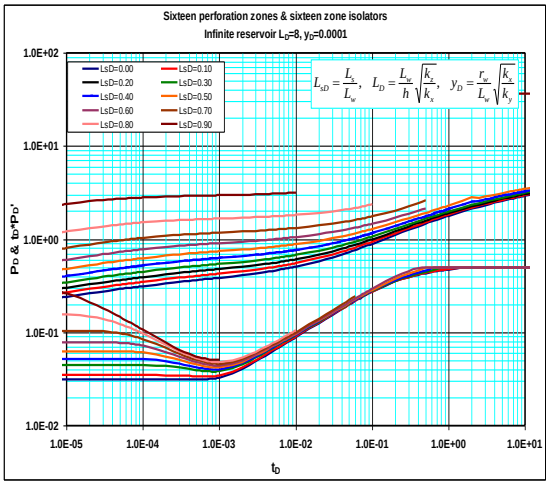

Figure A-24: Pressure and pressure derivative plot.

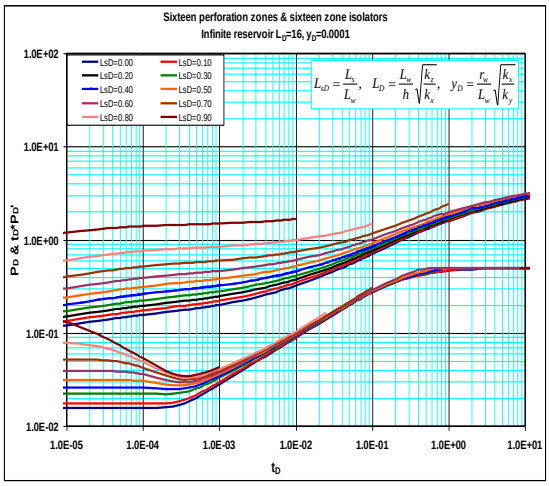

Figure A-25: Pressure and pressure derivative plot.

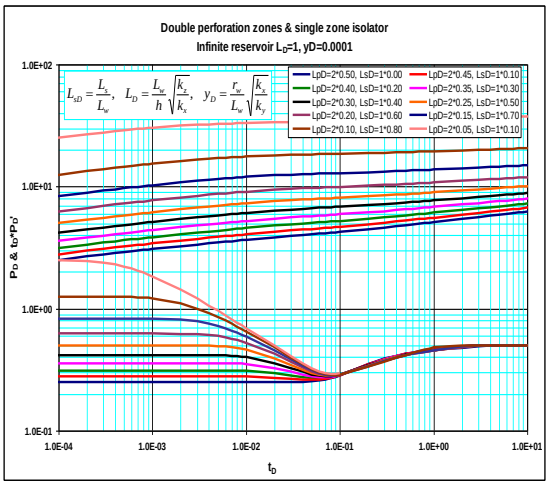

Figure A-26: Pressure and pressure derivative plot.

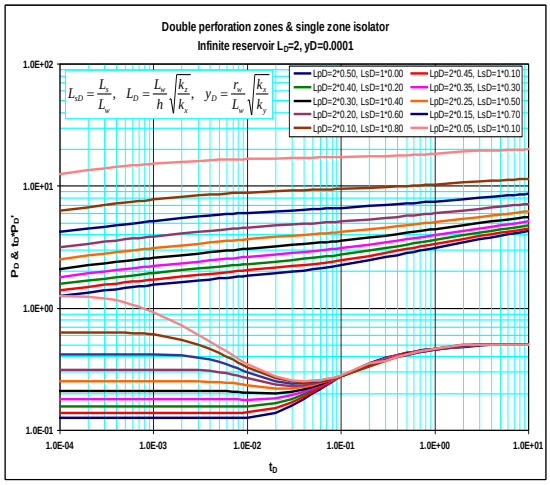

Figure A-27: Pressure and pressure derivative plot.

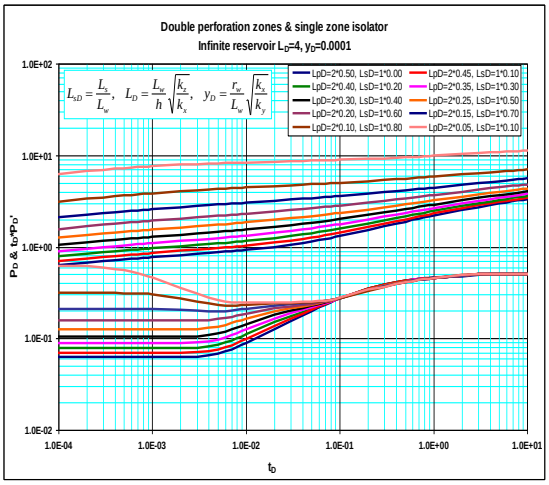

Figure A-28: Pressure and pressure derivative plot.

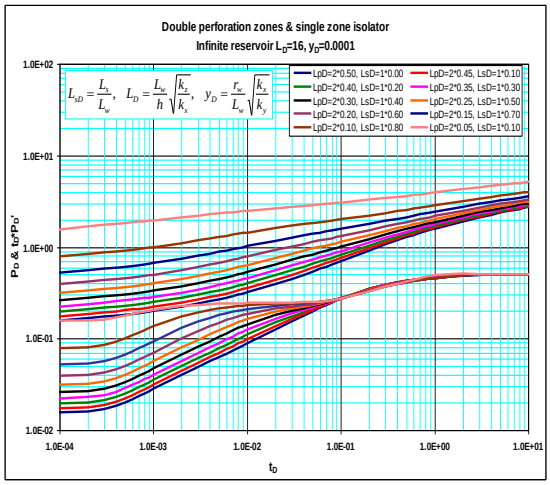

Figure A-29: Pressure and pressure derivative plot.

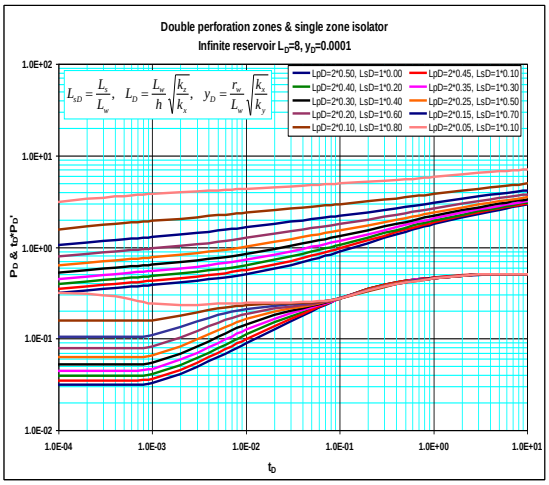

Figure A-30: Pressure and pressure derivative plot.

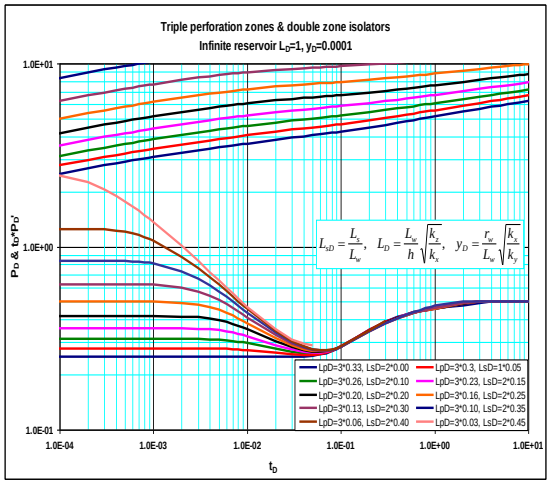

Figure A-31: Pressure and pressure derivative plot.

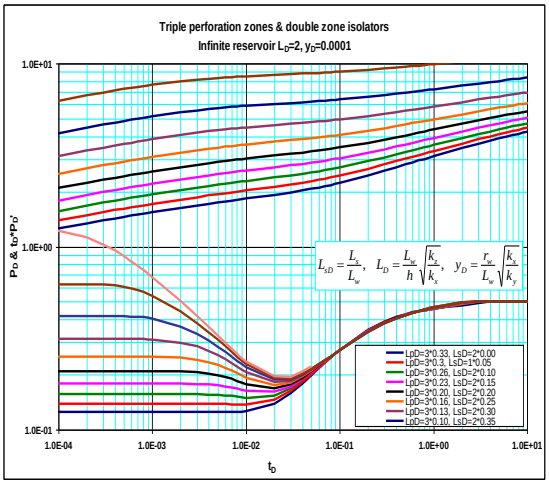

Figure A-32: Pressure and pressure derivative plot.

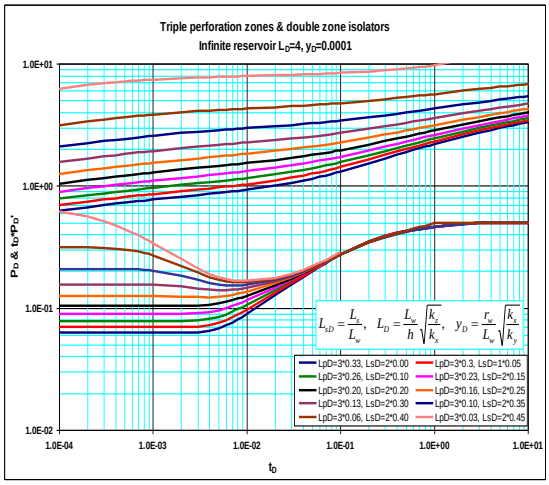

Figure A-33: Pressure and pressure derivative plot.

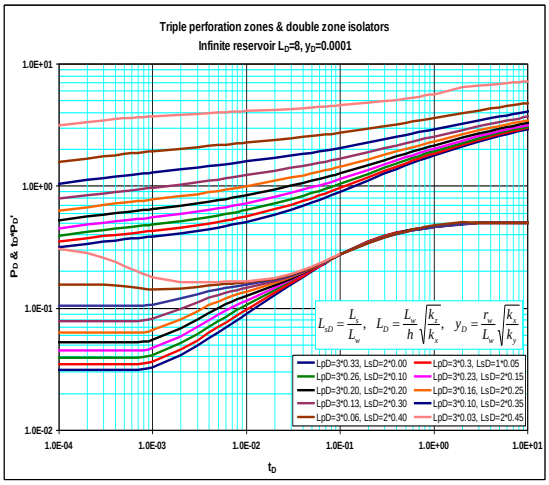

Figure A-34: Pressure and pressure derivative plot.

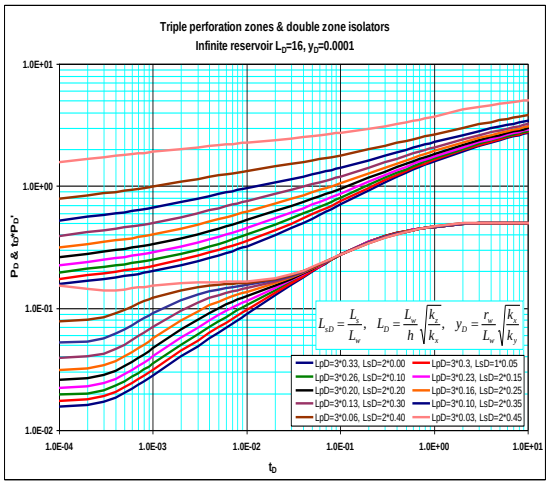

Figure A-35: Pressure and pressure derivative plot.

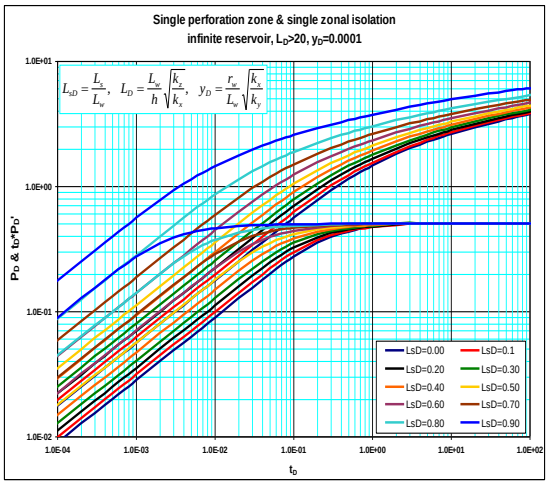

Figure A-36: Pressure and pressure derivative plot.

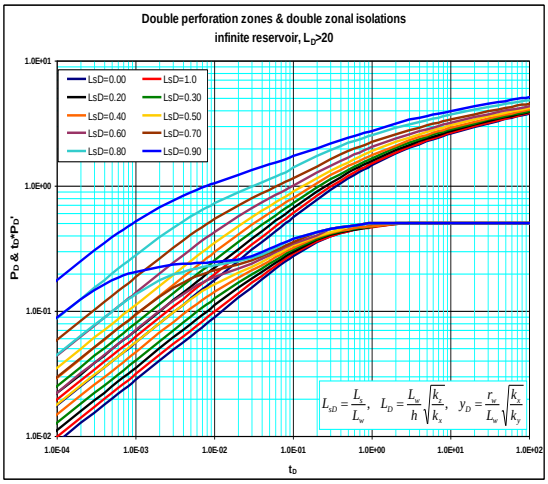

Figure A-37: Pressure and pressure derivative plot.

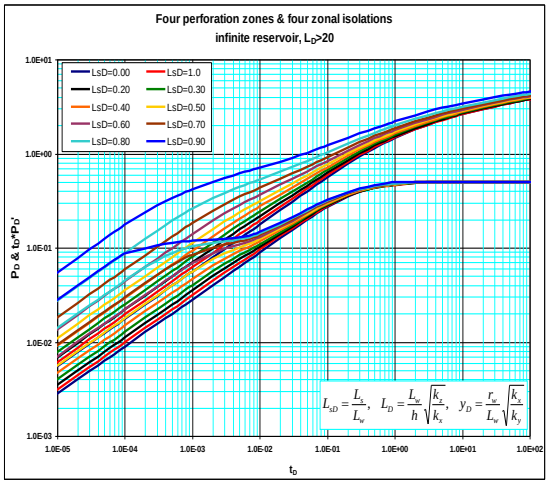

Figure A-38: Pressure and pressure derivative plot.

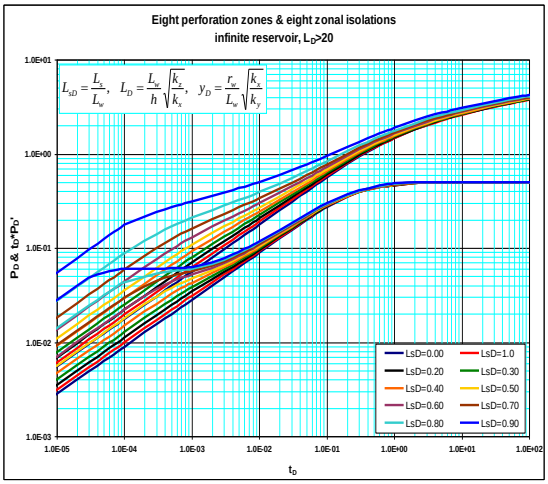

Figure A-39: Pressure and pressure derivative plot.

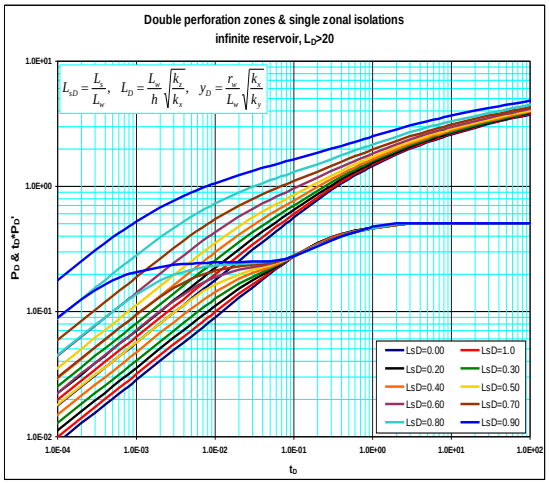

Figure A-40: Pressure and pressure derivative plot.

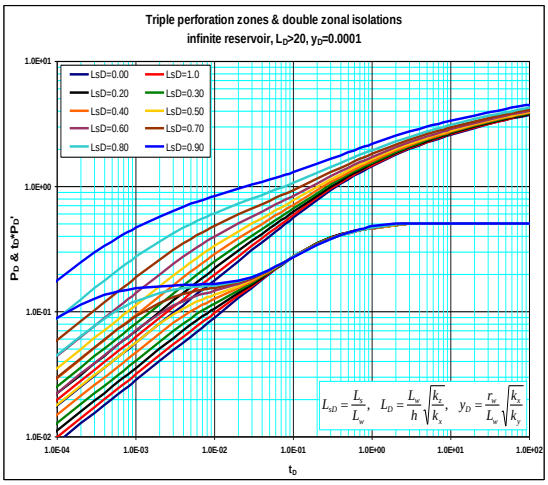

Figure A-41: Pressure and pressure derivative plot.

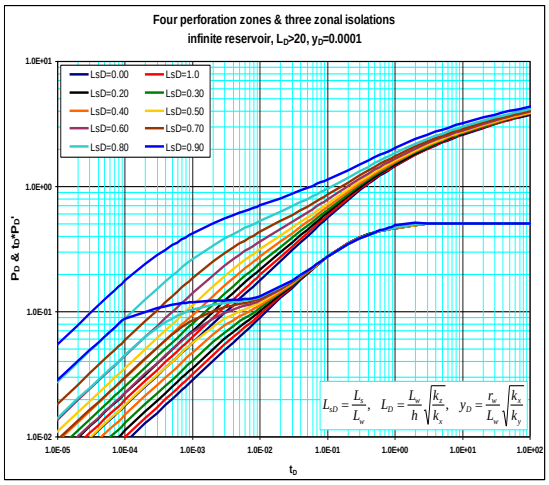

Figure A-42: Pressure and pressure derivative plot.

APPENDIX-B: Plots for multiple inclined hydraulic fractures.

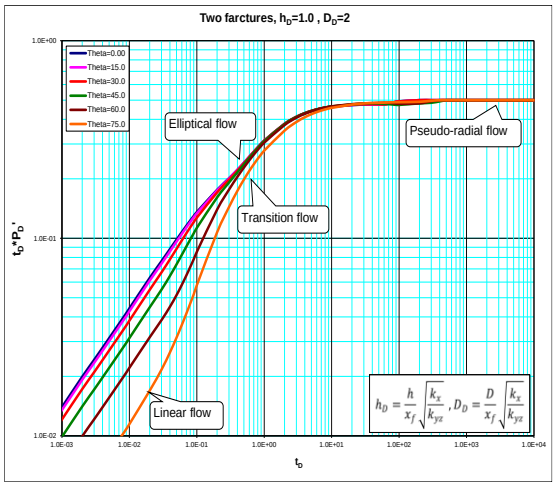

Figure B-1: Pressure and pressure derivative plot.

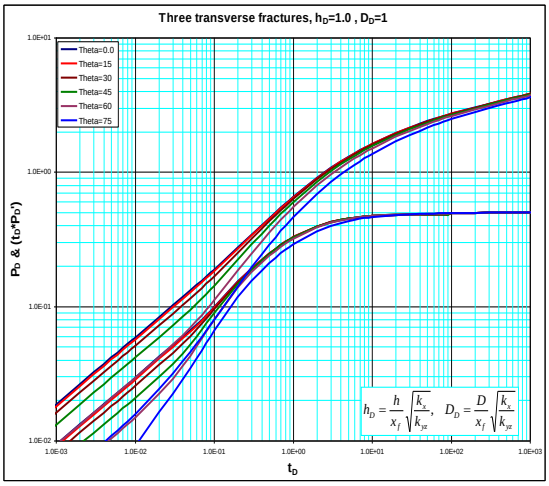

Figure B-2: Pressure and pressure derivative plot.

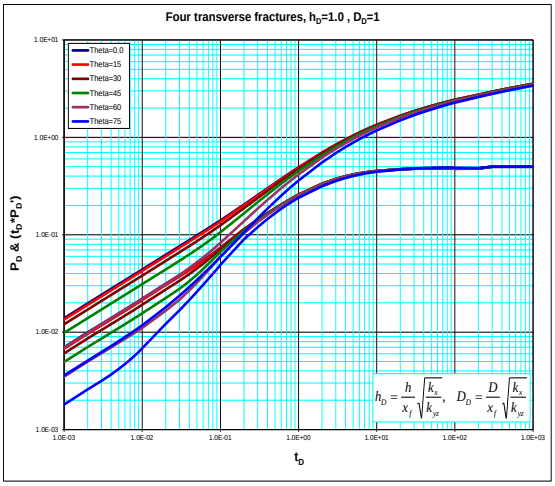

Figure B-3: Pressure and pressure derivative plot.

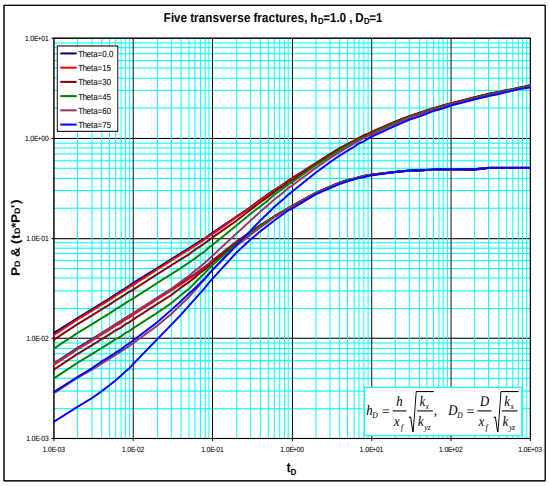

Figure B-4: Pressure and pressure derivative plot.

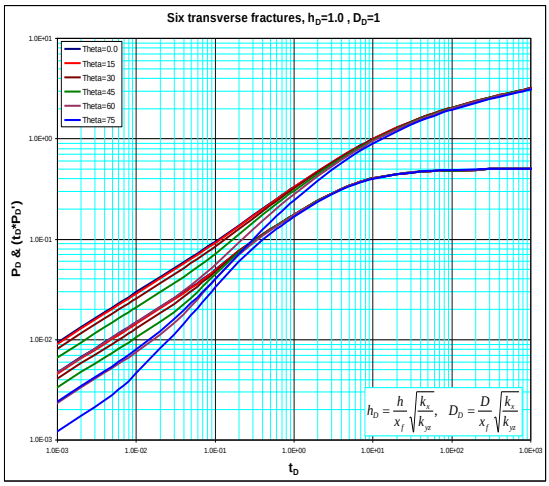

Figure B-5: Pressure and pressure derivative plot.

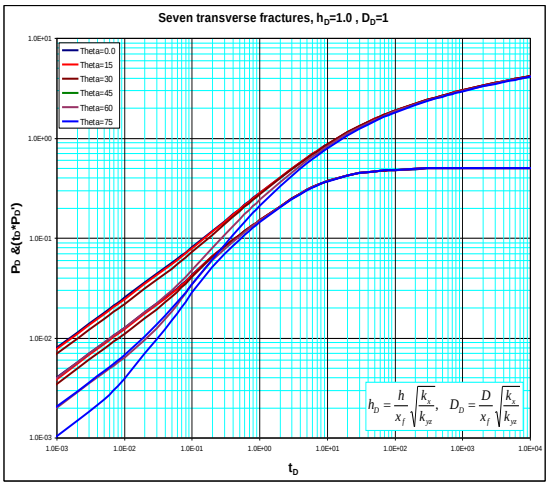

Figure B-6: Pressure and pressure derivative plot.

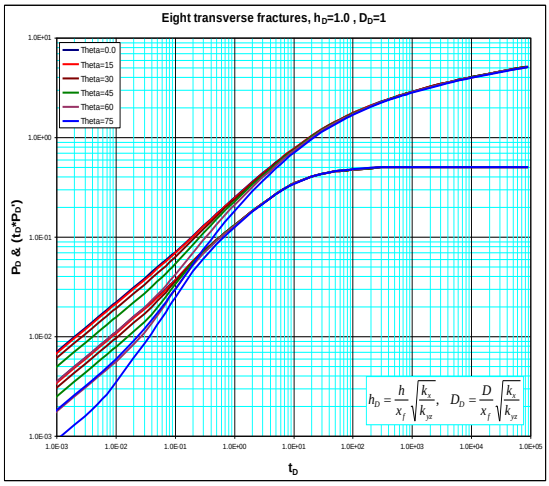

Figure B-7: Pressure and pressure derivative plot.

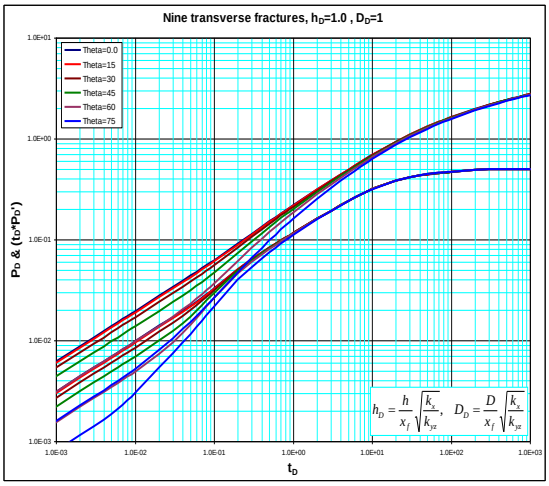

Figure B-8: Pressure and pressure derivative plot.

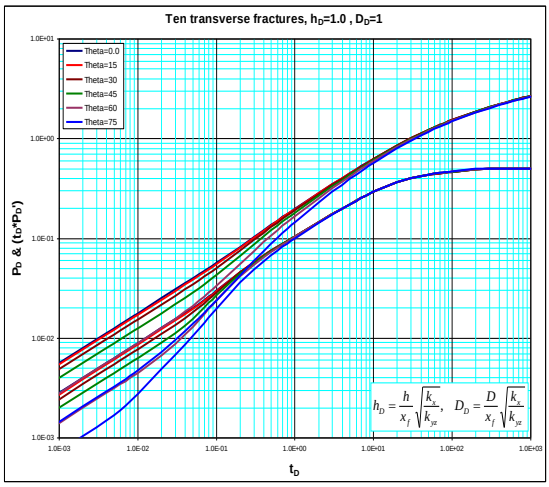

Figure B-9: Pressure and pressure derivative plot.

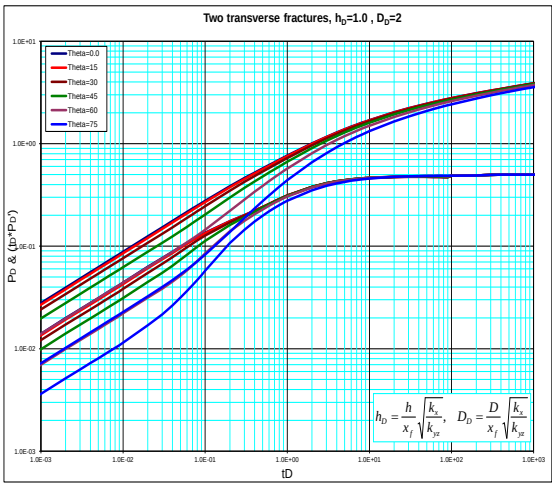

Figure B-10: Pressure and pressure derivative plot.

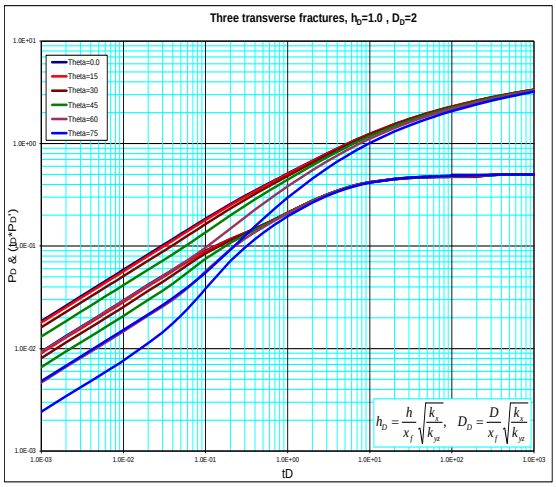

Figure B-11: Pressure and pressure derivative plot.

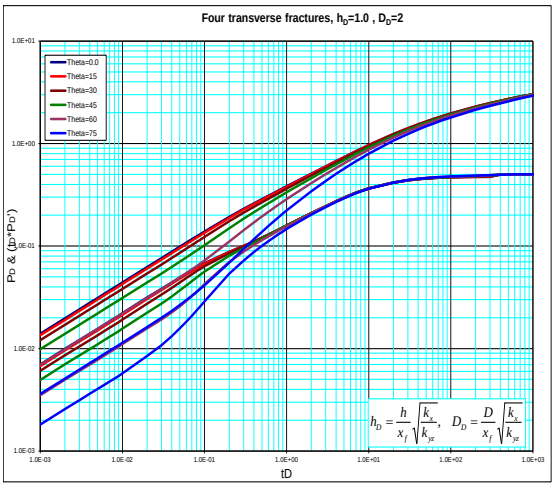

Figure B-12: Pressure and pressure derivative plot.

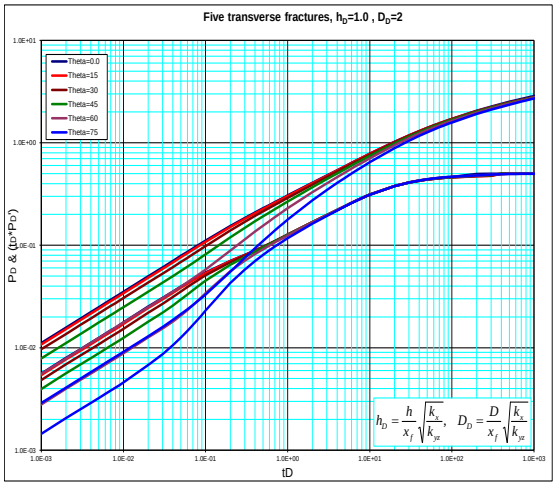

Figure B-13: Pressure and pressure derivative plot.

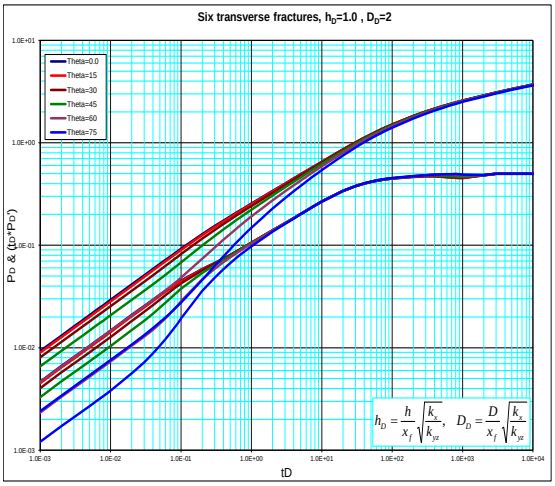

Figure B-14: Pressure and pressure derivative plot.

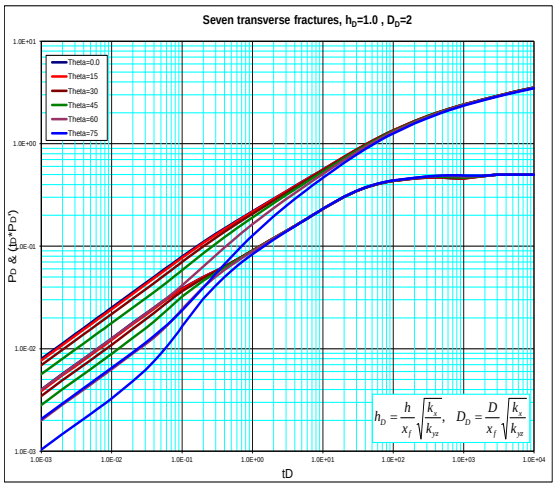

Figure B-15: Pressure and pressure derivative plot.

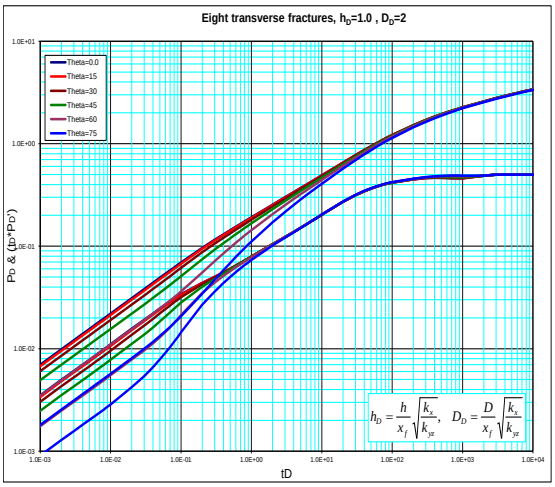

Figure B-16: Pressure and pressure derivative plot.

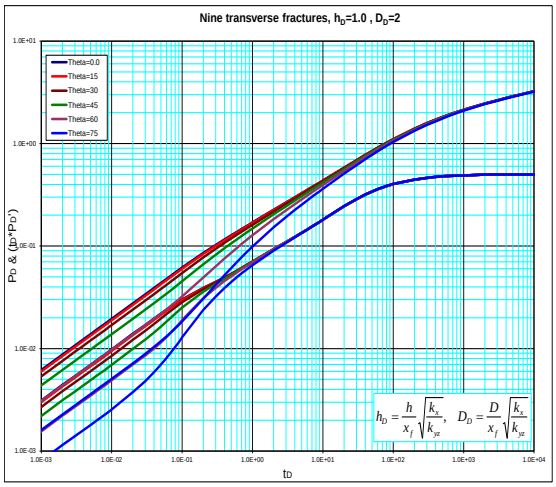

Figure B-17: Pressure and pressure derivative plot.

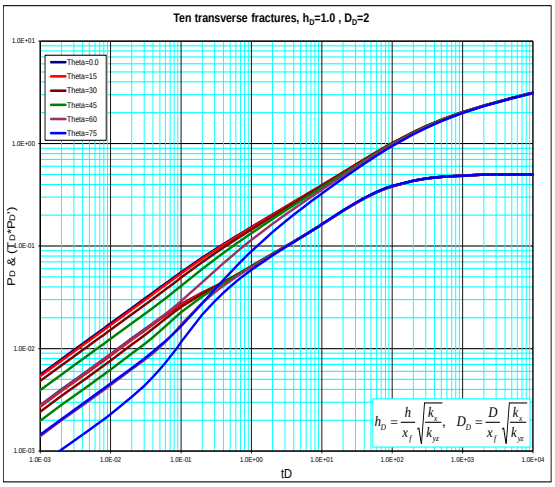

Figure B-18: Pressure and pressure derivative plot.

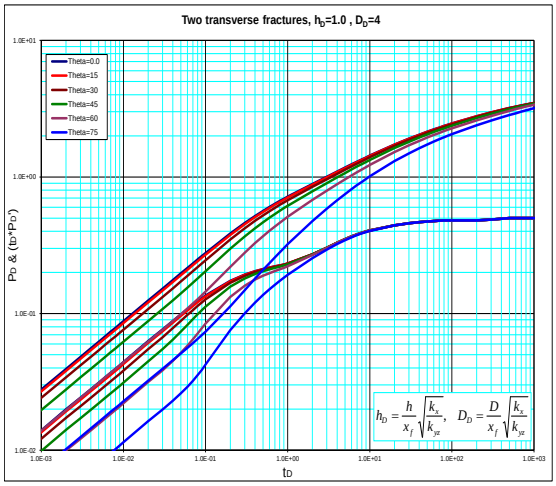

Figure B-19: Pressure and pressure derivative plot.

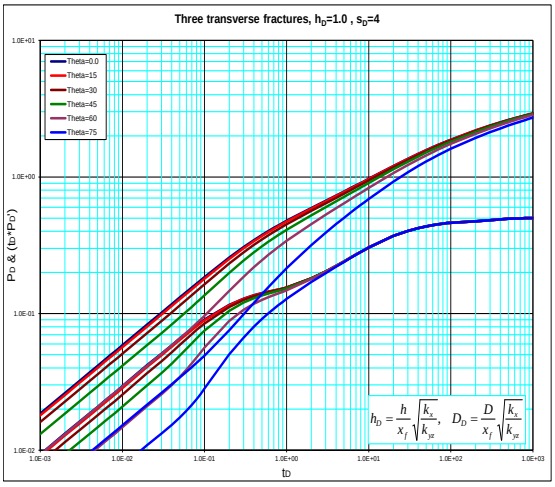

Figure B-20: Pressure and pressure derivative plot.

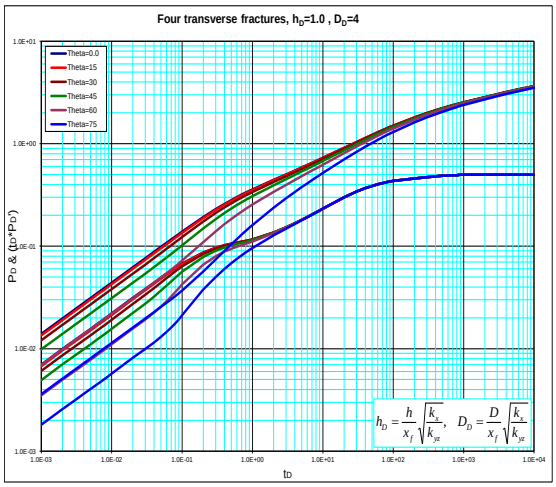

Figure B-21: Pressure and pressure derivative plot.

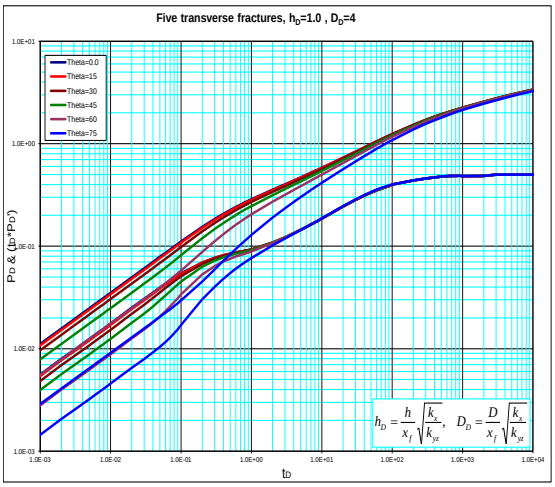

Figure B-22: Pressure and pressure derivative plot.

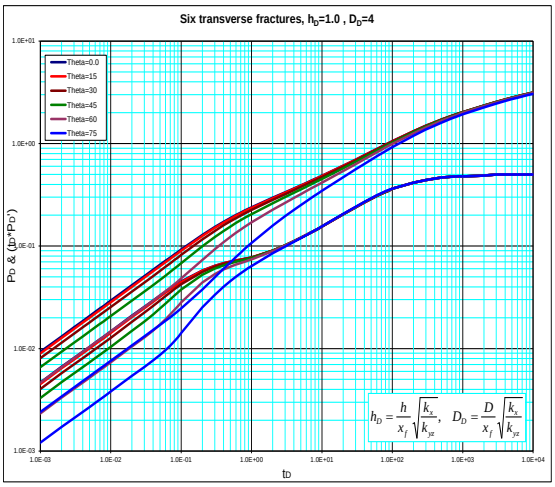

Figure B-23: Pressure and pressure derivative plot.

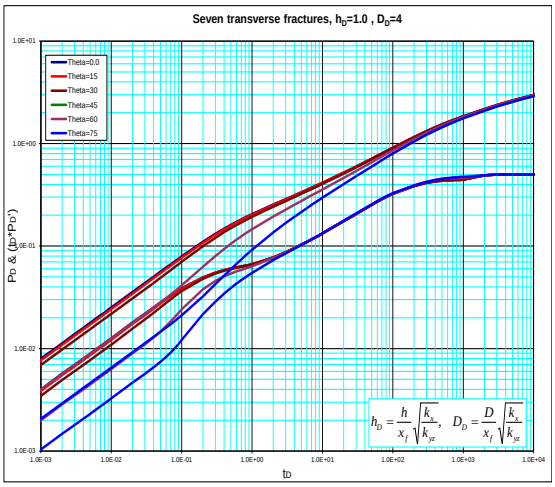

Figure B-24: Pressure and pressure derivative plot.

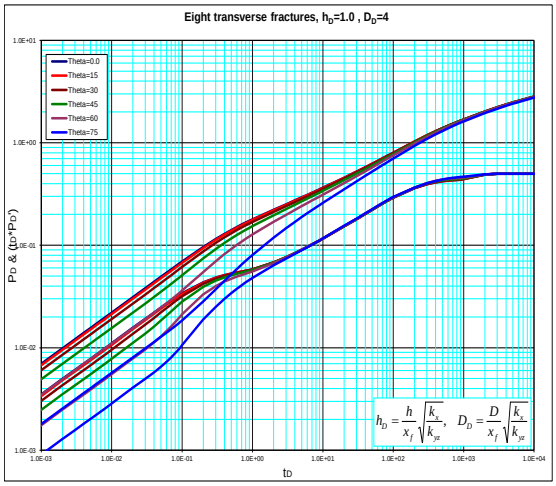

Figure B-25: Pressure and pressure derivative plot.

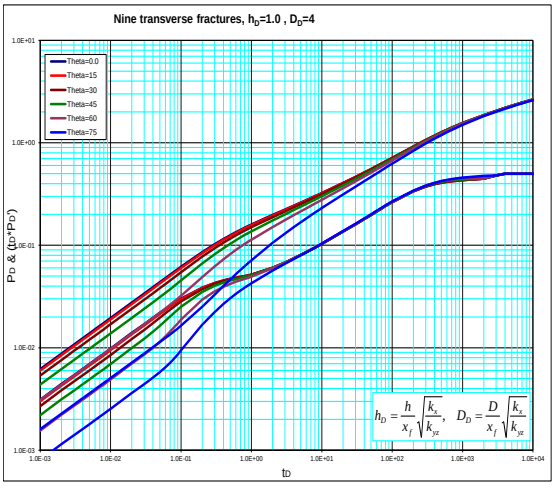

Figure B-26: Pressure and pressure derivative plot.

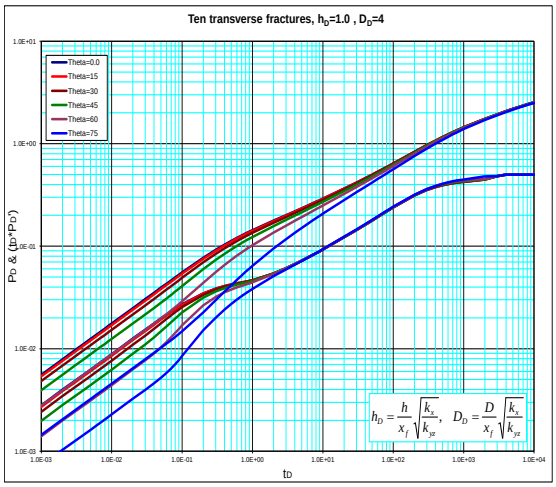

Figure B-27: Pressure and pressure derivative plot.

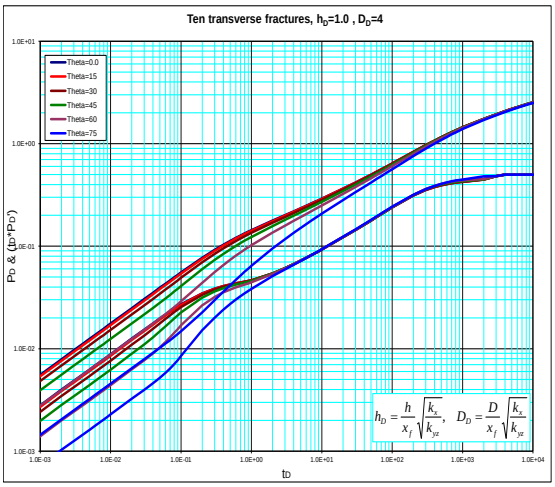

Figure B-28: Pressure and pressure derivative plot.

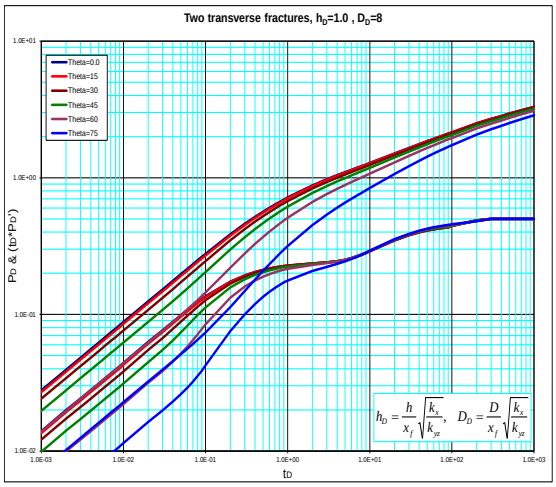

Figure B-29: Pressure and pressure derivative plot.

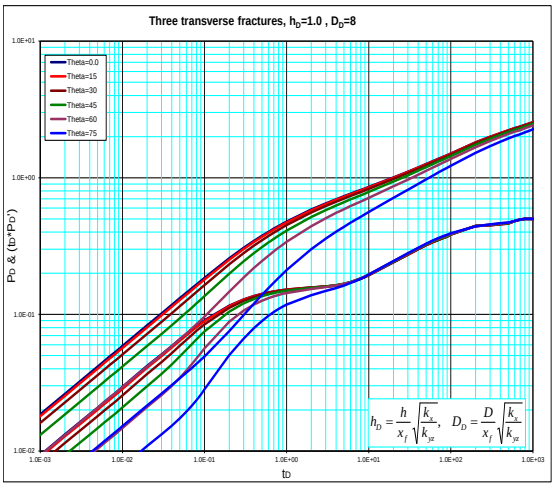

Figure B-30: Pressure and pressure derivative plot.

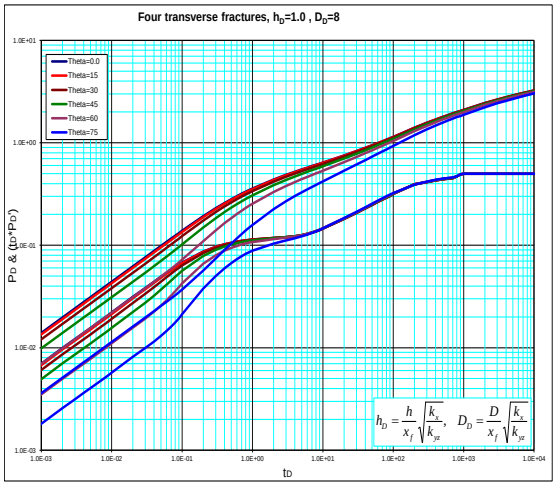

Figure B-31: Pressure and pressure derivative plot.

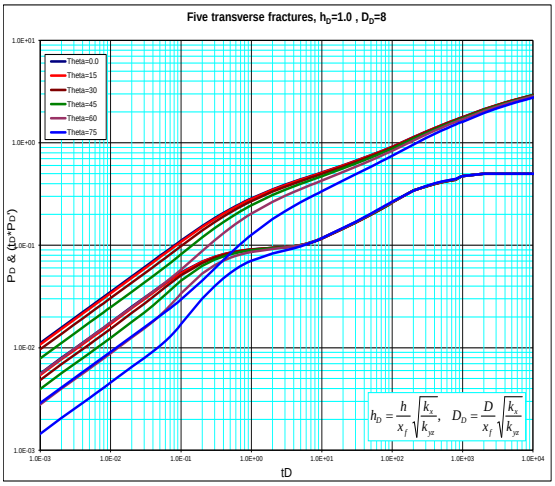

Figure B-32: Pressure and pressure derivative plot.

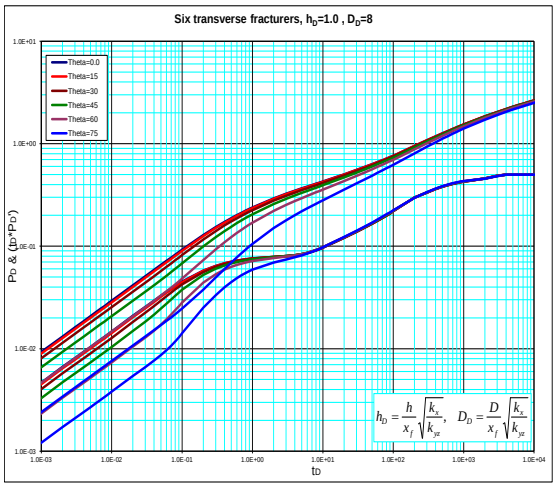

Figure B-33: Pressure and pressure derivative plot.

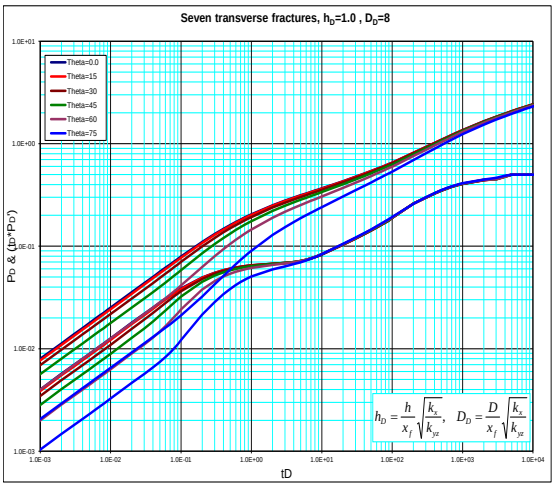

Figure B-34: Pressure and pressure derivative plot.

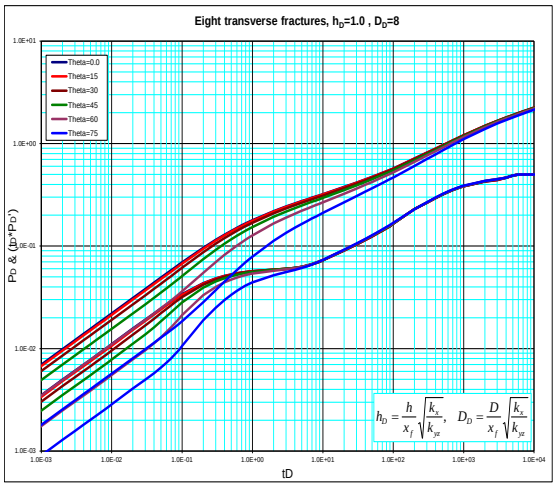

Figure B-35: Pressure and pressure derivative plot.

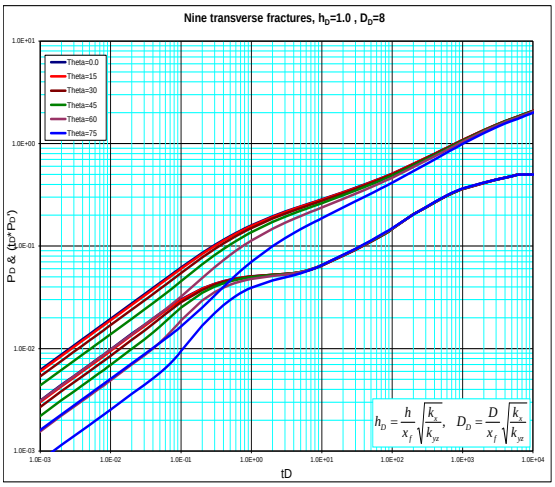

Figure B-36: Pressure and pressure derivative plot.

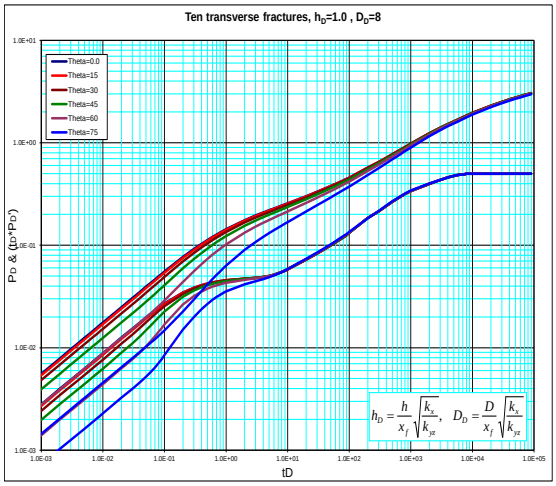

Figure B-37: Pressure and pressure derivative plot.

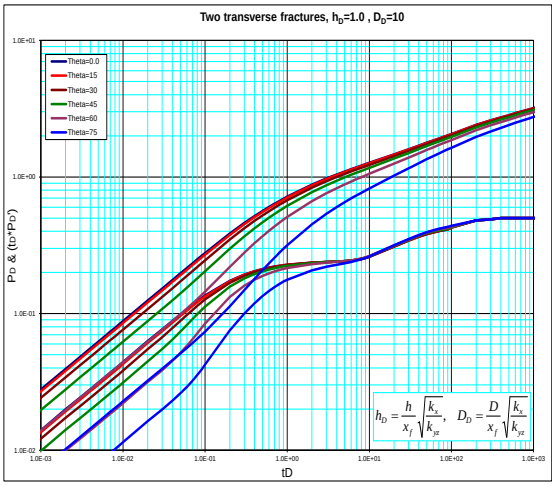

Figure B-38: Pressure and pressure derivative plot.

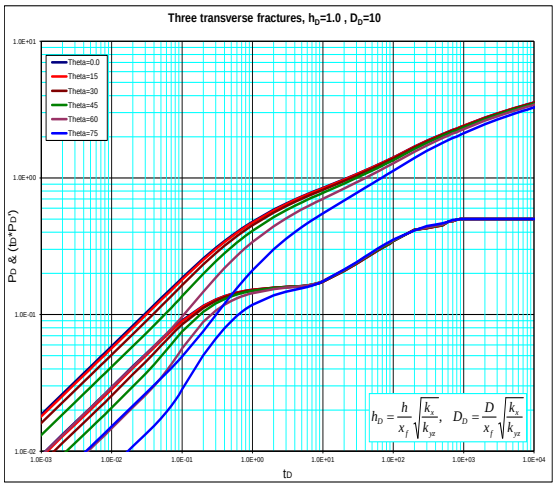

Figure B-39: Pressure and pressure derivative plot.

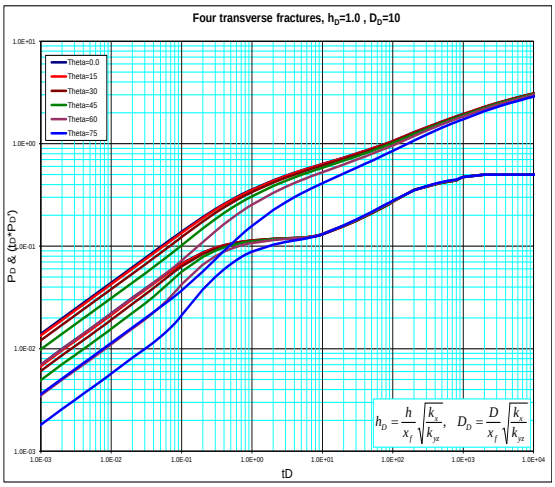

Figure B-40: Pressure and pressure derivative plot.

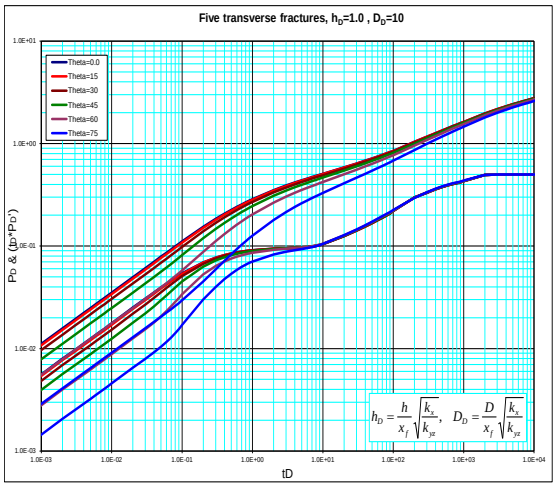

Figure B-41: Pressure and pressure derivative plot.

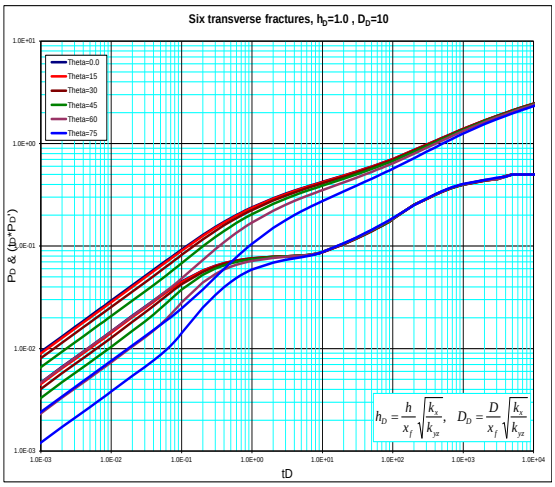

Figure B-42: Pressure and pressure derivative plot.

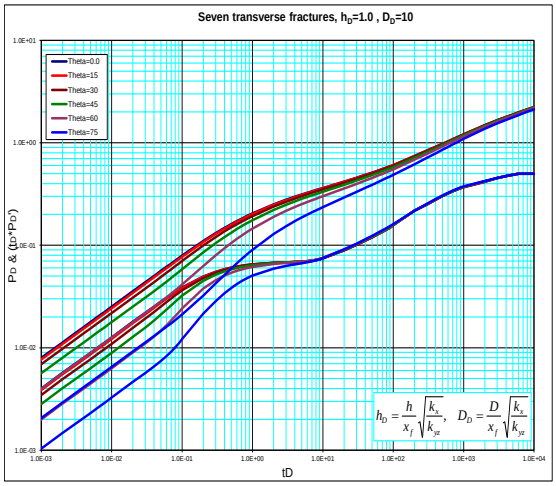

Figure B-43: Pressure and pressure derivative plot.

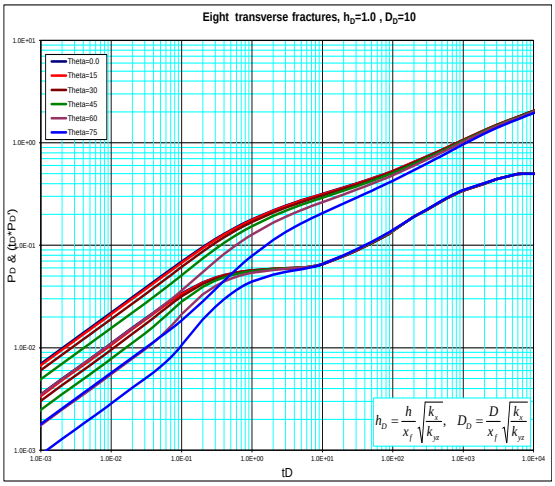

Figure B-44: Pressure and pressure derivative plot.

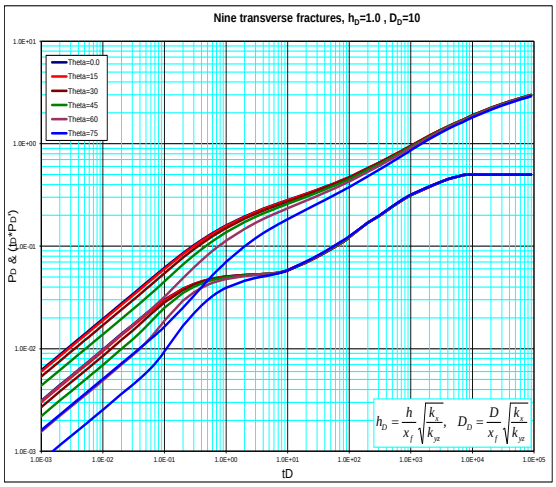

Figure B-45: Pressure and pressure derivative plot.

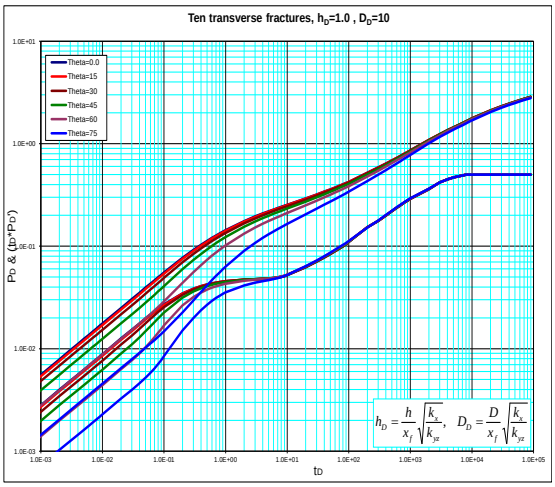

Figure B-46: Pressure and pressure derivative plot.

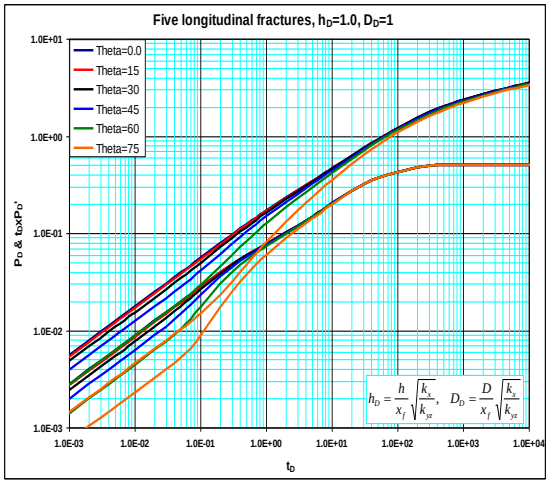

Figure B-47: Pressure and pressure derivative plot.

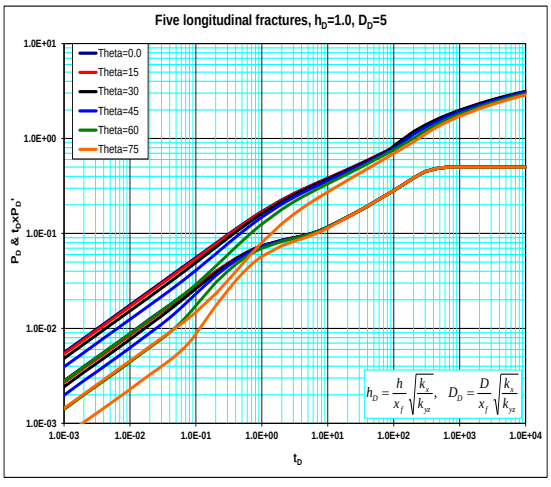

Figure B-48: Pressure and pressure derivative plot.

APPENDIX-C: Plots for partially penetrating multiple inclined hydraulic fractures.

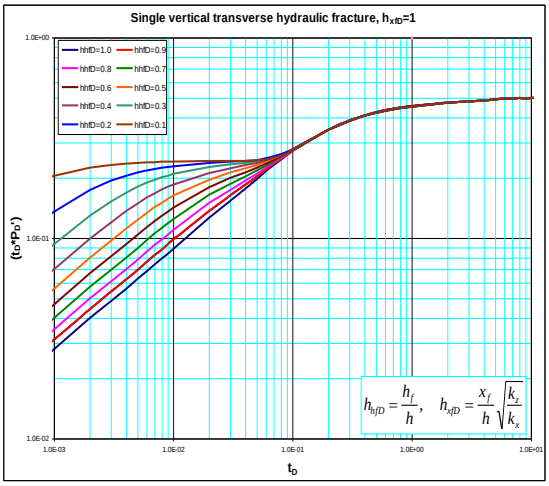

Figure C-1: Pressure and pressure derivative plot.

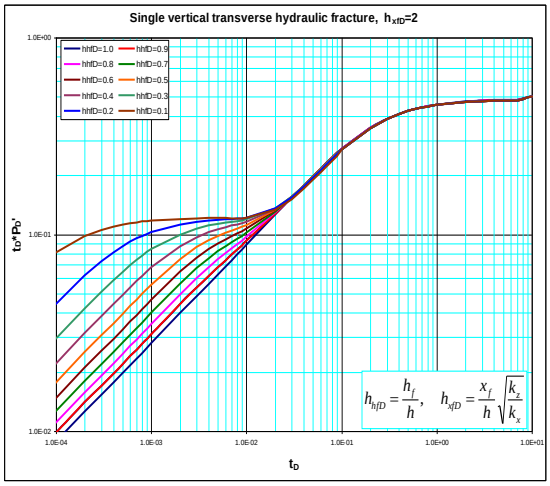

Figure C-2: Pressure and pressure derivative plot.

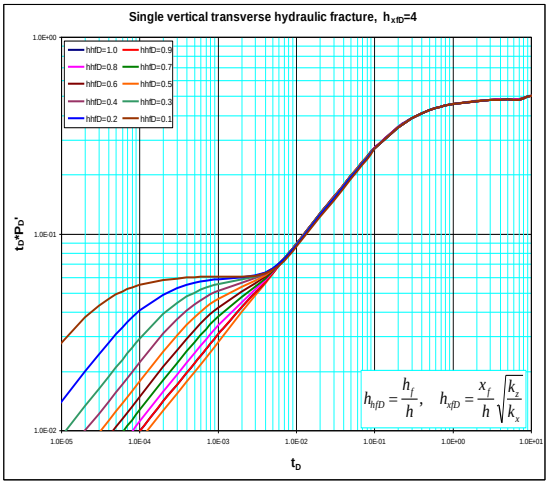

Figure C-3: Pressure and pressure derivative plot.

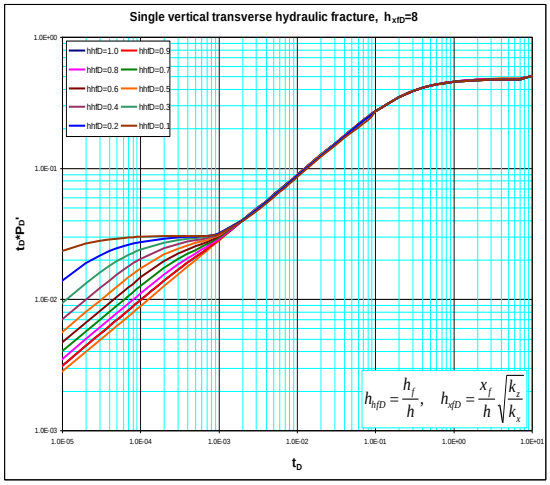

Figure C-4: Pressure and pressure derivative plot.

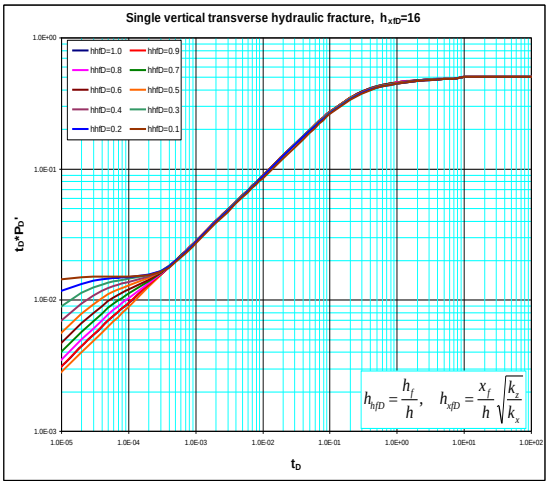

Figure C-5: Pressure and pressure derivative plot.

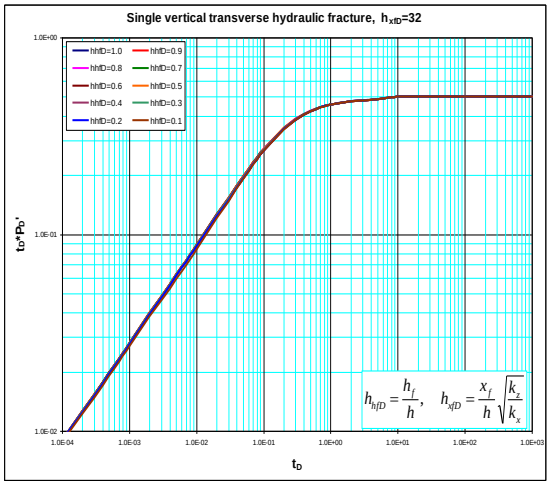

Figure C-6: Pressure and pressure derivative plot.

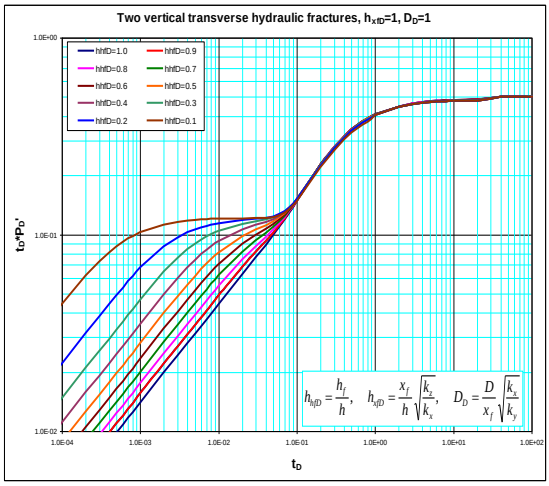

Figure C-7: Pressure and pressure derivative plot.

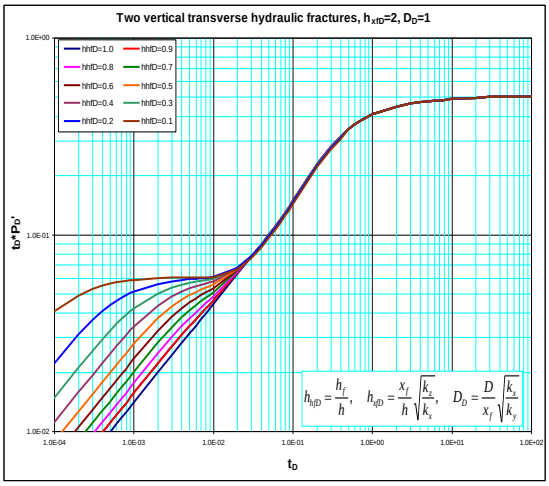

Figure C-8: Pressure and pressure derivative plot.

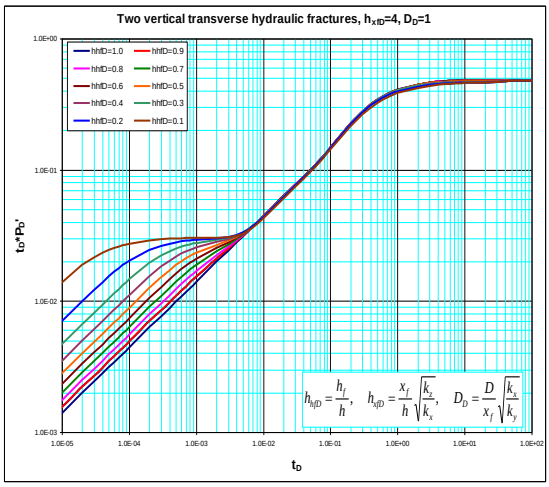

Figure C-9: Pressure and pressure derivative plot.

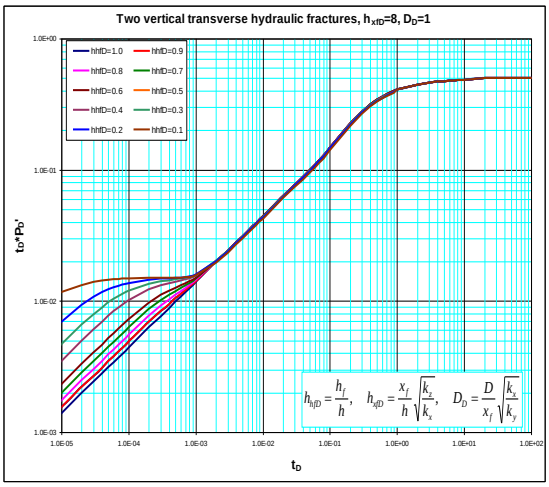

Figure C-10: Pressure and pressure derivative plot.

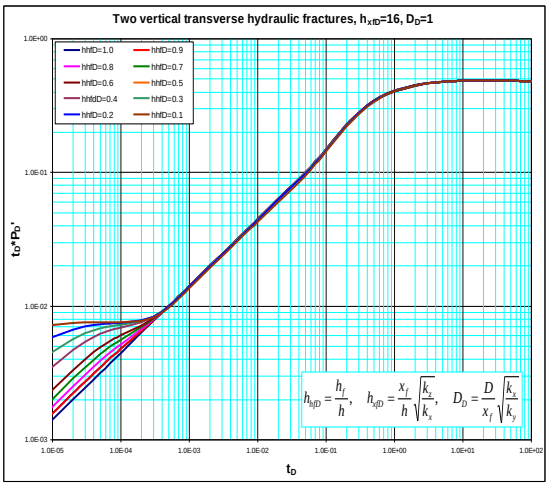

Figure C-11: Pressure and pressure derivative plot.

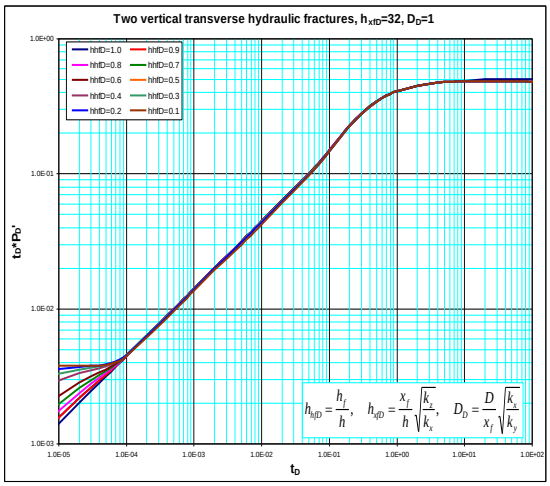

Figure C-12: Pressure and pressure derivative plot.

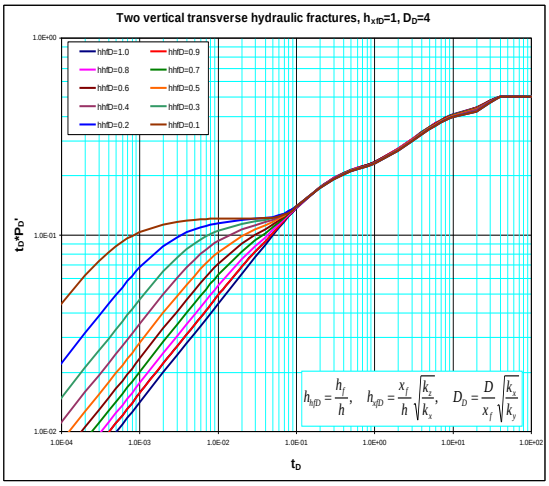

Figure C-13: Pressure and pressure derivative plot.

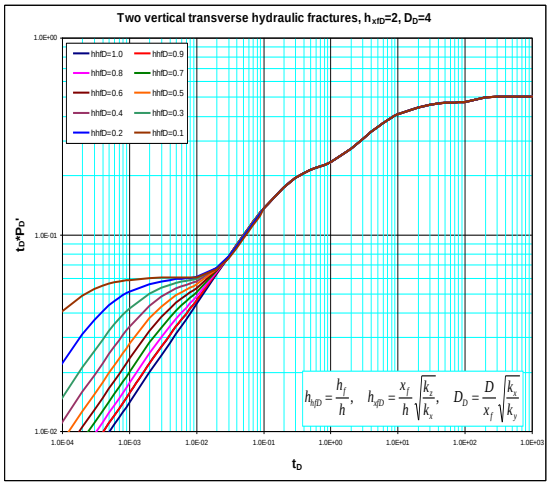

Figure C-14: Pressure and pressure derivative plot.

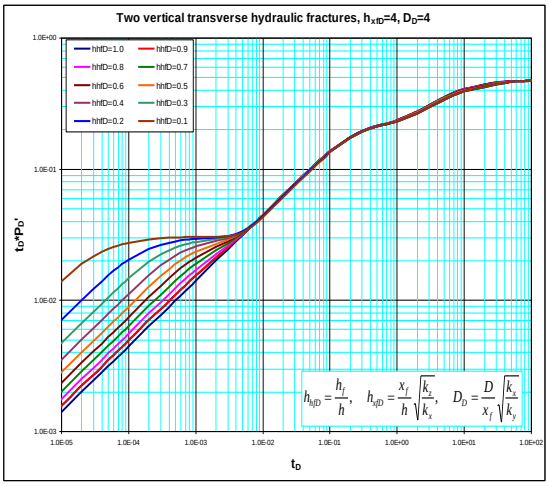

Figure C-15: Pressure and pressure derivative plot.

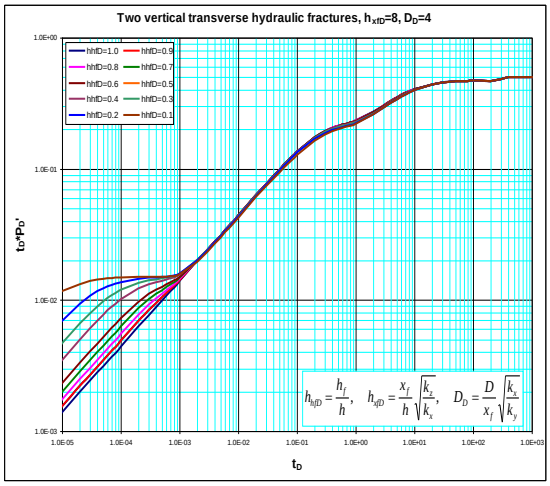

Figure C-16: Pressure and pressure derivative plot.

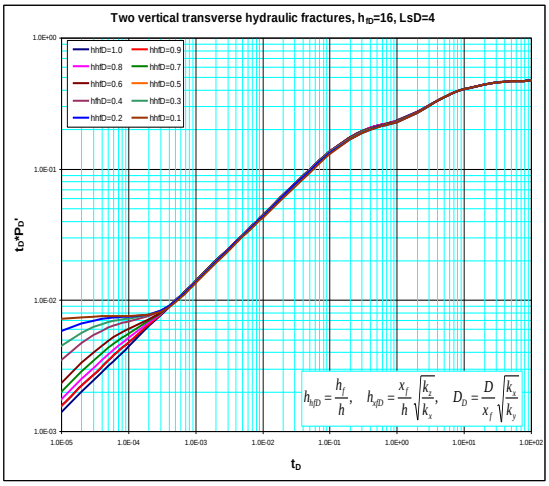

Figure C-17: Pressure and pressure derivative plot.

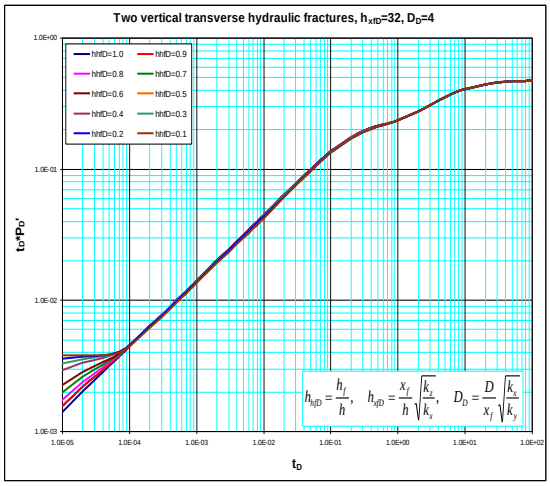

Figure C-18: Pressure and pressure derivative plot.

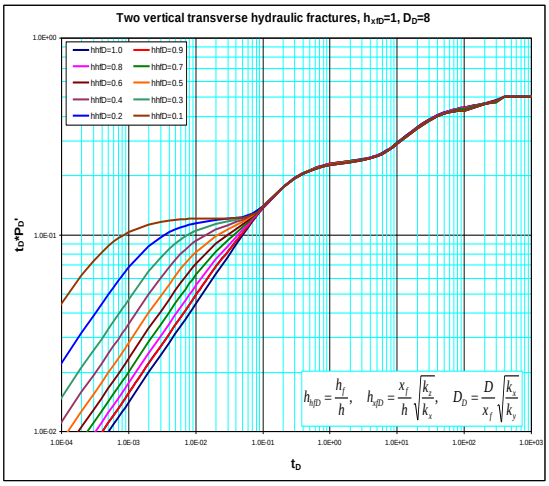

Figure C-19: Pressure and pressure derivative plot.

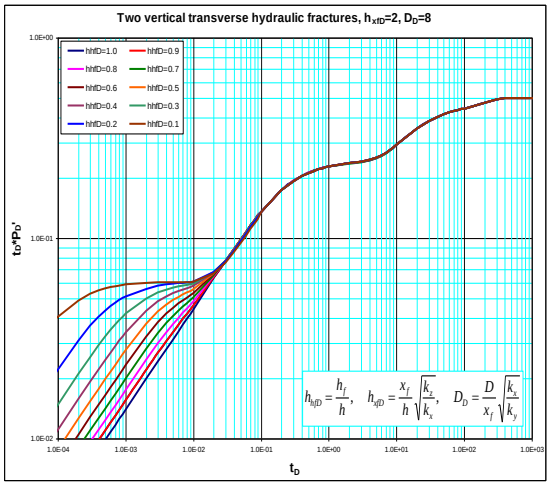

Figure C-20: Pressure and pressure derivative plot.

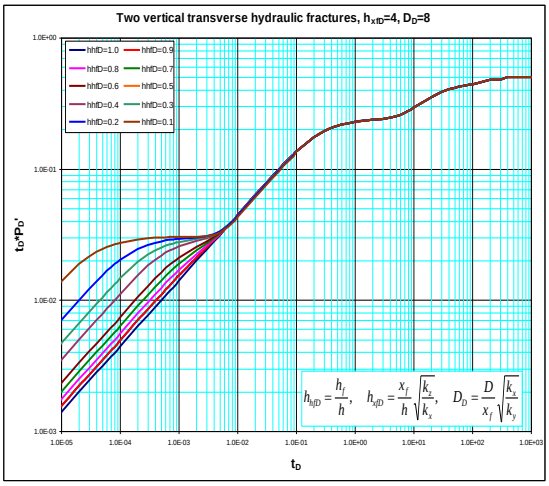

Figure C-21: Pressure and pressure derivative plot.

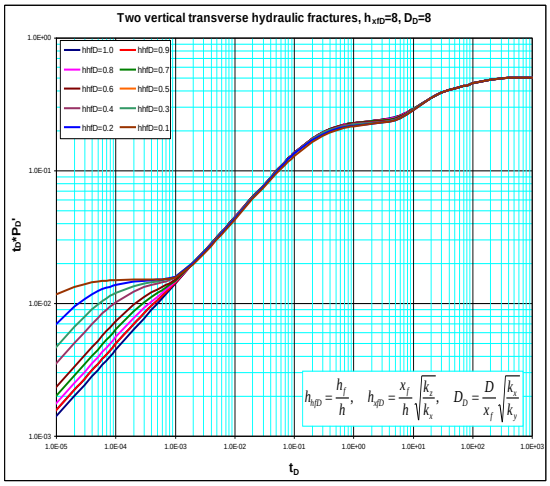

Figure C-22: Pressure and pressure derivative plot.

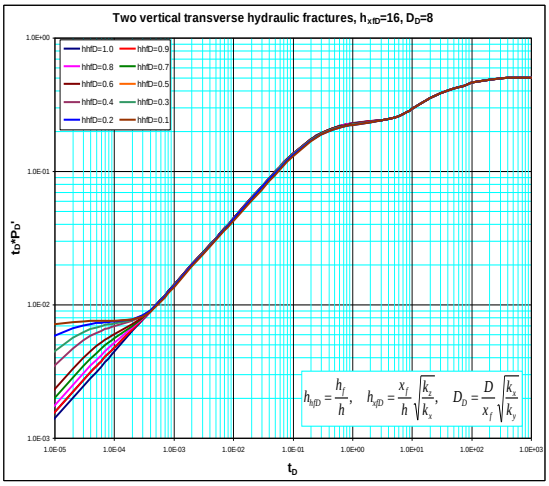

Figure C-23: Pressure and pressure derivative plot.

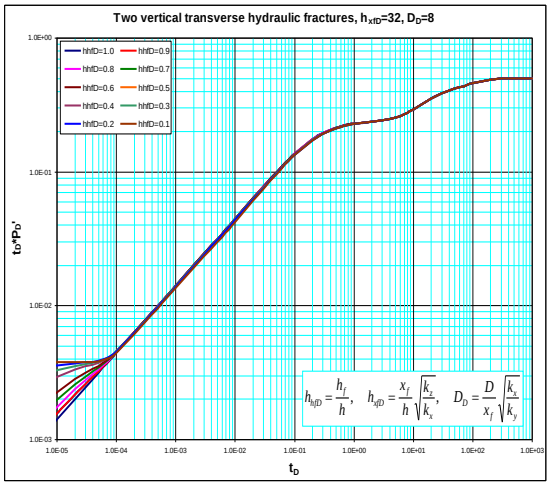

Figure C-24: Pressure and pressure derivative plot.

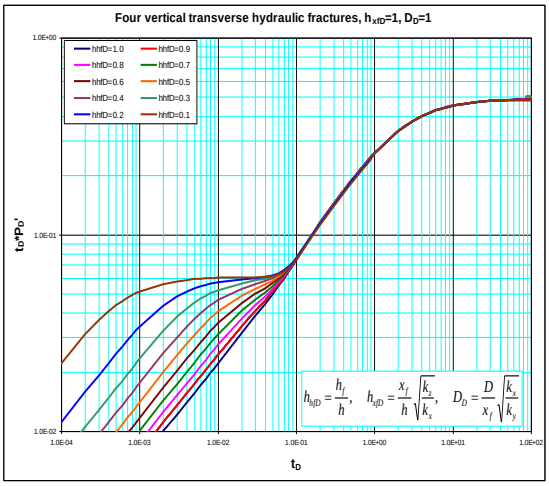

Figure C-25: Pressure and pressure derivative plot.

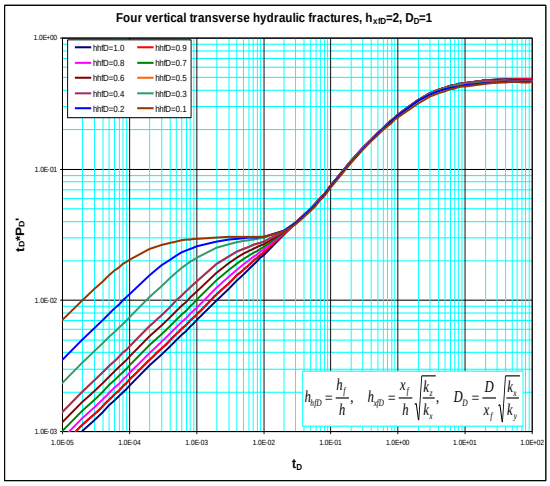

Figure C-26: Pressure and pressure derivative plot.

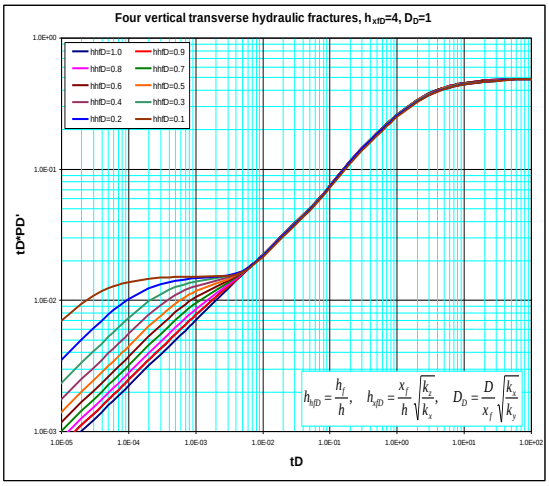

Figure C-27: Pressure and pressure derivative plot.

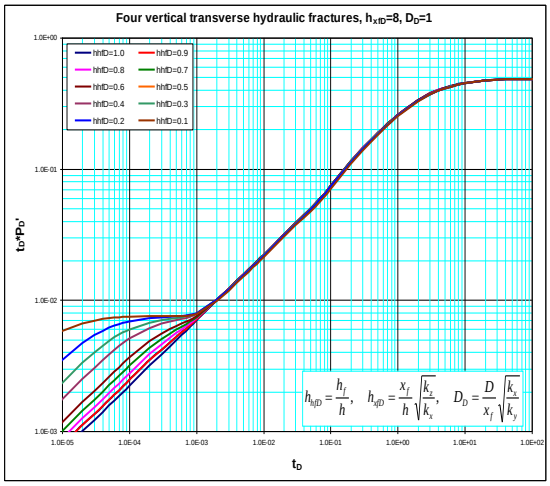

Figure C-28: Pressure and pressure derivative plot.

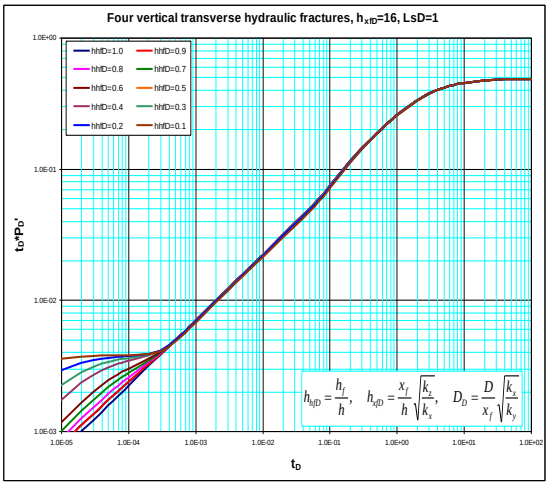

Figure C-29: Pressure and pressure derivative plot.

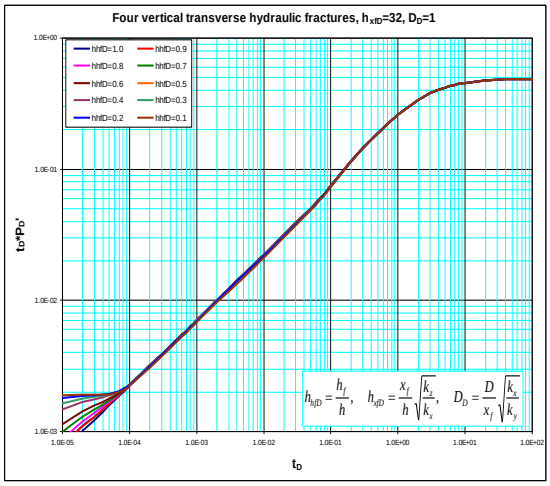

Figure C-30: Pressure and pressure derivative plot.

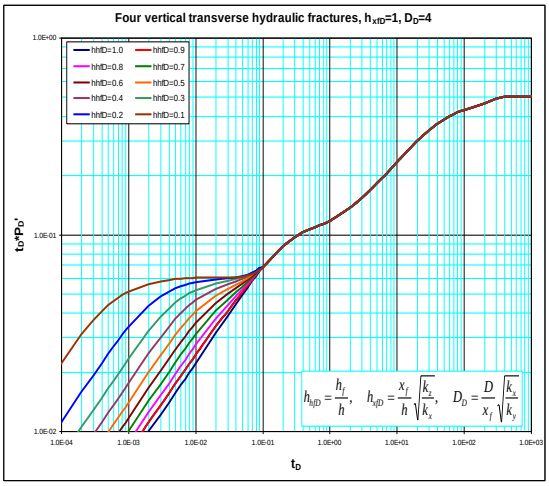

Figure C-31: Pressure and pressure derivative plot.

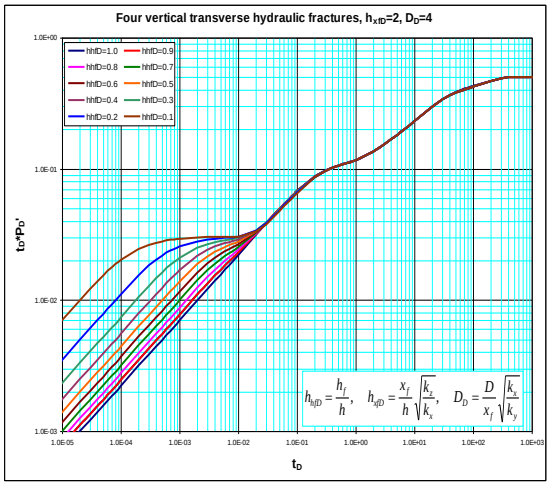

Figure C-32: Pressure and pressure derivative plot.

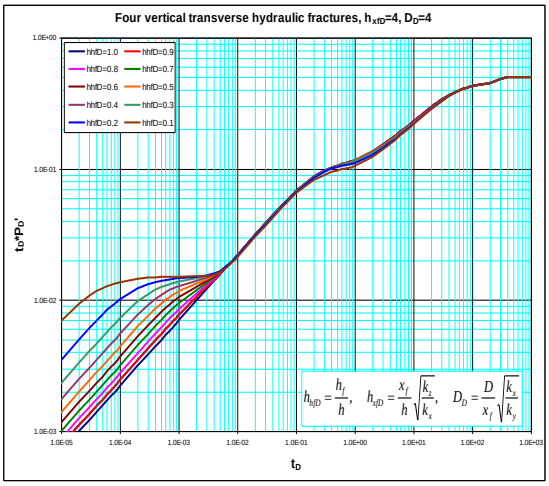

Figure C-33: Pressure and pressure derivative plot.

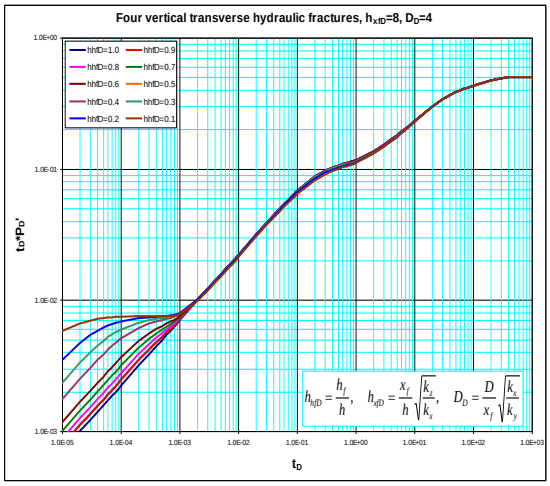

Figure C-34: Pressure and pressure derivative plot.

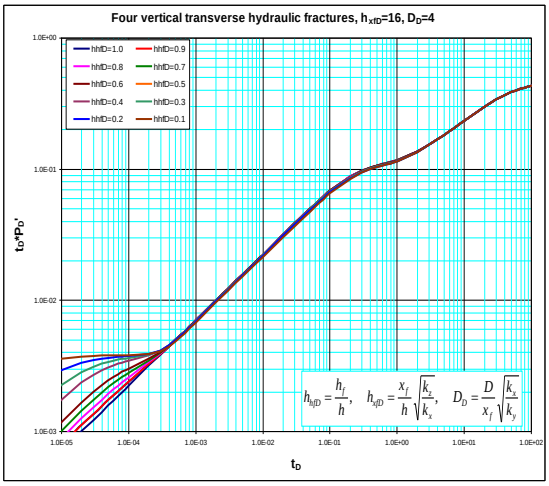

Figure C-35: Pressure and pressure derivative plot.

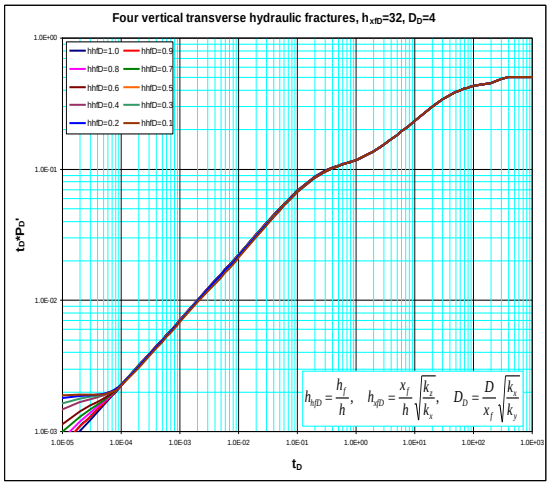

Figure C-36: Pressure and pressure derivative plot.

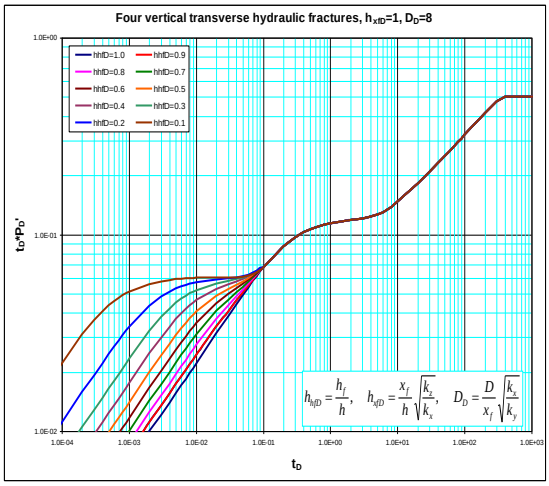

Figure C-37: Pressure and pressure derivative plot.

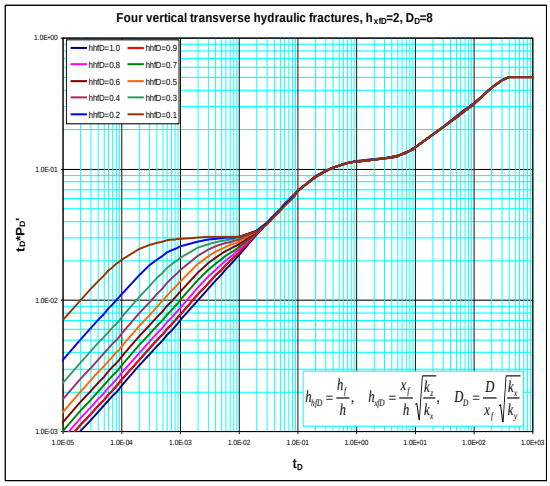

Figure C-38: Pressure and pressure derivative plot.

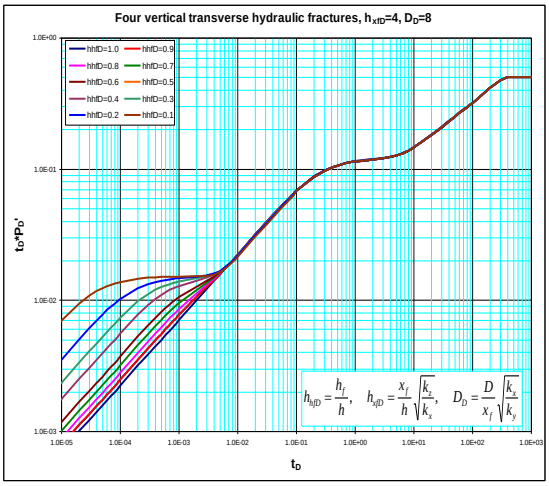

Figure C-39: Pressure and pressure derivative plot.

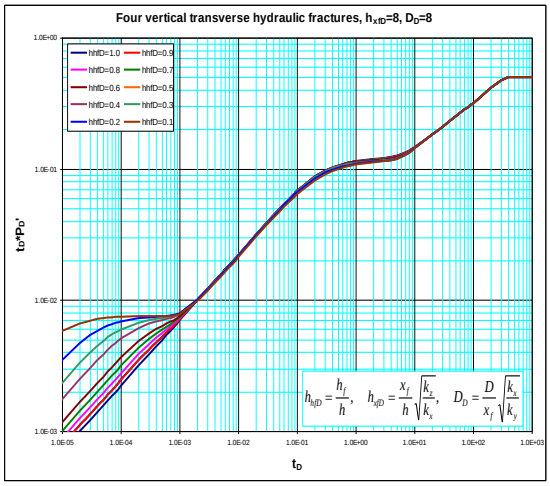

Figure C-40: Pressure and pressure derivative plot.

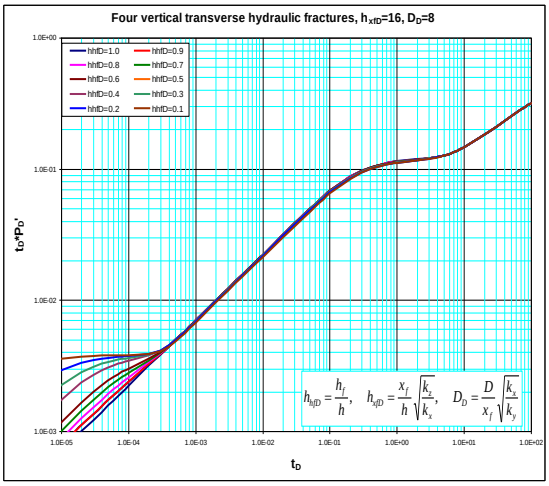

Figure C-41: Pressure and pressure derivative plot.

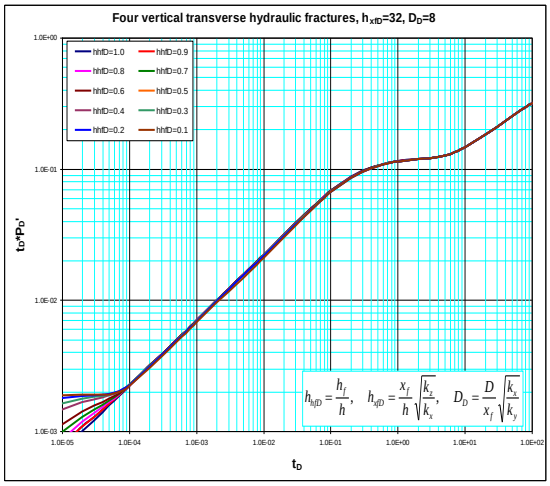

Figure C-42: Pressure and pressure derivative plot.

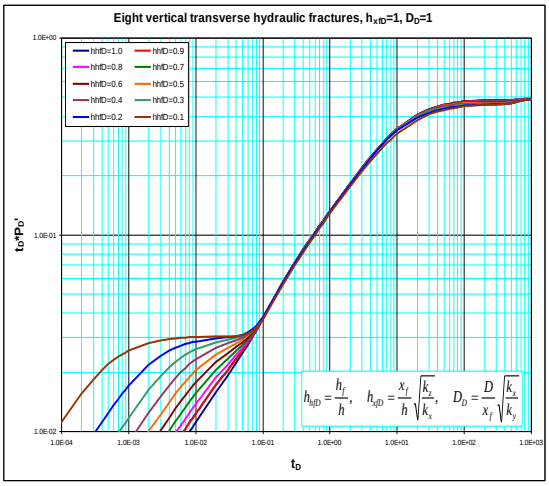

Figure C-43: Pressure and pressure derivative plot.

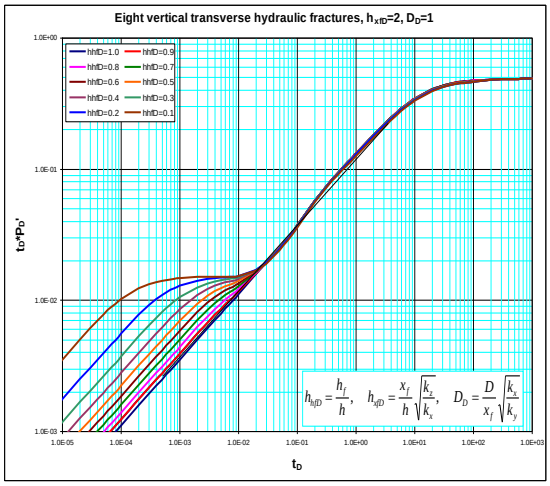

Figure C-44: Pressure and pressure derivative plot.

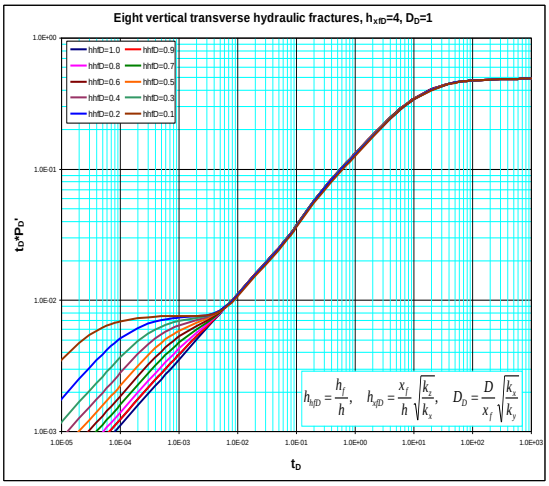

Figure C-45: Pressure and pressure derivative plot.

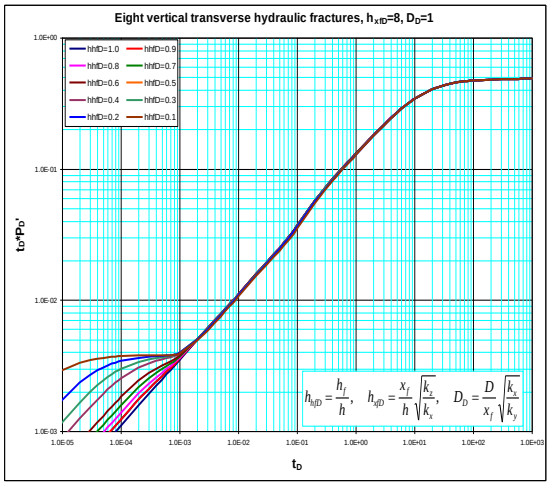

Figure C-46: Pressure and pressure derivative plot.

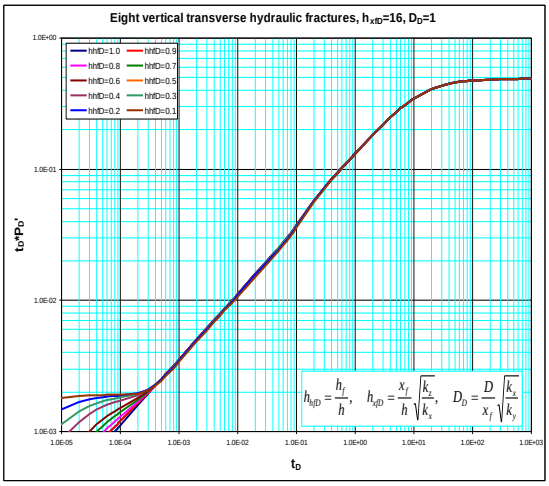

Figure C-47: Pressure and pressure derivative plot.

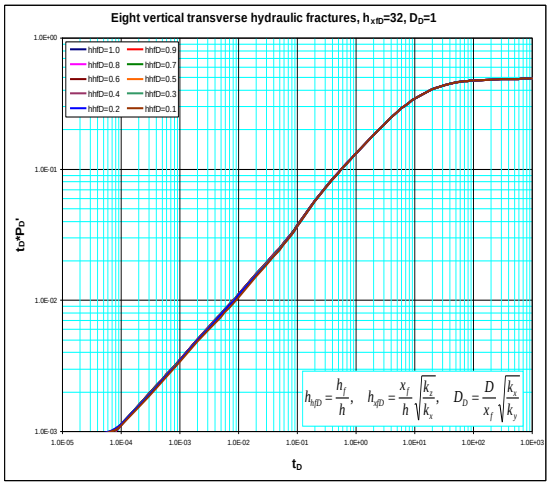

Figure C-48: Pressure and pressure derivative plot.

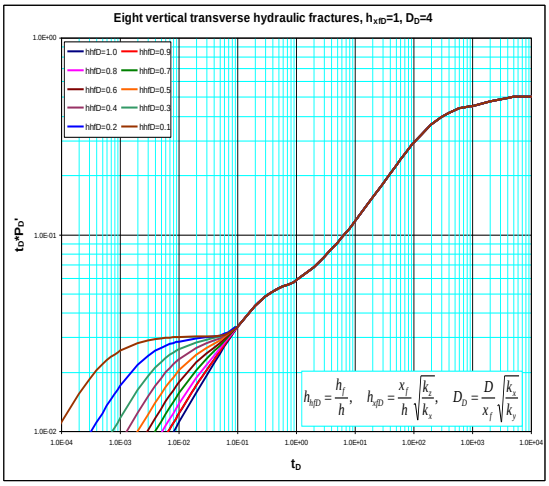

Figure C-49: Pressure and pressure derivative plot.

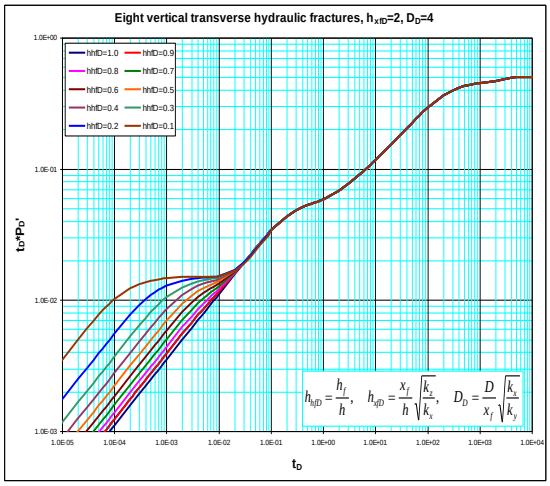

Figure C-50: Pressure and pressure derivative plot.

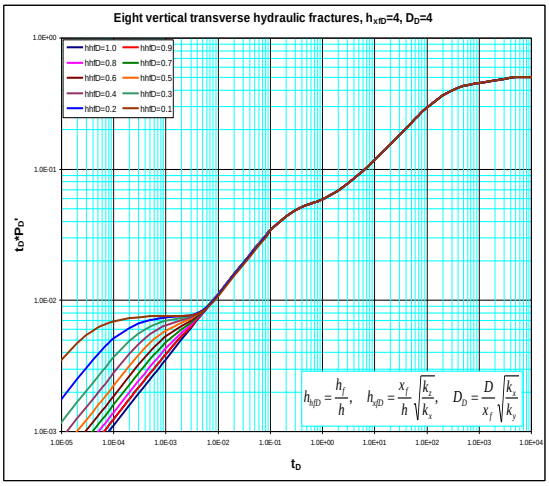

Figure C-51: Pressure and pressure derivative plot.

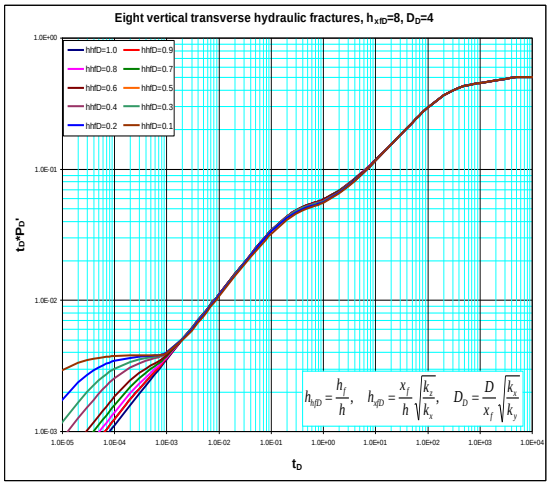

Figure C-52: Pressure and pressure derivative plot.

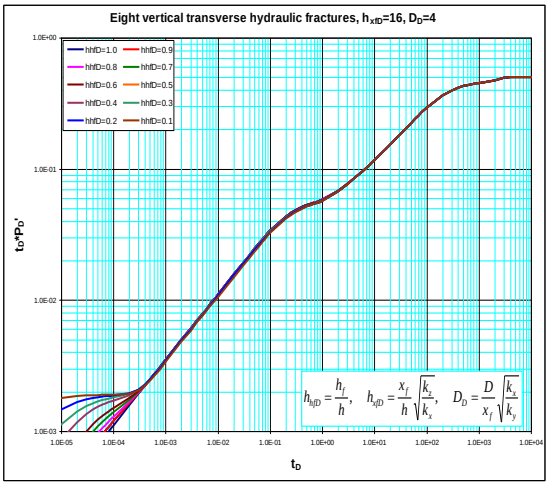

Figure C-53: Pressure and pressure derivative plot.

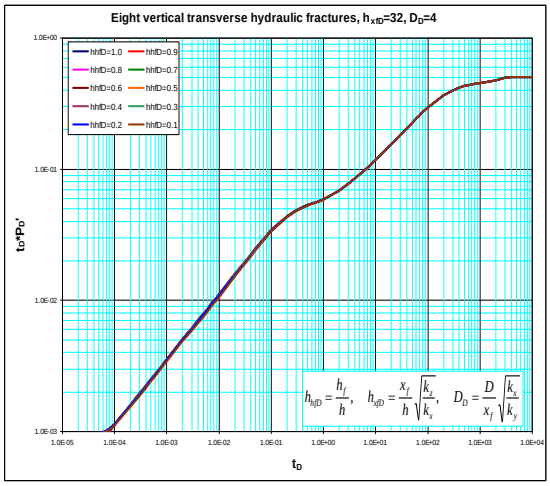

Figure C-54: Pressure and pressure derivative plot.

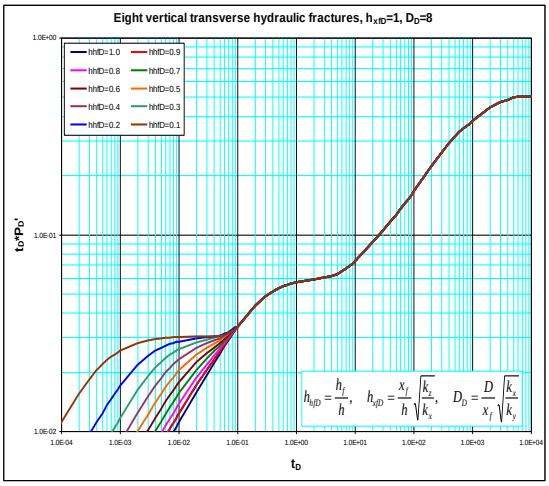

Figure C-55: Pressure and pressure derivative plot.

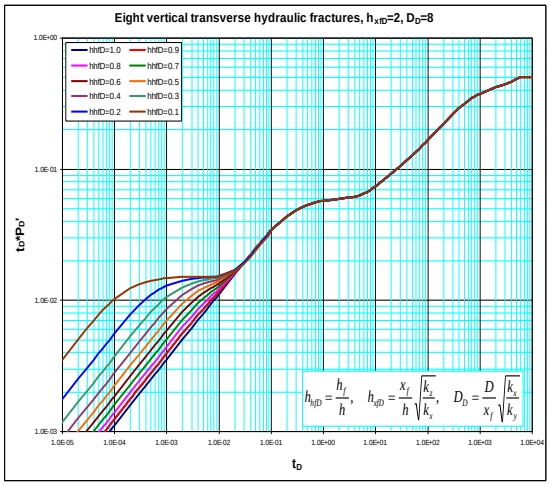

Figure C-56: Pressure and pressure derivative plot.

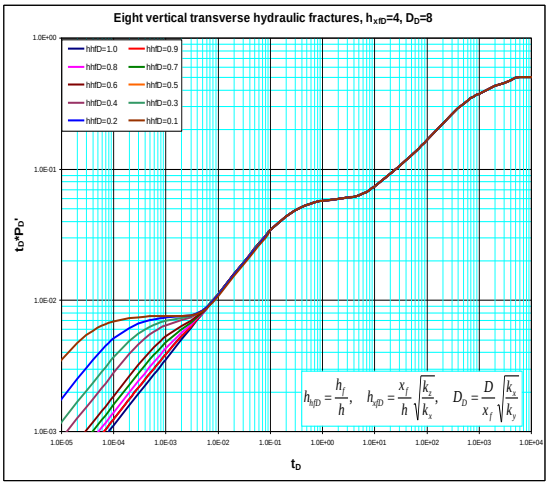

Figure C-57: Pressure and pressure derivative plot.

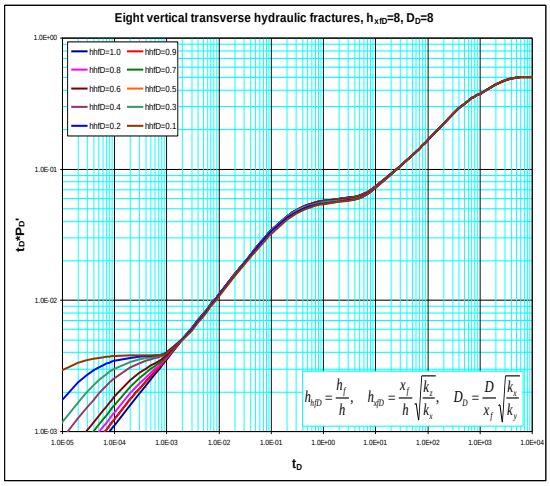

Figure C-58: Pressure and pressure derivative plot.

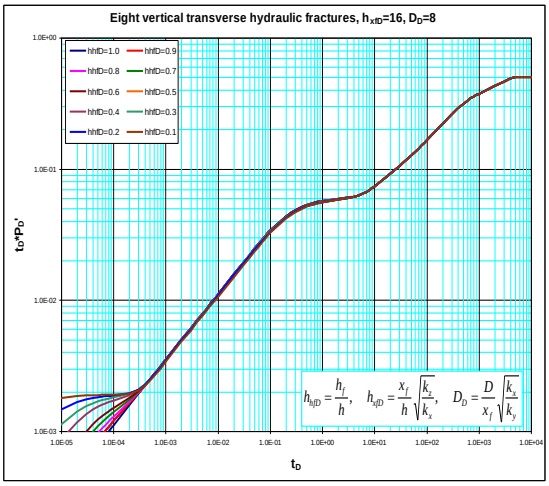

Figure C-59: Pressure and pressure derivative plot.

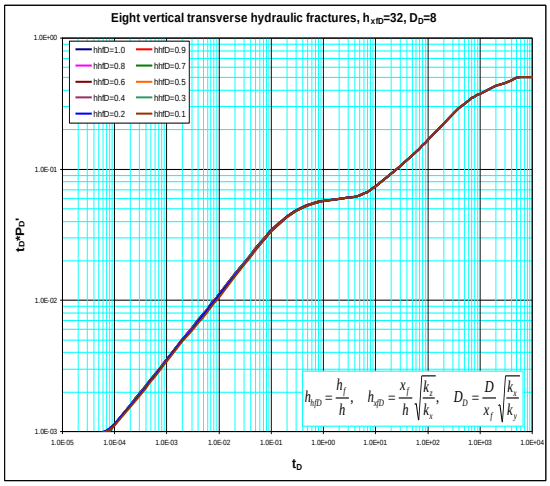

Figure C-60: Pressure and pressure derivative plot.

APPENDIX-D: Pseudo skin factor for multiple inclined hydraulic fractures.

Two Transverse Fractures					
	D_D=1	**D_D=2**	**D_D=5**	**D_D=8**	**D_D=10**
$\theta_v = 0.0$	**-0.620**	**-0.971**	**-1.489**	**-1.556**	**-1.774**
$\theta_v = 15$	**-0.629**	**-0.976**	**-1.492**	**-1.566**	**-1.778**
$\theta_v = 30$	**-0.655**	**-0.994**	**-1.501**	**-1.597**	**-1.793**
$\theta_v = 45$	**-0.706**	**-1.035**	**-1.526**	**-1.658**	**-1.828**
$\theta_v = 60$	**-0.794**	**-1.126**	**-1.589**	**-1.767**	**-1.912**
$\theta_v = 75$	**-1.05**	**-1.291**	**-1.789**	**-2.000**	**-2.134**

Four Transverse Fractures					
	D_D=1	**D_D=2**	**D_D=5**	**D_D=8**	**D_D=10**
$\theta_v = 0.0$	**-1.309**	**-1.876**	**-2.520**	**-2.764**	**-2.994**
$\theta_v = 15$	**-1.312**	**-1.877**	**-2.521**	**-2.768**	**-2.995**
$\theta_v = 30$	**-1.324**	**-1.881**	**-2.526**	**-2.783**	**-3.000**
$\theta_v = 45$	**-1.346**	**-1.889**	**-2.538**	**-2.812**	**-3.012**
$\theta_v = 60$	**-1.381**	**-1.912**	**-2.569**	**-2.866**	**-3.044**
$\theta_v = 75$	**-1.464**	**-1.971**	**-2.666**	**-2.979**	**-3.146**

Six Transverse Fractures					
	D_D=1	**D_D=2**	**D_D=5**	**D_D=8**	**D_D=10**
$\theta_v = 0.0$	**-1.700**	**-2.312**	**-3.029**	**-3.368**	**-3.608**
$\theta_v = 15$	**-1.702**	**-2.313**	**-3.030**	**-3.371**	**-3.608**
$\theta_v = 30$	**-1.709**	**-2.315**	**-3.033**	**-3.381**	**-3.610**
$\theta_v = 45$	**-1.723**	**-2.320**	**-3.041**	**-3.399**	**-3.614**
$\theta_v = 60$	**-1.745**	**-2.335**	**-2.061**	**-3.433**	**-3.627**
$\theta_v = 75$	**-1.793**	**-2.373**	**-3.125**	**-3.507**	**-3.679**

Eight Transverse Fractures					
	D_D=1	**D_D=2**	**D_D=5**	**D_D=8**	**D_D=10**
$\theta_v = 0.0$	**-1.980**	**-2.617**	**-3.360**	**-3.768**	**-4.095**
$\theta_v = 15$	**-1.982**	**-2.620**	**-3.361**	**-3.770**	**-4.095**
$\theta_v = 30$	**-1.987**	**-2.622**	**-3.363**	**-3.776**	**-4.095**
$\theta_v = 45$	**-1.997**	**-2.626**	**-3.369**	**-3.790**	**-4.096**
$\theta_v = 60$	**-2.013**	**-2.637**	**-2.384**	**-3.815**	**-3.099**
$\theta_v = 75$	**-2.046**	**-2.664**	**-3.432**	**-3.868**	**-4.114**

Ten Transverse Fractures					
	D_D=1	**D_D=2**	**D_D=5**	**D_D=8**	**D_D=10**
$\theta_v = 0.0$	**-2.195**	**-2.881**	**-3.733**	**-4.048**	**-4.394**
$\theta_v = 15$	**-2.196**	**-2.881**	**-3.733**	**-4.049**	**-4.394**
$\theta_v = 30$	**-2.200**	**-2.882**	**-3.733**	**-4.054**	**-4.394**
$\theta_v = 45$	**-2.209**	**-2.883**	**-3.734**	**-4.064**	**-4.395**
$\theta_v = 60$	**-2.221**	**-2.887**	**-3.737**	**-4.085**	**-4.396**
$\theta_v = 75$	**-2.246**	**-2.903**	**-3.750**	**-4.127**	**-4.405**

Five Semi-Transverse Fractures, D_D=1			
	$\theta_v = 0.0$	$\theta_v = 30$	$\theta_v = 60$
$\theta_h = 15$	**-1.255**	**-1.390**	**-1.432**
$\theta_h = 30$	**-1.343**	**-1.424**	**-1.463**
$\theta_h = 45$	**-1.411**	**-1.464**	**-1.500**
$\theta_h = 60$	**-1.456**	**-1.498**	**-1.531**
$\theta_h = 75$	**-1.471**	**-1.519**	**-1.551**
$\theta_h = 90$	**-1.490**	**-1.527**	**-1.558**

Five Semi-Transverse Fractures, D_D=5			
	$\theta_v = 0.0$	$\theta_v = 30$	$\theta_v = 60$
$\theta_h = 15$	**-2.794**	**-2.798**	**-2.820**
$\theta_h = 30$	**-2.802**	**-2.805**	**-2.827**
$\theta_h = 45$	**-2.811**	**-2.814**	**-2.836**
$\theta_h = 60$	**-2.820**	**-2.823**	**-2.844**
$\theta_h = 75$	**-2.827**	**-2.830**	**-2.850**
$\theta_h = 90$	**-2.829**	**-2.832**	**-2.852**

Five Longitudinal Fractures		
	D_D=1	D_D=5
$\theta_v = 0.0$	**-2.507**	**-2.870**
$\theta_v = 15$	**-2.508**	**-2.897**
$\theta_v = 30$	**-2.511**	**-2.905**
$\theta_v = 45$	**-2.551**	**-2.948**
$\theta_v = 60$	**-2.587**	**-3.048**
$\theta_v = 75$	**-2.664**	**-3.142**

APPENDIX-E Pseudo skin factor for partially penetrating hydraulic fractures.

Single vertical fractures						
H_{hfD}	**h_{xfD}=1**	**h_{xfD}=2**	**h_{xfD}=4**	**h_{xfD}=8**	**h_{xfD}=16**	**h_{xfD}=32**
0.0	-0.01804	-0.01804	-0.01804	-0.01804	-0.01804	-0.01804
0.1	0.017739	-0.00137	-0.01044	-0.01734	-0.01804	-0.01804
0.2	0.060897	0.018669	-0.00156	-0.01655	-0.01804	-0.01804
0.3	0.112727	0.042644	0.008382	-0.01569	-0.01804	-0.01804
0.4	0.175179	0.071546	0.019082	-0.01482	-0.01804	-0.01804
0.5	0.251176	0.106756	0.030047	-0.01398	-0.01804	-0.01804
0.6	0.345206	0.149289	0.040626	-0.01321	-0.01804	-0.01804
0.7	0.466256	0.1978	0.050048	-0.01256	-0.01804	-0.01804
0.8	0.632365	0.246128	0.057515	-0.01207	-0.01804	-0.01804
0.9	0.83231	0.283126	0.062322	-0.01177	-0.01804	-0.01804

Two vertical fractures, L_D=1						
H_{hfD}	**h_{xfD}=1**	**h_{xfD}=2**	**h_{xfD}=4**	**h_{xfD}=8**	**h_{xfD}=16**	**h_{xfD}=32**
0.0	-0.58441	-0.63443	-0.63443	-0.63443	-0.63443	-0.63443
0.1	-0.56756	-0.6344	-0.6344	-0.6344	-0.6344	-0.6344
0.2	-0.54732	-0.63437	-0.63437	-0.63437	-0.63437	-0.63437
0.3	-0.52314	-0.63434	-0.63434	-0.63434	-0.63434	-0.63434
0.4	-0.49407	-0.6343	-0.6343	-0.6343	-0.6343	-0.6343
0.5	-0.4586	-0.63427	-0.63427	-0.63427	-0.63427	-0.63427
0.6	-0.41527	-0.63424	-0.63424	-0.63424	-0.63424	-0.63424
0.7	-0.36473	-0.63421	-0.63421	-0.63421	-0.63421	-0.63421
0.8	-0.313	-0.6342	-0.6342	-0.6342	-0.6342	-0.6342
0.9	-0.27247	-0.63418	-0.63418	-0.63418	-0.63418	-0.63418

Two vertical fractures, L_D=8						
H_{hfD}	**h_{xfD}=1**	**h_{xfD}=2**	**h_{xfD}=4**	**h_{xfD}=8**	**h_{xfD}=16**	**h_{xfD}=32**
0.0	-1.59554	-1.59554	-1.59554	-1.59554	-1.59554	-1.59554
0.1	-1.58661	-1.59551	-1.59551	-1.59551	-1.59551	-1.59551
0.2	-1.57643	-1.59548	-1.59548	-1.59548	-1.59548	-1.59548
0.3	-1.56546	-1.59545	-1.59545	-1.59545	-1.59545	-1.59545
0.4	-1.55425	-1.59542	-1.59542	-1.59542	-1.59542	-1.59542
0.5	-1.5434	-1.59538	-1.59538	-1.59538	-1.59538	-1.59538
0.6	-1.53349	-1.59535	-1.59535	-1.59535	-1.59535	-1.59535
0.7	-1.52511	-1.59533	-1.59533	-1.59533	-1.59533	-1.59533
0.8	-1.51873	-1.59531	-1.59531	-1.59531	-1.59531	-1.59531
0.9	-1.51474	-1.5953	-1.5953	-1.5953	-1.5953	-1.5953

Four vertical fractures, L_D=1						
H_{hfD}	**h_{xfD}=1**	**h_{xfD}=2**	**h_{xfD}=4**	**h_{xfD}=8**	**h_{xfD}=16**	**h_{xfD}=32**
0.0	-1.27819	-1.27819	-1.27819	-1.27819	-1.27819	-1.27819
0.1	-1.27372	-1.27818	-1.27819	-1.27819	-1.27819	-1.27819
0.2	-1.26862	-1.27816	-1.27819	-1.27819	-1.27819	-1.27819
0.3	-1.26313	-1.27814	-1.27819	-1.27819	-1.27819	-1.27819
0.4	-1.25752	-1.27813	-1.27819	-1.27819	-1.27819	-1.27819
0.5	-1.25209	-1.27811	-1.27819	-1.27819	-1.27819	-1.27819
0.6	-1.24713	-1.27811	-1.27819	-1.27819	-1.27819	-1.27819
0.7	-1.24293	-1.27808	-1.27819	-1.27819	-1.27819	-1.27819
0.8	-1.23974	-1.27807	-1.27819	-1.27819	-1.27819	-1.27819
0.9	-1.23775	-1.27807	-1.27819	-1.27819	-1.27819	-1.27819

Four vertical fractures, L_D=8						
H_{hfD}	**h_{xfD}=1**	**h_{xfD}=2**	**h_{xfD}=4**	**h_{xfD}=8**	**h_{xfD}=16**	**h_{xfD}=32**
0.0	-2.70685	-2.70685	-2.70685	-2.70685	-2.70685	-2.70685
0.1	-2.70238	-2.70683	-2.70685	-2.70685	-2.70685	-2.70685
0.2	-2.69729	-2.70682	-2.70685	-2.70685	-2.70685	-2.70685
0.3	-2.69181	-2.7068	-2.70685	-2.70685	-2.70685	-2.70685
0.4	-2.6862	-2.70678	-2.70685	-2.70685	-2.70685	-2.70685
0.5	-2.68077	-2.70677	-2.70685	-2.70685	-2.70685	-2.70685
0.6	-2.67582	-2.70675	-2.70685	-2.70685	-2.70685	-2.70685
0.7	-2.67163	-2.70674	-2.70685	-2.70685	-2.70685	-2.70685
0.8	-2.66844	-2.70673	-2.70685	-2.70685	-2.70685	-2.70685
0.9	-2.66645	-2.70673	-2.70685	-2.70685	-2.70685	-2.70685

Eight vertical fractures, L_D=1						
H_{hfD}	**h_{xfD}=1**	**h_{xfD}=2**	**h_{xfD}=4**	**h_{xfD}=8**	**h_{xfD}=16**	**h_{xfD}=32**
0.0	-2.03185	-2.03185	-2.03185	-2.03185	-2.03185	-2.03185
0.1	-2.03185	-2.03185	-2.03185	-2.03185	-2.03185	-2.03185
0.2	-2.03185	-2.03185	-2.03185	-2.03185	-2.03185	-2.03185
0.3	-2.03185	-2.03185	-2.03185	-2.03185	-2.03185	-2.03185
0.4	-2.03185	-2.03185	-2.03185	-2.03185	-2.03185	-2.03185
0.5	-2.03185	-2.03185	-2.03185	-2.03185	-2.03185	-2.03185
0.6	-2.03185	-2.03185	-2.03185	-2.03185	-2.03185	-2.03185
0.7	-2.03185	-2.03185	-2.03185	-2.03185	-2.03185	-2.03185
0.8	-2.03185	-2.03185	-2.03185	-2.03185	-2.03185	-2.03185
0.9	-2.03185	-2.03185	-2.03185	-2.03185	-2.03185	-2.03185

Eight vertical fractures, L_D=8						
H_{hfD}	**h_{xfD}=1**	**h_{xfD}=2**	**h_{xfD}=4**	**h_{xfD}=8**	**h_{xfD}=16**	**h_{xfD}=32**
0.0	-3.81424	-3.81424	-3.81424	-3.81424	-3.81424	-3.81424
0.1	-3.81424	-3.81424	-3.81424	-3.81424	-3.81424	-3.81424
0.2	-3.81424	-3.81424	-3.81424	-3.81424	-3.81424	-3.81424
0.3	-3.81424	-3.81424	-3.81424	-3.81424	-3.81424	-3.81424
0.4	-3.81424	-3.81424	-3.81424	-3.81424	-3.81424	-3.81424
0.5	-3.81424	-3.81424	-3.81424	-3.81424	-3.81424	-3.81424
0.6	-3.81424	-3.81424	-3.81424	-3.81424	-3.81424	-3.81424
0.7	-3.81424	-3.81424	-3.81424	-3.81424	-3.81424	-3.81424
0.8	-3.81424	-3.81424	-3.81424	-3.81424	-3.81424	-3.81424
0.9	-3.81424	-3.81424	-3.81424	-3.81424	-3.81424	-3.81424

Two inclined fractures, L_D=1				**Two inclined fractures, L_D=8**		
	h_{xfD}=1, h_{hfD}=1	**h_{xfD}=10, h_{hfD}=1**	**h_{xfD}=10, h_{hfD}=0.5**	**h_{xfD}=1, h_{hfD}=1**	**h_{xfD}=10, h_{hfD}=1**	**h_{xfD}=10, h_{hfD}=0.5**
$\theta_v = 0.0$	-0.605	-0.605	-0.605	-1.542	-1.618	-1.618
$\theta_v = 15$	-0.600	-0.605	-0.605	-1.537	-1.618	-1.618
$\theta_v = 30$	-0.583	-0.605	-0.605	-1.520	-1.618	-1.618
$\theta_v = 45$	-0.550	-0.605	-0.605	-1.487	-1.618	-1.618
$\theta_v = 60$	-0.498	-0.605	-0.605	-1.436	-1.618	-1.618
$\theta_v = 75$	-0.439	-0.605	-0.605	-1.376	-1.618	-1.618

APPENDIX-F: Synthetic data for Examples.

Example 3-1

t,hrs	Pwf, psi	t,hrs	Pwf, psi	t,hrs	Pwf, psi	t,hrs	Pwf, psi
0.0000	5000.00	0.512	4939.59	102.39	4807.26	15358.36	4529.54
0.0017	4965.95	0.683	4937.47	119.45	4799.61	17064.85	4523.58
0.0034	4962.89	0.853	4935.60	136.52	4792.86	34129.69	4484.44
0.0051	4961.10	1.024	4933.92	153.58	4786.84	51194.54	4461.54
0.0068	4959.83	1.195	4932.36	170.65	4781.39	68259.39	4445.29
0.0085	4958.85	1.365	4930.92	341.30	4744.54	85324.23	4432.68
0.0102	4958.04	1.536	4929.57	511.95	4721.64		
0.0119	4957.36	1.706	4928.29	682.59	4705.39		
0.0137	4956.77	3.413	4918.13	853.24	4692.78		
0.0154	4956.25	5.119	4910.70	1023.89	4682.49		
0.0171	4955.79	6.826	4904.71	1194.54	4673.78		
0.0341	4952.73	8.532	4899.61	1365.19	4666.24		
0.0512	4950.94	10.239	4895.13	1535.84	4659.59		
0.0683	4949.67	11.945	4891.08	1706.48	4653.63		
0.0853	4948.69	13.652	4887.38	3412.97	4614.49		
0.1024	4947.88	15.358	4883.95	5119.45	4591.59		
0.1195	4947.20	17.065	4880.75	6825.94	4575.34		
0.1365	4946.61	34.130	4856.39	8532.42	4562.73		
0.1536	4946.08	51.195	4839.57	10238.91	4552.44		
0.1706	4945.60	68.259	4826.64	11945.39	4543.73		
0.3413	4942.12	85.324	4816.12	13651.88	4536.19		

Example 3-2

t,hrs	Pwf, psi	t,hrs	Pwf, psi	t,hrs	Pwf, psi	t,hrs	Pwf, psi
0.0000	5000.00	0.273	4984.05	54.61	4870.45	8191.13	4469.33
0.0014	4998.96	0.410	4980.45	68.26	4860.52	9556.31	4454.52
0.0027	4998.49	0.546	4977.42	81.91	4851.74	10921.50	4441.69
0.0041	4998.13	0.683	4974.77	95.56	4843.82	12286.69	4430.37
0.0055	4997.83	0.819	4972.41	109.22	4836.57	13651.88	4420.25
0.0068	4997.56	0.956	4970.26	122.87	4829.88	27303.75	4353.66
0.0082	4997.32	1.092	4968.30	136.52	4823.65	40955.63	4314.70
0.0096	4997.10	1.229	4966.49	273.04	4777.17	54607.51	4287.06
0.0109	4996.89	1.365	4964.80	409.56	4746.07	68259.39	4265.63
0.0123	4996.69	2.730	4952.38	546.08	4722.59	81911.26	4248.11
0.0137	4996.51	4.096	4944.23	682.59	4703.70	95563.14	4233.30
0.0273	4995.02	5.461	4938.13	819.11	4687.88	109215.02	4220.47
0.0410	4993.88	6.826	4933.22	955.63	4674.27		
0.0546	4992.92	8.191	4929.07	1092.15	4662.31		
0.0683	4992.07	9.556	4925.45	1228.67	4651.64		
0.0819	4991.31	10.922	4922.22	1365.19	4642.00		
0.0956	4990.60	12.287	4919.28	2730.38	4576.38		
0.1092	4989.95	13.652	4916.57	4095.56	4535.92		
0.1229	4989.33	27.304	4896.34	5460.75	4508.28		
0.1365	4988.75	40.956	4882.03	6825.94	4486.84		

Example 3-3

t,hrs	Pwf, psi	t,hrs	Pwf, psi	t,hrs	Pwf, psi	t,hrs	Pwf, psi	t,hrs	Pwf, psi
0.0000	5000.00	0.039	4969.10	2.12	4949.15	57.64	4885.13	3943.88	4643.11
0.0006	4982.55	0.042	4968.86	2.43	4947.87	60.68	4883.14	4247.25	4638.33
0.0009	4981.25	0.046	4968.64	2.73	4946.70	91.01	4866.05	4550.63	4633.88
0.0012	4980.32	0.049	4968.43	3.03	4945.63	121.35	4852.56	4854.00	4629.73
0.0015	4979.60	0.052	4968.24	3.34	4944.63	151.69	4841.39	5157.38	4625.82
0.0018	4979.01	0.055	4968.05	3.64	4943.69	182.03	4831.86	5460.75	4622.13
0.0021	4978.52	0.058	4967.88	3.94	4942.81	212.36	4823.55	5764.13	4618.65
0.0024	4978.09	0.061	4967.71	4.25	4941.98	242.70	4816.17	6067.50	4615.34
0.0027	4977.71	0.091	4966.41	4.55	4941.19	273.04	4809.55	9101.25	4589.21
0.0030	4977.37	0.121	4965.47	4.85	4940.43	303.38	4803.53	12135.00	4570.67
0.0033	4977.06	0.152	4964.65	5.16	4939.70	333.71	4798.01	15168.75	4556.29
0.0036	4976.78	0.182	4963.99	5.46	4939.01	364.05	4792.92	18202.50	4544.54
0.0039	4976.52	0.212	4963.43	5.76	4938.33	394.39	4788.19	21236.25	4534.60
0.0042	4976.28	0.243	4962.92	6.07	4937.68	424.73	4783.77	24270.00	4526.00
0.0046	4976.06	0.273	4962.46	9.10	4932.05	455.06	4779.63	27303.75	4518.41
0.0049	4975.85	0.303	4962.03	12.14	4927.36	485.40	4775.73	30337.50	4511.62
0.0052	4975.66	0.334	4961.62	15.17	4923.21	515.74	4772.04	33371.26	4505.47
0.0055	4975.47	0.364	4961.24	18.20	4919.43	546.08	4768.55	36405.01	4499.87
0.0058	4975.30	0.394	4960.87	21.24	4915.92	576.41	4765.22	39438.76	4494.71
0.0061	4975.13	0.425	4960.52	24.27	4912.64	606.75	4762.05	42472.51	4489.93
0.0091	4973.83	0.46	4960.18	27.30	4909.54	910.13	4736.47	45506.26	4485.49
0.0121	4972.90	0.49	4959.85	30.34	4906.60	1213.50	4717.74	48540.01	4481.33
0.0152	4972.18	0.52	4959.53	33.37	4903.81	1516.88	4704.69	51573.76	4477.42
0.0182	4971.59	0.55	4959.22	36.41	4901.14	1820.25	4692.94	54607.51	4473.74
0.0212	4971.10	0.58	4958.93	39.44	4898.58	2123.63	4683.00	57641.26	4470.25
0.024	4970.67	0.61	4958.63	42.47	4896.13	2427.00	4674.40	60675.01	4466.95
0.027	4970.29	0.91	4956.07	45.51	4893.77	2730.38	4666.81	91012.51	4440.81
0.030	4969.95	1.21	4953.96	48.54	4891.49	3033.75	4660.02		
0.033	4969.64	1.52	4952.15	51.57	4889.30	3337.13	4653.87		
0.036	4969.36	1.82	4950.56	54.61	4887.18	3640.50	4648.27		

Example 5-1

t,hrs	Pwf, psi	t,hrs	Pwf, psi	t,hrs	Pwf, psi	t,hrs	Pwf, psi	t,hrs	Pwf, psi
0.0000	6000.00	0.046	5976.51	2.29	5821.30	68.81	5439.59	4587.03	4146.90
0.0008	5996.97	0.054	5974.62	3.06	5794.93	76.45	5424.82	5351.54	4066.44
0.0015	5995.71	0.061	5972.87	3.82	5773.24	152.90	5315.11	6116.04	3995.66
0.0023	5994.75	0.069	5971.23	4.59	5754.85	229.35	5238.44	6880.55	3932.50
0.0031	5993.93	0.076	5969.67	5.35	5738.87	305.80	5176.95	7645.05	3883.79
0.0038	5993.22	0.153	5957.10	6.12	5724.76	382.25	5124.56	15290.10	3461.72
0.0046	5992.57	0.229	5947.41	6.88	5712.13	458.70	5078.42	22935.15	3214.82
0.0054	5991.98	0.306	5939.11	7.65	5700.70	535.15	5036.93	30580.20	3039.64
0.0061	5991.42	0.382	5931.65	15.29	5623.06	611.60	4999.03	38225.26	2903.76
0.0069	5990.90	0.459	5924.74	22.94	5576.24	688.05	4964.02	45870.31	2792.74
0.0076	5990.41	0.535	5918.25	30.58	5542.38	764.51	4931.38	53515.36	2698.88
0.0153	5986.44	0.612	5912.09	38.23	5515.50	1529.01	4662.66	61160.41	2617.57
0.0229	5983.39	0.688	5906.23	45.87	5492.92	2293.52	4486.38	68805.46	2545.85
0.0306	5980.82	0.765	5900.62	53.52	5473.22	3058.02	4350.61	76450.51	2481.69
0.0382	5978.55	1.529	5854.86	61.16	5455.61	3822.53	4240.07		

Example 5-2

t,hrs	Pwf, psi	t,hrs	Pwf, psi	t,hrs	Pwf, psi	t,hrs	Pwf, psi	t,hrs	Pwf, psi
0.0000	10000.00	0.0114	9914.60	0.57	9628.89	17.06	8874.51	1137.66	7282.04
0.0002	9988.95	0.0133	9907.90	0.76	9593.99	18.96	8838.68	1327.27	7219.46
0.0004	9984.38	0.0152	9901.74	0.95	9564.35	37.92	8592.78	1516.88	7165.25
0.0006	9980.86	0.0171	9896.03	1.14	9538.27	56.88	8444.23	1706.48	7117.44
0.0008	9977.90	0.0190	9890.70	1.33	9514.78	75.84	8338.78	1896.09	7074.67
0.0009	9975.29	0.0379	9850.93	1.52	9493.31	94.80	8257.49	3792.19	6793.28
0.0011	9972.94	0.0569	9824.44	1.71	9473.43	113.77	8191.51	5688.28	6628.68
0.0013	9970.77	0.0758	9804.54	1.90	9454.86	132.73	8136.07	7584.38	6511.90
0.0015	9968.75	0.0948	9788.56	3.79	9312.07	151.69	8088.34	9480.47	6421.31
0.0017	9966.85	0.1138	9775.14	5.69	9210.44	170.65	8046.53	11376.56	6347.30
0.0019	9965.06	0.1327	9763.52	7.58	9130.30	189.61	8009.40	13272.66	6284.72
0.0038	9950.59	0.1517	9753.20	9.48	9063.94	379.22	7728.02	15168.75	6230.52
0.0057	9939.49	0.1706	9743.88	11.38	9007.27	568.83	7563.42	17064.85	6182.70
0.0076	9930.15	0.1896	9735.34	13.27	8957.83	758.44	7446.63	18960.94	6139.93
0.0095	9921.95	0.3792	9672.57	15.17	8913.95	948.05	7356.05	37921.88	5858.55

Example 5-3

t, hrs	Pwf, psi	t, hrs	Pwf, psi	t, hrs	Pwf, psi	t, hrs	Pwf, psi
0.0000	8000.00	0.2133	7935.40	42.662	7365.71	6399.32	5248.28
0.0007	7996.27	0.2844	7925.40	49.772	7330.51	7110.35	5192.49
0.0014	7994.73	0.3555	7916.61	56.883	7298.37	14220.71	4825.47
0.0021	7993.54	0.4266	7908.67	63.993	7268.64	21331.06	4610.77
0.0028	7992.54	0.4977	7901.39	71.104	7240.89	28441.41	4458.45
0.0036	7991.66	0.5688	7894.64	142.207	7028.27	35551.76	4340.29
0.0043	7990.86	0.6399	7888.34	213.311	6879.55	42662.12	4243.75
0.0050	7990.13	0.7110	7882.42	284.414	6764.33	49772.47	4162.13
0.0057	7989.45	1.4221	7836.72	355.518	6670.19	56882.82	4091.42
0.0064	7988.81	2.1331	7804.50	426.621	6590.59	63993.17	4029.06
0.0071	7988.21	2.8441	7778.83	497.725	6521.67	71103.53	3973.27
0.0142	7983.32	3.5552	7757.00	568.828	6460.91	142207.05	3606.25
0.0213	7979.57	4.2662	7737.73	639.932	6406.60	213310.58	3391.55
0.0284	7976.41	4.9772	7720.34	711.035	6357.50	284414.11	3239.23
0.0356	7973.63	5.6883	7704.42	1422.071	6003.16	355517.63	3121.07
0.0427	7971.11	6.3993	7689.71	2133.106	5799.60	426621.16	3024.53
0.0498	7968.79	7.1104	7676.01	2844.141	5653.70	497724.69	2942.91
0.0569	7966.64	14.2207	7573.50	3555.176	5539.97	568828.21	2872.20
0.0640	7964.62	21.3311	7503.99	4266.212	5462.97	639931.74	2809.84
0.0711	7962.70	28.4414	7450.02	4977.247	5381.35		
0.1422	7947.25	35.5518	7404.98	5688.282	5310.64		

Example 7-1

t,hrs	Pwf, psi	t,hrs	Pwf, psi	t,hrs	Pwf, psi	t,hrs	Pwf, psi
0.000000	5000.00	0.0030	4995.98	0.61	4971.01	364.05	4739.89
0.000006	4999.76	0.0036	4995.76	1.21	4960.61	424.73	4724.94
0.000012	4999.66	0.0042	4995.57	1.82	4953.41	485.4	4711.16
0.000018	4999.58	0.0049	4995.41	2.43	4947.9	546.08	4698.32
0.000024	4999.52	0.0055	4995.25	3.03	4943.44	606.75	4686.27
0.000030	4999.46	0.0061	4995.11	3.64	4939.7	1213.5	4592.89
0.000036	4999.41	0.0121	4993.99	4.25	4936.48	1820.25	4526.84
0.000043	4999.36	0.0182	4993.13	4.85	4933.64	2427	4475.29
0.000049	4999.32	0.0243	4992.41	5.46	4931.1	3033.75	4432.96
0.000055	4999.27	0.0303	4991.78	6.07	4928.79	3640.5	4397.07
0.000061	4999.23	0.0364	4991.2	12.14	4912.48	4247.25	4365.94
0.000121	4998.92	0.0425	4990.68	18.20	4901.52	4854	4338.49
0.000182	4998.68	0.0485	4990.19	24.27	4892.83	5460.75	4313.95
0.000243	4998.48	0.0546	4989.73	30.34	4885.44	6067.5	4291.78
0.000303	4998.31	0.0607	4989.29	36.41	4878.92	12135	4142.55
0.000364	4998.16	0.1214	4985.77	42.47	4873.04	18202.5	4053.79
0.000425	4998.03	0.1820	4983.07	48.54	4867.66	24270	3983.97
0.000485	4997.91	0.2427	4980.8	54.61	4862.67	30337.5	3929.82
0.000546	4997.80	0.3034	4978.79	60.68	4858.02	36405.01	3885.57
0.000607	4997.70	0.3641	4976.98	121.35	4822.17	42472.51	3848.16
0.001214	4997.00	0.4247	4975.33	182.03	4796.11	48540.01	3815.76
0.00182	4996.56	0.4854	4973.79	242.7	4774.77	54607.51	3787.17
0.00243	4996.23	0.5461	4972.36	303.38	4756.33	60675.01	3761.6

Example 7-2

t,hrs	Pwf, psi	t,hrs	Pwf, psi	t,hrs	Pwf, psi	t,hrs	Pwf, psi	t,hrs	Pwf, psi
0	10000	0.000777	9994.95	0.1553	9971.73	23.299	9479.96	3106.56	6668.39
7.77E-06	9999.47	0.0016	9993.35	0.233	9966.34	31.066	9391.53	3883.2	6510.57
1.55E-05	9999.25	0.0023	9992.35	0.311	9961.44	38.832	9314.31	4659.84	6381.28
2.33E-05	9999.09	0.0031	9991.61	0.388	9956.8	46.6	9245.3	5436.48	6271.79
3.11E-05	9998.94	0.0039	9991.03	0.466	9952.35	54.36	9182.67	6213.12	6176.88
3.88E-05	9998.82	0.0047	9990.55	0.544	9948.04	62.13	9125.24	6989.76	6093.16
4.66E-05	9998.71	0.0054	9990.14	0.621	9943.86	69.9	9072.15	7766.4	6018.29
5.44E-05	9998.6	0.0062	9989.77	0.699	9939.78	77.66	9022.76		
6.21E-05	9998.51	0.007	9989.45	0.777	9935.8	155.33	8657.22		
6.99E-05	9998.42	0.0078	9989.16	1.553	9900.11	232.99	8416.47		
7.77E-05	9998.33	0.0155	9986.99	2.33	9869.83	310.66	8236.67		
0.000155	9997.64	0.0233	9985.41	3.107	9843.21	388.32	8093.13		
0.000233	9997.12	0.0311	9984.09	3.883	9819.25	465.98	7973.71		
0.000311	9996.68	0.0388	9982.92	4.66	9797.32	543.65	7871.5		
0.000388	9996.3	0.0466	9981.86	5.436	9777	621.31	7782.17		
0.000466	9995.98	0.0544	9980.89	6.213	9757.99	698.98	7702.85		
0.000544	9995.68	0.0621	9979.98	6.99	9740.07	776.64	7631.51		
0.000621	9995.41	0.0699	9979.13	7.766	9723.09	1553.28	7154.65		
0.000699	9995.17	0.0777	9978.33	15.533	9585.47	2329.92	6871.03		